Tropical Cyclone-induced Storm Surges

A. Capel

Supervisors:

Prof.dr.ir. G.S. Stelling	(TU Delft / WL|Delft Hydraulics)
Prof.dr.ir. J.A. Battjes	(TU Delft)
Dr.ir. H. Gerritsen	(WL|Delft Hydraulics)
Dr.ir. J.A. Roelvink	(TU Delft / WL|Delft Hydraulics)

M.Sc. thesis
Faculty of Civil Engineering and Geosciences
Delft University of Technology

December, 2001

Preface

This report has been written in the framework of my Master of Science thesis for my study Civil Engineering at the faculty of Civil Engineering and Geosciences at Delft University of Technology. It has been carried out at WL|Delft Hydraulics. In this report, a study of tropical cyclone-induced storm surges has been performed.

I would like to thank my supervisors, prof.dr.ir. G.S. Stelling (Delft University of Technology and WL|Delft Hydraulics), prof.dr.ir. J.A. Battjes (Delft University of Technology), dr.ir. H. Gerritsen (WL|Delft Hydraulics) and dr.ir. J.A. Roelvink (Delft University of Technology and WL|Delft Hydraulics) for their suggestions and comments during my research.

Furthermore I am grateful to my girlfriend, family, friends and fellow-students for their support during my research project and everybody else who was willing to help me during my stay at WL|Delft Hydraulics.

Summary

Many cyclone models, which predict the induced storm surge in coastal areas have been developed over the years. These models have either been developed and calibrated for specific areas or they are more general and can be applied in different areas. Significant input in the surge prediction is the predicted track of the cyclone. However, even when it is predicted correctly, errors in computed and observed water levels or other phenomena still occur. One reason for this could be the absence of wind-wave influences in the computations.

In this study, a literature survey has been carried out into the phenomena, which are incorporated in the cyclone-models and how they are described. This survey showed that wind-waves are not taken into account in any of the models and therefore further research on the influence of waves is performed.

First a schematic model experiment has been carried out in which both wind set-up and wave set-up were computed for a simplified situation. It has been shown in the surge computations that about 15 percent of the storm surge can be ascribed to wave set-up. This percentage differs for different drag coefficients and when a conversion is made from a two-dimensional model to a three-dimensional model. It is also shown that wave set-up can be parameterised by increasing the drag coefficient. Finally the computations showed that grid refinement is of importance for wind set-up, but hardly important for wave set-up.

These conclusions were verified in a cyclone model that was developed for Andhra Pradesh. For this cyclone model, a wave module was incorporated in the existing model to compute the wind-waves which were generated by the cyclonic winds. The interaction between these modules could only be carried out by using stationary winds in the wave module. Four different cases have been researched. Apart from a change in landfall point, which was either Andhra Pradesh or the Ganges Delta, the computations were carried out using either a two-dimensional or three-dimensional model. None of these four cases showed a difference in storm surge level generated due to wave-induced set-up. The cause can probably be found in both the coarse resolution of the grid for computing wave set-up as well as the interaction between the two modules, which required stationary wind input in the wave-module.

Improvement can only be made when non-stationary wind input is available in the wave computation. A fine-grid resolution near the coastline is also necessary for computing wave-induced set-up. Finally, when including wave effects in the drag coefficient within Delft3D, this would lead to a physically more realistic drag coefficient.

Table of Contents

Preface ..... **i**

Summary ..... **iii**

List of Figures ..... **viii**

List of Tables ..... **xiii**

List of Symbols ..... **xiv**

1 Problem analysis **1–1**

1.1 Introduction 1–1

1.2 Problem definition 1–1

1.3 Objective 1–2

1.4 Outline 1–2

2 Literature review **2–1**

2.1 Introduction 2–1

2.2 Depth-averaged hydrodynamic equations 2–1

2.2.1 Non-linear interaction 2–5

2.3 Outline of cyclone modelling 2–6

2.3.1 Wind and pressure fields 2–6

2.4 Wind Stress and atmospheric pressure gradient forces 2–14

2.5 Description of existing Cyclone models 2–18

2.5.1 SLOSH 2–18

2.5.2 Special applications 2–21

2.6 Conclusion for further research 2–23

3 Modelling in Delft3D **3–1**

3.1 Introduction 3–1

3.2 Delft3D-Flow 3–1

3.2.1 Hydrodynamic equations 3–1

3.2.2 The staggered grid 3–3

3.2.3 Boundary conditions 3–4

3.2.4 Turbulence 3–4

3.3 Delft3D-Wave 3–5

3.3.1 Physical Background 3–6

3.4 Wave-Current interaction 3–8

4 Experiments....4–1
4.1 Introduction....4–1
4.2 Model Set-up....4–1
4.2.1 Introduction....4–1
4.2.2 Bathymetry....4–1
4.2.3 Offshore boundary....4–3
4.2.4 Domain....4–3
4.2.5 Depth-averaged or three-dimensional approach....4–6
4.2.6 Grid Size....4–8
4.2.7 Time Step....4–9
4.2.8 Numerical Parameters....4–9
4.2.9 Duration....4–12
4.3 Wind friction versus slope-gradient force....4–14
4.4 Wave Growth....4–19
4.5 Wind and Wave forcing....4–21
4.6 Dependence of the drag coefficient on the wave set-up....4–26
4.7 Sensitivity analysis....4–29
4.8 Conclusions....4–31

5 Case Study....5–1
5.1 Introduction....5–1
5.2 Approach....5–3
5.3 Cases....5–3
5.3.1 2D Andhra Pradesh....5–4
5.3.2 3D Andhra Pradesh....5–5
5.3.3 2D Ganges Delta....5–6
5.3.4 3D Ganges Delta....5–7
5.4 Input changes....5–8
5.5 Conclusions....5–9

6 Conclusions and Recommendations....6-1
6.1 Introduction....6-1
6.2 Conclusions....6-1
6.3 Recommendations....6-2

References....7-1

Appendix A Description of Delft3D-Flow and its interaction with Delft3D-Wave

A.1 Delft3D-Flow A-1

A.2 Flow-Wave interaction A-12

Appendix B: Batch files listing for case study

B.1 Description of computational method B-1

Appendix C: Case Study results

C.1 Stricken areas in the Bay of Bengal C-1

C.2 Water level registration at Andhra Pradesh C-3

C.3 Water level registration at the Ganges Delta C-13

C.4 Water level set-up due to waves in 2D Andhra Pradesh case C-20

C.5 Wave height and Dissipation for 2D Andhra Pradesh case C-29

C.6 Water level set-up due to waves in 3D Andhra Pradesh case C-38

C.7 Wave height and Dissipation for 3D Andhra Pradesh case C-47

C.8 Water level set-up due to waves in 2D Ganges Delta case C-56

C.9 Wave height and Dissipation for 2D Ganges Delta case C-65

C.10 Water level set-up due to waves in 3D Ganges Delta case C-74

C.11 Wave height and Dissipation for 3D Ganges Delta case C-83

C.12 Set-up computation with wind profile B C-92

List of Figures

Figure 2-1: Radial distribution of pressure profiles....2-9
Figure 2-2: Radial distributions of gradient winds.... 2-10
Figure 2-3: Radial distribution of gradient winds described by empirical formulae.... 2-12
Figure 2-4: Multiplying factor of the wind speed in the dependence relations of 2-14
Wu and Van Dorn
Figure 2-5: Dependence of the wind shear stress on the wind speed according the 2-15
formulations of Wu and Van Dorn
Figure 3-1: Example of s-grid....3-3
Figure 3-2: The staggered grid....3-4
Figure 4-2: Model grid definition; Wind vectors perpendicular to coastline....4-2
Figure 4-3: Water level at the shoreline for two computations when varying the bottom gradient 4-3
Figure 4-4: Wind direction at 100 km away from the eye of the cyclone 4-4
Figure 4-5: Typical sketch of wind vectors of a cyclone: eye of the cyclone overland 4-5
in the Krishna Delta
Figure 4-6: 2DH simulation of 25 days. Slow disappearing of the initialisation effect....4-7
Figure 4-7: 3D simulation, lasting 25 days. Energy dissipated already within 4-7
14.400 minutes (10 days)
Figure 4-8: Water level in station at shoreline drawn for one model run with 4-9
Dx=100m and one with Dx=1000m
Figure 4-9: Water level in observation point halfway. 2DH model run with a=100 4-12
and Dmar=0.1 m
Figure 4-10: Damping out of oscillations.... 4-12
Figure 4-11: Storm Surge at a wind speed of 40 m/s for several Drag coefficients.... 4-15
Figure 4-12: Storm Surge at a wind speed of 60 m/s for several Drag coefficients.... 4-15
Figure 4-13: Wind set-up for 3 different wind speeds with a Drag coefficient of 0.0025 4-16
Figure 4-14: Wind set-up for 3 different wind speeds with a Drag coefficient of 0.0050 4-16
Figure 4-15: Wind set-up for 3 different wind speeds with a Drag coefficient of 0.0075 4-17
Figure 4-16: Wind set-up for 3 different wind speeds with a Drag coefficient of 0.0100 4-17
Figure 4-17: Amplification factor in surge height for 4 drag coefficients.... 4-18
Figure 4-18: Significant Wave Height for 3 different wind velocities; computed 4-20
using Delft3D-Wave
Figure 4-19: Water levels in model area in final situation 4-21
Figure 4-20: Water levels in model area, zooming in at the last 20 km of previous figure.... 4-22
Figure 4-21: Root Mean Square Wave Height for wind blowing 50 m/s over model.... 4-23
area onshore
Figure 4-22: Wave Force per square metre.... 4-24
Figure 4-23: Energy Dissipation by bottom friction and wave breaking computed.... 4-25
by Delft3D-Wave
Figure 4-24: Water level for simulation in which hinterland is flooded.... 4-26

Figure 4-25: Relative increase of the water level by the influence of waves for several computations 4-27
Figure 4-26: Water levels along the x-axis for 4 computations; 2 computations with wind and wave forcing and 2 computations with just wind forcing 4-28
Figure 4-27: Water levels at the shoreline; variation in grid size and in number of layers 4-29
Figure 4-28: Water levels at the shoreline; increase of level due to enlarging of number of layers for the depth 4-30
Figure 4-29: Relative increase of water level due to waves for several computations by varying the spatial and vertical resolution 4-31
Figure 5-1: Grid of computational area 5-1
Figure 5-2: Schematic bottom profile of Bay of Bengal 5-2
Figure 5-3: Cyclone wind profiles used in case study and for verifying 5-3
Figure C-1: Overview of Bay of Bengal including selected areas C-1
Figure C-2: Andhra Pradesh selected area C-2
Figure C-3: Ganges Delta selected area C-2
Figure C-4: Water level registration at Andhra Pradesh: station 1 ..... C-3
Figure C-5: Water level registration at Andhra Pradesh: station 2 ..... C-4
Figure C-6: Water level registration at Andhra Pradesh: station 3 ..... C-5
Figure C-7: Water level registration at Andhra Pradesh: station 4 ..... C-6
Figure C-8: Water level registration at Andhra Pradesh: station 5 ..... C-7
Figure C-9: Water level registration at Andhra Pradesh: station 6 ..... C-8
Figure C-10: Water level registration at Andhra Pradesh: station 7 ..... C-9
Figure C-11: Water level registration at Andhra Pradesh: station 8 ..... C-10
Figure C-12: Water level registration at Andhra Pradesh: station 9 ..... C-11
Figure C-13: Water level registration at Andhra Pradesh: station 10 ..... C-12
Figure C-14: Water level registration at Ganges Delta: station 1 ..... C-13
Figure C-15: Water level registration at Ganges Delta: station 2 ..... C-14
Figure C-16: Water level registration at Ganges Delta: station 3 ..... C-15
Figure C-17: Water level registration at Ganges Delta: station 4 ..... C-16
Figure C-18: Water level registration at Ganges Delta: station 5 ..... C-17
Figure C-19: Water level registration at Ganges Delta: station 6 ..... C-18
Figure C-20: Water level registration at Ganges Delta: station 7 ..... C-19
Figure C-21: Water level set-up due to waves in 2D Andhra Pradesh case: 06/11/1996, 10:00 .... C-20
Figure C-22: Water level set-up due to waves in 2D Andhra Pradesh case: 06/11/1996, 14:00 .... C-21
Figure C-23: Water level set-up due to waves in 2D Andhra Pradesh case: 06/11/1996, 18:00 .... C-22
Figure C-24: Water level set-up due to waves in 2D Andhra Pradesh case: 06/11/1996, 22:00 .... C-23
Figure C-25: Water level set-up due to waves in 2D Andhra Pradesh case: 07/11/1996, 02:00 .... C-24
Figure C-26: Water level set-up due to waves in 2D Andhra Pradesh case: 07/11/1996, 06:00 .... C-25
Figure C-27: Water level set-up due to waves in 2D Andhra Pradesh case: 07/11/1996, 10:00 .... C-26
Figure C-28: Water level set-up due to waves in 2D Andhra Pradesh case: 07/11/1996, 14:00 .... C-27
Figure C-29: Water level set-up due to waves in 2D Andhra Pradesh case: 07/11/1996, 18:00 .... C-28

Figure C-30: Wave height for 2D Andhra Pradesh case: 06/11/1996, 10:00 ....C-29
Figure C-31: Dissipation for 2D Andhra Pradesh case: 06/11/1996, 10:00 ....C-29
Figure C-32: Wave height for 2D Andhra Pradesh case: 06/11/1996, 14:00 ....C-30
Figure C-33: Dissipation for 2D Andhra Pradesh case: 06/11/1996, 14:00 ....C-30
Figure C-34: Wave height for 2D Andhra Pradesh case: 06/11/1996, 18:00 ....C-31
Figure C-35: Dissipation for 2D Andhra Pradesh case: 06/11/1996, 18:00 ....C-31
Figure C-36: Wave height for 2D Andhra Pradesh case: 06/11/1996, 22:00 ....C-32
Figure C-37: Dissipation for 2D Andhra Pradesh case: 06/11/1996, 22:00 ....C-32
Figure C-38: Wave height for 2D Andhra Pradesh case: 07/11/1996, 02:00 ....C-33
Figure C-39: Dissipation for 2D Andhra Pradesh case: 07/11/1996, 02:00 ....C-33
Figure C-40: Wave height for 2D Andhra Pradesh case: 07/11/1996, 06:00 ....C-34
Figure C-41: Dissipation for 2D Andhra Pradesh case: 07/11/1996, 06:00 ....C-34
Figure C-42: Wave height for 2D Andhra Pradesh case: 07/11/1996, 10:00 ....C-35
Figure C-43: Dissipation for 2D Andhra Pradesh case: 07/11/1996, 10:00 ....C-35
Figure C-44: Wave height for 2D Andhra Pradesh case: 07/11/1996, 14:00 ....C-36
Figure C-45: Dissipation for 2D Andhra Pradesh case: 07/11/1996, 14:00 ....C-36
Figure C-46: Wave height for 2D Andhra Pradesh case: 07/11/1996, 18:00 ....C-37
Figure C-47: Dissipation for 2D Andhra Pradesh case: 07/11/1996, 18:00 ....C-37
Figure C-48: Water level set-up due to waves in 3D Andhra Pradesh case: 06/11/1996, 10:00 ....C-38
Figure C-49: Water level set-up due to waves in 3D Andhra Pradesh case: 06/11/1996, 14:00 ....C-39
Figure C-50: Water level set-up due to waves in 3D Andhra Pradesh case: 06/11/1996, 18:00 ....C-40
Figure C-51: Water level set-up due to waves in 3D Andhra Pradesh case: 06/11/1996, 22:00 ....C-41
Figure C-52: Water level set-up due to waves in 3D Andhra Pradesh case: 07/11/1996, 02:00 ....C-42
Figure C-53: Water level set-up due to waves in 3D Andhra Pradesh case: 07/11/1996, 06:00 ....C-43
Figure C-54: Water level set-up due to waves in 3D Andhra Pradesh case: 07/11/1996, 10:00 ....C-44
Figure C-55: Water level set-up due to waves in 3D Andhra Pradesh case: 07/11/1996, 14:00 ....C-45
Figure C-56: Water level set-up due to waves in 3D Andhra Pradesh case: 07/11/1996, 18:00 ....C-46
Figure C-57: Wave height for 3D Andhra Pradesh case: 06/11/1996, 10:00 ....C-47
Figure C-58: Dissipation for 3D Andhra Pradesh case: 06/11/1996, 10:00 ....C-47
Figure C-59: Wave height for 3D Andhra Pradesh case: 06/11/1996, 14:00 ....C-48
Figure C-60: Dissipation for 3D Andhra Pradesh case: 06/11/1996, 14:00 ....C-48
Figure C-61: Wave height for 3D Andhra Pradesh case: 06/11/1996, 18:00 ....C-49
Figure C-62: Dissipation for 3D Andhra Pradesh case: 06/11/1996, 18:00 ....C-49
Figure C-63: Wave height for 3D Andhra Pradesh case: 06/11/1996, 22:00 ....C-50
Figure C-64: Dissipation for 3D Andhra Pradesh case: 06/11/1996, 22:00 ....C-50
Figure C-65: Wave height for 3D Andhra Pradesh case: 07/11/1996, 02:00 ....C-51
Figure C-66: Dissipation for 3D Andhra Pradesh case: 07/11/1996, 02:00 ....C-51
Figure C-67: Wave height for 3D Andhra Pradesh case: 07/11/1996, 06:00 ....C-52
Figure C-68: Dissipation for 3D Andhra Pradesh case: 07/11/1996, 06:00 ....C-52
Figure C-69: Wave height for 3D Andhra Pradesh case: 07/11/1996, 10:00 ....C-53
Figure C-70: Dissipation for 3D Andhra Pradesh case: 07/11/1996, 10:00 ....C-53

Figure C-71: Wave height for 3D Andhra Pradesh case: 07/11/1996, 14:00 .....C-54
Figure C-72: Dissipation for 3D Andhra Pradesh case: 07/11/1996, 14:00 ..... C-54
Figure C-73: Wave height for 3D Andhra Pradesh case: 07/11/1996, 18:00 .....C-55
Figure C-74: Dissipation for 3D Andhra Pradesh case: 07/11/1996, 18:00 .....C-55
Figure C-75: Water level set-up due to waves in 2D Ganges Delta case: 06/11/1996, 02:00 .....C-56
Figure C-76: Water level set-up due to waves in 2D Ganges Delta case: 06/11/1996, 06:00 .....C-57
Figure C-77: Water level set-up due to waves in 2D Ganges Delta case: 06/11/1996, 10:00 .....C-58
Figure C-78: Water level set-up due to waves in 2D Ganges Delta case: 06/11/1996, 14:00 .....C-59
Figure C-79: Water level set-up due to waves in 2D Ganges Delta case: 06/11/1996, 18:00 .....C-60
Figure C-80: Water level set-up due to waves in 2D Ganges Delta case: 06/11/1996, 22:00 .....C-61
Figure C-81: Water level set-up due to waves in 2D Ganges Delta case: 07/11/1996, 02:00 .....C-62
Figure C-82: Water level set-up due to waves in 2D Ganges Delta case: 07/11/1996, 06:00 .....C-63
Figure C-83: Water level set-up due to waves in 2D Ganges Delta case: 07/11/1996, 10:00 .....C-64
Figure C-84: Wave height for 2D Ganges Delta case: 06/11/1996, 02:00 .....C-65
Figure C-85: Dissipation for 2D Ganges Delta case: 06/11/1996, 02:00 .....C-65
Figure C-86: Wave height for 2D Ganges Delta case: 06/11/1996, 06:00 .....C-66
Figure C-87: Dissipation for 2D Ganges Delta case: 06/11/1996, 06:00 .....C-66
Figure C-88: Wave height for 2D Ganges Delta case: 06/11/1996, 10:00 .....C-67
Figure C-89: Dissipation for 2D Ganges Delta case: 06/11/1996, 10:00 .....C-67
Figure C-90: Wave height for 2D Ganges Delta case: 06/11/1996, 14:00 .....C-68
Figure C-91: Dissipation for 2D Ganges Delta case: 06/11/1996, 14:00 .....C-68
Figure C-92: Wave height for 2D Ganges Delta case: 06/11/1996, 18:00 .....C-69
Figure C-93: Dissipation for 2D Ganges Delta case: 06/11/1996, 18:00 .....C-69
Figure C-94: Wave height for 2D Ganges Delta case: 06/11/1996, 22:00 .....C-70
Figure C-95: Dissipation for 2D Ganges Delta case: 06/11/1996, 22:00 .....C-70
Figure C-96: Wave height for 2D Ganges Delta case: 07/11/1996, 02:00 .....C-71
Figure C-97: Dissipation for 2D Ganges Delta case: 07/11/1996, 02:00 .....C-71
Figure C-98: Wave height for 2D Ganges Delta case: 07/11/1996, 06:00 .....C-72
Figure C-99: Dissipation for 2D Ganges Delta case: 07/11/1996, 06:00 .....C-72
Figure C-100: Wave height for 2D Ganges Delta case: 07/11/1996, 10:00 .....C-73
Figure C-101: Dissipation for 2D Ganges Delta case: 07/11/1996, 10:00 .....C-73
Figure C-102: Water level set-up due to waves in 3D Ganges Delta case: 06/11/1996, 02:00 .....C-74
Figure C-103: Water level set-up due to waves in 3D Ganges Delta case: 06/11/1996, 06:00 .....C-75
Figure C-104: Water level set-up due to waves in 3D Ganges Delta case: 06/11/1996, 10:00 .....C-76
Figure C-105: Water level set-up due to waves in 3D Ganges Delta case: 06/11/1996, 14:00 .....C-77
Figure C-106: Water level set-up due to waves in 3D Ganges Delta case: 06/11/1996, 18:00 .....C-78
Figure C-107: Water level set-up due to waves in 3D Ganges Delta case: 06/11/1996, 22:00 .....C-79
Figure C-108: Water level set-up due to waves in 3D Ganges Delta case: 07/11/1996, 02:00 .....C-80
Figure C-109: Water level set-up due to waves in 3D Ganges Delta case: 07/11/1996, 06:00 .....C-81
Figure C-110: Water level set-up due to waves in 3D Ganges Delta case: 07/11/1996, 10:00 .....C-82
Figure C-111: Wave height for 3D Ganges Delta case: 06/11/1996, 02:00 .....C-83

Figure C-112: Dissipation for 3D Ganges Delta case: 06/11/1996, 02:00 ..... C-83
Figure C-113: Wave height for 3D Ganges Delta case: 06/11/1996, 06:00 ..... C-84
Figure C-114: Dissipation for 3D Ganges Delta case: 06/11/1996, 06:00 ..... C-84
Figure C-115: Wave height for 3D Ganges Delta case: 06/11/1996, 10:00 ..... C-85
Figure C-116: Dissipation for 3D Ganges Delta case: 06/11/1996, 10:00 ..... C-85
Figure C-117: Wave height for 3D Ganges Delta case: 06/11/1996, 14:00 ..... C-86
Figure C-118: Dissipation for 3D Ganges Delta case: 06/11/1996, 14:00 ..... C-86
Figure C-119: Wave height for 3D Ganges Delta case: 06/11/1996, 18:00 ..... C-87
Figure C-120: Dissipation for 3D Ganges Delta case: 06/11/1996, 18:00 ..... C-87
Figure C-121: Wave height for 3D Ganges Delta case: 06/11/1996, 22:00 ..... C-88
Figure C-122: Dissipation for 3D Ganges Delta case: 06/11/1996, 22:00 ..... C-88
Figure C-123: Wave height for 3D Ganges Delta case: 07/11/1996, 02:00 ..... C-89
Figure C-124: Dissipation for 3D Ganges Delta case: 07/11/1996, 02:00 ..... C-89
Figure C-125: Wave height for 3D Ganges Delta case: 07/11/1996, 06:00 ..... C-90
Figure C-126: Dissipation for 3D Ganges Delta case: 07/11/1996, 06:00 ..... C-90
Figure C-127: Wave height for 3D Ganges Delta case: 07/11/1996, 10:00 ..... C-91
Figure C-128: Dissipation for 3D Ganges Delta case: 07/11/1996, 10:00 ..... C-91
Figure C-129: Water level registration at Andhra Pradesh using wind profile B: Station 6 ..... C-92
Figure C-130: Water level set-up due to waves using wind profile B in 2D Andhra Pradesh case 07/11/1996, 12:00 ..... C-92

List of Tables

Table 4-1: Water level set-up at the shoreline for different grid sizes 4-8
Table 4-2: Coefficients of equation (4-78)..... 4-13
Table 5-1: Comparison of maximum H_{rms} and Dissipation for 2D and 5-5
3D Andhra Pradesh computations
Table 5-2: Comparison of maximum H_{rms} and Dissipation for 2D and 5-7
3D Ganges Delta computations

List of Symbols

C, C_{2D}	: 2D Chézy coefficient	$m^{1/2}/s$
C_{3D}	: 3D Chézy coefficient	$m^{1/2}/s$
C_d	: wind drag coefficient	-
c_D	: constant relating mixing length, turbulent kinetic energy and dissipation in k-ε turbulence model	-
C_z	: drag coefficient in shear stress at bed due to current	-
c_μ	: calibration constant	-
$c_{\mu'}$	: constant in Kolmogorov-Prandtl's eddy viscosity formulation	-
$c_x, c_y, c_\theta, c_\omega$	: wave group velocity in x,y,θ,ω direction	m/s
D_h, D_v	: eddy diffusivity in the horizontal and vertical direction	m^2/s
D	: energy dissipation	$kg\ m^2/s^3$
D	: depth to horizontal reference plane	m
E	: wave energy density	J/m^2
E	: evaporation	m/s
E_k, E_p	: kinetic and potential Energy	$kg\ m^2/s^2$
f	: Coriolis coefficient	1/s
f_w	: wave friction factor	-
F	: fetch length	m
$\tilde{F}$	: dimensionless fetch length	-
F_ξ	: turbulent momentum flux in ξ-direction	m/s^2
F_x	: radiation stress gradient in x-direction	m/s^2
F_η	: turbulent momentum flux in η-direction	m/s^2
F_y	: radiation stress gradient in y-direction	m/s^2
g	: acceleration of gravity	m/s^2
$\sqrt{G_{\xi\xi}}$	: coefficient used to transform curvi-linear to rectangular co-ordinates	m
$\sqrt{G_{\eta\eta}}$	: coefficient used to transform curvi-linear to rectangular co-ordinates	m
h	: total water depth (h=D+ζ)	m
$H_{1/3}$	: significant wave height	m
$\tilde{H}$	: dimensionless wave height	-
H_{rms}	: root-mean-square wave height	m
k	: turbulent kinetic energy	m^2/s^2
k, k_x, k_y	: wave number	1/m
k_s	: Nikuradse roughness length	m
L	: mixing length	m
$L_{1/3}$	: wave length of significant wave	m
M_ξ	: source or sink of momentum in ξ-direction	m/s^2
M_η	: source or sink of momentum in η-direction	m/s^2
M^S_x,	: depth-averaged mass flux due to Stokes drift in x-direction	kg m/s
M^S_y,	: depth-averaged mass flux due to Stokes drift in y-direction	kg m/s
N	: action density spectrum	Js/m^2
n	: Manning's coefficient	$m^{1/3}/s$
p	: hydrostatic water pressure	$kg/m/s^2$
p	: surface atmospheric pressure	$kg/m/s^2$
p_c	: central atmospheric pressure	$kg/m/s^2$
p_∞	: ambient atmospheric pressure	$kg/m/s^2$

Δp	: difference in ambient and central pressure	$kg/m/s^2$
P	: precipitation	m/s
P_ξ	:gradient hydrostatic pressure in ξ -direction in (ξ,η,z) co-ordinate system	$kg/m^2/s^2$
P_η	:gradient hydrostatic pressure in η -direction in (ξ,η,z) co-ordinate system	$kg/m^2/s^2$
P_k	: production term in transport equation for the turbulent kinetic energy	m^2/s^3
P_ε	: production term in transport equation for the dissipation of turbulent kinetic energy	m^2/s^4
q_{in}	: local source per unit volume	1/s
q_{out}	: local sink per unit volume	1/s
Q	: global source or sink per unit area	m/s
r_0	: radius of maximum wind	m
Ri	: gradient Richardson's number	-
S_{xx}	: onshore flux of onshore momentum	N/m
S_{xy}	: longshore flux of onshore momentum	N/m
t	: time co-ordinate	s
$T_{1/3}$	: wave period of significant wave height	s
$\widetilde{T}$	: dimensionless wave period	-
u	: velocity in the x, ξ -direction	m/s
u_*	: friction velocity	m/s
U_{10}	: wind speed at 10 metres above the surface	m/s
U	: depth-averaged velocity in x, ξ -direction	m/s
$\overline{u_*}$	: vertical averaged friction velocity	m/s
u_b	: velocity at bed boundary layer in x, ξ-direction	m/s
u_{*b}	: friction velocity at the bed	m/s
u_*^b	: modified friction velocity near bed	m/s
$\widetilde{u_*}$	: friction velocity near bed due to current and waves	m/s
$\lvert\underline{u}_b\rvert$	: magnitude of velocity at the computational sea bed layer = $\sqrt{(u_b^2+v_b^2)}$	m/s
u_*^s	: friction velocity at the free surface	m/s
$\lvert\underline{U}\rvert$	: magnitude of depth-averaged horizontal velocity vector $(U,V)^T$	m/s
$\hat{U}_{orb}$	: amplitude of the near-bottom wave orbital velocity	m/s
u_S	: Stokes drift in y-direction	m/s
$\tilde{u}$	: total velocity due to flow and Stokes drift in x-direction	m/s
v	: velocity in the y, η -direction	m/s
V	: depth-averaged velocity in y, η-direction	m/s
V_c, V_g	: wind speed	m/s
w	: velocity in z-direction in the Cartesian frame of reference	m/s
w	: wind speed	m/s
w_c	: critical wind speed	m/s
W_m, V_m	: maximum wind speed	m/s
x,y	: spatial co-ordinates	-
z_0	: bed roughness length	m
$\widetilde{z}_0$	: enhanced bed roughness length due to current and waves	m
Δz_b	: thickness of the bed layer	m
Δz_s	: thickness of the surface layer	m

ε	: dissipation in transport equation for turbulent kinetic energy	m^2/s^3
Φ	: latitude	deg.
θ	: spectral direction	deg.
ν^{3D}	: part of eddy viscosity due to 3D turbulence	m^2/s
ν_H	: horizontal eddy viscosity (ξ- and η-direction)	m^2/s
ν_{mol}	: molecular eddy viscosity (ξ- and η-direction)	m^2/s
ν_V	: vertical eddy viscosity	m^2/s
ω	: velocity in the s-direction in the s co-ordinate system	m/s
ω	: angular frequency waves	1/s
ρ	: density of water	kg/m^3
ρ_a	: density of air	kg/m^3
ρ_0	: reference density of water	kg/m^3
σ	: scaled vertical co-ordinate $\sigma=(z - \zeta)/(D+\zeta)$ (surface: $\sigma=0$; bed: $\sigma=-1$)	-
σ	: relative frequency of waves	1/s
τ	: shear stress	$kg/m/s^2$
$\tau_{b\xi},\tau_{bx}$	: shear stress at bed in ξ,x-direction	$kg/m/s^2$
$\tau_{b\eta},\tau_{by}$	: shear stress at bed in η,y-direction	$kg/m/s^2$
τ_c	: magnitude of the shear stress at bed due to current alone	$kg/m/s^2$
τ_w	: magnitude of the shear stress at bed due to waves alone	$kg/m/s^2$
τ_m	: magnitude of the wave-averaged shear stress at bed for combined waves and current	$kg/m/s^2$
τ_{max}	: magnitude of the maximum bed shear stress for combined waves and current	$kg/m/s^2$
$\tau_{s\xi},\tau_{sx}$	: shear stress at surface in ξ,x-direction	$kg/m/s^2$
$\tau_{s\eta},\tau_{sy}$	: shear stress at surface in η,y-direction	$kg/m/s^2$
ξ, η	: horizontal, curvilinear spatial co-ordinates	-
ζ	: water level above some reference datum	m
ζ_0	: hydrostatic water height	m

1 Problem analysis

1.1 Introduction

Each year, many areas of the world are struck by tropical cyclones. A tropical cyclone develops over tropical or subtropical waters. At the Northern Hemisphere they follow a anti-clockwise pattern and on the Southern Hemisphere a clockwise pattern. They can be classified into three different categories:
Tropical Depressions with maximum sustained winds of 60 kilometres per hour, Tropical Storms with maximum sustained wind speeds between 60 and 120 kilometres an hour and Hurricanes/ Typhoons with maximum sustained winds of 120 kilometres per hour and higher.
The most severe tropical cyclones are thus hurricanes/ typhoons. They have a characteristic area of low pressure in their centre, called the eye. The name hurricane or typhoon depends on where they are formed. The names stand for the same phenomenon. They are called hurricanes when they are formed in the North Atlantic or eastern North Pacific, and typhoons when they are formed in the western Pacific. Their track speed ranges from 0 to 15 m/s and they measure 320 to 480 kilometres across and may bring winds up to 290 kilometres an hour.

Tropical cyclones can cause immense damage by wind, pressure, rain and indirectly through storm surges and waves. The greatest potential for loss of life related to a tropical cyclone is from the storm surge and associated flooding, which historically has claimed nine of ten victims, often due to the lack of warning and insufficient preparedness.
A storm surge is an abnormal rise of the water level above the predicted water level of the astronomical tide, due to wind and/ or pressure. The rise in water level begins with a local atmospheric low pressure that lifts the sea surface. Mainly, in the eye of the cyclone, where the lowest pressures are, the water level can be raised by 0.5 till 1 metre. The winds that arise from this low-pressure field amplify the surge due to the shear stress that is most effective over shallow water. In extreme cases, surges of more than 8 metres have been observed and obviously, these storm surges cause severe flooding of the area behind with all consequences related to that.

1.2 Problem definition

Over the years, numerical models have been made to forecast the high water and flooding resulting from a certain cyclone. The impact is computed and areas which are threatened by flooding, are made visible by these computations. Steps can then be taken to minimise the damage and so these models can improve the warning.
However these forecasts are not always right. Significant input in the surge prediction is the predicted track of the cyclone. This track is very hard to predict, but even when is it

predicted correctly, errors in computed and observed water levels, flow velocities, etc. still occur.
One of these numerical models is Delft3D. This model has been used for tropical cyclone-induced storm surge computations in Vietnam and India. Good results have been obtained by calibrating the model with observed data, but some of these coefficients do not make any sense physically. One aspect that is not taken into account in the computations for Vietnam and India are the wind-waves. The impression is that by including the waves in the computations, this will also lead to a more physically justifiable basis.

1.3 Objective

This study is aimed to obtain some more insight in aspects that play a role in storm surges. This will be done in two ways. First a literature study will be carried out in which the phenomena, that are included in existing hurricane models, are reviewed. Secondly, the impact of waves on storm surges will be investigated with the program Delft3D, developed by Delft Hydraulics.

1.4 Outline

The outline of this report is as follows:

In Chapter 2, a literature review on the state of cyclone modelling is given. Treated are the wind and pressure fields of a cyclone and how they are mathematically described, and existing models with respect to the aspects they take into account in cyclone modelling.

In Chapter 3, two modules of the computer software package Delft3D, used for calculating water levels, flow and wind waves are discussed. Treated are the background of the two modules and the interaction between them.

Chapter 4 deals with the numerical experiments that have been carried out to examine the influence of waves on surges. Comparison is made between theory and model runs.

In Chapter 5 a case study is performed for the Bay of Bengal. Four computations have been carried out and the results of each computation are discussed.

The conclusions and recommendations from this study are given in Chapter 6.

Appendix A gives a detailed outline of Delft3D-Flow and its interaction with Delft3D-Wave.

Appendix B shows the listing of the files which where used for the computations.

Appendix C plots the output of the case study for all four variants that were examined.

2 Literature review

2.1 Introduction

This literature review deals with storm surges caused by cyclones. In the first paragraph the depth-averaged hydrodynamic equations are treated. These equations describe the water movement caused by the forces acting on it. One of these forces can be the wind from a cyclone. Paragraph 2.3 deals therefore with the way wind and pressure fields are mathematically described in cyclones. Paragraph 2.4 treats how the wind forces act on the water surface. Subsequently, existing hurricane models, which make use of the theory, described in paragraph 2.2 to 2.4 are reviewed in paragraph 2.5. Finally a conclusion is presented for further research.

2.2 Depth-averaged hydrodynamic equations

Storm surges are meteorologically generated motions in a coastal area or inland water bodies. They typically last for a period between a few hours and several days. Storm surges belong to the same class of motion as tides, that is, long gravity waves.
Tides are large-scale horizontal phenomena, characterised by vertical flow accelerations that are much smaller than acceleration of gravity. The dynamical theory of tides and surges is therefore based on depth-averaged hydrodynamic equations. The elimination of the vertical dependence gives a useful simplification of the problem. The water is assumed to be incompressible and homogeneous. Thus in Cartesian co-ordinates, that is x, y-axes in the horizontal plane, the depth-averaged equations of motion and continuity are

$$\frac{\partial U}{\partial t}+U\frac{\partial U}{\partial x}+V\frac{\partial U}{\partial y}-fV=-g\frac{\partial \zeta}{\partial x}-\frac{1}{\rho}\frac{\partial p}{\partial x}+\frac{1}{\rho h}\left(\tau_{sx}-\tau_{bx}\right)+\Gamma_x \qquad (2\text{-}1)$$

$$\frac{\partial V}{\partial t}+U\frac{\partial V}{\partial x}+V\frac{\partial V}{\partial y}+fU=-g\frac{\partial \zeta}{\partial y}-\frac{1}{\rho}\frac{\partial p}{\partial y}+\frac{1}{\rho h}\left(\tau_{sy}-\tau_{by}\right)+\Gamma_y \qquad (2\text{-}2)$$

$$\frac{\partial \zeta}{\partial t}+\frac{\partial (hU)}{\partial x}+\frac{\partial (hV)}{\partial y}=0 \qquad (2\text{-}3)$$

where:

t	= time	[s]
ζ	= elevation of the sea surface	[m]
U,V	= components of depth-averaged current	[m/s]
τ_{sx},τ_{sy}	= components of the wind-stress, τ_s, on the sea surface	[N/m^2]
τ_{bx},τ_{by}	= components of the bottom stress τ_b	[N/m^2]
p	= atmospheric pressure on the sea surface	[Pa]
h	= the total water depth (D + ζ, where D is depth)	[m]
ρ	= the density of the sea water, assumed uniform	[kg/m^3]

g	= the acceleration due to gravity	[m/s^2]
f	= the Coriolis parameter (2 ω sin ϕ, where ω is the angular speed of the Earth's rotation and ϕ is latitude)	[1/s]
Γ_x, Γ_y	= tide generating body forces	[m/s^2]

Equations (2-1) and (2-2) equate the acceleration of the water to the forces (per unit mass) acting on it. The meteorological forces, which generate storm surges, are thus the wind stress and horizontal gradients of surface atmospheric pressure.

As can be seen in equations (2-1) and (2-2), the wind stress is divided by the water depth. This means that the wind stress is less effective in generating surges in deep water than in shallow water. This is not applicable to the influence of pressure variations, namely, the relevant terms in equation (2-1) and equation (2-2) are independent of the depth. In deep water, then, surges are produced mainly by changes in atmospheric pressure, but in shallow water, and in particular on continental shelves and near coasts, wind stress forcing dominates.
Equation (2-3) is the continuity equation, expressing conservation of water. Changes in surface elevation, associated with the tide or storm surge, are related to net fluxes of water in or out across its sides.
The last equation, generally used for solving the hydrodynamic equations mathematically, is the bottom stress related to the depth mean current in a quadratic law:

$$\tau_b = \kappa \rho U |U| \tag{2-4}$$

Here κ is a dimensionless bottom friction parameter, typically 2.5 x 10^{-3}. For relating the wind stress to the surface wind velocity, *w* [m/s], another quadratic law is used:

$$\tau_s = C_d \rho_a w |w| \tag{2-5}$$

Here ρ_a is the air density [kg/m^3] and C_d is the drag coefficient [-], which may itself be a function of wind speed. According to Flather and Khandker (1993), Wu used for example the following relationship:

$$C_d \times 10^3 = 0.8 + 0.065 \cdot w \tag{2-6}$$

for any wind speed (m/s) from breeze to hurricane. Here *w* is the wind speed at 10 m above the sea level.

From equation (2-5) we see that an accurate knowledge of the wind field is essential since, for example, a 10% error in wind speed translates into a 21% error in the wind stress that generates the surge.
The dynamical problem is now to solve equations (2-1)-(2-5) within a region in which p and w are prescribed functions of position and time, and subject to appropriate boundary conditions.

With simplifying assumptions, some analytical solutions are possible. In the depth-averaged equations, there are no vertical velocities. When assuming hardly any horizontal velocities and no stresses or tide acting on the water level, then, in equations (2-1) and (2-2) all terms other than the first two on the right hand sides can be neglected. Integrated over a distance between two locations, one gets,

$$\Delta\zeta = -\Delta p / \rho g \tag{2-7}$$

where $\Delta\zeta$ is the difference in surge height between two locations at which atmospheric pressure differs by Δp.

A second analytical solution is possible when looking at the effect of steady wind, no tide and negligible pressure gradient. The solution must be stationary and this is only possible when no velocities remain. Equations (2-1) and (2-2) give by neglecting the pressure term:

$$\frac{\partial\zeta}{\partial s} = \frac{\tau_s}{\rho g h} \tag{2-8}$$

where s is the distance (in the direction of the wind stress). This gives the balance between the slope of the sea surface due to surge and the wind stress magnitude.

With further assumptions, this may be integrated to give an estimate of surge height. For example, a wind stress, τ_s directed towards the shore over a continental shelf of width L and uniform depth h, bounded by a deep ocean where the wind induced surge height was zero, would produce a surge at the coast given by

$$\zeta = \frac{\tau_s}{\rho g h} L \tag{2-9}$$

Next to the basic depth-averaged equations, there are researchers who use these equations with some small alterations, like Ebersole (1985). He developed a numerical model for hurricane-induced storm surge in the Atchafalaya River Delta. In his momentum equations, the advective terms are neglected and the water elevation is related to the hydrostatic elevation of the atmospheric pressure deficit from ambient pressure, ζ_a. The bottom friction is modelled with the Chezy coefficient and the wind shear stress is related to the water density and a dimensionless wind stress coefficient k.

Momentum equations:

$$\frac{\partial U}{\partial t} - fV + g\frac{\partial}{\partial x}(\zeta - \zeta_a) + \frac{gU}{C^2 h}\left(U^2 + V^2\right)^{\frac{1}{2}} + \frac{1}{\rho h}\tau_{sx} = 0 \qquad (2\text{-}10)$$

$$\frac{\partial V}{\partial t} + fU + g\frac{\partial}{\partial y}(\zeta - \zeta_a) + \frac{gV}{C^2 h}\left(U^2 + V^2\right)^{\frac{1}{2}} + \frac{1}{\rho h}\tau_{sy} = 0 \qquad (2\text{-}11)$$

The wind stresses τ_{sx}, τ_{sy} were calculated by the following equations:

$$\tau_{sx} = \rho k |\vec{w}| w_x \qquad (2\text{-}12)$$

$$\tau_{sy} = \rho k |\vec{w}| w_y \qquad (2\text{-}13)$$

in where:

ρ = the water density [kg/m^3]

$|\vec{w}|$ = the magnitude of the wind speed [kn]

The wind stress coefficient k was based on a formulation given by Van Dorn (1953). This coefficient was assumed to be a function of wind speed such that

$$k = k_1 \text{ for } |\vec{w}| \le w_c \qquad (2\text{-}14)$$

$$k = k_1 + k_2\left(1 - \frac{w_c}{|\vec{w}|}\right)^2 \text{ for } |\vec{w}| > w_c \qquad (2\text{-}15)$$

where k_1 =1.1 x 10^{-6}, k_2 = 2.5 x 10^{-6}, and w_c is a critical wind speed defined to be 14 knots.

2.2.1 Non-linear interaction

A specific problem for analytical treatment concerns the terms in equations (2-1)-(2-4) that contain products of the dependent variables, ζ, U and V. Dimensional analysis indicates that these non-linear terms are important in shallow water, where they generate an interaction between components of the motion. In particular, where the tides are large and the water shallow, interaction occurs between the tide and surge making the two components interdependent. Thus the surge produced by given meteorological forces at a certain state of the tide may differ significantly from the surge resulting from identical forcing at a different stage of the tide or under the assumption that there is no tide.

The main surge effect is generated by the wind acting over the continental shelves. Due to cyclonic rotation, maximum onshore winds, and hence also the maximum surge levels, tend to occur on the right of the storm track as it crosses the coast. A negative surge associated with the offshore winds on the left of the storm centre may also appear. The speed and angle of approach of the storm, relative to the coastline, influence the magnitude of surge, and convergence of coastlines in a bay or estuary can produce substantial amplification. Other dynamical factors may also modify the response. The resonant coupling mechanism occurs when the speed of a travelling atmospheric disturbance matches that of free gravity waves.

The apparent importance of non-linear effects suggests that dynamical tide-surge interaction must also play a part here.
If tides are close to resonance, then a change in mean sea level (MSL) could produce a larger change in the tides than would otherwise be the case. Since a rise in MSL increases water depth, the wavelength, λ, of the tide would increase. For a shelf with $L > \lambda/4$, this could bring the regime closer to resonance, increasing the tidal range for certain constituents.
If the shoreline comprises a vertical wall, high enough not to be overtopped by the raised levels giving a bathymetric profile with a step, then water depths will increase and as a consequence storm surges should be reduced in magnitude.
If the bathymetric profile in the nearshore region has a linear slope, then the shoreline will advance inland as MSL rises so that the area of sea below a given water depth will remain broadly unchanged. Correspondingly, surge magnitudes may be unaltered. So, when tide and surge are both substantial their timing becomes critical in determining the maximum water level; the level may be large if tidal high water and peak surge occur at the same time, but much less if they occur at different times (Flather and Khandker, 1993).

In order to forecast coastal flooding, it is necessary first to be able to describe the development and distribution of winds within the cyclones, which generate the surges, and then to relate coastal water levels to the meteorological variables.

The next paragraph will deal with the distribution of wind and the pressure fields within a cyclone. Several ways of prescribing these topics will be examined.

2.3 Outline of cyclone modelling

2.3.1 Wind and pressure fields

Through out the world storm surge models have made to predict or to hindcast surge heights caused by hurricanes or typhoons. Tropical Cyclones, which generated an enormous storm surge, most of time causing severe flooding, were recorded and models were developed, calibrated and verified on only these few cyclones that originated in that typical bay or sea. Therefore there exist a large number of indepently developed models, but all these models tackle the problem in near enough the same way. However, the different assumptions made about dependence of surface atmospheric pressure and wind speed on the distance from the storm centre make it difficult to evaluate the different storm surge models.
In most of the model studies of storm surges, idealised cyclone models are used, most of them with circular symmetry, moving along straight-line tracks with constant speed of propagation. Here, an outline will be given of the approaches that were made by several researchers in the past.

The central pressure is one of the key parameters in defining the intensity of a storm. It is considered that a mound of water is formed below the storm centre in the open sea and this propagates as a solitary wave, moving with the same speed as that of the storm.

The Bay of Bengal is one of the most vulnerable areas in the world. According to Murty et al. (1986), Das attempted to develop a storm surge model for this area. He assumed that the atmospheric pressure could be described by

$$p = p_{\infty} - \Delta p \left[1 + \left(r / r_0 \right)^2 \right]^{-1} \tag{2-16}$$

where:

p	= surface atmospheric pressure p = p(r)	[Pa]
r	= radial distance from the storm centre	[m]
p_∞	= ambient pressure at large distance	[Pa]
Δp	= difference between the ambient and central pressure	[Pa]
r_0	= radius at which the wind attains its maximum speed	[m]

He made the assumption that winds were in cyclostrophic balance and therefore could be described by

$$W_c = \sqrt{\frac{r}{\rho_a} \frac{\partial p}{\partial r}} \tag{2-17}$$

in which ρ_a is the air density in kg/m^3.

The maximum wind speed at r_0 is then

$$W_m^2 = \frac{\Delta p}{2\rho_a} \tag{2-18}$$

Johns et al. (1980) used some alternative definitions. They assumed that the pressure distribution was best described with

$$p = p_\infty - \Delta p \cdot e^{\frac{-r}{R}} \tag{2-19}$$

where R is the e-folding radius of the cyclone.
They calculated the wind speed from a gradient balance [1]

$$W_g = \sqrt{\frac{r}{\rho_a}\frac{\partial p}{\partial r} + \left(\frac{1}{2}rf\right)^2} - \frac{rf}{2} \tag{2-20}$$

f is the Coriolis parameter that changes with latitude (Murty et al., 1986).

The analytic model that Holland (1980) used relates the wind and pressure fields in a hurricane again in a different way. The pressure field was first normalised to eliminate variations due to different central and ambient pressures through the following parameter:

$$\frac{p - p_c}{\Delta p} \tag{2-21}$$

where:

p	= pressure at radius r	[Pa]
p_c	= central pressure	[Pa]
Δp	= difference between ambient pressure, p_∞, and central pressure	[Pa]

This parameter plotted against the radial distance from the centre for a number of hurricanes gives a curve that looks like a rectangular hyperbola and was approximated by

$$r^B \ln\left[\frac{\Delta p}{p - p_c}\right] = A \tag{2-22}$$

where A and B are scaling parameters. Taking the antilogarithm of this equation and rearranging gives

$$p = p_c + \Delta p \cdot e^{-\frac{A}{r^B}} \tag{2-23}$$

Making use of the gradient wind relation, the wind profile can be expressed as

[1] *The formula written in Murty et al. (1986) is not correct. The second term on the right-hand side must be divided by two to get the correct equation for the gradient wind balance.*

$$V_g = \sqrt{AB \cdot \Delta p \cdot \frac{e^{\frac{-A}{r^B}}}{\rho r^B} + \frac{r^2 f^2}{4}} - \frac{rf}{2} \tag{2-24}$$

where V_g is the gradient wind at radius r, f is the Coriolis parameter, and ρ is the density of air (1.15 kg·m^{-3}).
In the area of maximum sustained wind speed, the pressure gradient and centrifugal forces are dominant and the Coriolis force can be ignored. Thus, for the cyclostrophic equilibrium one can write

$$V_c = \sqrt{AB \cdot \Delta p \cdot \frac{e^{\frac{-A}{r^B}}}{\rho r^B}} \tag{2-25}$$

The radius of maximum winds, R_w, is obtained by setting dV$_c$/dr equal to zero:

$$R_w = A^{1/B} \tag{2-26}$$

Thus, R$_w$ is determined only by the scaling parameters A and B and is not dependent on the central and ambient pressures. To obtain the maximum wind speed, V_m, equation (2-26) is substituted into equation (2-25) to give

$$V_m = C\sqrt{\Delta p} \tag{2-27}$$

with

$$C \equiv \sqrt{\frac{B}{\rho e}}$$

where e is the base of natural logarithms.

From the above relations it can be seen that the maximum wind speed is independent of the radius of maximum winds but it depends on the shape of the pressure profile through B. From equation 2-23 the radius R_p of maximum pressure gradient is given by

$$R_p = \left[\frac{AB}{B+1}\right]^{1/B} \tag{2-28}$$

From equation (2-26) and (2-28)

$$\frac{R_p}{R_w} = \left(\frac{B}{B+1}\right)^{1/B} \tag{2-29}$$

Based on observed data, a lower limit for B is found to be 1.0. An upper bound is 3.0 and a representative value was found to be 2.5. Then from equation (2-26), one can determine A by using the observed R_w values.

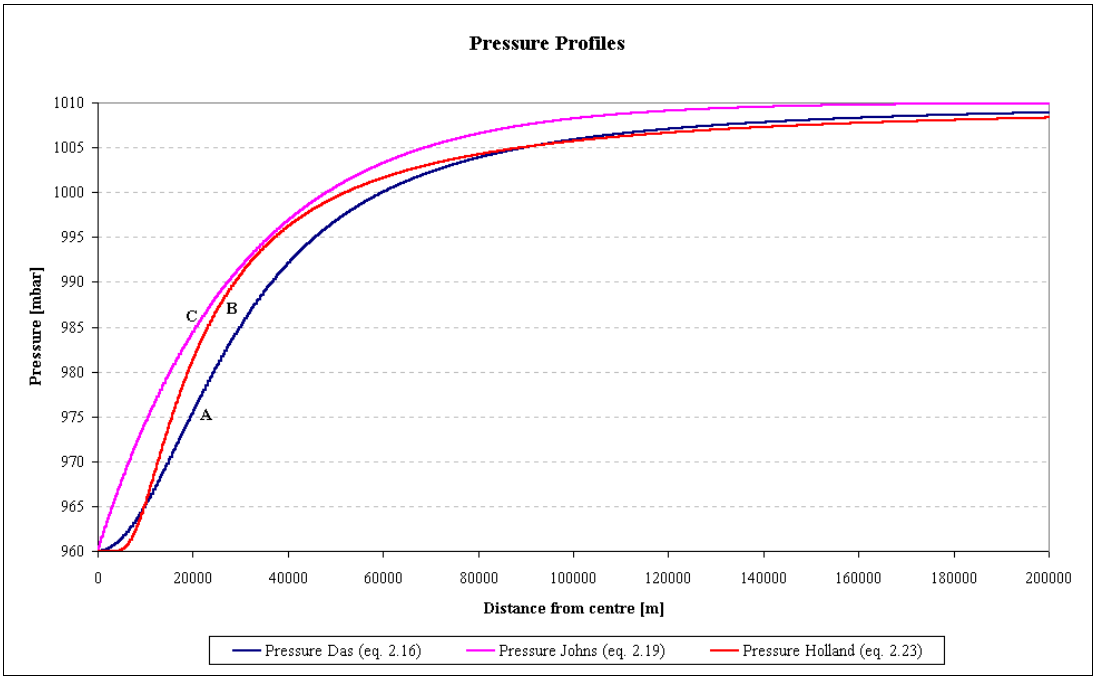

Figure 2-1: Radial distribution of pressure profiles
Curve A: using equation (2-16) with Δp=50 mb, p_∞=1010 mb and r_0=30 km
Curve B: using equation (2-19) with same Δp, p_∞ and R=30 km
Curve C: using equation (2-23) with A=900 km, B=1.4 and p_c=960 mb

In Figure 2-1 three different pressure profiles are depicted against the distance from the centre of the cyclone. Abstract values have been assigned to the parameters: Δp=50 mb, p_∞= 1010 mb and therefore p_c=960mb and r_0, R=30km. For the pressure profile of Holland, the constants A and B are taken 900 km and 1.4 respectively. Pressure profile A is the only one that over about the first 5 km from the centre, in here, retains a constant central pressure of 960 mb.

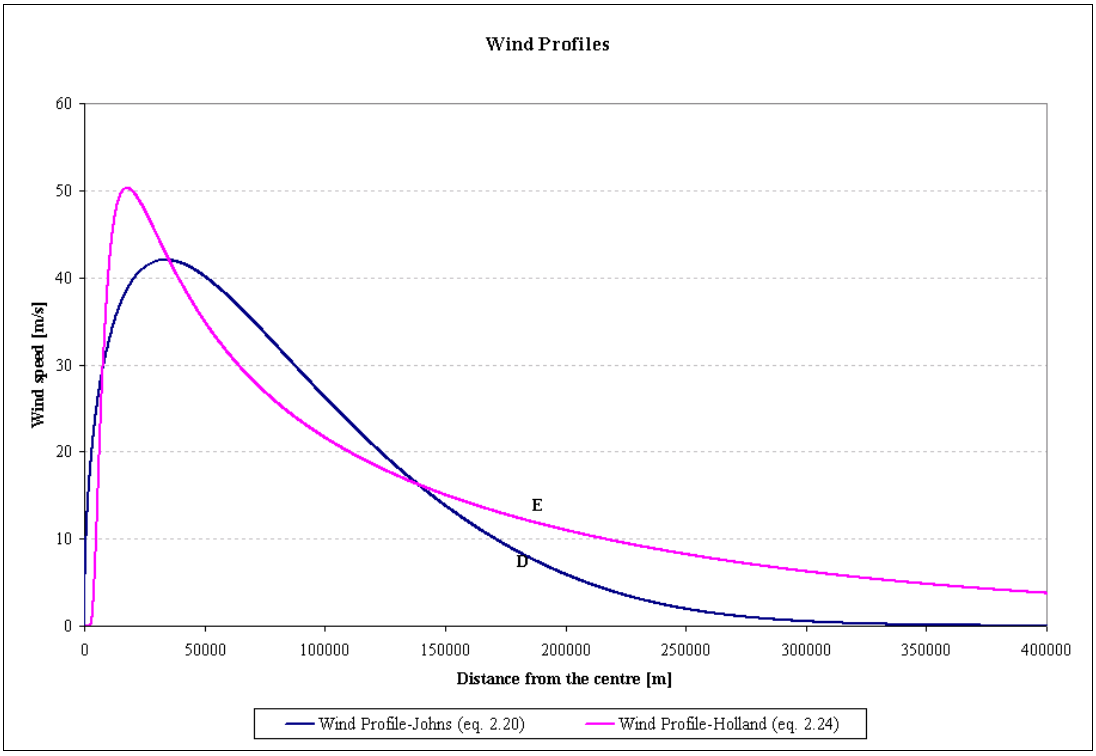

Figure 2-2: Radial distributions of gradient winds
Curve D: using equation (2-20) with pressure profile of equation (2-19)
Curve E: using equation (2-24) with A=900 km and B=1.4

In Figure 2-2 two mathematically described wind profiles are depicted.
Curve D is due to Johns and Curve E is due to Holland. Curve E describes the wind at distance better than Curve D and the maximum wind speed is also greater than the one of Curve D.

In addition to the analytical approaches for wind and pressure fields, empirical ones exist.

An empirical formulation for the wind was according to Murty et al. (1986) developed by Jelesnianski and used by Johns and Ali.

$$W_j = \begin{cases} W_m \left(r / r_0 \right)^{3/2} & \text{for } 0 \le r \le r_0 \\ W_m \left(r_0 / r \right)^{1/2} & \text{for } r \ge r_0 \end{cases} \tag{2-30}$$

It was used for a tropical cyclone in the Bay of Bengal but winds were overestimated over areas at large distance from the core. (See curve F in Figure 2-3).

Dube et al. proposed a new wind model for the Bay of Bengal (ibid.), because none of the formulae considered above provided satisfactory estimates of the actual wind fields.

$$W_D = \begin{cases} W_m \cdot e^{\frac{r - r_0}{\alpha}} & \text{for } 0 \le r \le r_0 \\ W_m \cdot e^{\frac{r_0 - r}{\beta}} & \text{for } r \ge r_0 \end{cases} \tag{2-31}$$

Later on a combination of W_D and W_j was proposed by Johns and a modified version of it too.

$$W_{DJ} = \begin{cases} W_m \left(r / r_0 \right)^{3/2} & \text{for } 0 \le r \le r_0 \\ W_m \cdot e^{\frac{r_0 - r}{\alpha}} & \text{for } r_0 < r \le r_1 \\ W_m \cdot e^{\frac{r_0 - r_1}{\alpha}} \cdot e^{\frac{r_1 - r}{\beta}} & \text{for } r > r_1 \end{cases} \tag{2-32}$$

in which r_1 denotes the distance from the centre of the cyclone from where the wind speed will reduce rapidly.
However, the far-field winds derived from (2-32) (curve H in Figure 2-3) are too weak to generate significant surges, so that the surge response is confined to a much shorter stretch of the coast than would otherwise have been the case (Murty et al., 1986).

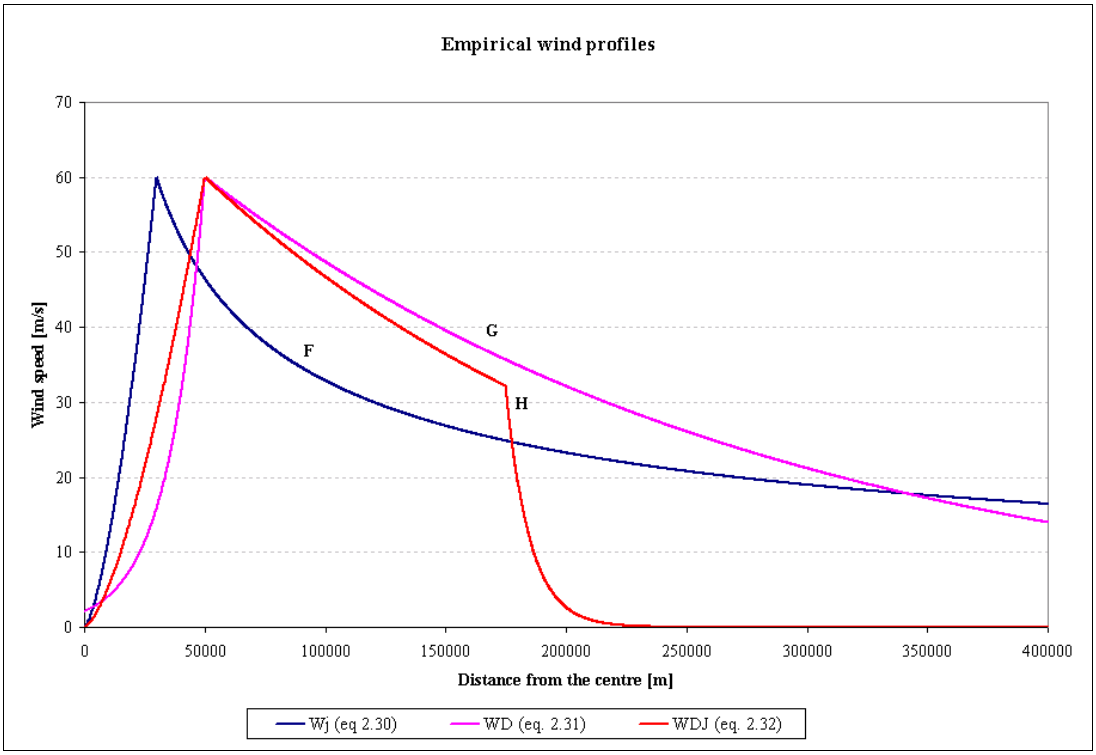

Figure 2-3: Radial distribution of gradient winds described by empirical formulae
Curve F: using equation (2-30) with r_0=30 km
Curve G: using equation (2-31) with α=15 km and β=240 km and W_m=60m/s
Curve H: using equation (2-32) with r_0=50 km, r_1=175 km and α,β
are 200 km and 10 km respectively.

In figure 2-3 three wind profiles are drawn. These profiles are derived from the empirical formulae for the Bay of Bengal. The horizontal and vertical axis are the distance to the centre in metres and the wind speed in m/s respectively.
Curve F and H start with a wind speed of 0 m/s at the core of the cyclone and increase to 60 m/s at 30 km and 50 km from the centre respectively. Then they decrease slowly, whereby Curve H decreases rapidly to 0 m/s after 175 km distance from the centre of the cyclone, whereas Curve F at 400 km still has a value of 18 m/s. Curve G starts at 2 m/s at the centre and increases to 60 m/s at 50 km from the core. Hereafter it slowly decreases, but it still has a value of 16 m/s at 400 km from the core.

For tropical cyclones it is unrealistic to have the maximum wind speed at a distance more than 50 km away from the core. Moreover a significant wind speed should be retained over a large distance. According to Murty et al. (1986), the part of the wind field which is most effective in surge generation depends on the ratio between the radius of maximum wind speed and the shelf width, r_0/L. If this ratio is about 1 then the strongest winds are most significant. If this ratio is small then the strongest winds will act effectively only over a small area of the shelf, and weaker winds beyond the core acting over a larger area and longer fetch will be more effective.
Although the wind profiles in Figure 2-2 are physically more realistic than the profiles of figure 2-3, because they have no discontinuities, it is hard to say which profile leads to the best computed results. A profile choice will presumably depend on model tests whereafter observed and computed surges can be compared. The wind profile, which leads to the best-computed results, is probably area-dependent.

Next to the wind profile, there is another parameter, the wind stress that is important for computing storm surges. This parameter will be the subject of the next paragraph.

2.4 Wind Stress and atmospheric pressure gradient forces

The main forcing functions for the generation of storm surges are the wind stress on the water surface and the atmospheric pressure gradient forces, whereas bottom stress is the main retarding force. Since the ocean surface is not rigid, kinetic energy can be transferred from the atmosphere to the ocean by tangential stresses, which produce accelerations parallel to the surface, and by normal pressure forces.
Friction at the air-water interface is not large enough to account for the energy of wind-driven ocean currents and for exciting inertial oscillations. Thus, momentum and energy must be transferred from the wind to the ocean by processes other than viscous shear at the interface. Predominantly, short-period wind waves provide such a mechanism (Murty, 1984).

In paragraph 2.3 two different formulations for the dependence of the shear stress to the wind speed were already mentioned (eq. (2-6) and (2-14)/(2-15)). Both formulations use the wind speed at 10 metres above the sea surface. Comparing both formulations by focussing on the factor which the wind speed is multiplied with, the following figure is the result:

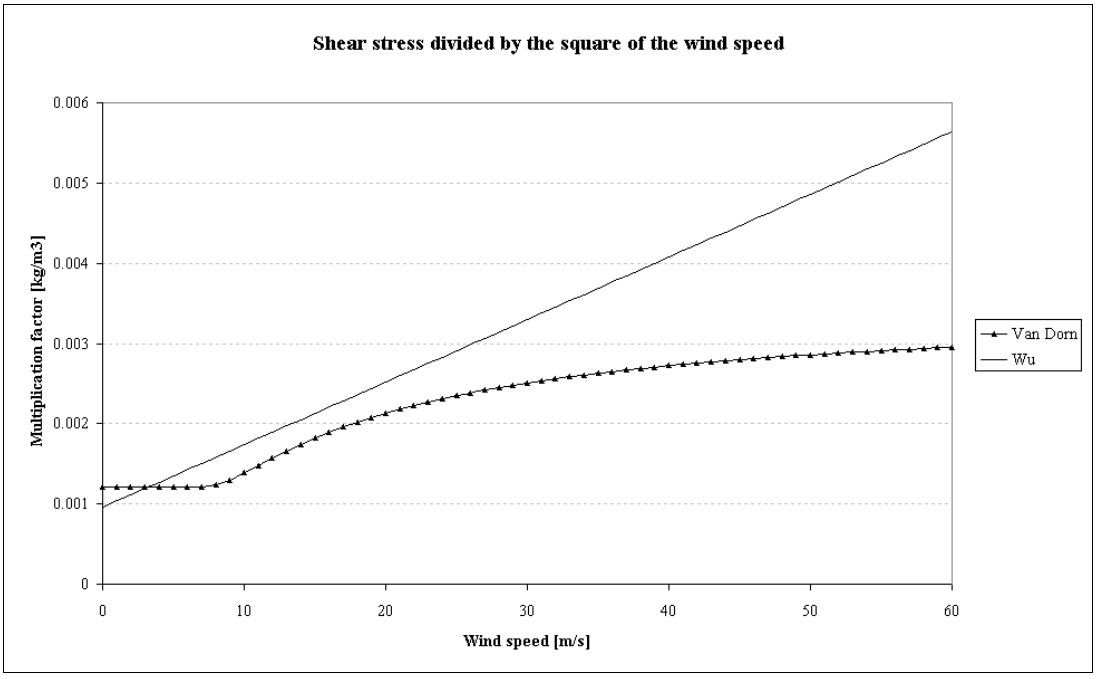

Figure 2-4: Multiplying factor of the wind speed in the dependence relations of Wu and Van Dorn

So in Figure 2-4, the parameters $\rho_a C_D$ and $\rho_w k$, in which C_D is according to the formulation of Wu and k is according to Van Dorn (1953), are drawn. The formulation of Van Dorn gives lower values than the formulation of Wu. Wu relates his drag coefficient just to the wind speed and Van Dorn uses a formulation in where a critical wind speed of 7 m/s is defined. This implies that for lower wind speed values a constant factor is used in the formulation and for larger wind speed values, this constant factor plus a factor related to the ratio of the critical wind speed to the actual wind speed.
Van Dorn (1953) distinguishes two kinds of water surface states and relates the wind stress to both states. Van Dorn defines the water surface as smooth for wind speed values less than

a certain 'critical' wind speed value. Above this specified value the water surface is called rough. The wind stress for a smooth water surface is therefore just determined by a 'friction' drag which is proportional to the square of the wind speed, but for a rough surface an additional 'form' drag is added to the wind. This second kind of drag is related to the surface waves. In Figure 2-4, it is seen that the drag does hardly increase for storm conditions. This means that although larger winds generate higher waves they do not increase the roughness of the sea state, which is the case in the formulation of Wu as can be seen in the same figure.

In Figure 2-5 the wind shear stress is plotted. For wind speed values less than 25 m/s, the two formulations do not differ that much, but for larger values this difference increases quite fast.

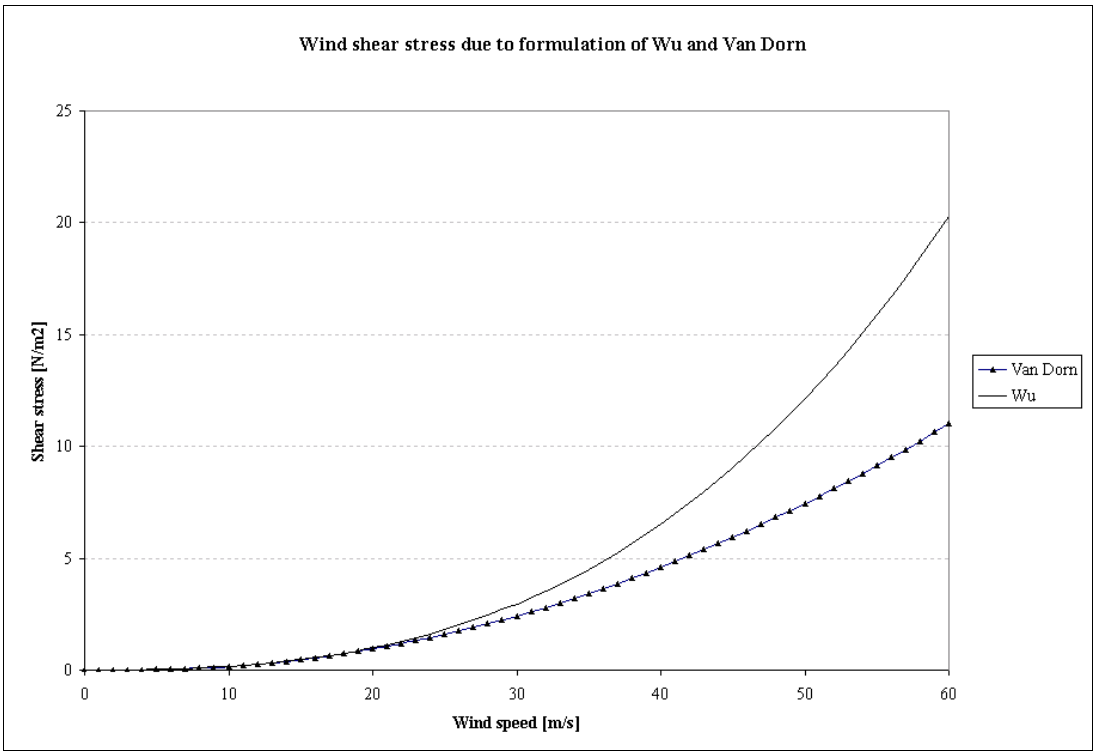

Figure 2-5: Dependence of the wind shear stress on the wind speed according the formulations of Wu and Van Dorn

The wind shear stress which is most effective in shallow water, as can be seen in the momentum equations (eq. (2-1), (2-2)) is thus under storm conditions very significant in the storm surge. Correct drag relations are thus of very importance in determining the surge.

In the next paragraph, which is mainly a selection of Murty (1984), several types of relations are discussed.
In the past, the wind-drag coefficient was a function of wind speed only and the actual sea state was not explicitly taken into account.

According to Murty, Taylor was one of the first and suggested for the wind stress:

$$\tau = \rho_a \gamma^2 w^2 \qquad (2\text{-}33)$$

In which γ^2 was equal to 2.6 x 10^{-3} according to Rossby and ρ_a is the density of air. w is the wind speed at 15 m above the sea surface.

Stewart considered the question of transfer of momentum from the atmosphere to the water and stated that a very large fraction of the momentum transfer is in the form of wave generation. Baines showed that when the wind wave spectrum in shallow water is approximately independent of wind speed due to the combined effects of white capping and bottom friction, then the wave-induced drag coefficient has a maximum value when the wind speed is twice the maximum wave speed, and as the wind speed increases further, the drag coefficient slowly decreases.

Charnock proposed a relation between the roughness length (z_0) and the friction velocity over the water surface (u_*). Charnock's formula represents the surface roughness near full development when most of the stress is supported by short gravity waves. The formula does not contain any wave parameters and therefore corresponds to a classical wind speed – drag coefficient relation. A constant α in the relation compensate the missing sea state (Van den Boogaard et al., 1991).

Simons made the important point that numerical models for hindcasting storm surges usually require drag coefficients (for wind stress) as high as 3 x 10^{-3} whereas observations appear to indicate a value about half of this. Donelan resolved this problem by suggesting that the form stress (due to wave drag) is large if the sea state is not in equilibrium with the wind (i.e. during the initial stages of a storm when the waves are developing). However, once the wave field has adjusted to the wind, the drag coefficient decreases.

The stress produced by wind blowing over a water body consists partly of skin friction and partly form drag. Taylor and Gent showed the dependence of the drag coefficient on certain wave parameters such as steepness and wave age. Donelan showed through observational data that the drag coefficient is dependent on inverse wave age and wave height and can be approximated well by a simple model involving the form drag τ_f and the skin drag τ_s.

Of the form drag τ_f, a portion τ_w adds or subtracts momentum directly from the gravity wave spectrum. The remaining part τ_c generates changes in the currents. Of the momentum flux τ_w, a portion τ_η produces a net growth or decay of the wave momentum. The remaining part τ_d is lost from the wave field by viscous dissipation and whitecapping. Hence, the total drag τ between air and water is:

$$\tau = \tau_s + \tau_\eta + \tau_d + \tau_c \tag{2-34}$$

where

$$\tau_w \equiv \tau_\eta + \tau_d \tag{2-35}$$

and

$$\tau_f \equiv \tau_w + \tau_c \tag{2-36}$$

The problem here is to determine the wave field and wind stress, given the wind at a 10 metres height. For predicting the wave field, τ_η must be known and for the determination of the wind stress, τ - τ_η must be known. Donelan stated 'to the hydrodynamic modeller, to whom wind waves are a sub-grid scale process, the appropriate wind stress is not the total τ, but the total less that which is carried away by the waves τ_η. If, as we believe, the waves significantly affect the drag coefficient and the local surface stress is depleted by the growth

and advection of the wave field, then the prediction of the surface stress depends rather critically on a knowledge of the wave field.'(Murty, 1984)

Wind Stress and Drag Coefficients

It is well known that wind stress depends on the stability of the atmospheric surface layer. In earlier observations of drag coefficients, little attention was paid to atmospheric stability conditions. Wu summarised the wind stress coefficients over the sea surface for neutral conditions. He presented a scaling law for wind stress coefficients; the coefficient increases with wind velocity and decreases with fetch.

Smith considered the question of wind stress over the ocean for strong winds (i.e. gale force). He also showed that the drag coefficient increases gradually with increasing wind speed.

Plate and Wengefeld used a similar approach as Donelan, but wrote the equations somewhat differently. The work done by the air on the water is divided into two parts: one part produces the energy change of the mean water motion and the other part maintains the wave pattern. The energy balance equation for the first part can be written as

$$\frac{dE_w}{dt} = \frac{dE_{k_w}}{dt} + \frac{dE_{p_w}}{dt} - D_w + \frac{dW_w}{dt} = 0 \qquad (2\text{-}37)$$

where the subscript 'w' refers to water, E_k, E_p and E are the means of the kinetic, potential, and total energies, respectively, W_w is the work done on the water body, and D_w is the mean energy dissipation inside the water column.

The second part that maintains the waves against energy loss due to radiation and dissipation can be written as

$$\frac{dE_0}{dt} = \frac{dE_{k_0}}{dt} + \frac{dE_{p_0}}{dt} - D_0 + \frac{dW_0}{dt} = 0 \qquad (2\text{-}38)$$

where subscript 0 stands for the wave field and W_0 is the work done to maintain the wave field. The total work done by the air on the water surface is $W_w + W_0$. However, it is not clear how this partitioning can be specified. Under the assumptions that the mean flow does not vary in x, the flux of vertical momentum at a height δ is constant and is equal to τ_∞. Closer to the surface, a part of the momentum flux is transferred downward through shear stresses, which gives rise to a surface shear stress δ_D. The remaining part τ_∞ is converted into a pressure pattern and this creates a form drag given by an average stress τ_F (Murty, 1984).

A literature survey to the dependence of surface drag on waves was carried out by Van den Boogaard et al. (1991). They investigated whether and how for storm conditions numerical models could improve by using a wave dependent drag coefficient instead of the 'traditional' form in which only wind speed is incorporated. They pointed out that C_d formulae could be divided into two classes, one class that uses the complete spectral density and one class that uses just a few wave parameters. This latter was therefore more an empirical description for the surface drag. Here, the so-called wave age, which is the ratio of the phase velocity of the dominant wave and the friction velocity, is the key parameter for the surface roughness. They concluded that inclusion of wave information in the drag coefficient should improve the storm surge predictions, which was verified with their Continental Shelf Model.

Later on, in Chapter 4, the drag coefficient and its influence on wind and waves will be examined in the experiments.

2.5 Description of existing Cyclone models

Cyclone models have been developed and improved all over the years. These models contain the hydrodynamic equations, the wind and pressure fields of cyclones and the wind stress parameters, all discussed before. Some of these models are general and can therefore be used at different locations. Others are just made for the location of interest. Here some of these models are described.

2.5.1 SLOSH

Jelesnianski (1992) developed the models SPLASH (Special Program to List Amplitudes of Surges from Hurricanes) and SLOSH (Sea, Lake and Overland Surges from Hurricanes) for predicting storm surges due to hurricanes. The latter was an extended version of SPLASH and was developed for real-time forecasting of hurricane storm surges. It permitted overtopping of barriers, channel flow and flow through barrier cuts.

A continuously varying polar grid system was chosen for the SLOSH model. The equations of momentum do not include advective terms and are depth-averaged. The equations were derived from the so-called Ekman equations in a rotating frame of reference:

$$\frac{\partial u}{\partial t} = -g\frac{\partial \zeta}{\partial x} + fv + \frac{\partial}{\partial z'}\left(\nu \frac{\partial u}{\partial z'}\right) \tag{2-39}$$

$$\frac{\partial v}{\partial t} = -g\frac{\partial \zeta}{\partial y} - fu + \frac{\partial}{\partial z'}\left(\nu \frac{\partial v}{\partial z'}\right) \tag{2-40}$$

$$\frac{\partial \zeta}{\partial t} = -\frac{\partial M}{\partial x} - \frac{\partial N}{\partial y} \tag{2-41}$$

where $$(M, N) \equiv \int_{-D}^{\zeta} (u, v) dz'$$

These momentum equations are then transformed into complex form following Welander

$$\frac{\partial W}{\partial t'} = q - ifW + \nu \frac{\partial^2 W}{\partial z'^2} \tag{2-42}$$

in where:

$$W = (u + iv)D$$

and

$$q = -g\left[\frac{\partial(\eta-\eta_0)}{\partial x} + i\frac{\partial(\eta-\eta_0)}{\partial y}\right]$$

In (Jelesnianski et al, 1992) the full derivation can be found. In here, it is shown that depth-dependent parameters were introduced and after some more assumptions were taken into account this set of momentum equations was, on a Cartesian frame of Reference, rewritten into:

$$\frac{\partial M}{\partial t} = -g(D+\zeta)\left[B_r\frac{\partial(\zeta-\zeta_0)}{\partial x} - B_i\frac{\partial(\zeta-\zeta_0)}{\partial y}\right] + f(A_rN + A_iM) + C_r\frac{\tau_{sx}}{\rho} - C_i\frac{\tau_{sy}}{\rho} \quad (2\text{-}43)$$

$$\frac{\partial N}{\partial t} = -g(D+\zeta)\left[B_r\frac{\partial(\zeta-\zeta_0)}{\partial y} - B_i\frac{\partial(\zeta-\zeta_0)}{\partial x}\right] - f(A_rM - A_iN) + C_r\frac{\tau_{sy}}{\rho} + C_i\frac{\tau_{sx}}{\rho} \quad (2\text{-}44)$$

$$\frac{\partial\zeta}{\partial t} = -\frac{\partial M}{\partial x} - \frac{\partial N}{\partial y} \quad (2\text{-}45)$$

where

t	= time	[s]
ζ	= elevation of the sea surface	[m]
ζ_0	= hydrostatic water height	[m]
M,N	= components of depth-averaged mass transport	[m^2/s]
D	= depth to horizontal reference plane	[m]
f	= Coriolis parameter	[1/s]
g	= gravitational constant	[m/s^2]
ρ	= water density	[kg/m^3]
τ_{sx}, τ_{sy}	= components of surface stress	[N/m^2]
$A_r,..,C_I$	= depth dependent bottom stress coefficients	[-]

These equations are now linear with the variable coefficients, which are real and imaginary functions of the total depth. They are ascertained empirically and therefore not physically justifiable.

The SLOSH model incorporates finite amplitude effects and uses time-history bottom stress, corrected for finite amplitude affects. Classical bottom-stress formulations are not used, instead, 'Ekman' formulations are used with invariant eddy viscosity and slip coefficients for all storms and in all regions. If a fast-moving storm landfalls or moves alongshore, and if waters just offshore are deep or intermediate in depth, then a surge model need not include bottom stress to compute peak coastal surges associated with the storm. In some cases, however, after passage of an alongshore-moving storm, secondary, or free, waves are generated. These waves are trapped between the nearshore region and the coast, and are sensitive to bottom stress.

In SLOSH, the short-term action from wind-waves is absent but crude approximations for the long-term effects are present.

For SPLASH and SLOSH a constant drag coefficient has been used, even though it may be a function of storm, storm track, basin terrain, basin geometry, wind speed, etc.

The wind model in SLOSH computes pressure and wind inflow direction for a stationary, circularly symmetric storm. The computations are based on a balance of forces given by

$$\frac{1}{\rho_a}\frac{dp}{dr} = \frac{k_s w^2}{\sin\phi} - w\frac{dw}{dr} \tag{2-46}$$

$$\frac{1}{\rho_a}\frac{dp}{dr}\cos\phi = fw + \frac{w^2}{r}\cos\phi - w^2\frac{d\phi}{dr}\sin\phi + k_n w \tag{2-47}$$

Here, r is the distance from the storm centre, p(r) is the pressure, ϕ(r) the inflow angle across circular isobars toward the storm centre, and w(r) is the wind speed. The terms k_s and k_n are empirically determined coefficients, and f is the Coriolis parameter. The two equations can be solved for p and ϕ, on a ray from the storm centre, if the form of the wind speed profile w(r) is supplied, as in

$$w(r) = w_R\frac{2Rr}{R^2 + r^2} \tag{2-48}$$

The parameter R is the radius of maximum wind in miles and w_R is the maximum wind speed in mph.
The storm friction coefficients are arbitrarily pre-set as

$$k_s = 1.15k_n = \alpha\sqrt{\frac{10^{-4}R}{0.3\cdot w_R + 60}} \tag{2-49}$$

α=1 for ocean winds.

For lake winds

$$\alpha = 4\sqrt{22/R} \tag{2-50}$$

is taken.

k_s = coefficient of wind friction in the tangential direction
k_n = coefficient of wind friction in the radial direction

The storm surge model has an overall accuracy of ± 20% in the prediction of surge levels, only when hurricanes are well described.

2.5.2 Special applications

SPLASH and SLOSH are models, originally developed for general storm surges due to hurricanes and were not typically made for special areas. Several models were, however, just developed for typical bays.

Das' extended model for example included the non-linear advective terms and he showed that inclusion of the tide-surge interaction advanced the time of arrival of the peak surge by two hours (see Murty et al., 1986).

Johns' model was based on equations (2-19) and (2-20), described earlier, and applied to the Bay of Bengal. An idealised tidal oscillation was introduced on the southern boundary of the model. He used an analysis area large enough to allow the recording of 3 days surge-generating capacity of a cyclone before landfall at the Bangladesh coastline. They concluded that the surge development depends critically on the diameter and track of the cyclone, that tide-surge interaction is important in shallow water regions, suggesting the necessity of using a non-linear model for the northern part of the Bay of Bengal; and that the surge can penetrate deep inland causing a flood hazard along the river systems (Johns et al., 1980).

Models with symmetric and asymmetric storms have been developed too. The surge magnitudes were substantially different, demonstrating that it is essential to specify surface wind as accurately as possible. Tide-surge interaction was also examined. A fully three-dimensional spectral model was also established and surge computations carried out to determine the influence of three-dimensionality. Surge responses were similar, elevations from the three-dimensional model being up to 10% higher than the equivalent from the depth-averaged model (Murty et al., 1986).

Dekker (1995) developed a storm surge model application for the Enore Coal Port in India. He calculated the wind set-up assuming the water surface has such a slope that the hydrostatic forces are in equilibrium with the wind friction forces. The approach contained several uncertainties. In the computation the bottom friction was neglected. Taking this factor into account would lead to a higher wind set-up, because the current at the bottom is seaward and thus the bottom friction leads to a shore directed force on a column of water.

For the barometric pressure difference, $S_{\Delta p}$, Dekker used an expression from Bretschneider to estimate the effect

$$S_{\Delta p} = 0.01\left(p_n - p_0\right)\left(1 - e^{-\frac{R}{r}}\right) \tag{2-51}$$

where p_n is the pressure at the periphery of the storm, p_0 the central pressure in millibar, r the radial distance from the storm centre to the prediction point on the traverse line and R the distance from the storm centre to the point where the region of maximum winds intersect the shoreline.

Flather (1993) developed a numerical cyclone surge model that allowed to simulate the complex network of linked channels that makes up the Ganges Delta. His formulation allowed the delta to be included in a more complete and realistic manner than hitherto. This was achieved by a modification of the standard depth-averaged storm surge equations to allow them to represent either one-dimensional flow, as in a channel, or two-dimensional flow, as in the open sea.

He included advection, the rotation of the earth, and several variations within the model of surface atmospheric pressure.

The scheme he used, makes use of an analytical model for the surface pressure and wind field distribution in a tropical cyclone. The formulation is due to Holland (1980), with data on cyclone position, maximum wind speed, radius to maximum winds, and central pressure provided by the Joint Typhoon Warning Center. Cyclone evolution is taken into account and arbitrary tracks and cyclone motion are allowed.

The atmospheric forces, which generate storm surges, are thus wind stress and horizontal gradients of surface atmospheric pressure.

The empirical relation

$$W_m = 6.7\left(p_\infty - p_c\right)^{0.66} \tag{2-52}$$

was used to estimate the central pressure, p_c (hPa), of the cyclone from the maximum wind speed, W_m given in knots. The ambient pressure, p_∞, was taken as 1010 hPa. The numbers 6.7 and 0.66 here are fitting parameters, in which the first one must have a dimension.

2.6 Conclusion for further research

This literature review has given an overview of the aspects, which are or can be taken into account in cyclone models. In none of the models, wind-waves are included. They all include the hydrodynamic equations without wind-wave terms and some of them simplify the equations by neglecting the advective terms. All of the models are depth-averaged.

The next chapters will deal with incorporating waves in the model. First, on a simplified basis, the impact of wave-induced set-up will be investigated. Later on, in Delft3D, a more sophisticated wave model will be implemented into the existing cyclone surge model, which is already in use for the Andhra Pradesh (India).

3 Modelling in Delft3D

3.1 Introduction

Delft3D is an integrated modelling system with several modules. It is able to compute several situations in coastal, river and estuarine areas. The two modules used for calculating water levels, flow and wind waves are Delft3D-Flow and -Wave. These modules are able to interact with each other. Delft3D-Flow simulates non-steady flow and transport phenomena that result from tidal and meteorological forcing on a grid. Delft3D-Wave contains two wave models that can calculate the wave phenomena. The HISWA wave model (HIndcast Shallow WAter waves) is the standard option and is used for the experiments, which will be discussed in Chapter 4. It is a second-generation wave model and developed for stationary simulations. The SWAN wave model (Simulating WAves Nearshore) is a third generation model which has been incorporated within Delft3D and although the SWAN wave model is able to simulate non-stationary model runs, at present only stationary simulations, like in HISWA, can be made with Delft3D-Wave.

In the next paragraphs, an outline will be given of the most important features of these two modules, Flow and Wave, in Delft3D. First the Flow module is described, then the Wave module and finally the interaction between the two modules. In appendix A, more details can be found on Delft3D-Flow and -Wave and their interaction.

3.2 Delft3D-Flow

Delft3D-Flow solves the unsteady shallow water equations in two (depth-averaged) or in three dimensions. The system of equations comprises the horizontal equations of motion, the continuity equation and the transport equations for conservative constituents. These equations are formulated in orthogonal curvilinear co-ordinates or in spherical co-ordinates on the globe within Delft3D. The flow can be forced by tide at the open boundaries, wind stress at the free surface, pressure gradients due to free surface gradients or density gradients (barotropic and baroclinic flow). The discharge and withdrawal of water can be included in the equations as well.

3.2.1 Hydrodynamic equations

Delft3D-Flow solves the shallow water equations, under the Boussinesq assumption. This set of partial differential equations in combination with an appropriate set of initial and boundary conditions is solved on a finite difference grid. The depth-averaged equations are already discussed in paragraph 1.2, although in comparison with Delft3D, some terms were neglected there. The three-dimensional hydrodynamic equations used in Delft3D are defined as:

$$\frac{\partial u}{\partial t}+u\frac{\partial u}{\partial x}+v\frac{\partial u}{\partial y}+\frac{\omega}{D+\zeta}\frac{\partial u}{\partial \sigma}-fv=\frac{P_x}{\rho_0}+F_x+\frac{1}{(D+\zeta)^2}\frac{\partial}{\partial \sigma}\left(\nu_v\frac{\partial u}{\partial \sigma}\right)+M_x \qquad (3\text{-}1)$$

$$\frac{\partial v}{\partial t}+u\frac{\partial v}{\partial x}+v\frac{\partial v}{\partial y}+\frac{\omega}{D+\zeta}\frac{\partial v}{\partial \sigma}+fu=\frac{P_y}{\rho_0}+F_y+\frac{1}{(D+\zeta)^2}\frac{\partial}{\partial \sigma}\left(\nu_v\frac{\partial v}{\partial \sigma}\right)+M_y \qquad (3\text{-}2)$$

$$\frac{\partial \zeta}{\partial t}+\frac{\partial[(D+\zeta)u]}{\partial x}+\frac{\partial[(D+\zeta)v]}{\partial y}+\frac{\partial \omega}{\partial \sigma}=h\cdot(q_{in}-q_{out}) \qquad (3\text{-}3)$$

where:

u,v	= velocity in x,y-directions	[m/s]
x,y	= horizontal spatial co-ordinates	[m]
t	= time co-ordinate	[s]
f	= Coriolis coefficient	[1/s]
ω	= velocity in the σ -direction in the σ co-ordinate system	[m/s]
σ	= scaled vertical co-ordinate	[-]
ρ_0	= reference density of water	[kg/m^3]
P_x , P_y	= gradient hydrostatic pressure in x-,y-direction	[kg/m^2/s^2]
F_x , F_y	= turbulent momentum flux in x-,y-direction	[m/s^2]
D	= depth to horizontal reference plane	[m]
ζ	= water level above reference	[m]
ν_v	= vertical eddy viscosity	[m^2/s]
M_x , M_y	= source or sink of momentum in x-, y-direction respectively	[m/s^2]
q_{in}, q_{out}	= local source, sink per unit volume	[1/s]

Density variations are neglected, except in the baroclinic pressure terms, which are represented by the pressure gradients P_x and P_y. The forces F_x and F_y in the momentum equations represent the unbalance of horizontal Reynold's stresses. M_x and M_y represent the contributions due to external sources or sinks of momentum, for example by hydraulic structures and wave stresses, or tide generating forces as internal body forces.

At the surface the effect of precipitation and evaporation is taken into account by the terms q_{in} and q_{out}.

The σ-coordinate used in the vertical direction is a scaled co-ordinate and is defined as

$$\sigma=\frac{z-\zeta}{D+\zeta}=\frac{z-\zeta}{h} \qquad (3\text{-}4)$$

where:

h	= total water depth	[m]
z	= reference level in the vertical with z=0 at the top of the undisturbed depth	[m]

At the bottom σ = -1 and at the free surface σ = 0. So the σ-co-ordinate system is boundary fitted both to the bottom and to the moving free surface.
The vertical velocity ω is defined at the iso σ-surfaces. ω is the vertical velocity relative to the moving σ-plane. It may be interpreted as the velocity associated with up- or downwelling motions.

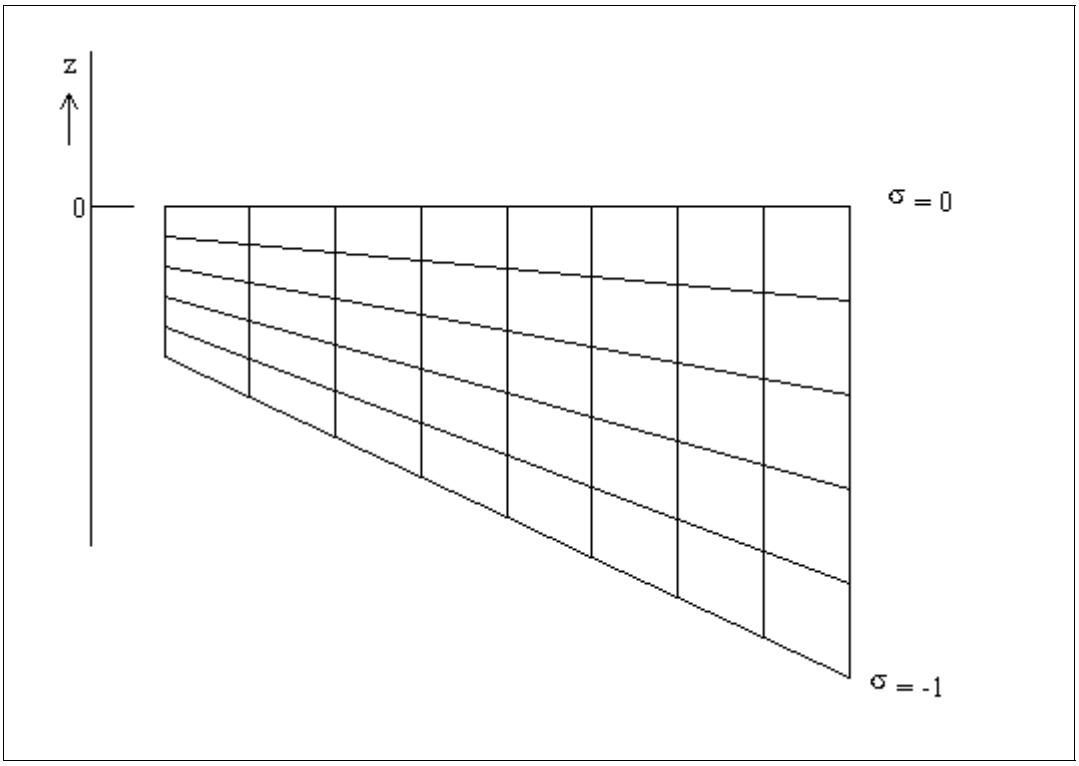

Figure 3-1: Example of σ-grid

3.2.2 The staggered grid

In Delft3D-Flow, a staggered grid is applied, which means that not all quantities are defined at the same location in the numerical grid.

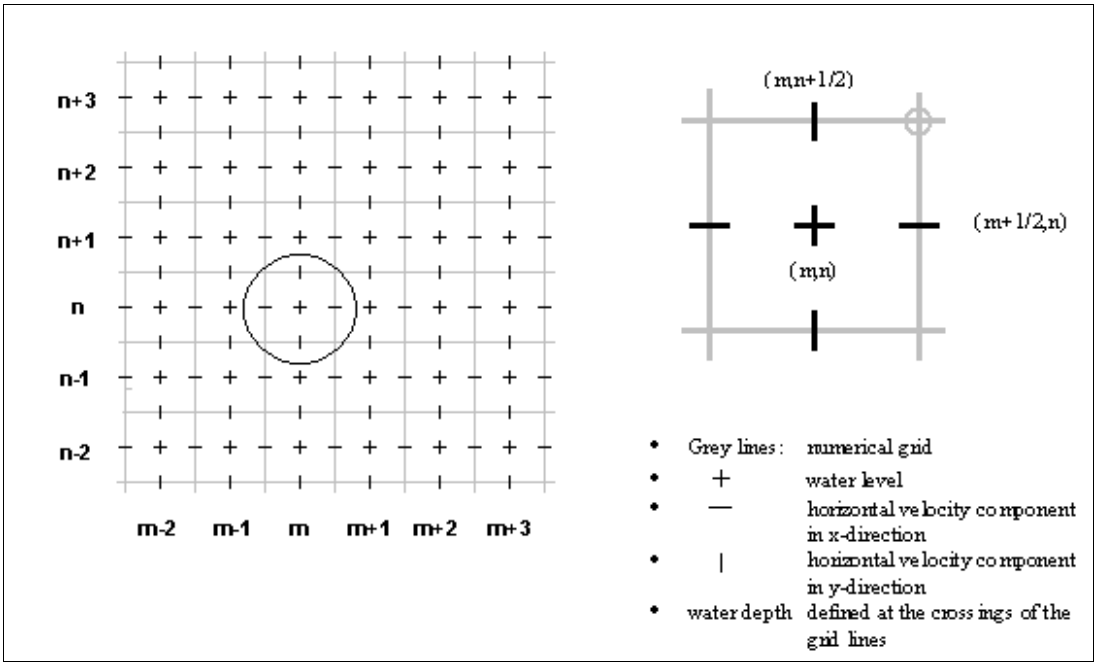

Figure 3-2: The staggered grid

In Figure 3-2 , the staggered grid of Delft3D-Flow is depicted. This grid is, because of its particular arrangement of the variables called the Arakawa C-grid. The water level points are defined in the centre of a cell. The velocity components are perpendicular to the grid cell faces, where they are situated. The depth is defined in the right top corner of the grid cell. Together with the water level at (m,n) and the u- and v-velocities at respectively (m+1/2,n) and (m,n+1/2), these 4 parameters use the same grid co-ordinates in the equations, (m,n).

3.2.3 Boundary conditions

Most applications concern a limited area only. Fictitious boundaries are defined to separate the waterbody that is being modelled from the remainder of the world 's oceans. Then, for solving the 3D and 2D depth-averaged shallow water equations, a set of initial and boundary conditions for water levels and horizontal velocities must be specified. There are two types of boundaries, closed boundaries, which are the land-water lines and open boundaries, which are artificial and are introduced to restrict the computational area and so the computational time. In Appendix A, these boundary conditions are outlined.

3.2.4 Turbulence

Delft3D-Flow solves the shallow water equations for an incompressible fluid, see eqs. (3-1)-(3-3) in discretised form on a computational grid. Usually the grid (horizontal and/or vertical) is too coarse and the time step too large to resolve the turbulent scales of motion. The primitive variables are space- and time-averaged quantities. This leads to the need of appropriate closure assumptions.

In Delft3D-Flow, four turbulence closure models have been implemented to determine the vertical viscosity coefficient, ν_v, and the eddy diffusivity coefficient, D_v. These models can only be chosen in three-dimensional model runs and not in depth-averaged model runs.

The first one is the simplest closure model based on a constant value. The constant eddy viscosity will lead to parabolic vertical velocity profiles, which is correct for laminar flow. The other three turbulence closure models are based on the so-called eddy viscosity concept of Kolmogorov and Prandtl.

The turbulence closure models differ in their prescription of the turbulent kinetic energy, k, the dissipation rate of turbulent kinetic energy, ε, and/or the mixing length, L.

The algebraic eddy viscosity model (AEM) does not involve transport equations for the turbulent quantities. This so-called zero order closure scheme is a combination of two algebraic formulations. This model uses analytical (algebraic) formulae to determine k and L.

The third closure model for the eddy viscosity involves one transport equation for k and is called a first order turbulence closure scheme. The mixing length L is prescribed analytically and the same formulation is used as for the AEM turbulence model. However, to find the kinetic energy k, a transport equation is solved. This turbulence closure model is known as the k-L model.

The fourth model is the k-ε model, which is a second order turbulence closure model. In this model both the turbulence energy k and dissipation rate of turbulent kinetic energy ε are calculated by a transport equation. From k and ε, the mixing length L and viscosity ν_V are determined. The mixing length is now a property of the flow, and in the case of stratification no damping functions are needed.

For the combination of flow and waves, the effect of the orbital velocities on the production of turbulence is modelled indirectly by the enhancement of the bed roughness. The shear production is determined only from the wave-averaged velocities.

A more detailed description of the algebraic turbulence model, a combination of Algebraic Closure Model and Prandtl's Mixing Length model, the k-L Turbulence Model and the k-ε Turbulence Model can be found in Appendix A.

3.3 Delft3D-Wave

Delft3d-Wave can be used for simulating the evolution of wind-generated waves in coastal waters. The module computes for a given bottom topography, stationary wind field, water level and current field in waters from deep till finite depth:

- wave propagation
- wave generation by wind
- depth and current induced shoaling

- non-linear wave-wave interactions and dissipation due to depth-induced breaking or bottom friction
- wave refraction over a bottom of variable depth and/or a spatially varying ambient current
- wave blocking by strong counter currents (in HISWA)

The HISWA (Booij and Holthuijsen, 1995) and SWAN (Holthuijsen et al., 2000) models are based on the spectral action balance equation and the wave propagation is based on linear wave theory. The wave computations are carried out on a rectangular grid. Non-stationary situations are simulated as quasi stationary with repeated model runs within the HISWA model. Wave computations are performed at specified, intermediate time levels. SWAN can deal with non-stationary winds, but within Delft3D-Wave, this feature is not implemented.

3.3.1 Physical Background

Action/Energy Balance
HISWA and SWAN are based on a spectral action balance. Wave propagation is determined across the grid according to the Eulerian approach. This means that wave information is available at the mesh points of the rectangular grid.

The action density A is defined as:

$$N(t,x,y,\theta,\omega) = \frac{E(t,x,y,\theta,\omega)}{\sigma} \tag{3-5}$$

where :

N	= wave action density	[Js/m^2]
x,y	= co-ordinates in propagation and wave crest direction	[m]
t	= time	[s]
E	= wave energy density	[J/m^2]
ω	= wave frequency	[1/s]
θ	= spectral direction	[°]
σ	= relative frequency of wave and current	[1/s]

$$\sigma = \omega - k \cdot U_c \tag{3-6}$$

where:

k	= wave number	[1/m]
U_c	= Current velocity vector	[m/s]

The action balance equation is written as

$$\frac{\partial N}{\partial t} + \frac{\partial (c_x N)}{\partial x} + \frac{\partial (c_y N)}{\partial y} + \frac{\partial (c_\theta N)}{\partial \theta} + \frac{\partial (c_\omega N)}{\partial \omega} = \frac{S}{\sigma} \tag{3-7}$$

where

c_x, c_y = wave group velocity in x,y direction [m/s]

c_θ, c_ω = wave group velocity in θ, ω direction [m/s]

S = sum total of all processes that generate or dissipate wave action [Js/m^2]

The first term in this equation represents the local rate of change of action density. The other terms on the left-hand side represent the net transport of action in the x-, y-, θ-, and ω-domain respectively. The total effect of generation and dissipation of action is represented by the source term S.

In HISWA a simplified form of the spectral action balance is used. The model was developed for stationary situations and the time dependent parameters can therefore be left out of the action balance. The second simplification comprises the parameterisation of the frequencies in the spectral action balance. Two quantities propagate in each spectral direction, a frequency-integrated energy density, $A_0(\theta)$, and a mean frequency, $\omega_0(\theta)$. These quantities vary across the geographic area. They can be defined as:

$$A_0(\theta) = m_0(\theta) \tag{3-8}$$

$$\omega_0(\theta) = \frac{m_1(\theta)}{m_0(\theta)} \tag{3-9}$$

where:

$A_0(\theta)$ = one-dimensional directional action spectrum [J/m^2]

$\omega_0(\theta)$ = mean frequency directional action spectrum [1/s]

$m_0(\theta)$ = zeroth order moment of the action density spectrum [J/m^2]

$m_1(\theta)$ = first order moment of the action density spectrum [J/sm^2]

The moments $m_n(\theta)$ of the action density spectrum are defined as:

$$m_n(\theta) = \int_0^\infty \omega^n A(\omega,\theta)\, d\omega \tag{3-10}$$

When the zeroth and first order moments of the action density spectrum are used, the following two evolution equations are obtained from the spectral action balance:

$$\frac{\partial}{\partial x}\left(c_x^* A_0\right) + \frac{\partial}{\partial y}\left(c_y^* A_0\right) + \frac{\partial}{\partial \theta}\left(c_\theta^* A_0\right) = T_0 \tag{3-11}$$

and

$$\frac{\partial}{\partial x}\left(c_x^{**} A_1\right) + \frac{\partial}{\partial y}\left(c_y^{**} A_1\right) + \frac{\partial}{\partial \theta}\left(c_\theta^{**} A_1\right) = T_1 \tag{3-12}$$

The propagation speed of the waves are represented as $c_x^*, c_y^*, c_\theta^*, c_x^{**}, c_y^{**}, c_\theta^{**}$ where the subscripts *x, y* and θ stand for the spatial directions and where the superscripts * and ** stand for the frequency integrated spectral direction and for the mean frequency respectively. The propagation speeds in x- and y-direction represent rectilinear propagation including shoaling. Generation and dissipation of A_0 and A_1 are represented by the source terms T_0 and T_1 respectively. Refraction is accounted for by shifting energy from one direction to another during propagation with the speed c_θ in the θ-direction, as can be seen in equation (3-11) and (3-12).

Whereas HISWA uses a simplified form of the action density spectrum, SWAN does not. The local rate of change of the action density in time and the shifting of the relative frequency due to variations in depths and currents is fully taken into account in SWAN. Moreover, the source term T in the action balance equation comprises more physical phenomena than HISWA, like the non-linear wave-wave interaction. SWAN does not require waves to propagate in forward direction within a specified degree range, like HISWA does.

Whereas HISWA will be used for the schematic experiments in chapter 4, SWAN will be used for the case study in chapter 5, because of the limitations of HISWA to deal with waves propagating in all directions.

3.4 Wave-Current interaction

Wave action is important in shallow areas. It enhances the bed shear stress, which affects the stirring up of sediments and increases the bed friction. Due to whitecapping and surf breaking, turbulence is generated near the surface. Averaged over a number of waves, a net mass flux is generated, which has some effect on the current profile, especially in cross-shore direction. Variations in wave-induced momentum flux occur especially in the surf zone and give rise to strong long-shore currents and cross-shore set-up.

Forcing by radiation stress gradients
Delft3D-Flow solves the wave-averaged velocities and water levels. The wave averaging of the non-linear terms introduces external forces on the right hand side of the momentum equations. These forces are the gradients of the so-called radiation stresses.

The radiation stresses are related to wave parameters of the wave model. The pressure part of the radiation stresses is not capable to drive currents and can therefore be neglected. The radiation stresses are then modelled as:

$$F_x = \frac{\partial S_{xx}}{\partial x} + \frac{\partial S_{yx}}{\partial y} \tag{3-13}$$

and

$$F_y = \frac{\partial S_{xy}}{\partial x} + \frac{\partial S_{yy}}{\partial y} \tag{3-14}$$

In cross-shore direction, this leads to a set-up gradient and in longshore direction this leads to a wave-driven current.
In (Dingemans et al., 1987) it is indicated that wave energy dissipation is the most significant term in determining the radiation stresses. The wave forcing term can therefore be approximated by the dissipation rate D divided by the celerity of the wave ω / k, so resulting in:

$$F_x \approx \frac{D}{\omega} k_x \tag{3-15}$$

and

$$F_y \approx \frac{D}{\omega} k_y \tag{3-16}$$

These quantities are computed in one of the wave modules of Delft3D-Wave and stored in the communication file. This file is read by a new Flow computation when interaction is intended. These wave forces are one of the forces represented by M_x, M_y in equations (3-1), (3-2).

Enhancement of the bed shear stress by waves
The bed shear stress is enhanced due to a combination of waves and current. This value is in addition to the value, which would result from a linear addition of the bed stress due to waves, τ_w, and the bed stress due to current, τ_c. There is namely a non-linear interaction between the wave and current boundary layer. The effect of the orbital velocities under waves on the bed shear stress can be modelled by an artificial enhancement of the bed roughness. Soulsby developed a parameterisation of several wave-current interaction models that describe the bottom boundary layer under combined current and wave action and the resulting virtual roughness. These models are implemented in Delft3D-Flow (Delft Hydraulics, 1999).

Stokes-drift
The fluid particles in waves describe an orbital motion. The net horizontal displacement for a fluid particle is not zero. This wave induced drift velocity, which is called the Stokes-drift, is always in the direction of the wave propagation. Only in three-dimensional computations, the waves-induced Stokes drift is added to the Eulerean mean velocity and this total velocity is taken in the hydrodynamic equations. In the present implementation, the drift is assumed to be uniform over the vertical. It is a function of the wave energy, the wave propagation speed, water depth and water density. Some more details can be found in appendix A.

4 Experiments

4.1 Introduction

In the previous Chapter, Delft3D-Flow, -Wave and the interaction between these two modules are discussed. In this Chapter a model is set up for research simulations. With these simulations, a comparison will be made between surge levels, only caused by wind, and surge levels caused by wind and waves.

In the next paragraph the model set-up is discussed. Subsequently the balance between wind friction and the water-gradient force is treated. Then the theory about wave growth will be discussed. In paragraph 4.5, results from the storm surge computations, including the influence of waves are compared with the results from wind forcing only. Paragraph 4.6 deals with the dependence of the drag coefficient on the wave set-up and paragraph 4.7 the results of the sensitivity analysis will be shown. Finally, the main conclusions of this Chapter will be given.

4.2 Model Set-up

4.2.1 Introduction

In this section, the model set-up for the experiments is presented. The different assumptions for taking the chosen parameters can be found here. In succession, the following paragraphs will be treated: bathymetry, offshore boundary, domain, depth-averaged-three dimensional approach, grid size, time step, numerical parameters, duration.

4.2.2 Bathymetry

In areas of small depth, the wind stress is most effective. The larger the area of small depth, the higher the set-up. In the Bay of Bengal, an area where a lot of cyclones arise, a large part of the coastline is characterised by a shelf width of 100 km whereby the depth varies from 0 metres at the coastline to about 250 metres at the shelf break. From the shelfbreak, the depth increases quite fast to more than 1000 metres 50 kilometres further offshore.

In order to study propagation of the surge toward land in a more schematic setting, a schematisation of the bathymetry of the Bay of Bengal is made for most simulations. At a distance of 100 km from the shoreline a depth of 250 metres is taken. From there the depth decreases linearly to the shoreline. In Figure 4-1, this schematisation is drawn. Figure 4-2 presents a top view of the computational grid, and the co-ordinate definition.

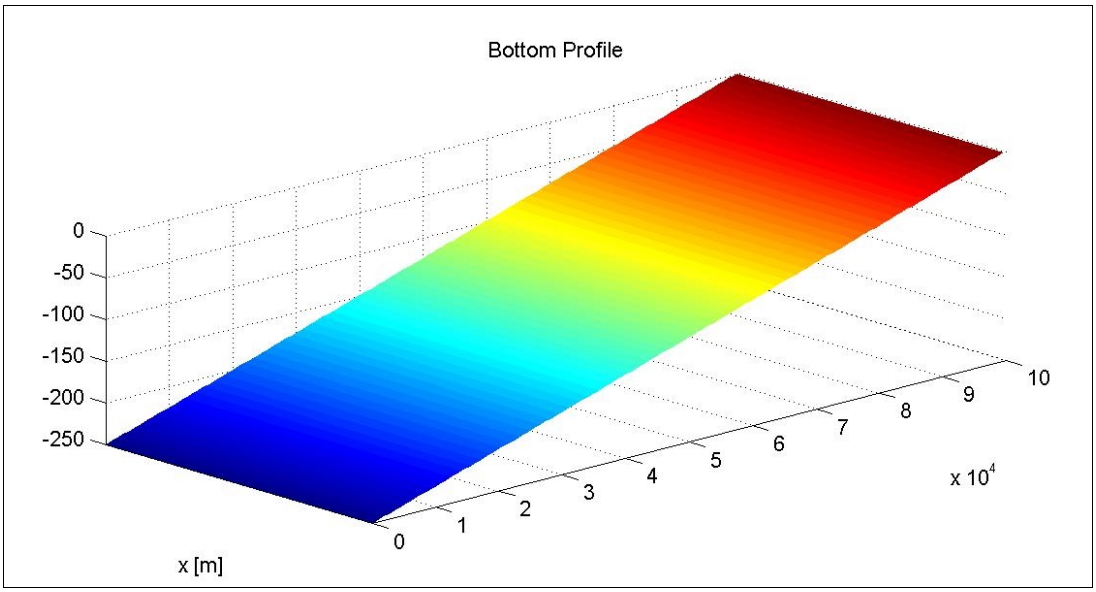

Figure 4-1: Bottom Profile

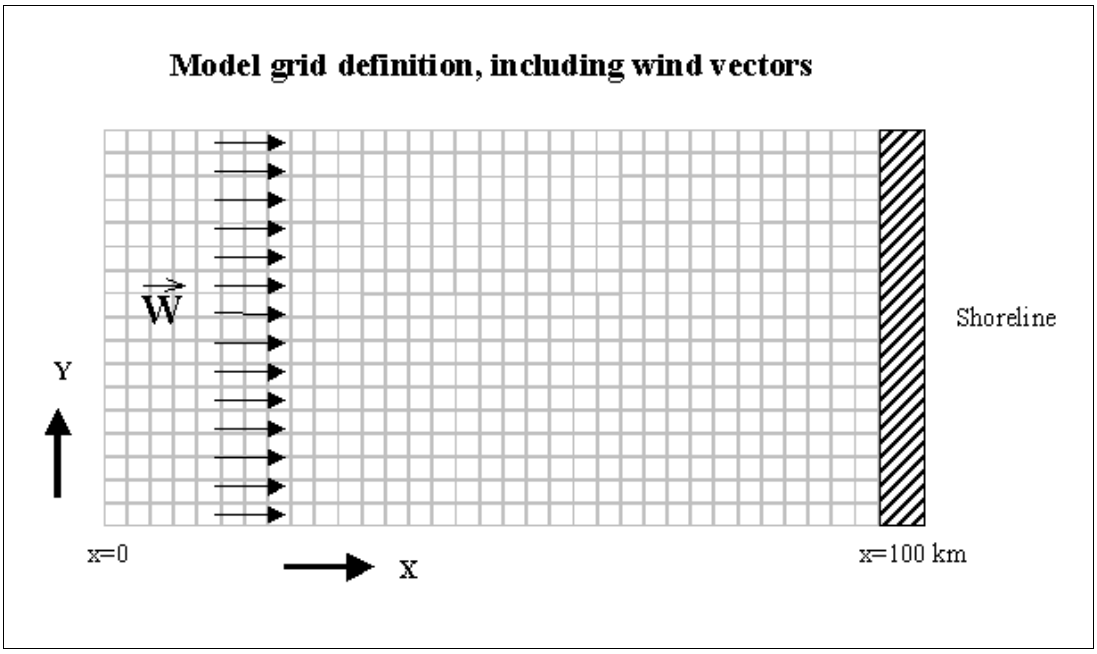

Figure 4-2: Model grid definition; Wind vectors perpendicular to coastline

In Figure 4-3, the water levels of two simulations with uniform wind directed toward the coast are depicted in which only the bottom profile is different from the other simulation. The simulation area was in both cases 50 km long, from x=50 till x=100 km, and for one simulation a starting bottom depth of 125 metres was taken, and having the same gradient as the bottom depicted in Figure 4-1. For the second simulation the bottom depth started at 250 metres. As can be seen in the figure, the water level elevation is a factor two larger halfway, at x = 25.000 m, and a factor 1.7 larger at the shoreline. These two simulations confirm that shallow water causes a larger set-up.

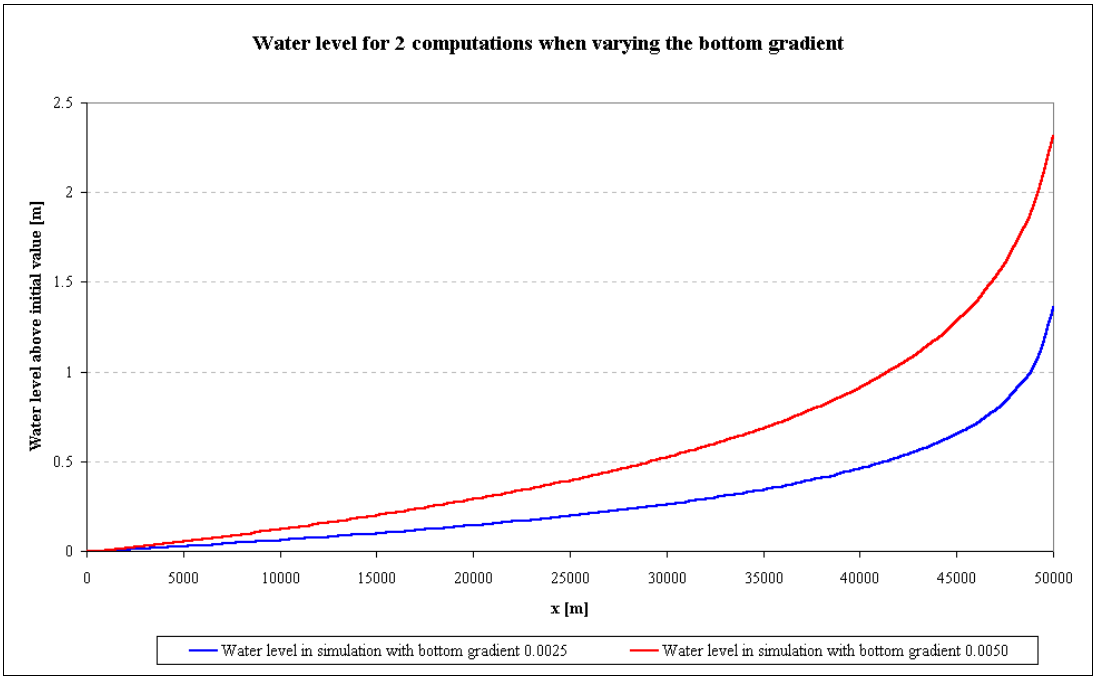

Figure 4-3: Water level at the shoreline for two computations when varying the bottom gradient

4.2.3 Offshore boundary

The area of interest in this project is mainly the shore, but the domain of the model has to be much larger to include all the effects of the surrounding area, especially the offshore area. At the boundaries of the computational domain boundary conditions have to be set.
In the paragraph 4.2.2 about the bathymetry, it is mentioned that the depth increases very fast from of the shelfbreak, which is at 100 km offshore, so in our model at x=0. The influence of the area outside our model has to be specified at this boundary. Because of the large depth, the mean water level is assumed to be constant at a value of 0 metres.

4.2.4 Domain

One important parameter for a surge caused by wind and waves is the fetch length. This length is namely the distance over where a constant wind, in speed and direction, is blowing. In the discussion of the bathymetry, paragraph 4.2.2, a length of 100 km is mentioned for the computational domain. Wind speed vectors, which are approximately pointing in the same direction over a length of 100 km, can only be found at a certain distance from the centre of the cyclone. This can be shown by describing the cyclone as circles and by plotting the wind vectors tangent to them. For example at a distance of 100 km from the centre, the incoming and outgoing vectors have an angle of 30°. In between this 100 km large area the angles of the vectors are less than that. Farther away, the angles of these incoming and outgoing vectors get smaller, but their corresponding wind speed too, which affects the rise in water level due to waves as well.

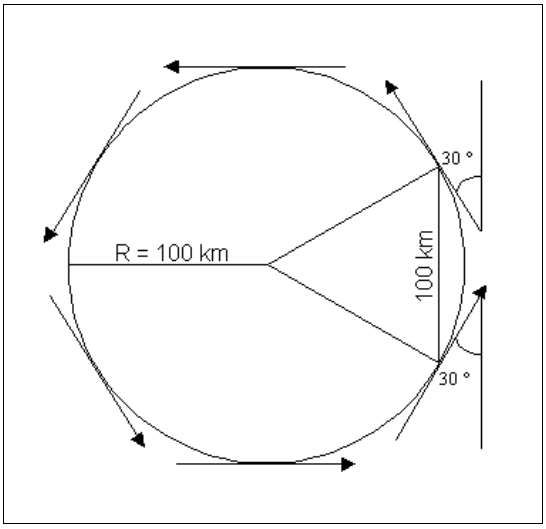

Figure 4-4: Wind direction at 100 km away from the eye of the cyclone

So for this model it is assumed that at a distance of 100 km from the eye of the cyclone the wind points in one direction and the wind speed is still large enough to generate large waves.
Looking at Curve H in Figure 2-3, a representative wind profile is depicted of a cyclone as one can occur. At a distance of about 100 km away from the centre, a wind with a speed of 50 m/s is blowing. This speed is taken as a first value to examine the influence of waves on storm surges.

For the model width the computational time has been taken as a constraint. The computational time is dependent of the number of cells in x-, y- and z-direction, in which here the x-direction represents the length, the y-direction the width, and obviously the z-direction the depth. The choice of the width is thus a combination of several aspects. The length was already discussed and later on in this chapter, the grid size and the number of layers in the vertical will be discussed, both of course influencing the computational time. The grid size and the number of layers in the vertical resulted therein, that for the width 1500 metres is taken. The left and right boundaries will not effect the solution, because in the simulations it is seen as a strip within a larger area. The wind has to blow only in the main direction, but this is assumed to be the case, at places sufficiently far away from the centre.

In Figure 4-5 a typical plot of wind vectors around the centre of a cyclone is drawn. The vectors drawn on the blue background represent flow directions of the water, but will not be of interest here.

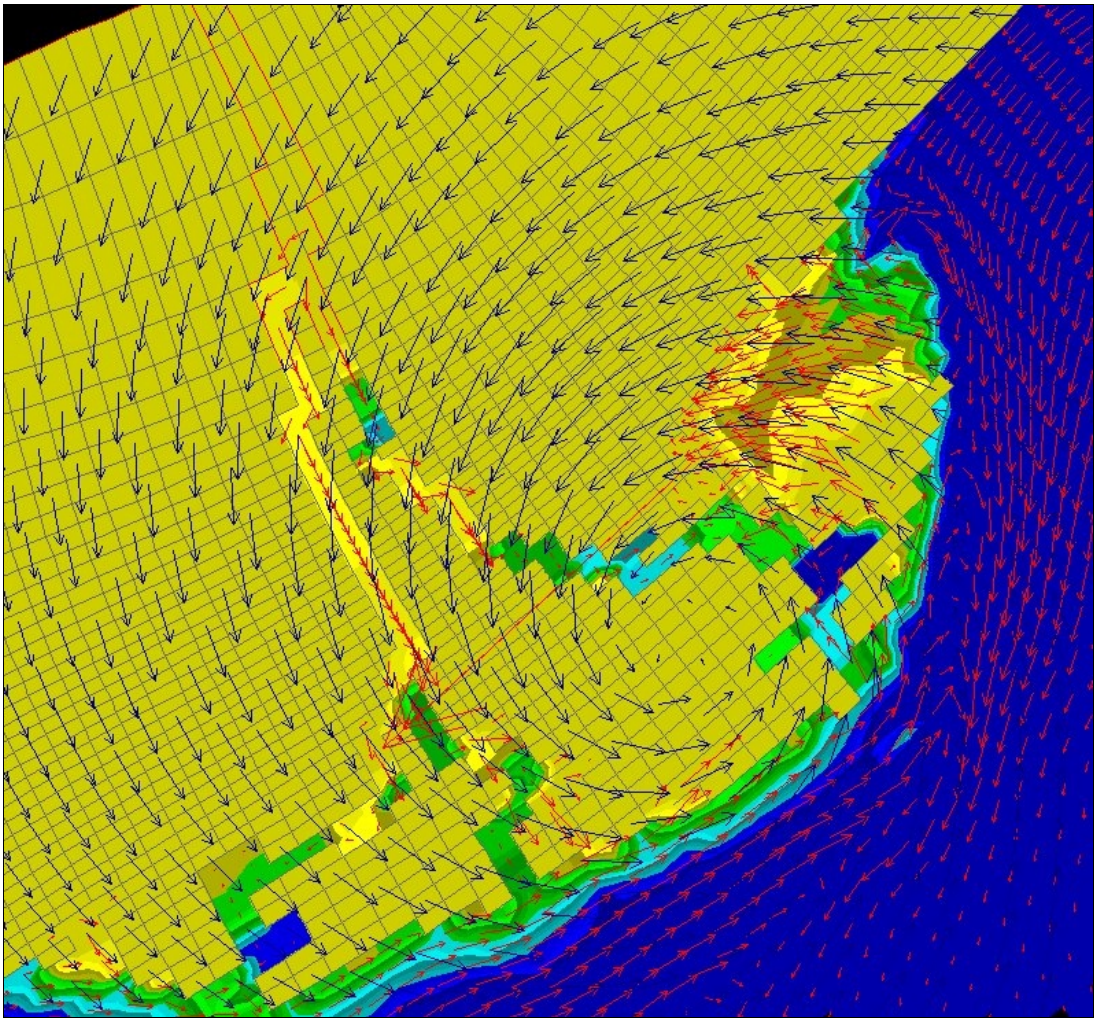

Figure 4-5: Typical sketch of wind vectors of a cyclone: eye of the cyclone overland in the Krishna Delta.

4.2.5 Depth-averaged or three-dimensional approach

For properly interpreting the numerical results an equilibrium solution is required. At the start of a simulation, velocities in the horizontal directions, u and v, as well as the water elevation, ζ, are 0. This cold start introduces initialisation effects and the numerical solution is not reached immediately. This initialisation effect is a wave, which starts propagating in the direction of the shore and reflects there.
More initialisation waves are introduced by the wind, because within the first six hours of the simulation it is increased from 0 m/s to its final prescribed value. For every time step, the wind speed increases and introduces therewith an initialisation wave. All these waves propagate through the computational area and reflect at the boundaries.

In a two-dimensional depth-averaged (2DH) model run, a stationary state is reached when the wind force is in equilibrium with the water surface slope. No velocities remain in the end situation. The bottom stress accounts for the loss of energy of the standing and propagating waves. However, it takes quite long to dissipate all the energy as the loss of energy is proportional to the square of the flow velocity. The amount of energy that is dissipated decreases per time step, because velocities are decreasing. Moreover, as can be seen in the momentum equations for U and V (Equations (2-1) and (2-2)), in the most right term the bottom stress is divided by the water depth and a large part of the models' domain, is situated in deep water. The bottom stress term is therefore negligible outside the onshore area and is therefore not significant for the decrease of the velocities.
In a three-dimensional (3D) model run, a stationary situation will be reached which includes a flow. This flow follows a clockwise pattern with velocities in onshore direction at the surface and in offshore direction at the bottom in this model. Because the velocities remain, continuously energy is taken out of the model due to bottom friction. A stationary state will be reached much more quickly than in a one-layer-model even though for two or more layers in depth more computational time is used. Figure 4-6 and 4-7 confirm this.

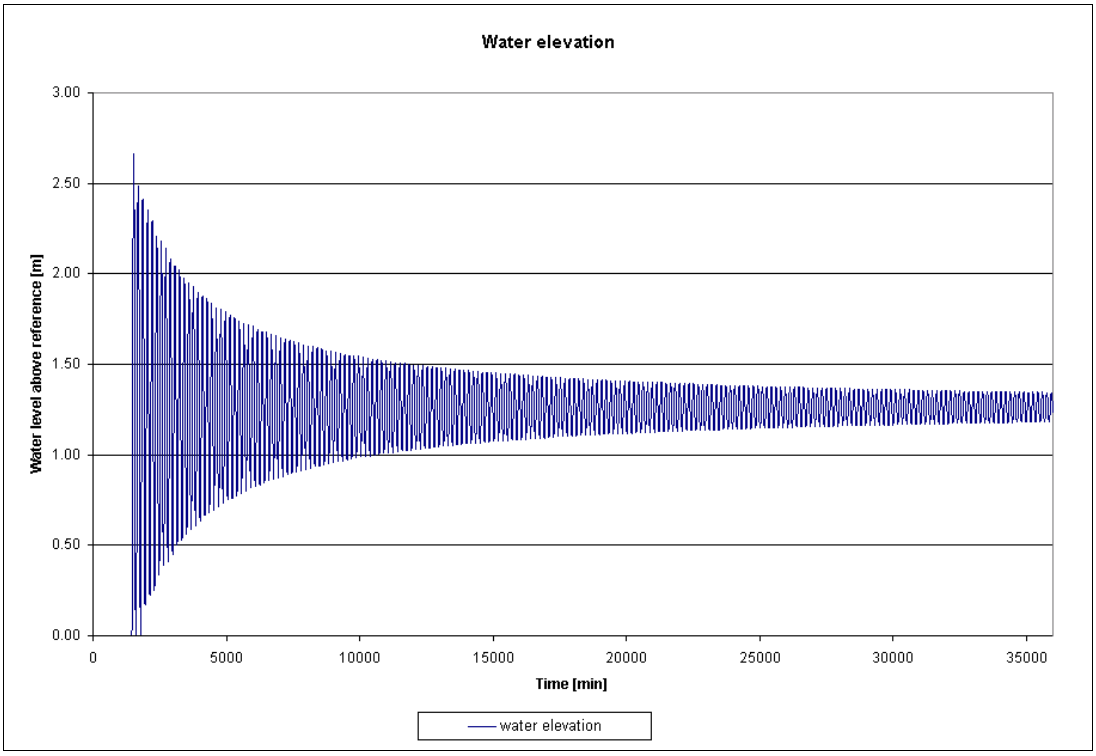

Figure 4-6: 2DH simulation of 25 days. Slow disappearing of the initialisation effect

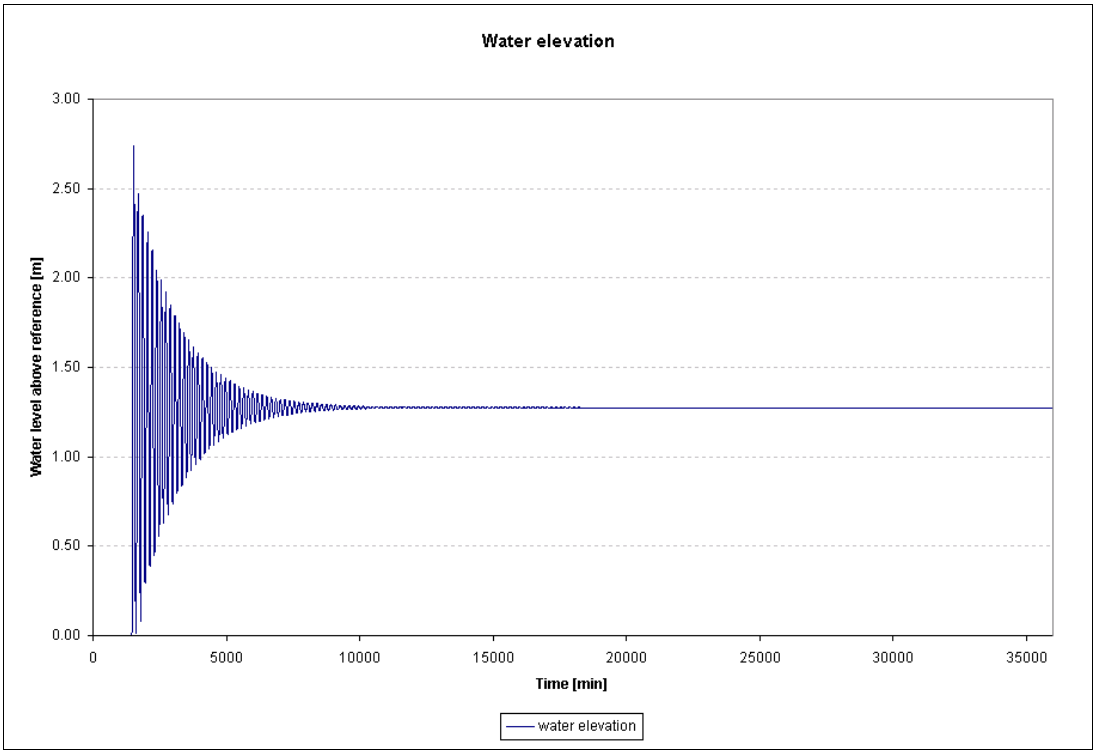

Figure 4-7: 3D simulation, lasting 25 days. Energy dissipated already within 14.400 minutes (10 days)

4.2.6 Grid Size

Numerical models generate errors. They can be divided into round-off errors and discretization errors. Discretization errors are caused by the finiteness of the grid size and the time step. These values of Δx and Δt also determine the stability of the calculation.
For determining the grid size and the time step, first the grid size is considered.

As the grid size and time step tend to zero, the values of the numerical solution should approach the values of the exact solution. However, a smaller grid size negatively affects the computational speed and therefore slows down the computation. It can cause loss of accuracy due to round-off errors as well. So, a grid size has to be found that guarantees a given level of accuracy. This is carried out in an empirical way.

In the next table the surge levels at the shoreline computed with three different grid-sizes are presented.

Table 4-1: Water level set-up at the shoreline for different grid sizes

Δx [m]	η [m]
500	3.343
250	3.415
50	3.475

These surge heights just slightly differ. Convergence is seen here in table 4-1 by the decrease of the difference in water height between two computations. The increase of computational time did decide to take a grid size of 250 metres in the schematic model experiments.

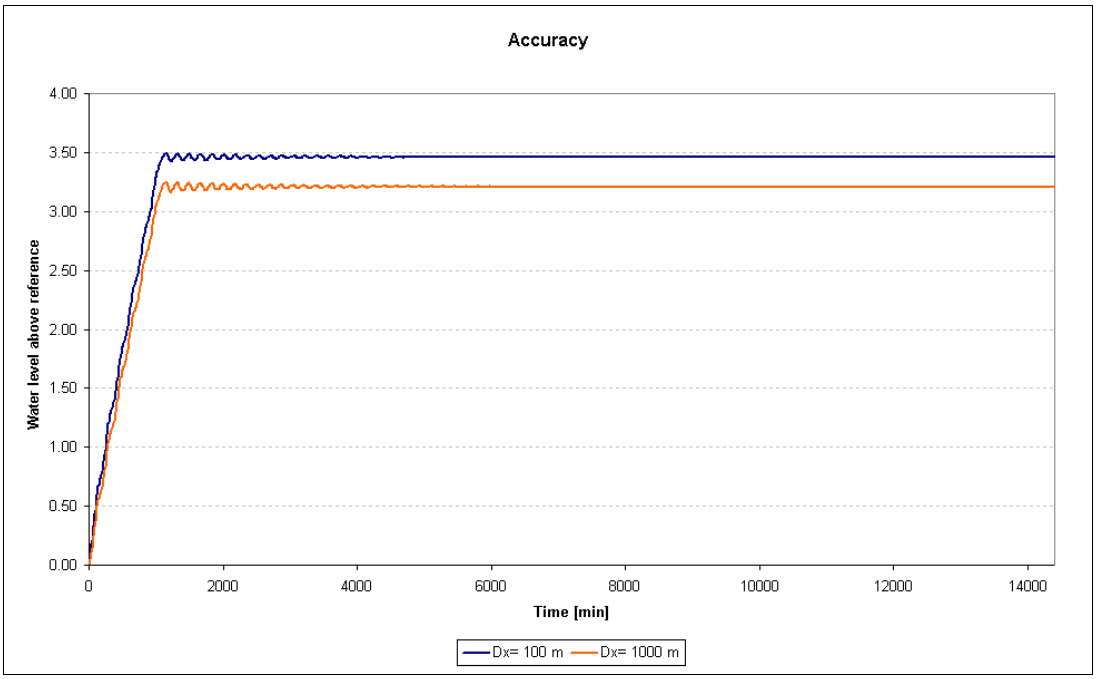

Figure 4-8: Water level in station at shoreline drawn for one model run with Dx=100m and one with Dx=1000m

Figure 4-8 depicts the water levels for two model runs, one in which the grid size is 100 metres and one in which the grid size is 1000 metres. The evolution in time is depicted. The difference in end values is easily seen. The water level computed with Dx=100 metres results in 8% higher set-up.

A high resolution is thus of importance for storm surge computations.

4.2.7 Time Step

The numerical schemes that Delft3D uses are all implicit and all the simulations are unconditionally stable and stability does not depend on the time step. The time step on the other hand influences the accuracy. So the time step cannot be taken too large and the Courant number will be used for that. For getting accurate results a Courant number of approximately 10 is advised, but larger numbers can be used in many cases without losing accuracy.

The Courant number is calculated by:

$$C_f = 2\Delta t \cdot c \cdot \sqrt{\frac{1}{\Delta x^2} + \frac{1}{\Delta y^2}} \tag{4-1}$$

whereby 'c' is the wave velocity.

For calculating c the next formula is used:

$$c = \sqrt{g \cdot H} \tag{4-2}$$

The Courant number is thus determined by the largest depth for constant grid size, here, 250 metres. When taking $\Delta t = 60$ seconds, and also having a grid size of 250 metres in x- and y-direction the Courant number is about 34. A simulation with $\Delta t = 30$ seconds was carried out and the results were the same as with $\Delta t = 60$. So this reduction did not lead to higher accuracy and further computations will be carried out with a 60 seconds time step.

4.2.8 Numerical Parameters

At the start of the computation, the water level at the shoreline, where the water depth D≡0, is zero. A propagating wave, which is generated at the start, reflects at the shoreline. The water depth in the grid cells at the shoreline becomes 0, because of this reflection. Delft3D consist of a special drying and flooding procedure. The way of computing the water depth in these grid cells, where drying and flooding occurs, can be changed in the program by the 'marginal depth'

When changing the marginal depth, Delft3D-Flow can determine the water levels in three different ways. When having the default value, the water depth in the standard Arakawa C grid is calculated by:

$$h^U_{m,n} = \overline{D}^{\eta} + \overline{\zeta}^{\xi} \tag{4-3}$$

in which

$$\overline{D}^{\eta} = \frac{\left(D_{m,n} + D_{m,n-1}\right)}{2} \quad \text{and} \quad \overline{\zeta}^{\xi} = \frac{\left(\zeta_{m,n} + \zeta_{m+1,n}\right)}{2}$$

In contrast with the average approach, an upwind approach is obtained when setting the marginal depth to a value different from the default value. The water depth is then calculated by:

$$h^U_{m,n} = \overline{D}^{\eta} + \theta^U_{m,n}\zeta_{m,n} + \left(1-\theta^U_{m,n}\right)\zeta_{m+1,n} \tag{4-4}$$

$\theta^U_{m,n}$ is determined by the following computational procedure:

If $\left(h^U_{m,n} > D_{mar}\right)$ *Then*

$$\theta^U_{m,n} = 0.5$$

Else

$$\theta^U_{m,n} = \begin{cases} 1.0 \;\; if \;\; U_{m,n} > 0 \\ 0.0 \;\; if \;\; U_{m,n} < 0 \\ 1.0 \;\; if \;\; \eta_{m,n} \geq \eta_{m+1,n} \wedge U_{m,n} = 0 \\ 0.0 \;\; if \;\; \eta_{m,n} \leq \eta_{m+1,n} \wedge U_{m,n} = 0 \end{cases} \tag{4-5}$$

The drying and flooding procedure can introduce some numerical instabilities. Especially in cases of tidal flats or overtopping of riverbanks the upwind approach is more realistic. In this model grid cells near the shoreline are being exposed to this procedure as well. Therefore the marginal depth was changed into 0.1 and +999, which in the first case meant that $\theta^U_{m,n}$ was almost always 0.5 and in the second case always 1.0. However, the solutions were not affected by changing this parameter. Oscillations introduced by the numerical procedures were not different after changing the marginal depth.

When starting the simulation from a cold start, waves are generated and are propagating through the model as explained before. These waves cannot pass through the open boundary by prescribing the water level or velocity at this point. Passing of waves through the boundary can be accommodated by adding a term to the boundary prescription that allows for passing waves, which is tuneable by a factor α.

This α is namely multiplied by $\frac{\partial}{\partial t}$ of the Riemann invariant and then added to the prescribed water elevation, changing the boundary condition effectively into:

$$\zeta + \alpha \cdot \frac{\partial}{\partial t}\left(U \pm 2\sqrt{gh}\right) = 0 \qquad (4\text{-}6)$$

The default value of this parameter is zero and simulations were carried out with 3 different values, namely, α = 50, 100 and 1000.
The simulations in where different α's were used, did not seem to be influenced by the value of it. In Figure 4-9 a 2DH model run was done with α = 100. The oscillations in the water level are not damped out after running for 10 days.

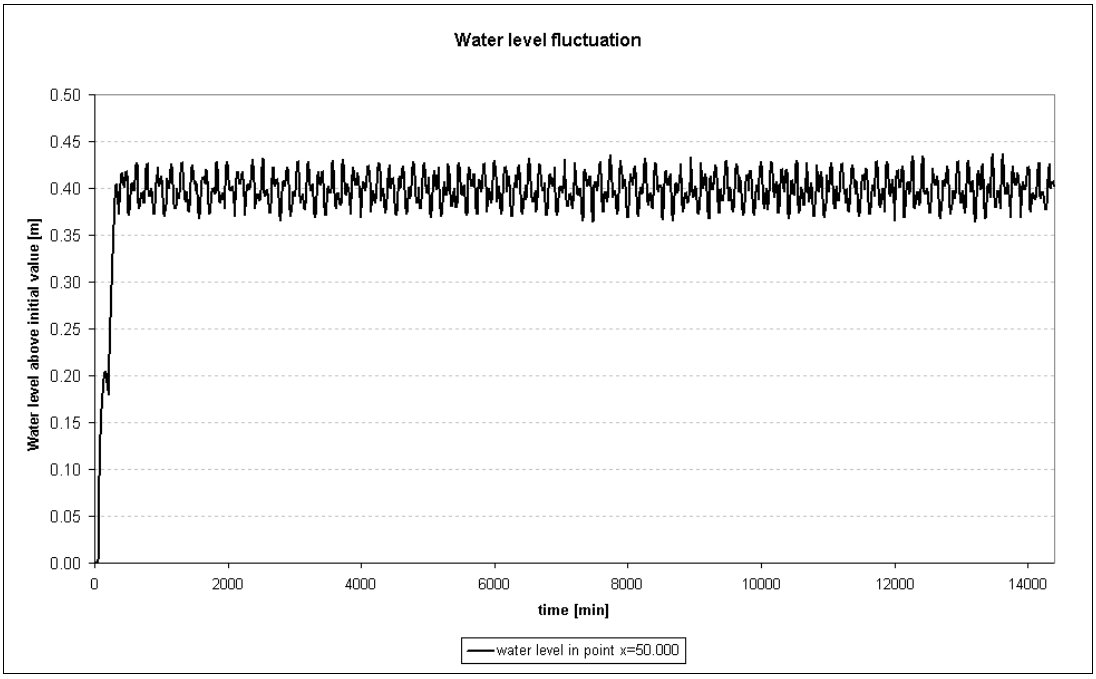

Figure 4-9: Water level in observation point halfway. 2DH model run with α = 100 and D_{mar} = 0.1 *m*

4.2.9 Duration

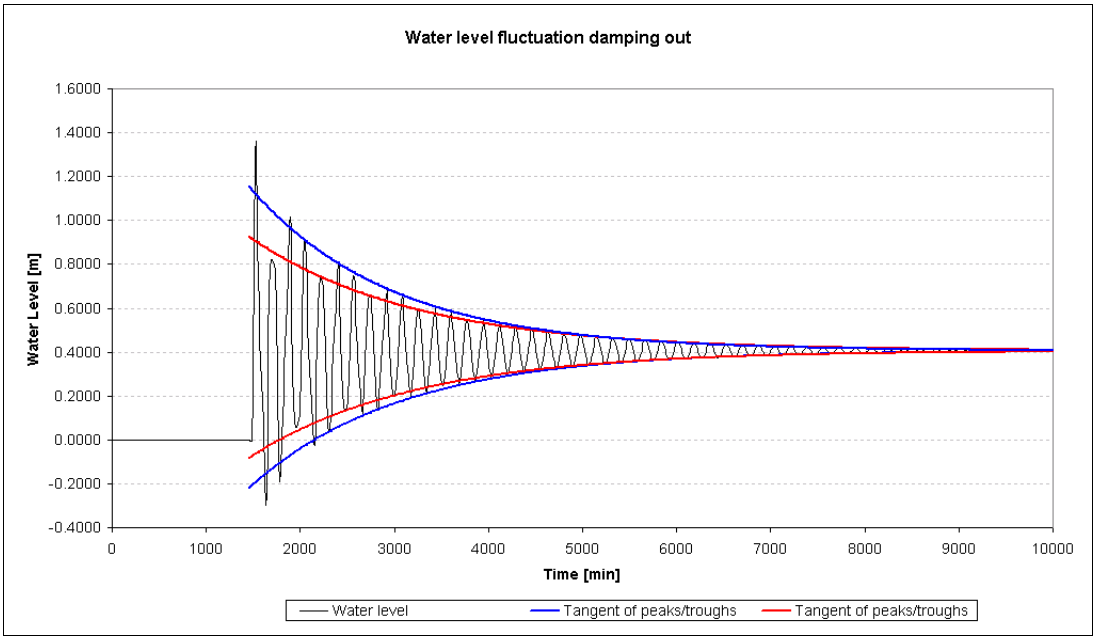

Figure 4-10: Damping out of oscillations

The figure above is a typical sketch of the water level that arises from the wind, which acts on the water. The water level for the first 10.000 minutes (7 days) is depicted here. After one day a wind of 50 m/s starts acting on the water. A wave is generated and propagates into the direction of the coast and reflects there to come back to where it was started and reflects there again. The wave height reduces in time due to the energy loss by bottom friction. The line that is drawn is thus the sum of several cosines with different amplitudes. These cosines have frequencies with the same base, $\cos(k\omega_0)$, whether they are travelling towards the coast or from the coast.
This is the reason why the sketch still looks like a cosine, so still having the same period over the whole time.

As can be seen in the figure, there are 4 exponential lines that follow the maximum or minimum amplitudes of the water level. All of these lines can be written in the form:

$$h_0 \cdot e^{-\alpha(t-t_0)} + h_\infty . \qquad (4\text{-}7)$$

The next table gives the values of the coefficients for the 4 exponential lines

Table 4-2: Coefficients of equation (4-78)

h_0 [m]	α [-]	t_0 [min]	h_∞ [m]
0.752	$6.66 \cdot 10^{-4}$	1450	$4.057 \cdot 10^{-1}$
0.521	$5.71 \cdot 10^{-4}$	1450	$4.057 \cdot 10^{-1}$
-0.490	$5.66 \cdot 10^{-4}$	1450	$4.057 \cdot 10^{-1}$
-0.625	$6.16 \cdot 10^{-4}$	1450	$4.057 \cdot 10^{-1}$

By taking the reciprocal of alpha, a value between about 1500 and 1750 minutes is found. This means that it takes 1500-1750 minutes for the amplitude to decrease with order of magnitude e of its original value. So for a simulation of 10 days the amplitude is decreased by a factor of e^8, that is about 3000. The amplitude in the above simulation is then in the order of tenth of millimetres, and one can say it has reached its equilibrium.

4.3 Wind friction versus slope-gradient force

A first approach is made by calculating the set-up by assuming the wind stress to be equal to the water level gradient in the depth-integrated equation:

$$g\frac{\partial \zeta}{\partial x} = \frac{\tau_{sx}}{\rho h} \tag{4-8}$$

in which h is the total water depth (D + ζ).

The set-up can then be expressed by:

$$\zeta(x) = \int_0^L \frac{\tau_{sx}}{\rho g(D(x)+\zeta(x))} dx \tag{4-9}$$

For the linearly increasing slope an analytical solution cannot be found for this integral and therefore it is solved numerically. Along the x-axis, the water depth is known; the wind stress, water density and the gravitational acceleration are prescribed constants. The only unknown in here is thus the set-up. The set-up exists in the expression at both sides. One can solve this numerically with the Riemann minimum values. That means that in the calculation, the new set-up is calculated by taking the sum of the previous set-ups in the denominator.

This has been carried out, and 2 variables of wind stress have been changing, the drag coefficient and the wind speed. In Figure 4-11 and Figure 4-12, the set-up is drawn for four different drag coefficients and two different wind velocities.
The depth profile is schematised linearly, following Figure 4-1, so having a depth of 250 metres at x=0 and 0 metres at the shoreline at x=100000 metres.

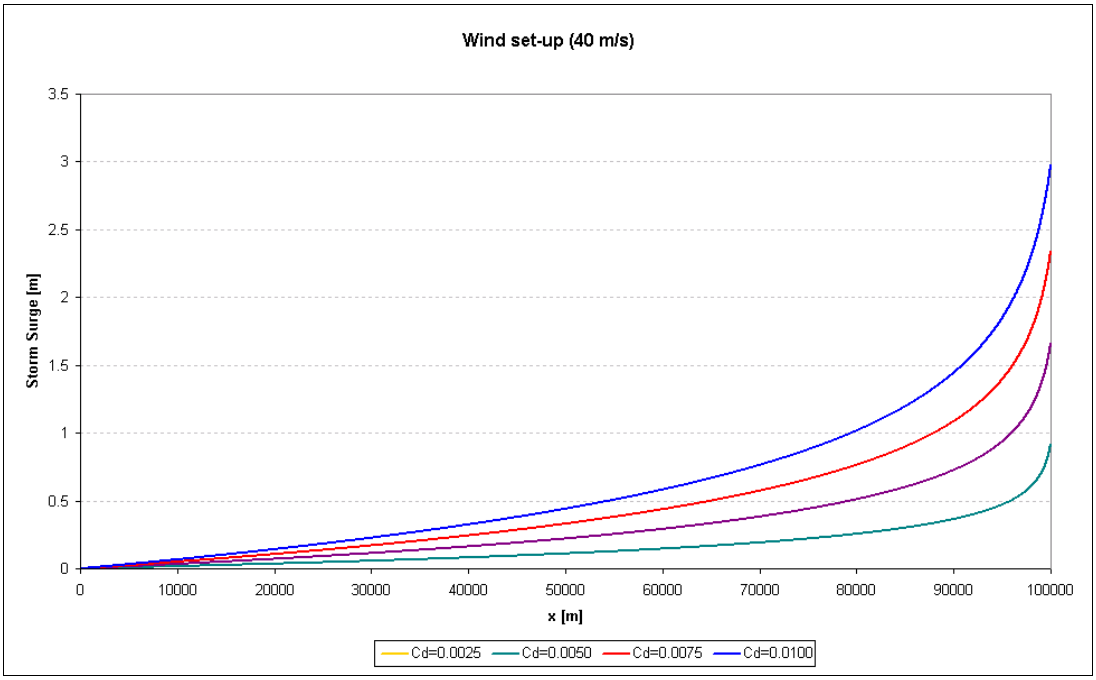

Figure 4-11: Storm Surge at a wind speed of 40 m/s for several Drag coefficients

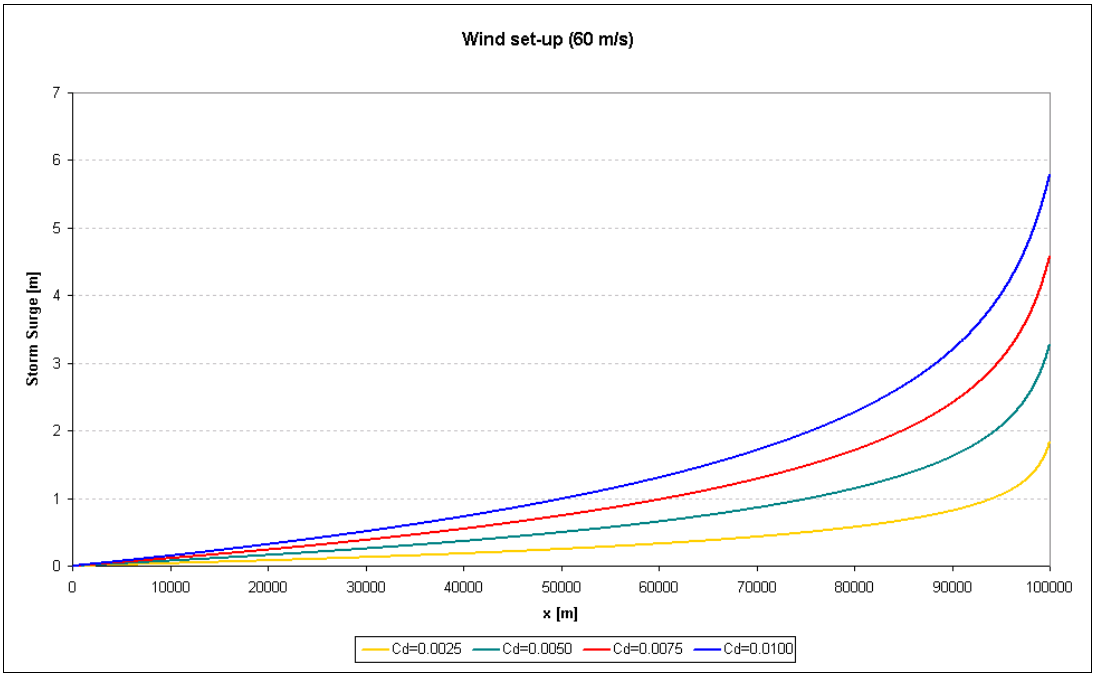

Figure 4-12: Storm Surge at a wind speed of 60 m/s for several Drag coefficients

Figure 4-13 to Figure 4-16 compare the set-up for three different wind velocities, whereby the set-up is calculated with the same drag coefficient. When looking at the set-up caused by a wind speed of 40 m/s and 60 m/s, the velocity increases by a factor 1.5 and the resulting set-up by about a factor 2. One would assume that because of the fact that the shear stress is proportional to the square of the wind velocity, the resulting set-up would have been increased by a factor 2.25. This would only have been so when in expression (4-9) the denominator had been D(x) instead of (D(x)+ζ(x)). Non-linear effects are thus the reason for this difference.

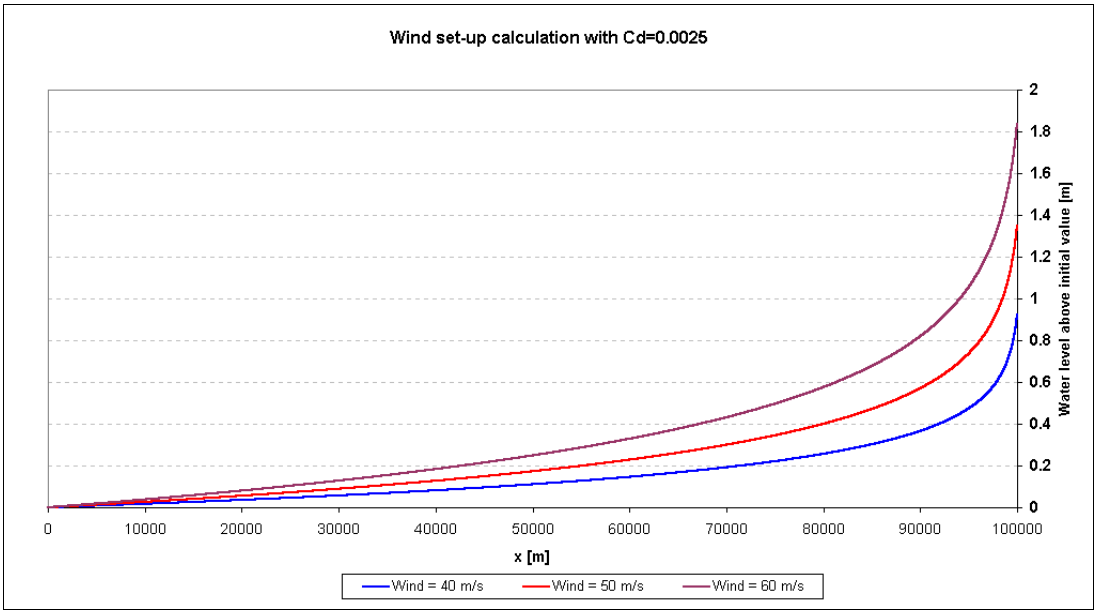

Figure 4-13: Wind set-up for 3 different wind speeds with a Drag coefficient of 0.0025

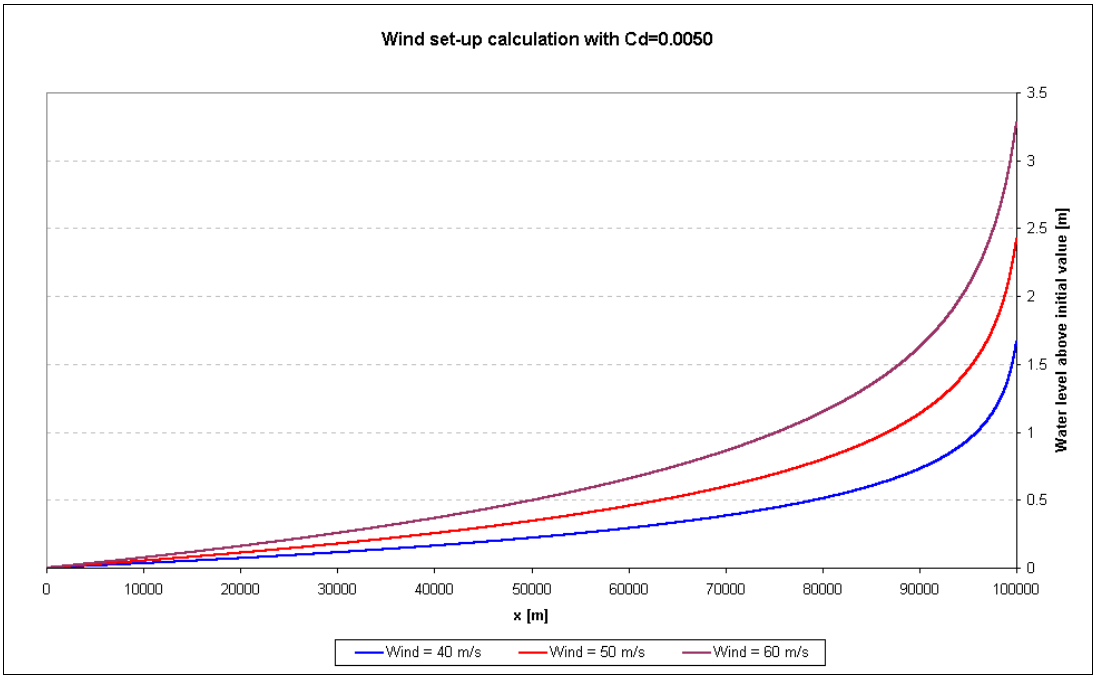

Figure 4-14: Wind set-up for 3 different wind speeds with a Drag coefficient of 0.0050

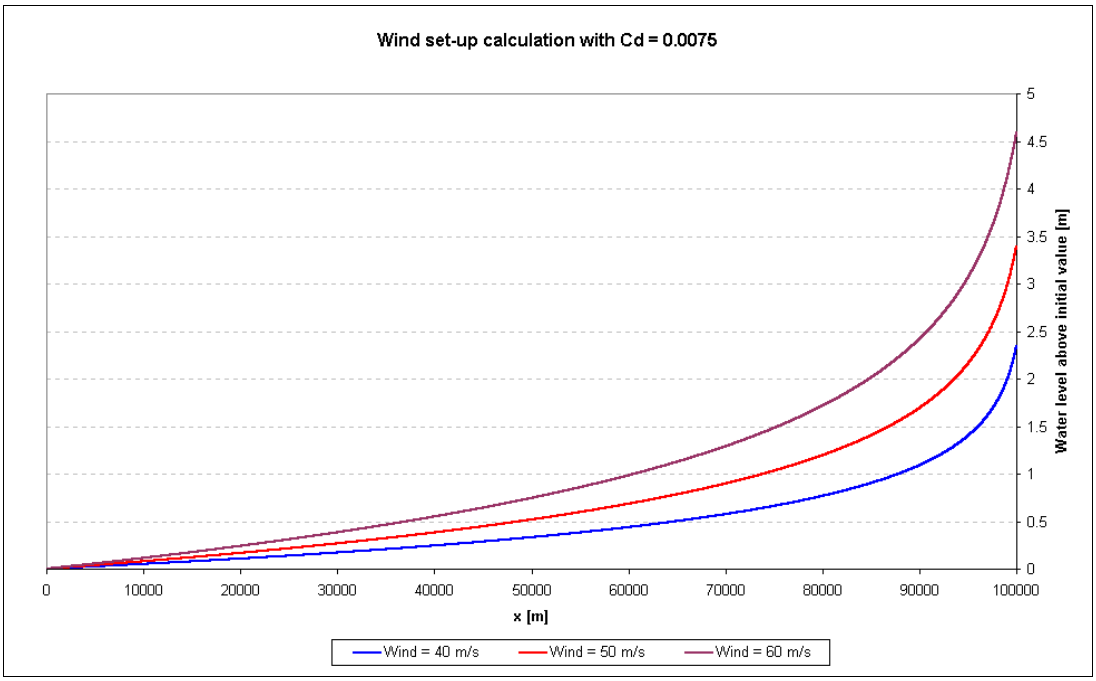

Figure 4-15: Wind set-up for 3 different wind speeds with a Drag coefficient of 0.0075

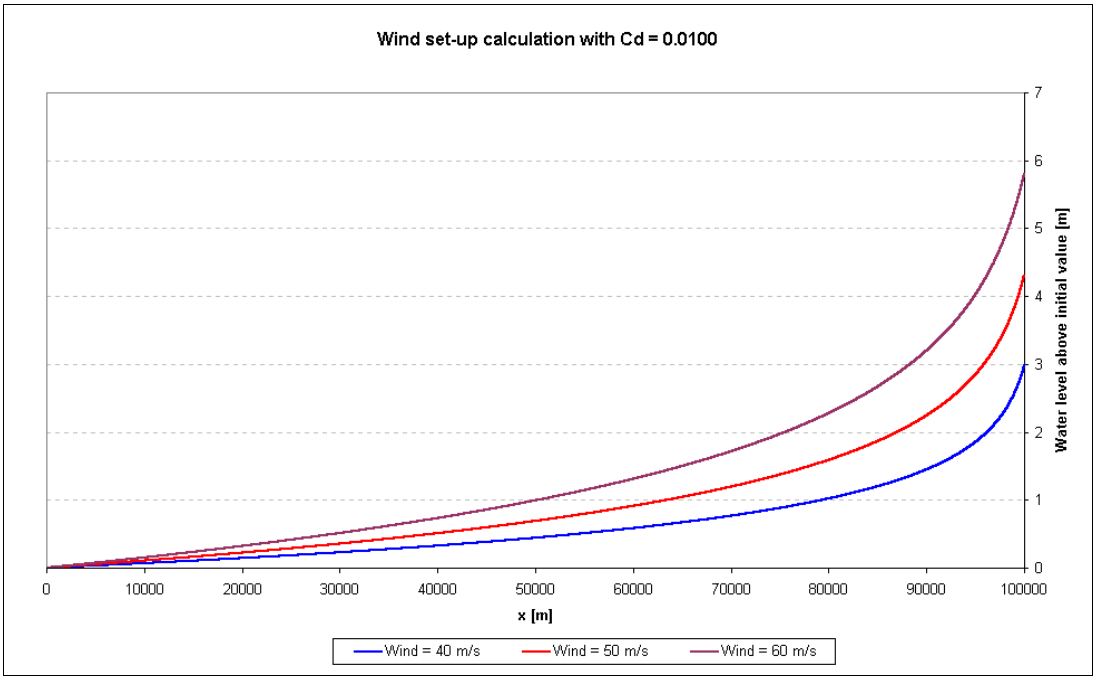

Figure 4-16: Wind set-up for 3 different wind speeds with a Drag coefficient of 0.0100

When plotting the amplification factor of the water level set-up generated by the winds of 40 m/s and 60 m/s, Figure 4-17, the amplification factor is at first 2.25 and later on, it decreases quite fast. The set-up is in comparison with the undisturbed water depth over the first 60 km negligible, less than 1%. At the shoreline on the other hand, the undisturbed water depth is negligible, comparing it with the set-up. For higher winds, these non-linearities are already visible in earlier state, which is logical, because their generated set-up is larger and thus earlier of interest.

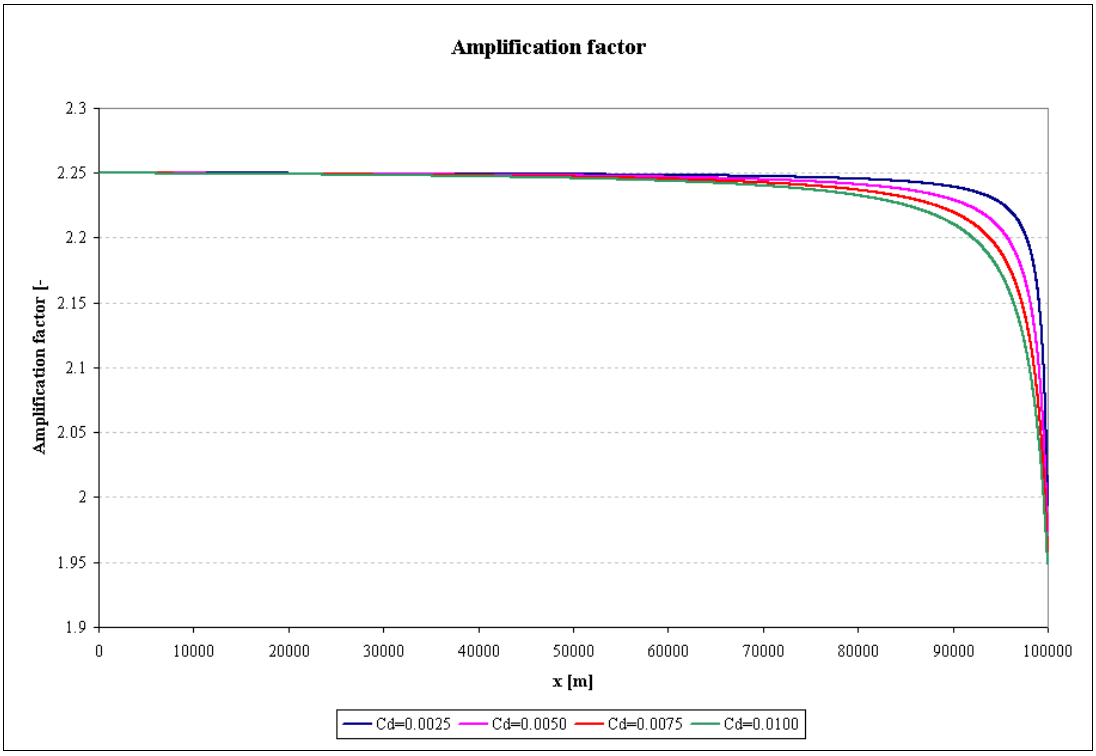

Figure 4-17: Amplification factor in surge height for 4 drag coefficients

All of these plots show that the drag coefficient is an important parameter as was already stated in paragraph 2.4. In the model a value of 0.0050 will be taken for a wind of 50 m/s. This value was also proposed by Wu with his expression (2-6). As can be seen later on, the storm surge model developed for the Andhra Pradesh coast uses about the same value.

4.4 Wave Growth

Before going to the computations carried out with the model described in section 4.2, two theories will be discussed for calculating important wind-wave parameters. The duration of the simulations is so long that a fully developed situation is reached. This means that the waves do not grow in time anymore and so they have reached a final height. The height of the waves depends on the fetch length, but the relation is not linear and at a certain point the waves cannot grow anymore because of the energy loss due to wave breaking, called whitecapping. A prediction of the wave height can be made.
The waves do not grow anymore when wind speed is equal to the phase speed of the waves. So in formula form:

$$\frac{g}{2\pi} T_{1/3} \approx U_{10} \tag{4-10}$$

For the wind speed, the speed at 10 metres above the surface water line is taken. In the computations, this value is prescribed. For winds of 20 m/s, the significant wave period is 12.8 seconds. The wave steepness at deep water $\frac{H_{1/3}}{L_{1/3}}$ is about 0.04-0.05. In dimensionless form, an expression can be formulated in which the dimensionless wave height, $\widetilde{H}$, is equal to the dimensionless wave period, $\widetilde{T}$:

$$\frac{H_{1/3}}{L_{1/3}} = \frac{\frac{g}{U_{10}^2}}{\frac{g}{U_{10}^2}} \cdot \frac{H_{1/3}}{L_{1/3}} = \frac{\widetilde{H}}{\frac{g}{U_{10}^2} \cdot \frac{g}{2\pi} \cdot T_{1/3}^2} = \frac{\widetilde{H}}{\widetilde{T}^2 / 2\pi} \approx 0.04 \tag{4-11}$$

So a significant wave period of 12.8 seconds gives a dimensionless water height of 0.25 and this is equal to a significant wave height of 10.2 metres.

A second method of calculating the wave height is the SMB-method (Sverdrup, Munk and Bretschneider method). Here the following expression is used:

$$\widetilde{H} = \widetilde{H}_{\infty} \cdot \tanh\left(k_1 \widetilde{F}^{m_1}\right) \tag{4-12}$$

in which H_∞ is the fully developed value and in which k_1, m_1 are constants what fit the observed values. According to (Holthuijsen, 1999), the Shore Protection Manual of 1973 gives values of $\widetilde{H}_{\infty} = 0.283$, $k_1 = 0.0125$ and $m_1 = 0.42$.

$\widetilde{F} = \frac{gF}{U_{10}^2}$ and is thus the dimensionless fetch length. For a fetch length of 100 kilometres and a wind velocity of 20 m/s, a dimensionless wave height, $\widetilde{H}$, of 0.09 is found and this

equals a significant wave height of 3.7 metres. This value is about a factor 3 less than the value found via equation (4-11). This means that a fully developed situation is not yet reached when having a fetch length of 100 kilometres. A fully developed situation would have been the case if the fetch length was about 5000 km. This is not realistic. Especially for winds which exceed 20 m/s, for example the wind from of a cyclone (40-50 m/s), the fetch length for a fully developed situation would have been more than 15000 km.

With those wind conditions, the significant wave height that would occur, when having a fetch length of 100 km, is about 11 metres. Delft3D-Wave gives the same results. In Figure 4-18 the significant wave height is drawn for 3 different wind velocities.

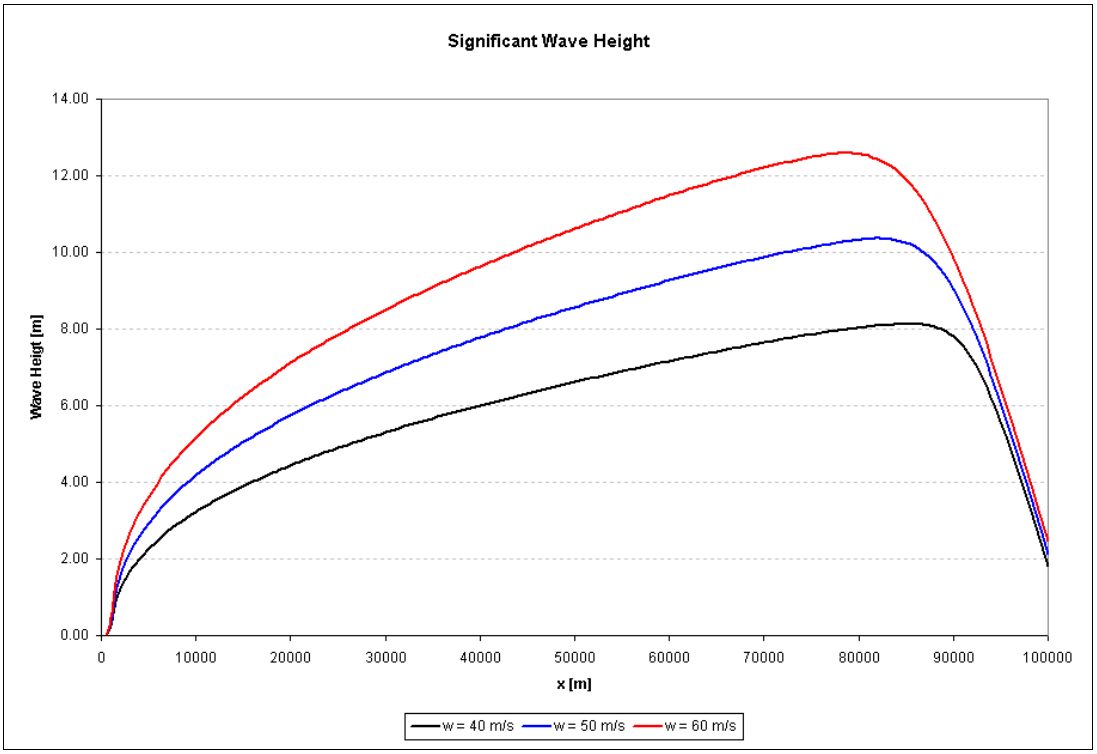

Figure 4-18: Significant Wave Height for 3 different wind velocities; computed using Delft3D-Wave

4.5 Wind and Wave forcing

A simulation is carried out in which the water level is forced by wind blowing with a velocity of 50 m/s over it. The drag coefficient taken in this case is 0.0050. The red line in Figure 4-19 is the water level resulting from the Flow computation. The influence of waves is not taken into account in this level. The blue line is on the other hand the water level including the influence of waves. The interaction of Flow and Wave gives thus a higher set-up as can be seen in the figure.

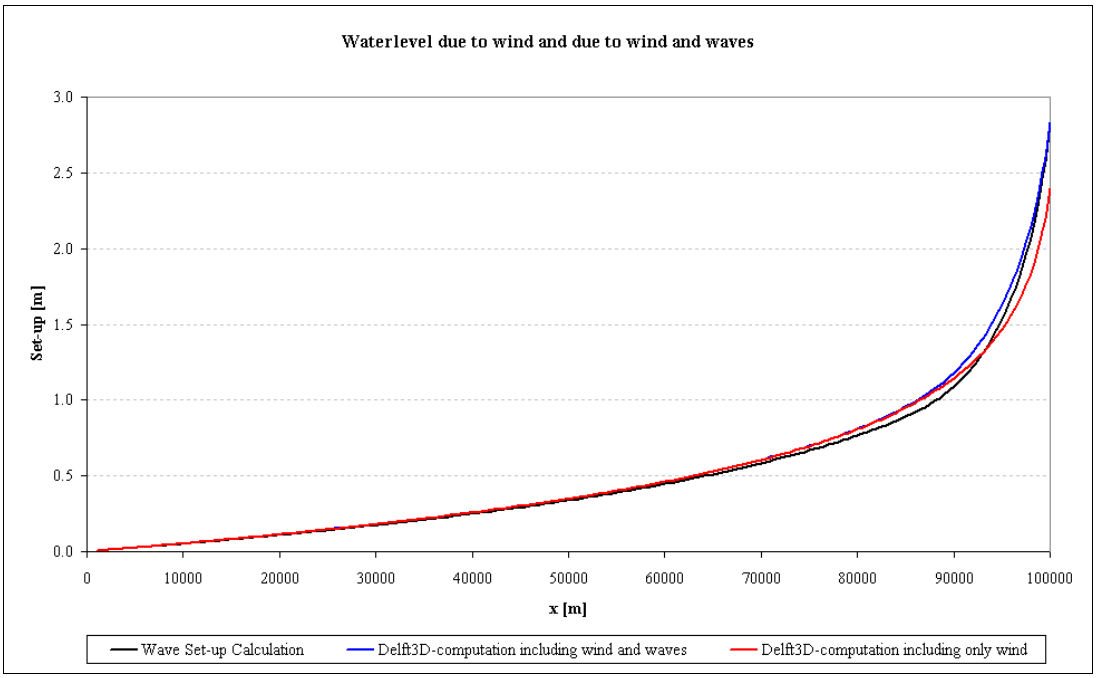

Figure 4-19: Water levels in model area in final situation

In Figure 4-20 the same figure is drawn, but only then for the last 20 km. The red and blue lines are from the start till about 80 km at approximately the same level and only differ in the last 20 km. This difference is caused by the wave set-up. The wave set-up starts from the point where dissipation of energy takes place. An extra force on the water is added and is, according to equation (3-15), equal to the dissipation divided by the wave velocity. This force is therefore causing an extra set-up. At the shoreline, an increase of the water level of 18 % is the result, which is in here 0,4 metres, and thus a significant difference.

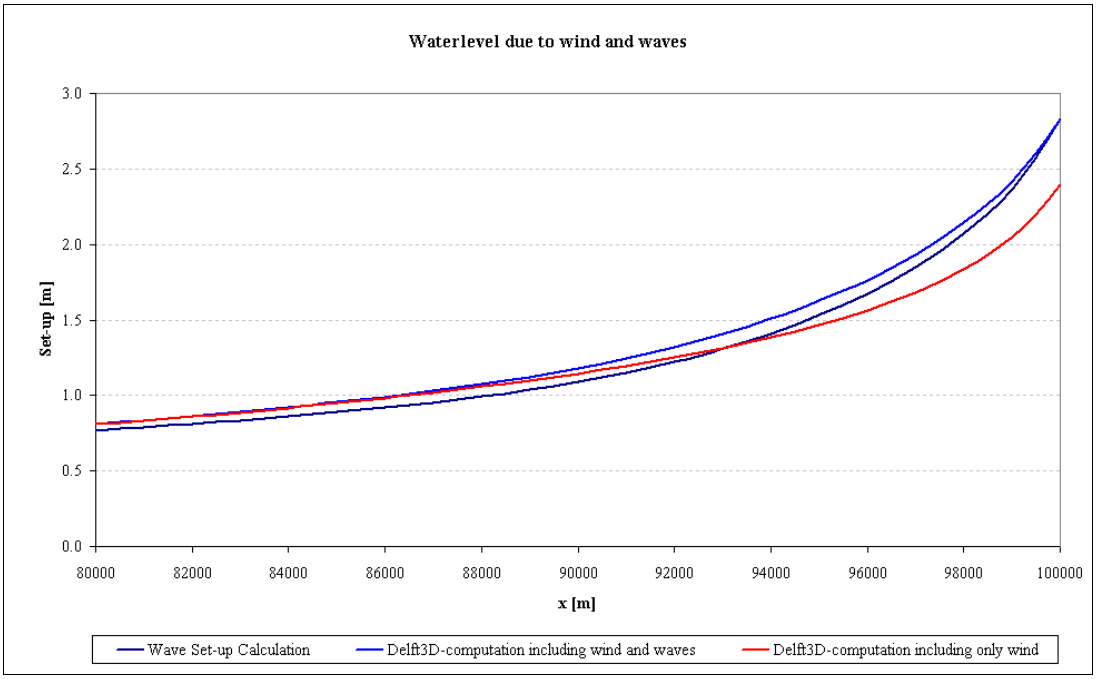

Figure 4-20: Water levels in model area, zooming in at the last 20 km of previous figure

A third black line can be seen in both Figures too. This is also a wave set-up but then calculated with the following equations (Battjes, 1998):

$$\frac{dS_{xx}}{dx} + \rho g h \frac{d\zeta}{dx} = 0 \tag{4-13}$$

In which h is the total water depth and η is the time-averaged value of the elevation of the sea surface. S_{xx} can be calculated with:

$$S_{xx} = (2n - 0.5)E \tag{4-14}$$

in which

$$n = 0.5 + \frac{kh}{\sinh(2kh)} \tag{4-15}$$

and

$$E = \frac{1}{8}\rho g H^2 \tag{4-16}$$

in which H is the root mean square value of the wave height

The total water depth, h, taken in equation (4-13) and (4-15) is the water depth resulting from the Flow-computation.

In Figure 4-21 the root-mean-square wave height is drawn:

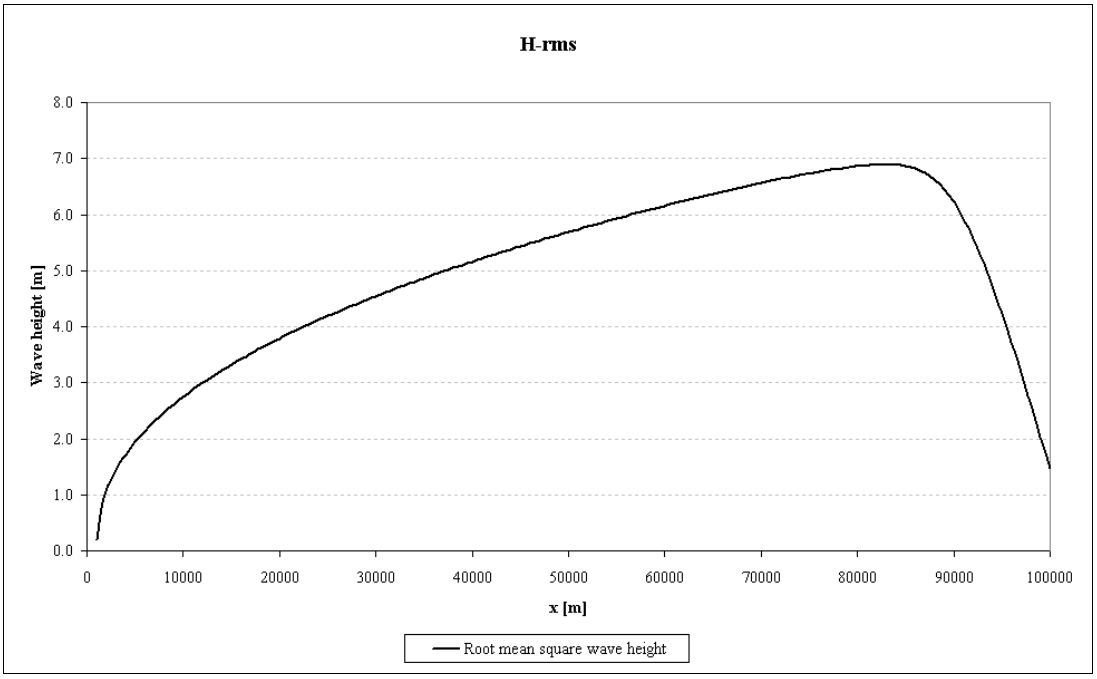

Figure 4-21: Root Mean Square Wave Height for wind blowing 50 m/s over model area onshore

This H_{rms}, computed by the Delft3d-Wave module, is used in equation (4-16). The onshore flux of onshore momentum, S_{xx}, increases due to the fact that the wave height is increasing too. The wave height increases because of the effect of shoaling at the breaker zone and because of the wind that is forcing on the waves over a larger distance (mainly). At the start the wave height is far too small for real situations. When having these circumstances, so a wind speed of 50 m/s, then the waves that travel into the computational area, are a few metres high. However, the radiation stress only plays a role there, where dissipation takes place and that is mainly in the breaker zone.
Assuming an initial wave height of 4 metres at the open boundary, some more dissipation would occur due to whitecapping in the area offshore from the breaker zone. However, the depth at this location is that large that the role of it is not important.
In Figure 4-22, a comparison is made between the wave force taken into account in Delft3D and the wave force calculated following equation (4-17):

$$F_x = \frac{dS_{xx}}{dx} + \frac{dS_{xy}}{dy} \tag{4-17}$$

The waves propagate perpendicular to the coast so the onshore flux of longshore momentum is 0 and only S_{xx} of equation (4-17) contributes to the wave force.

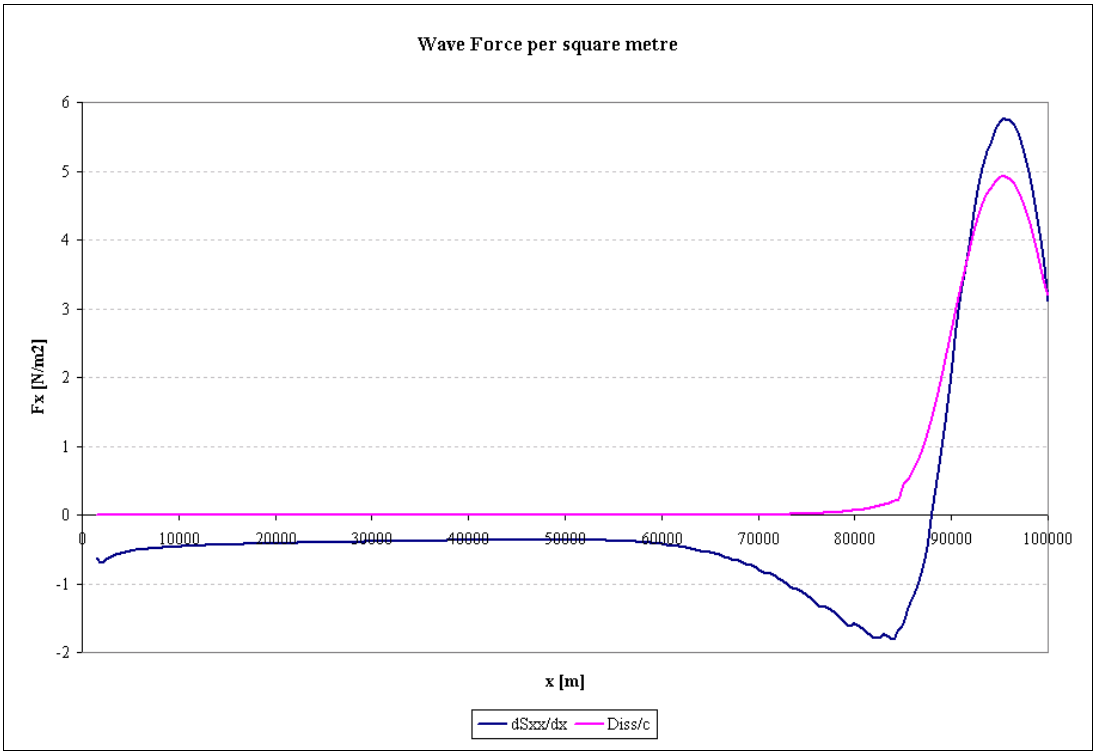

Figure 4-22: Wave Force per square metre

In Figure 4-22 two lines are drawn, giving the wave force per square metre according to the approach of Delft3D and the approach of equation (4-17). The black line, which is the line calculated with equation (4-17) starts increasing from point 85 km. The gradient is larger than the other, light-blue line and therefore, the water level, as can seen in Figure 4-20, is rising much faster than the water level computed by Delft3D. However, the final water level at the shoreline is in both cases the same and is about 18% larger than the one computed by only Flow. The fact that both computations lead to a similar set-up at the shoreline is more likely a co-incidence than logical.

As stated before, the wave set-up drawn in Figure 4-19 by the blue line starts differing from the red line at the 80.000 m point.
Figure 4-23 confirms this. It shows that dissipation starts at 80 km and finishes at the coastline. At this point waves are breaking mainly due to whitecapping and more onshore depth-induced breaking plays a significant role. The wave height decreases and therefore the wave energy, E, which is proportional to the square of the wave height (H_{rms}), decreases too. Equation (4-14) stated that there exist a linear relation between the radiation stress and the wave energy. The radiation stress decreases therefore too and because the gradient $\frac{dS_{xx}}{dx}$ is proportional to the wave force, dissipation can be indicated as the cause of the existing wave force.

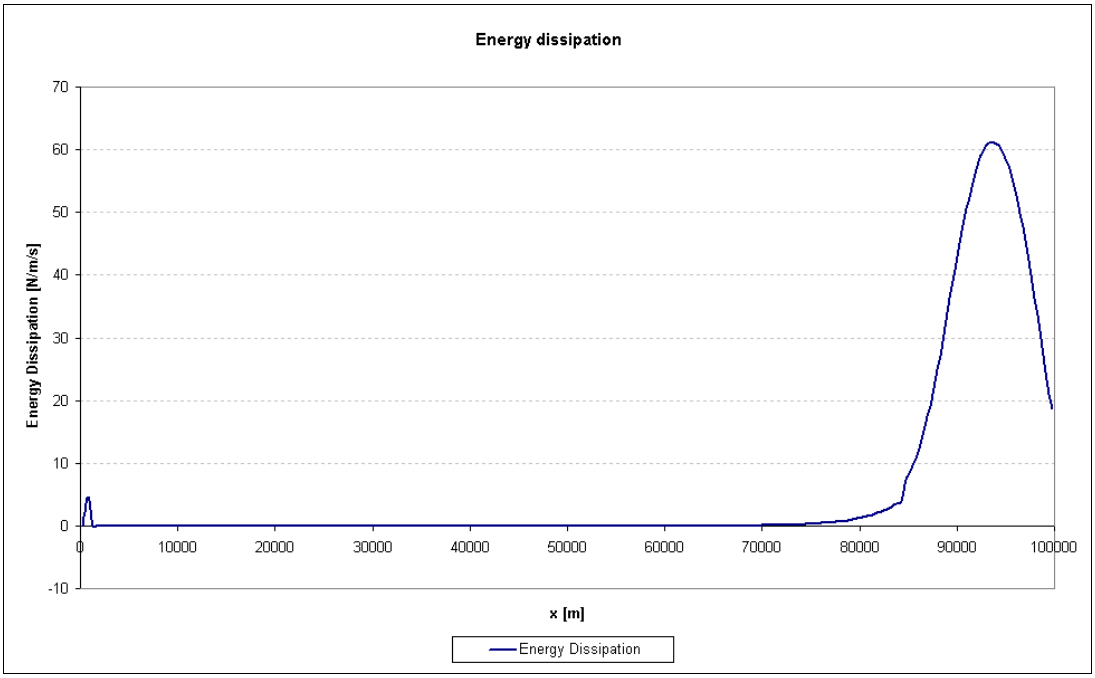

Figure 4-23: Energy Dissipation by bottom friction and wave breaking computed by Delft3D-Wave

As already stated, the computations are done for a x-length of 100000 metres. At this final point, D(x)=0. In real cases, inundation of the land behind would occur. To check whether the results are influenced by land above the reference level, a computation was carried out with a bottom profile, again starting with a depth of 250 metres at x=0 and linearly decreasing to a depth of 0 metres at x=100000 metres and then continuing with the same gradient to x=105000 m, having there a height of about 12,5 metres above the reference.

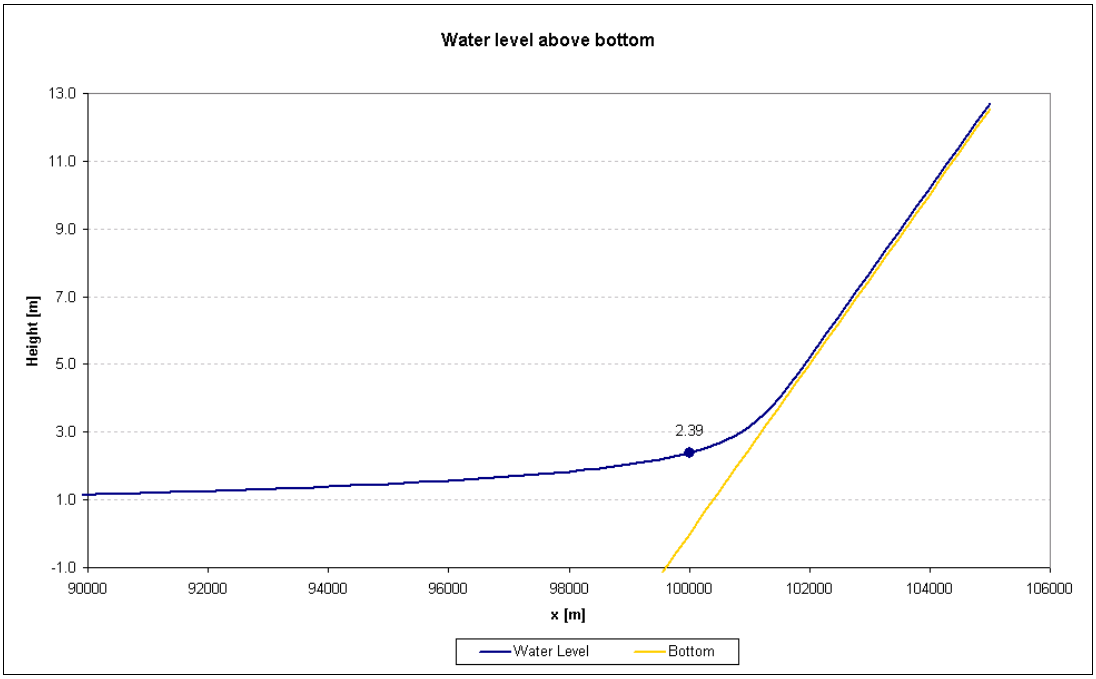

Figure 4-24: Water level for simulation in which hinterland is flooded

The computation was carried out with the same input values as the ones where the results are plotted in Figure 4-19. As can be seen in 4-24 the value of the water level reached at x=100.000 metres has in this extended bottom computation about the same value, namely 2.39 metres. So the Flow computation is not effected by the topography. Flooding of the hinterland will not affect the solution at the shoreline for this sustained forcing and steady state case.
This is also logical when knowing that Delft3D starts its calculations at the offshore boundary and computes from there till the land boundary. “It does not know” what exist at the end and when looking at the amount of water and comparing it to the amount that already is placed on top of the undisturbed water level, this extra piece of water is negligible. Water levels are thus the same.

4.6 Dependence of the wave set-up on the drag coefficient

In paragraph 4.3 it is indicated that the magnitude of the storm surge depends on the drag coefficient which is used. For the value of this drag coefficient several considerations are made by researchers as described in paragraph 2.4. We will have a closer look at the dependence of the increase of the water level at the shoreline on the drag coefficient.

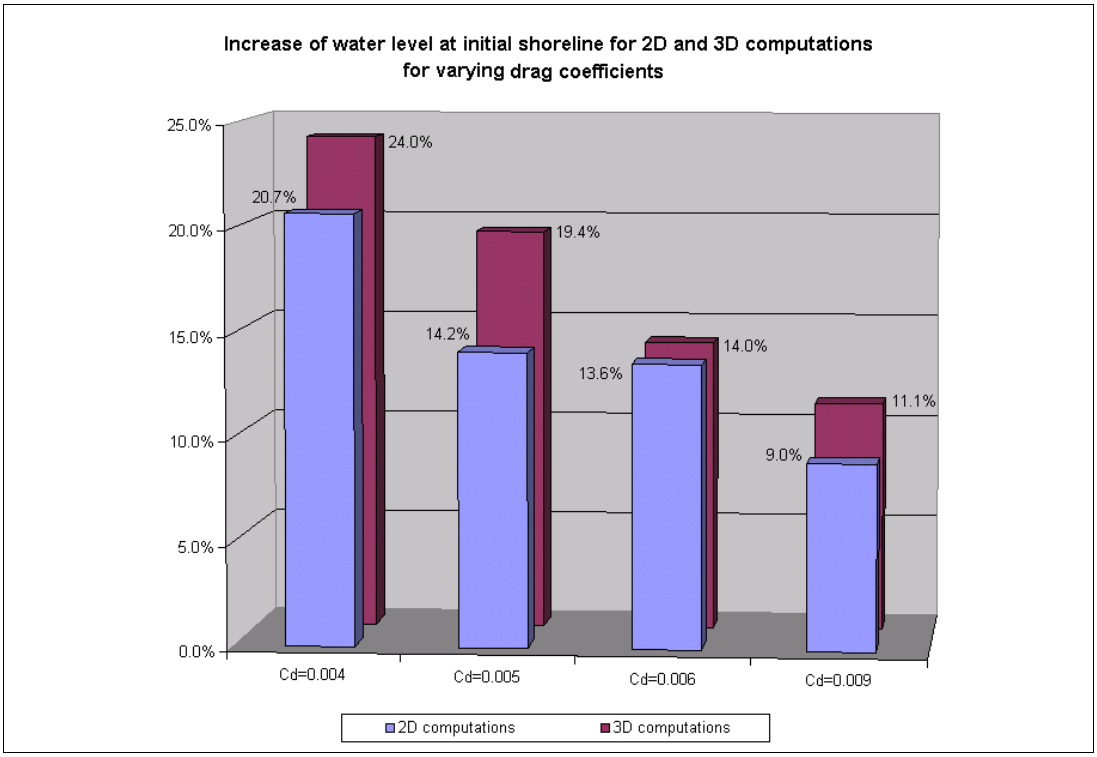

Figure 4-25: Relative increase of the water level by the influence of waves for several computations

Several computations have been carried out in which the drag coefficient was varied. Values of 0.004, 0.005, 0.006 and 0.009 have been taken and these have been put into 2D and 3D model runs. In figure 4-25 and 4-26 results of these computations are drawn. In figure 4-25, the bars at the front represent the increase of the water level at the initial shoreline for the 2D computations as a result of adding waves. The bars at the back represent the water level for the 3D computations. In this figure it is easily seen that the maximum increase of the water level at the shoreline occurs for the lowest value of the drag coefficient. This can be explained by the fact that larger drag coefficients generate a larger surge. The water depth is therefore larger and that means that fewer waves will break and so less dissipation will occur. Hence, the radiation stress that is determined by the dissipation divided by the wave velocity is less than for computations with smaller values of the drag coefficient. Even more, the wave velocity is larger in deeper water and reduces therewith the radiation stress term as well.

A second conclusion can be drawn from figure 4-25 too. The effect of incorporating waves in the model is larger for 3D computations than for 2D computations. This can be explained by knowing that the orbital motion of waves increases the bed stress. In this two-dimensional case, no flow velocities will remain, but in the three-dimensional case the bottom is forced by a flow in the offshore direction. Hence a bottom shear force acts in the opposite direction and together with the wind forcing a larger surge is generated.

The water level at the shoreline is important when looking to flooding. In figure 4-26, four of the storm surge levels of the computations are depicted. Of interest is thus the water level at the shoreline, x=100 km. The black and the blue line are levels in which just wind friction is accounted for. The yellow and red line are storm surge levels in which the influence of waves is included too. From this figure it is seen that the computation carried out with a

drag coefficient of 0.0050 and not taking the waves into account results in the same water level at the initial shoreline as the computation in which a drag coefficient of 0.0040 is taken and in which the influence of waves is included. The same applies for the computation with a drag coefficient of 0.0060 and where no waves are included, and the computation with a drag coefficient of 0.0050 in where the influence of the waves is accounted for. So, wave-induced set-up can be parameterised by increasing the drag coefficient.

The importance of both the drag coefficient as the influence of waves is shown by computations with the simplified model. The next paragraph will deal with the influence of the grid size when focussing on the influence of waves. In chapter 5 a case study on the influence of waves will be made to investigate whether the conclusions drawn above are still valid in the case study.

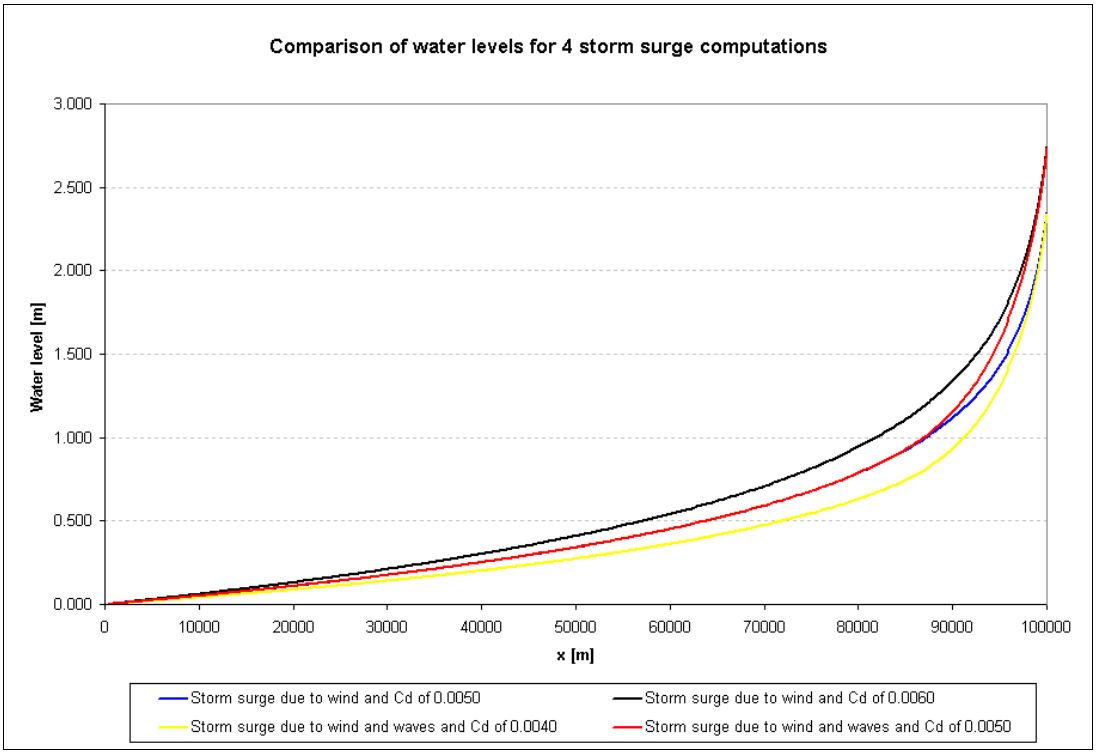

Figure 4-26: Water levels along the x-axis for 4 computations; 2 computations with wind and wave forcing and 2 computations with just wind forcing.

4.7 Sensitivity analysis

In this paragraph, the influence of the grid size and the number of layers in the vertical and their influence on the wave set-up will be examined. Three different grid sizes have been taken, 2000x2000, 1000x1000 and 250x250 metres, the one which was already used earlier in the model. For the depth 5 different cases have been carried out, 1 layer (2D-model) and 2, 3, 10 and 20 layers, all 3D models.
In figure 4-27, the water levels at the initial shoreline are plotted for each case. The front row of bars represents the cases with the largest grid size, the second row represents the cases with a grid size of 1000x1000 metres and the back row represents the cases with the finest grid size. From left to right the bars represent the cases for respectively, 1, 2, 3, 10 and 20 layers.

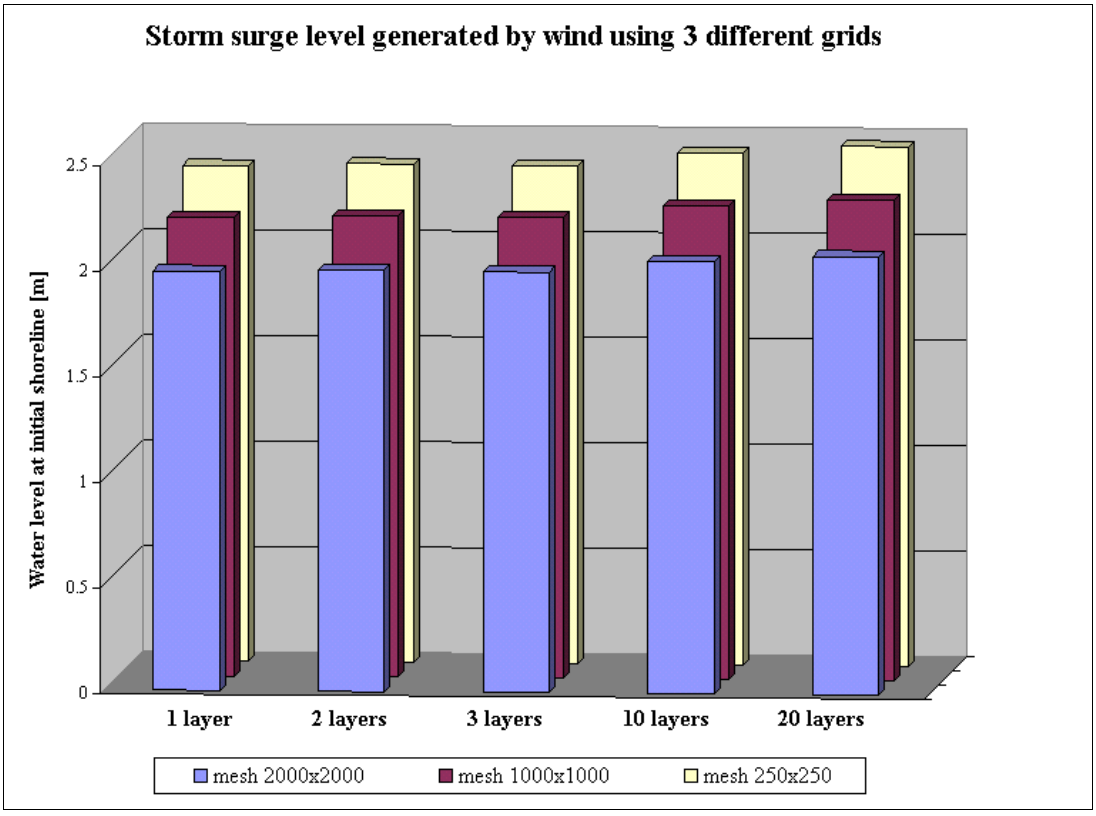

Figure 4-27: Water levels at the shoreline; variation in grid size and in number of layers

In this figure it is obvious that for all 2D and 3D model runs, the runs with the finest grid size generate the largest surge. Convergence plays a role in here, as was already stated in paragraph 4.2.6.

The influence of the number of layers in the vertical is again plotted in figure 4-28. Here it is clearly visible that an increase of layers results into a larger surge. This is most apparent for the third and the fourth bar in which the number of layers increases from three to ten.

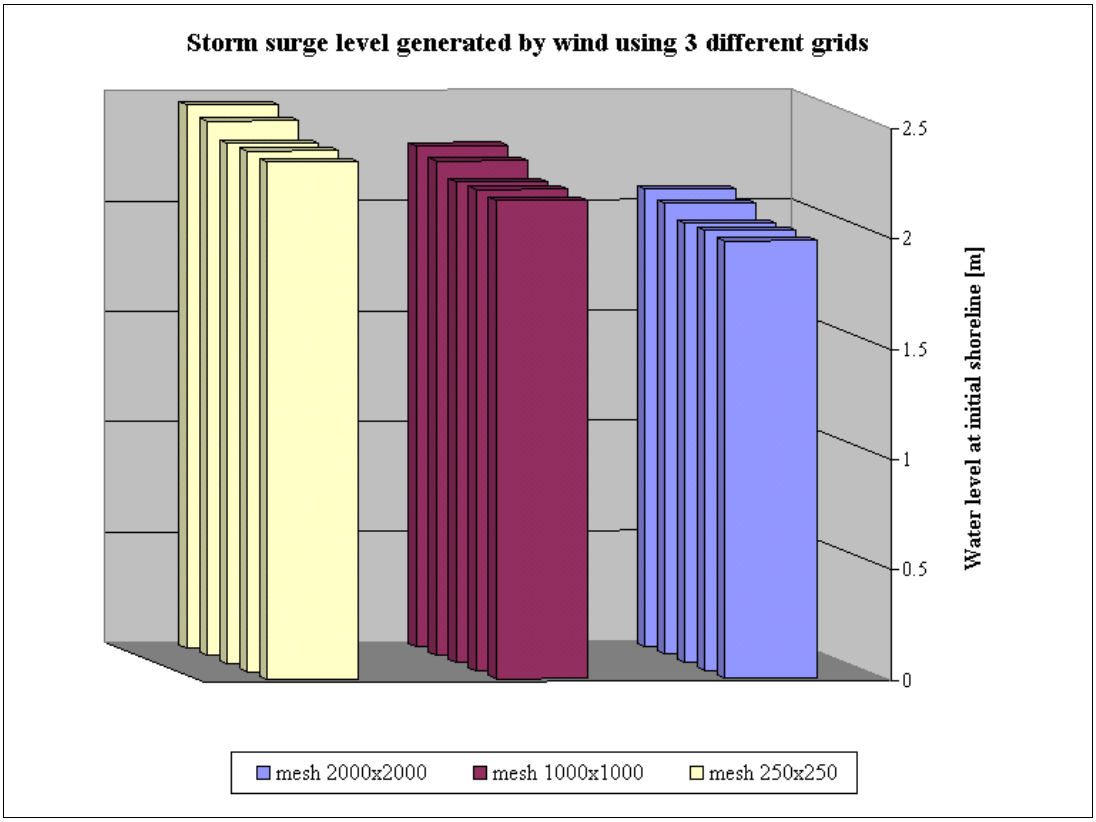

Figure 4-28: Water levels at the shoreline; increase of level due to enlarging of number of layers for the depth

In Figure 4-29, the relative increase comparing to the initial rise caused by only the wind is plotted with bars for each case. Two conclusions can be drawn from this figure: The relative increase of the water level due to influences of waves is not really dependent on the grid size taken and an increase of the number of layers results in a larger wave set-up. This latter can be explained by the fact that when using more layers for the depth, a better discription of the flow conditions at the bottom and therewith a more accurate bottom friction can be gained. Especially the case in which a fine mesh is used, 250x250 metres, shows that for having 10 layers in the vertical the relative increase of the storm surge level due to waves is added with another 3 percent, getting an almost 20% rise.
Athough from figure 4-29 for all the cases the conclusion can be drawn, namely an increase of the number of layers in the vertical will positively enlarge the storm surge level, a high resolution of the grid is however still more significant in determing the storm surge level as figure 4-27 showed.

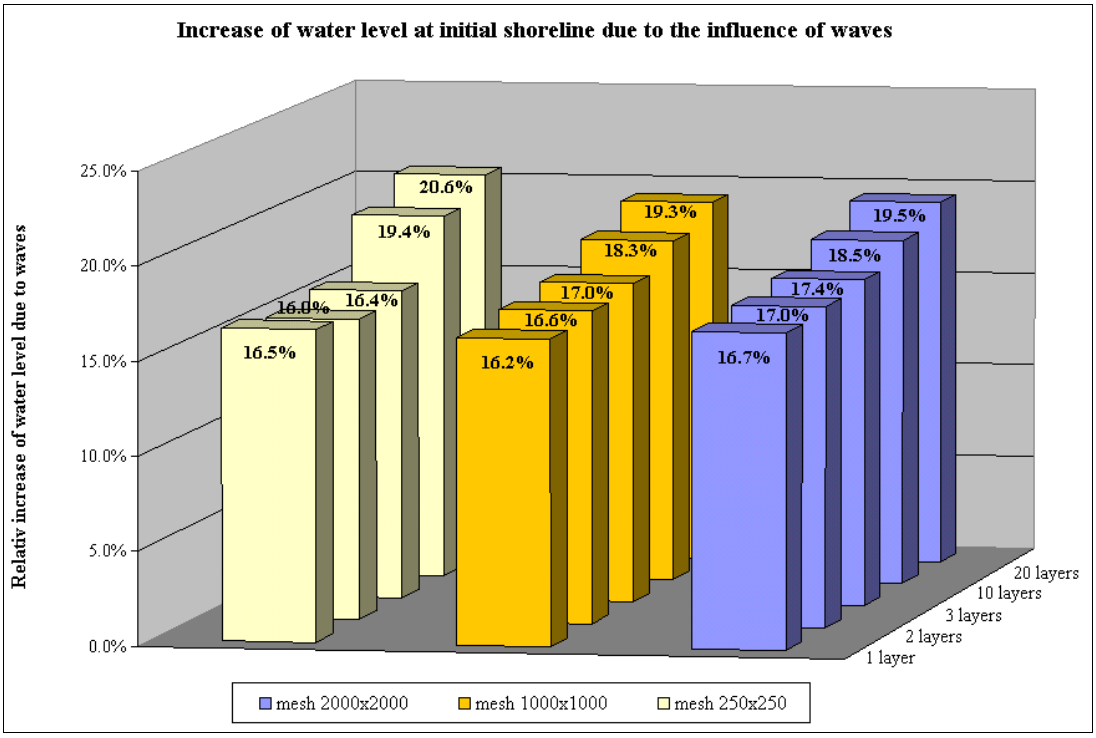

Figure 4-29: Relative increase of water level due to waves for several computations by varying the spatial and vertical resolution

4.8 Conclusions

- Modelled wind set-up is influenced by the grid resolution
- Modelled wind set-up is influenced by the bottom profile
- Modelled wind set-up is influenced by the drag coefficient
- Influence of waves plays a role near the shoreline
- The increase of the water level due to waves near the shoreline is significant
- When varying the drag coefficient and retaining the same wind speed, the lowest drag coefficient results in the largest relative wave set-up
- The relative wave set-up is not influenced by the grid resolution of the model
- Enlarging of the number of layers in the vertical (depth) results in a better description of the bed shear stress and induces therewith a larger set-up.

5 Case Study

5.1 Introduction

The coastline of the Andhra Pradesh is one of the most cyclone-prone areas in India. Delft Hydraulics got an assignment to develop a storm surge model for this area. They first developed an accurate tidal model for the Bay of Bengal (Van Holland et al., 2000). The design of the model grid and the schematisation of the bottom topography were the most important activities for the hydrodynamic model set-up. Later on the computational grid was extended with at least 60 km along the coast in order to assess the inundated area during cyclone events.
Since most of the cyclones in this area originate in the Andaman Sea before they start moving towards the Indian or Bangladesh coast, this sea was incorporated into the model.

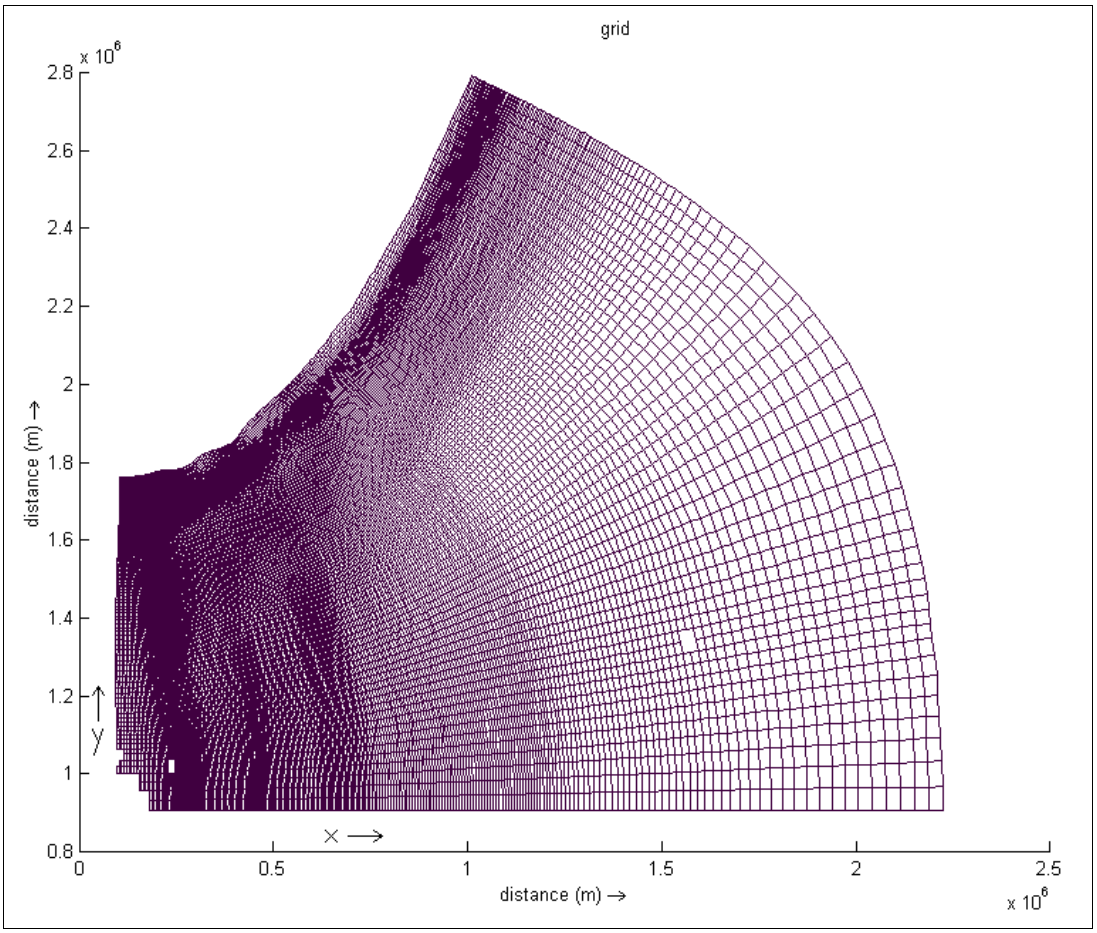

Figure 5-1: Grid of computational area

In Figure 5-1, the outline computational grid is drawn. The number of grid cells in this grid is 260x136 whereby the minimum grid sizes are 3.5 km and 1.5 km in the x- and y-direction. This high resolution is near the deltas of the Andhra Pradesh.

The Bay of Bengal is a very deep basin. The southern parts are over 3000-4000 metres deep. Going north the water depth gradually decreases and the rivers Ganges, Yamuna and Bramhaputra discharge here into the bay. The eastern and the western side of the basin are characterised by very steep slopes. The coastal shelf is narrow and relatively shallow. In the north, the coastline is, due to the big rivers a large river delta. The coastal shelf is much larger here and still relative shallow.

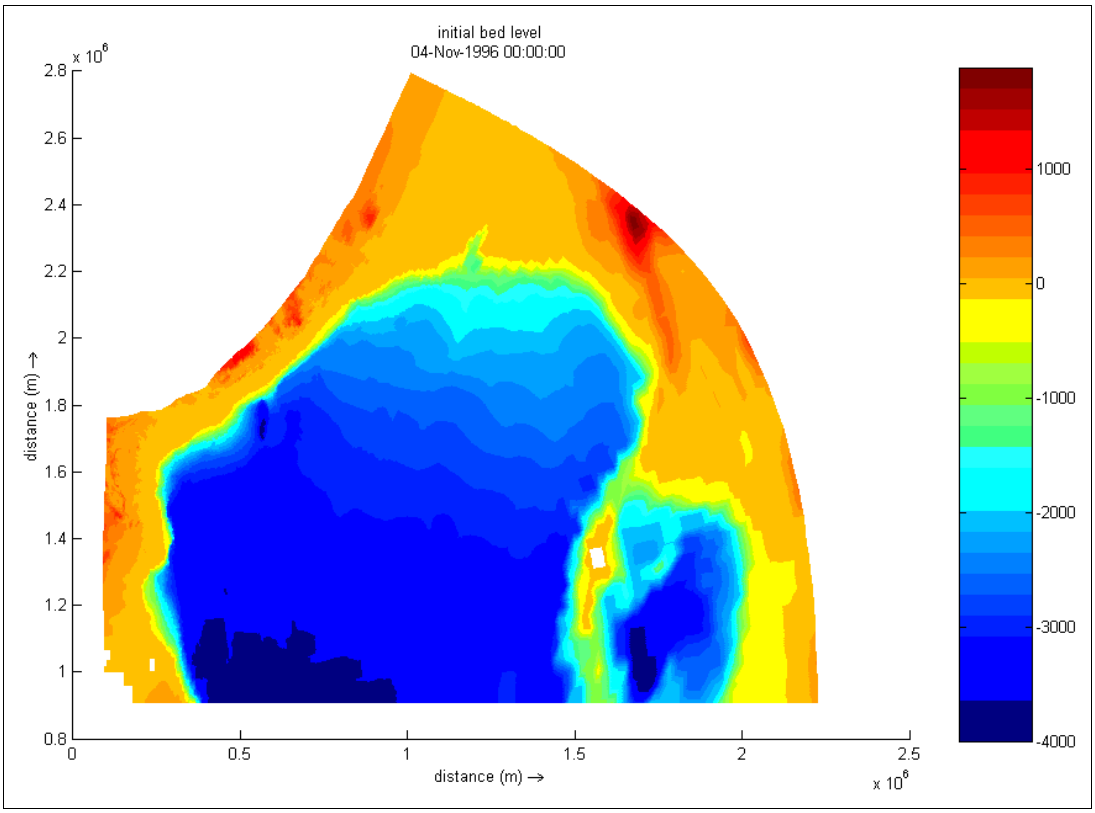

Figure 5-2: Schematic bottom profile of Bay of Bengal

At the open ocean boundary, tidal boundary conditions are set. The amplitudes and phases of the tidal constituents M_2, S_2, N_2, O_1 and K_1 have been prescribed in this boundary condition. The model subsequently was also applied for the surge computations.

In the model, the relation between the drag coefficient and the wind speed is described by the following formulation:

$$C_d = \begin{cases} 0.0025 + 0.0065w & \text{for w} \le 100 \text{ m/s} \\ 0.009 & \text{for w} > 100 \text{ m/s} \end{cases} \qquad (5\text{-}1)$$

in which w (m/s) is the wind speed.

The wind field consists of cyclonic winds superimposed on an overall background wind. The background wind is derived from Numerical Weather Prediction models and the cyclonic wind is generated with the program WES (Wind Enhanced Scheme). This program

computes surface winds and pressures around the specified location of the cyclone. More details about this program can be found in (Vatvani et al, 2001).

5.2 Approach

For this case study, two cyclones have been prepared with the programme WES, both based by prescribed maximum wind speed and pressure drop in the cyclone eye, which struck the Andhra Pradesh coast on November 1996. These cyclones propagate in a direct line towards the coast. Their maximum wind speed lies near 50 m/s. Their radius is 500 km and they do not weaken or intensify during their propagation. Several variants will be examined. As the original model is two-dimensional, a comparison will be made between two- and three-dimensional model runs. Moreover the path they follow will be alternated. Next to the cyclones, which will propagate towards Andhra Pradesh, a second path towards the Ganges delta in the north will be set as input, see figure C-1 in appendix C.1

For comparing the influence of waves on the storm surge level, first a computation has been carried out with Delft3D-Flow. No waves are incorporated in the model. This simulation lasts for three days, because the November-1996-Cyclone, which hit the Andhra Pradesh coast, is taken as input.

For taking the influences of waves into account, the simulation is separated into parts of two hours. A good interaction with the tide is then still possible. After every two hours of simulation, current, water level and bottom parameters of the flow simulation are taken next to the wind as input for the wave-simulation. The wind input does not change for the wave simulation. The output of this wave simulation is then taken as input for the flow simulation for the next two hours. By repeating this interaction, three days are simulated. The wave simulation is carried out by SWAN. Appendix B shows the batch files which are used for one of these computations. One significant limitation of this procedure is the fact that every two hours SWAN starts its simulation without taking the wave parameters from the previous simulation into account. For example, waves that are forced by wind blowing continuously into one direction can only grow for two hours. The next time that SWAN starts its computation, these waves are reset to the initial values. This will probably decrease the influence of waves, but different cases will be carried out to see whether this limitation is significant or not.

5.3 Cases

In Chapter 4, it was shown that the resolution near the coast is significant for the wind set-up but it was not significant for the wave set-up. The grid, which was made for the Andhra Pradesh Project, has in this case study a high resolution near Andhra Pradesh, but the grid size overhear is still about 5 km x 2 km large. Focussing on the Ganges Delta, the grid size is about 10 km x 50 km.

Four cases have been investigated. Case 1 is the model in which the cyclone propagates towards the Andhra Pradesh coast. A two dimensional model is used. Case 2 is the model in which the cyclone still propagates towards the Andhra Pradesh coast, but for which a three-dimensional model is used. The depth is divided in ten σ -layers. The k-ε turbulence model is used for describing the generated turbulence. In Case 3, the cyclone does not propagate

towards the Andhra Pradesh coast, but towards the Ganges Delta. For Case 3 a two-dimensional model is used and for Case 4 a three-dimensional model and also the depth describing by ten σ -layers.

5.3.1 2D Andhra Pradesh

For the Andhra Pradesh case several stations were set in the model to observe several time-related phenomena like for instance the water level. Figures C-4 through C-13 of Appendix C.2 show the results for ten observation stations. The ten stations, which are numbered in Figure C-2 show the water level record of the two computations, whereby the black dashed line represents the water level without wave influences and the black solid line represents the water level including the wave influences. This latter one shows a very irregular pattern for the time before the peak surge arrives in most of the plots. When the peak surge arises at the coast, both lines are nearly following the same pattern. Only the top levels differ by a few centimetres. Only station 1, which lies a bit more to the west of the place where the cyclone makes landfall, registered a higher water level due to wave influences. Stations 5 through 8 show clearly a lower water level of about 10 centimetres as maximum value. The increase of the bottom friction might be an explanation for this. A bulk of water around the cyclone eye propagates namely to the coast and experiences a larger friction which could reduce the maximum water level set-up.
A third aspect which is visible in these figures is the fact that the peak-surge-time is getting earlier when going from station 1 to station 10, so from left to right along the coastline. The peak-surge-time is for station 1 at 16:00 and for station 6 at 11:00, so five hours earlier. This is caused by the wind direction, which is pointing offshore for station 1 and resulting in a set-down when the cyclone almost makes landfall. Just when the cyclone eye is onshore, the wind points towards the coast and forces a set-up. Stations 5 through 8 have their maximum surge almost exactly when the cyclones makes landfall. The peak surge, is here mostly formed by the maximum wind speeds, which appear near the cyclone eye.

In appendix C.4, nine plots of the water level difference between the computations with and without waves are drawn in figures C-21 through C-29. In these plots, the wave vectors are drawn as well. There are two areas which turn blue and yellow during the time. These spots are located at (460, 1820) and (600, 1930). These two areas are most remarkable in this overview of the Andhra Pradesh. The change in water level is about 15 centimetres, either plus or minus compared to the water level generated without waves. However, this difference is caused by the oscillation which was already discussed in the previous paragraph and hence, it is not a general set-up or set-down, but rather a coincidence by plotting it this way. These overviews of the water level differences confirm that by including the waves the water level is only slightly changed.
Appendix C.5 shows figures of the root-mean-square wave height and the dissipation generated for the Andhra Pradesh case. Figures C-30 through C-47 show that the maximum wave height, from the start till 20 hours later (07/11 06:00), is about eight metres and then decreases quite fast towards seven, four and three metres maximum in chronological order. As can be seen with the iso-surfaces of same wave height, the wave height for a specified location increases till figure C-42 (07/11 10:00) and from that time it decreases. The waves on the right side of the cyclone would have been larger if the wave computation could have been carried out with non-stationary wind input and without restarting these computations

every two hours. More energy would have been transferred to the existing waves, resulting in larger waves.

The decrease of wave height, caused by the limiting depth, should induce wave forces, which would normally generate a wave set-up. The lack of dissipation, which is the main source for these wave forces results in, that no wave set-up is seen in the plots of appendix C.4. The reason for this could thus be the restarting procedure due to the requirement of stationary wind input. The lack of interaction between two successive wave computations is a limitation for wave growth, which resulted thus in little dissipation.

In the next three cases the above-described situation is also the case. In none of the four cases significant wave set-up is visible. In the description of the other three cases, the differences between them will be emphasised.

5.3.2 3D Andhra Pradesh

As stated in the previous paragraph, the 3D Andhra Pradesh case did not have any significant influence on the generation of wave set-up. Appendix C.6 shows the results of the incorporation of waves in the computation. These figures, C-48 through C-56, are almost identical with the ones of the 2D case in appendix C.4. Only figure C-54 and C-55 differ in one area, namely at the point where the cyclone makes landfall. This is also visible in figure C-8 of appendix C.2, where the 3D water levels are plotted with the 2D water levels recorded by the observation stations. Station 5 lies namely on the spot where the cyclone makes landfall. At 10:00 h on the 7th of November, the rise in surge stops almost straight away and within half an hour it starts increasing again very quickly for the computation without wave effects. Even more at time 14:00 h, it is visible that the two lines differ about 0.4 metres, in where the flow computation gives the higher values. This might be a huge difference, but it occurs at a very unimportant stage, namely at a stage in which the surge has already decreased to almost its initial state value. So it is not significant for flood prediction.

Focussing on the differences between the 2D and the 3D cases, table 5-1 is the result. In here, the maximum values of the root-mean-square wave height and the maximum dissipation are shown for each time a plot is generated. The plots can be found in appendix C.4 and C.6.

Table 5-1: Comparison of maximum Hrms and Dissipation for 2D and 3D Andhra Pradesh computations

2D Andhra Pradesh				**3D Andhra Pradesh**	
max. H_{rms} (m)	$Dissipation_{max}$ ($Nm/s/m^2$)	Date	Time	max. H_{rms} (m)	$Dissipation_{max}$ ($Nm/s/m^2$)
7.5-8.0	5-10	06-11-1996	10:00	8.0-8.5	5-10
8.0-8.5	20-50	06-11-1996	14:00	7.5-8.0	10-20
8.0-8.5	20-50	06-11-1996	18:00	7.5-8.0	10-20
8.0-8.5	20-50	06-11-1996	22:00	7.5-8.0	20-50
8.0-8.5	20-50	07-11-1996	02:00	7.5-8.0	20-50
8.0-8.5	20-50	07-11-1996	06:00	8.5-9.0	20-50
7.0-7.5	50-100	07-11-1996	10:00	7.0-7.5	50-100
4.0-4.5	20-50	07-11-1996	14:00	3.5-4.0	10-20
2.5-3.0	2-5	07-11-1996	18:00	2.5-3.0	2-5

As can be seen in this table, there is hardly any difference noticeable. The maximum root-mean-square wave height might be a bit larger in the two-dimensional case for when the cyclone is still in deep water, the overall wave heights however, drawn by the iso-surfaces, are the same for both the two- and three-dimensional case. So only in the eye of the cyclone, the wave height is about half a metre larger. The figures which show the dissipation are almost identical. The 2D computation is therefore already accurate enough to predict storm surges, and 3D computations only enlarge the computational time and are therefore less pratical for flood prediction.

5.3.3 2D Ganges Delta

In figures C-75 through C-83 nine stages of the wave directions caused by the cyclonic wind are drawn. Moreover, the differences in water level caused by these waves are drawn in here as well. The first plot is from the 6th of November at 02:00 h. Every four hours from that time another plot is drawn. The final plot is when the cyclone has made landfall and looses its strength.
All of these nine plots show that the water level is changed by the influences of waves, but not significantly. The water level is generally changed by 10 centimetres, either additional to the 'initial' storm surge level caused by only the wind or subtracted from it. Especially when the cyclone is in the neighbourhood of the coast this difference is observed. When the cyclone is still farther away, some spots are decreased by about 20 centimetres and others are increased by 30 centimetres, figure C-75. However, these changes might be significant at that time, the maximum surge is still about 14 hours later, as can be seen in figures C-14 through C-20. These figures show the water level as it is recorded at a specified station near the initial coastline. Figure C-3 shows these specified stations in the model grid together with the depth isolines in the north of the Bay of Bengal. These stations cover together about 350 km of the coast. Most extreme values have to be found here, because of the landfall of the cyclone in this area. Station 1 lies exactly on the path of the cyclone and at this station, the peak surge is immediately followed by a drop of four metres. Station 2, situated some more to west of the cyclone path records the largest set-down of about three metres. For station 3, the same can be said as station 1. The surge is immediately followed by a drop of almost five metres. This station lies on the cyclone path as well. Station 4 registered the largest set-up, 3.7 metres. Station 5, which lies near a bund, records the most variable values for the 4 variants. Again, when the maximum surge appears, the influence of the waves is just restricted to about 10 centimetres extra rise. The influence of the cyclone event is not visible anymore for stations 6 and 7. Generally, for the 2D Ganges Delta case, one can say that the waves do not have any influence on the peak storm surge level.

Focussing on the dissipation in the onshore area in figure C-84 through C-101 of appendix C.9, the shallow water depth has lead to a wider area where dissipation occurs than in the Andhra Pradesh case. However, the magnitude of this dissipation is primarily less than 20 J/s/m^2, which is far too less to generate a significant wave set-up. The low resolution in the Ganges Delta could be a reason for this too.
In the same appendix, the root mean square wave height is depicted for all nine stages. The main difference between the 2D Andhra Pradesh case and the 2D Ganges Delta case, is that the iso-surface of equal wave height are larger in the Ganges Delta case. So along a much wider coastline large waves can exist. This means that for computations in which for the determination of the dissipation the wave values of the previous computation will be used,

this would lead to much more dissipation, and hence, it could induce a significant wave set-up.

5.3.4 3D Ganges Delta

In the three cases described above, it was shown that there was not enough dissipation in the breaking zone to obtain large wave forces, which would generate a wave set-up. For the three-dimensional Ganges Delta case, SWAN was changed to operate in the third-generation mode. This means mainly that quadruplet interaction was taken into account, which would result in more dissipation. In Appendix C.11, figures C-112 through C-128 show that indeed more dissipation is generated. Already in deep water, around the eye of the cyclone, dissipation takes place and a lot more than described in the previous three cases. However, as can be seen in Appendix C.3 figures C-14 through C-20, the red solid line does hardly differ from the red dashed line, which is the line without the influence of waves. Comparing the 3D case and the 2D case water levels, registered at those stations, hardly any difference is noticed. For the peak surge, only in station 1 and 4 a difference of respectively 10 and 15 centimetres is noticed, however, this is just a four-percent-addition to the 2D-case water level and thus not really significant. For station 3, the opposite can be seen, namely a decrease of 10 centimetres, which is about 4% as well.
Focussing on the whole Ganges Delta, figures C-102 through C-110 of appendix C.10, the water level is changed by the waves just by a few centimetres with about 10 centimetres as maximum either plus or minus. For this case again, no significant difference is found between either computations incorporating the waves and disregarding the waves.
Like table 5-1, table 5-2 gives the difference between the 2D and 3D Ganges Delta cases. As was already stated, the 3D case would, due to taking the quadruplets into account within SWAN, generate more dissipation. Especially when the cyclone propagates into the onshore area on the 6th of November 22:00 h, the dissipation is fifty times larger than in the 2D case. For the root-mean-square wave height, it can be said that the maximum value differs about half a metre for the first twenty hours, but then when the cyclone arrives in the onshore area, the maximum wave height for the 3D case is far less, about 1,5 metres, in comparison with the 2D case.

Table 5-2: Comparison of maximum Hrms and Dissipation for 2D and 3D Ganges Delta computations

2D Ganges Delta				**3D Ganges Delta**	
max. H_{rms} (m)	$Dissipation_{max}$ (Nm/s/m^2)	Date	Time	max. H_{rms} (m)	$Dissipation_{max}$ (Nm/s/m^2)
5.5-6.0	2-5	06-11-1996	02:00	6.0-6.5	20-50
6.0-6.5	2-5	06-11-1996	06:00	6.0-6.5	20-50
6.5-7.0	20	06-11-1996	10:00	6.5-7.0	20-50
7.0-7.5	2-5	06-11-1996	14:00	7.5-8.0	50-100
7.0-7.5	10-20	06-11-1996	18:00	7.5-8.0	20-50
7.5-8.0	10-20	06-11-1996	22:00	7.0-7.5	500-1000
5.5-6.0	10-20	07-11-1996	02:00	4.0-4.5	200-500
3.5-4.0	5-10	07-11-1996	06:00	2.5-3.0	10-20
2.0-2.5	5-10	07-11-1996	10:00	1.5-2.0	2-5

This fourth case shows that a lot of dissipation is generated at the time that the cyclone arrives onshore. It might be the coarse resolution in this area that is responsible for the lack of wave set-up. Although in the schematic experiments hardly any difference was found in

the wave set-up by increasing the grid size, this might be of influence in this real case situation. The wave set-up is most of the time captured within a three-kilometres-zone starting from the coastline. The wave set-up is in this case covered by just one grid cell. Although in the experiments two kilometres large grid cells lead to a good description of the wave set-up, and so the wave set-up was also captured within 1,5 grid cell, this could be too coarse in a real case situation where tide and bottom changes play a part.

5.4 Input changes

In paragraph 5.3, it was stated that in none of the cases waves had a significant influence in the set-up. Trying to find a reason for this failure in wave set-up, the wind input for the above cases is compared with the wind input in the experiments. In the experiments a wind of 50 m/s is taken. The wind profile for the cases is drawn in figure 5-3. Here it is seen that the wind decreases very fast with increasing radius. So, at distance from the eye, the wind cannot generate large waves. So a different profile, profile B in figure 5-3, is taken as input to verify if this would result in a significant wave set-up. This new wind profile can generate larger waves and can therefore lead to some more dissipation near the coastline. Although this cyclone may not be a representative one, it is only used for verification.

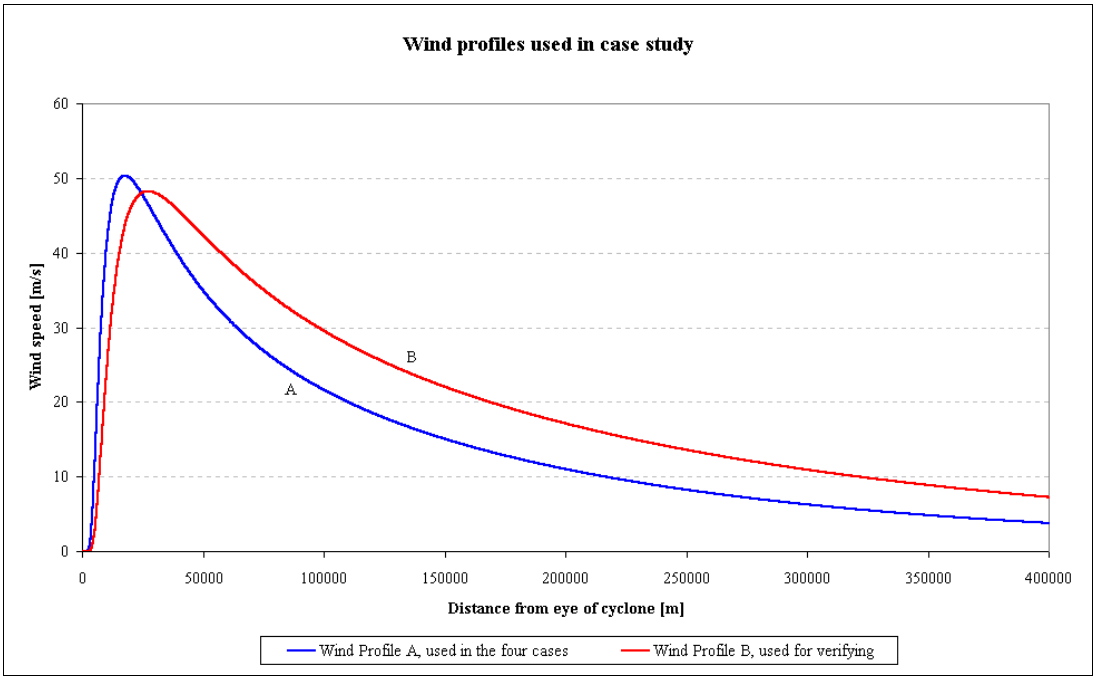

Figure 5-3: Cyclone wind profiles used in case study and for verifying

In Figure C-129 and C-130, two different plots are shown. Figure C-129 shows the water level as registered in station 6 at Andhra Pradesh. Again, it is obvious that the waves did not affect the water level much. Figure C-130 confirms the lack of wave set-up, when using wind profile B for the whole Andhra Pradesh area. However, the change in wind profile did lead to a much larger surge than for the 2D Andhra Pradesh case (Figure C-9). Stronger winds at distance from the eye of the cyclone are thus significant in the storm surge computations.

Trying to investigate whether the refining of the grid near the coastline would give other results, the limitations of the program WES came across. The 'stack space' used by the program was overflown due to the increase of grid cells. Wind input files could not be created anymore and a successful test was therefore excluded.

5.5 Conclusions

- The influence of waves on storm surges is not shown by one of the four cases.
- The three-dimensional cases do not generate more accurate values for the storm surge water levels.
- The maximum root-mean-square wave height is slightly higher for the Andhra Pradesh case than for the Ganges Delta case.
- The magnitude of dissipation is larger for the Andhra Pradesh cases when SWAN computes in the second-generation mode than for the Ganges Delta cases.
- The dissipation is much larger when SWAN computes in third-generation mode.
- Changing the wind profile to include larger winds at distance does not lead to wave-induced set-up either.
- Changing the wind profile did lead to major change in the results in terms of the peak surge.
- The time when the peak surge occurs is getting later when going from places on the right side of the cyclone towards the left side of the cyclone (Northern Hemisphere).
- The coarse resolution could be a reason for the lack of wave set-up.
- The lack of wave data from the previous run is harming the magnitude of energy dissipation.
- The wave-flow interaction, which required stationary wind input in the wave model, has negatively influenced the storm surge computation. In the onshore area, the energy dissipation is far too less as a result of the stationary wind input.

6 Conclusions and Recommendations

6.1 Introduction

In this thesis, a closer look has been taken at storm surges induced by tropical cyclones. A literature survey showed that existing storm surge models do not incorporate the effect of waves in their storm surge predictions. The impression exists that these wave influences cause surge predictions to be not always accurate. This impression has therefore led to a research on the influences of waves in storm surge prediction models. In the second part of this thesis the influence of waves is included in a simulation model. First an experiment has been carried out, using a model in which a lot of simplifications were applied and finally a realistic test was carried out with the storm surge model that was developed for the Andhra Pradesh coast in India.

6.2 Conclusions

From this study the following conclusions can be drawn:

- In the schematic experiments, wave set-up is significant in the storm surge level at the coastline. All computations resulted in about a 15% rise in surge level compared to the surge, which was generated without the effects of waves.

- Three-dimensional storm surge computations, which incorporated wave influences, have shown to generate slightly more wave set-up than the two-dimensional computations in the schematic experiments.

- Wave-induced set-up can be parameterised by increasing the drag coefficient.

- The realistic storm surge computations carried out for the Bay of Bengal have not shown any difference in storm surge level caused by the incorporation of waves in the model for either the Andhra Pradesh or the Ganges Delta. Altering between two-dimensional and three-dimensional storm surge computations including the waves by changing the number of layers in the vertical, did not result in a difference in storm surge level either.

- Three-dimensional computations carried out for the Andhra Pradesh and the Ganges Delta without taking the waves into account, did not show any difference in storm surge level when comparing it to two-dimensional computations for these areas.

6.3 Recommendations

- The small dissipation was mentioned as one of the reasons, because depth-induced breaking of waves generates dissipation, which is the main source for generating a wave set-up. The results of the case study show that by incorporating a wave model that can only take stationary wind as input does not lead to any significant wave set-up. To generate more dissipation in the model, Delft3D-Flow should be able to operate with non-stationary wind input in SWAN. SWAN itself is already able to compute with continuously changing wind speed and wind direction, so only the interaction between the two models has to be improved. When this is incorporated into Delft3D, storm surge computations can be carried out with incorporating wave influences, which then might generate a significant wave set-up.

- Refinement of the Bay of Bengal grid in the onshore zone is necessary for a more accurate computed wave set-up computation. Merging wind on a high-resolution grid has to be made possible within the program WES. Then, little dissipation might already lead to wave set-up. At this moment the coarse resolution can be a reason not to generate wave set-up.

- In paragraph 2.4, it was stated that the drag coefficient is related to the actual sea state. Delft3D-Flow uses however only a wind-drag relationship. By including wave parameters in a relationship for the drag coefficient, this would result in a better description of the actual drag and therewith affect the computational results and probably improve the simulations.

7 References

Battjes, J.A. (1998) *Korte Golven.* Technische Universiteit Delft, Faculteit Civiele Techniek en Geowetenschappen.

Booij, N., & L.H. Holthuijsen (1995). *User manual for the Program HISWA. Prediction of stationary, short-crested waves in shallow water with ambient currents.* Delft University of Technology. Department of Civil Engineering.

Dekker, J. (1995) *Enore Coal Port Project, India. Cyclone Hindcast Study. Report phase I. Part II, Report on numerical modelling*. Delft Hydraulics.

Delft Hydraulics. (1999) *Delft3D-FLOW User Manual*, Version 3.05

Delft Hydraulics. (2000) *Delft3D-WAVE User Manual*, Version 2.00

Dingemans, M.W., A.C. Radder, & H.J. de Vriend (1987). Computation of the driving forces of wave-induced currents. *Coastal Engineering, Vol. 11*.

Ebersole, B.A. (1985) *The Atchafalaya River Delta, Report 8, Numerical Modeling of Hurricane-induced storm surge*. US Army Engineer Waterways Experiment Station, Coastal Engineering Research Center.

Flather, R.A., & H. Khandker (1993) The storm surge problem and possible effects of sea level changes on coastal flooding in the Bay of Bengal. *Climate and sea level change:observations, projections and implications*.pp.229-245.

Flather, Roger A. (1993) A Storm Surge Prediction Model for the Northern Bay of Bengal with Application to the Cyclone Disaster in April 1991. *Journal of Physical Oceanography. Vol. 24*, pp. 172-190.

Holland, G.J. (1980) An analytical model of the wind and pressure profiles in hurricanes. *Monthly Weather Review. Vol. 108*, pp. 1212-1218.

Holthuijsen, L.H. (1999). *Windgolven*. Technische Universiteit Delft, Faculteit Civiele Techniek en Geowetenschappen.

Holthuijsen, L.H., N. Booij, R.C. Ris, IJ.G. Haagsma, A.T.M.M. Kieftenburg, & E.E. Kriezi. (2000). *SWAN Cycle III version 40.11 USER MANUAL (not the short version)*. Electronic version at http://swan.ct.tudelft.nl

Jelesnianski, Chester P., Jye Chen & Wilson A. Shaffer (1992) *SLOSH: Sea, Lake and Overland Surges from Hurricanes*. NOAA Technical Report NWS 48.

Johns, B., & M. Anwar Ali (1980) The numerical modelling of storm surges in the Bay of Bengal. *Quarterly Journal of the Royal Meteorological Society. Vol. 106*, pp. 1-18

Murty, T.S. (1984) *Storm Surges - Meteorological Ocean Tides*. Institute of Ocean Sciences, Department of Fisheries and Oceans, Ottawa.

Murty, T.S., R.A. Flather & R.F. Henry (1986) The storm Surge Problem in the Bay of Bengal. *Progress in Oceanography. Vol. 16*, pp. 195-233.

Van den Boogaard, H.F.P, R.E. Uittenboogaard, & H. Gerritsen (1991*). The dependence of surface drag on waves.* Z462, Delft Hydraulics.

Van Dorn, W.G. (1953). Wind stress on an Artificial Pond. *Journal of Marine Research, Vol. 12*, pp.249-276.

Van Holland, G., D. Vatvani & P.N.M. Shastri. (2000). *Tidal modelling of the Bay of Bengal, A model with high resolution along the Andhra Pradesh coast*. Z2270, Delft Hydraulics.

Vatvani, D., A.V.R.K. Rao, P.D. Namratha, & S. Goodchild (2001) *WES Scientific Document*. Delft Hydraulics.

Appendix A Description of Delft3D-Flow and its interaction with Delft3D-Wave

This appendix gives a more detailed description of Delft3D-Flow, -Wave and the interaction between Wave and Flow. The main aspects are already summarised in Chapter 3. Here, the hydrodynamic equations as they have been programmed in Delft3D are discussed. Subsequently, the boundary conditions and parameterisation of Soulsby for the interaction between wave and current are treated. Then the turbulence closure models, which can be chosen by the user, are discussed. Finally, a more detailed description is given of the dissipation terms in the action balance equation and the formulae for determining the magnitude of the Stokes-drift. Parts of the text in this appendix are taken from the Delft3D-Flow manual.

A.1 Delft3D-Flow

Hydrodynamic equations
In Delft3D-Flow the continuity and momentum equations are formulated in curvilinear co-ordinates. The velocity scale is in the physical space, but the components are perpendicular to the cell faces of the curvilinear grid. The grid transformation introduces curvature terms in the equations of motion. The terms $\sqrt{G_{\xi\eta}}, \sqrt{G_{\eta\xi}}$ are not found in the equations, because Delft3D assumes orthogonality and these cross terms are then equal to zero.
The meaning of the symbols used here in the appendix can be found in Chapter 3, where it is already discussed. Following the Delft3D-Flow manual, the governing equations are written in ξ- and η- co-ordinates instead of x- and y-co-ordinates. The symbol ζ is used for the water elevation.

For depth-averaged flow, the continuity equation yields:

$$\frac{\partial \zeta}{\partial t} + \frac{1}{\sqrt{G_{\xi\xi}}\sqrt{G_{\eta\eta}}} \frac{\partial \left[(D+\zeta) U \sqrt{G_{\eta\eta}} \right]}{\partial \xi} + \frac{1}{\sqrt{G_{\xi\xi}}\sqrt{G_{\eta\eta}}} \frac{\partial \left[(D+\zeta) V \sqrt{G_{\xi\xi}} \right]}{\partial \eta} = Q \qquad \text{(A-1)}$$

with Q [m/s] representing the contributions per unit area due to the discharge or withdrawal of water, evaporation, E [m/s], and precipitation, P [m/s]:

$$Q = h \int_{-1}^{0} \left(q_{in} - q_{out} \right) d\sigma + P - E \qquad \text{(A-2)}$$

with q_{in} and q_{out} the local sources and sinks of water per unit of volume, respectively.

The momentum equations in ξ- and η-direction are given by:

$$\frac{\partial U}{\partial t}+\frac{U}{\sqrt{G_{\xi\xi}}}\frac{\partial U}{\partial \xi}+\frac{V}{\sqrt{G_{\eta\eta}}}\frac{\partial U}{\partial \eta}+\frac{UV}{\sqrt{G_{\xi\xi}}\sqrt{G_{\eta\eta}}}\frac{\partial \sqrt{G_{\xi\xi}}}{\partial \eta}-\frac{V^2}{\sqrt{G_{\xi\xi}}\sqrt{G_{\eta\eta}}}\frac{\partial \sqrt{G_{\eta\eta}}}{\partial \xi} \tag{A-3}$$
$$= fV-\frac{P_\xi}{\rho_0\sqrt{G_{\xi\xi}}}+F_\xi+\frac{gV\sqrt{U^2+V^2}}{C_{2D}^2(D+\zeta)}+M_\xi$$

and

$$\frac{\partial V}{\partial t}+\frac{U}{\sqrt{G_{\xi\xi}}}\frac{\partial V}{\partial \xi}+\frac{V}{\sqrt{G_{\eta\eta}}}\frac{\partial V}{\partial \eta}+\frac{UV}{\sqrt{G_{\xi\xi}}\sqrt{G_{\eta\eta}}}\frac{\partial \sqrt{G_{\eta\eta}}}{\partial \xi}-\frac{U^2}{\sqrt{G_{\xi\xi}}\sqrt{G_{\eta\eta}}}\frac{\partial \sqrt{G_{\xi\xi}}}{\partial \eta} \tag{A-4}$$
$$= -fV-\frac{P_\eta}{\rho_0\sqrt{G_{\eta\eta}}}+F_\eta+\frac{gV\sqrt{U^2+V^2}}{C_{2D}^2(D+\zeta)}+M_\eta$$

In three-dimensional flow the momentum equations in horizontal direction, thus ξ- and η-direction are given by:

$$\frac{\partial u}{\partial t}+\frac{u}{\sqrt{G_{\xi\xi}}}\frac{\partial u}{\partial \xi}+\frac{v}{\sqrt{G_{\eta\eta}}}\frac{\partial u}{\partial \eta}+\frac{uv}{\sqrt{G_{\xi\xi}}\sqrt{G_{\eta\eta}}}\frac{\partial \sqrt{G_{\xi\xi}}}{\partial \eta}-\frac{v^2}{\sqrt{G_{\xi\xi}}\sqrt{G_{\eta\eta}}}\frac{\partial \sqrt{G_{\eta\eta}}}{\partial \xi} \tag{A-5}$$
$$+\frac{\omega}{D+\zeta}\frac{\partial u}{\partial \sigma}=fv-\frac{P_\xi}{\rho_0\sqrt{G_{\xi\xi}}}+F_\xi+\frac{1}{(D+\zeta)^2}\frac{\partial}{\partial \sigma}\left(\nu_v\frac{\partial u}{\partial \sigma}\right)+M_\xi$$

and

$$\frac{\partial v}{\partial t}+\frac{u}{\sqrt{G_{\xi\xi}}}\frac{\partial v}{\partial \xi}+\frac{v}{\sqrt{G_{\eta\eta}}}\frac{\partial v}{\partial \eta}+\frac{uv}{\sqrt{G_{\xi\xi}}\sqrt{G_{\eta\eta}}}\frac{\partial \sqrt{G_{\eta\eta}}}{\partial \xi}-\frac{u^2}{\sqrt{G_{\xi\xi}}\sqrt{G_{\eta\eta}}}\frac{\partial \sqrt{G_{\xi\xi}}}{\partial \eta} \tag{A-6}$$
$$+\frac{\omega}{D+\zeta}\frac{\partial v}{\partial \sigma}=-fu-\frac{P_\eta}{\rho_0\sqrt{G_{\eta\eta}}}+F_\eta+\frac{1}{(D+\zeta)^2}\frac{\partial}{\partial \sigma}\left(\nu_v\frac{\partial v}{\partial \sigma}\right)+M_\eta$$

The hydrostatic assumption, which is made in Delft3D, results therein, that there is no momentum equation in vertical direction. The vertical velocity ω in the adapting σ-co-ordinate system is therefore computed from the continuity equation:

$$\frac{\partial \zeta}{\partial t}+\frac{1}{\sqrt{G_{\xi\xi}}\sqrt{G_{\eta\eta}}}\frac{\partial[(d+\zeta)u\sqrt{G_{\eta\eta}}]}{\partial \xi}+\frac{1}{\sqrt{G_{\xi\xi}}\sqrt{G_{\eta\eta}}}\frac{\partial[(d+\zeta)v\sqrt{G_{\xi\xi}}]}{\partial \eta} \tag{A-7}$$
$$+\frac{\partial \omega}{\partial \sigma}=H\left(q_{in}-q_{out}\right)$$

In the momentum equations (A-3) – (A-6), P_ξ and P_η represent the pressure gradients in ξ and η direction. For water of constant density, these terms can be described as:

$$P_\xi = g\rho_0 \frac{\partial \zeta}{\partial \xi} + \frac{\partial P_{atm}}{\partial \xi} \tag{A-8}$$

and

$$P_\eta = g\rho_0 \frac{\partial \zeta}{\partial \eta} + \frac{\partial P_{atm}}{\partial \eta} \tag{A-9}$$

The unbalance of the horizontal Reynold's stresses, the forces F_ξ and F_η in the momentum equations, are formulated in large scale flow as follows:

$$F_\xi = \nu_H \left(\frac{1}{\sqrt{G_{\xi\xi}}\sqrt{G_{\xi\xi}}} \frac{\partial^2 u}{\partial \xi^2} + \frac{1}{\sqrt{G_{\eta\eta}}\sqrt{G_{\eta\eta}}} \frac{\partial^2 u}{\partial \eta^2} \right) \tag{A-10}$$

and

$$F_\eta = \nu_H \left(\frac{1}{\sqrt{G_{\xi\xi}}\sqrt{G_{\xi\xi}}} \frac{\partial^2 v}{\partial \xi^2} + \frac{1}{\sqrt{G_{\eta\eta}}\sqrt{G_{\eta\eta}}} \frac{\partial^2 v}{\partial \eta^2} \right) \tag{A-11}$$

Body forces are represented by the terms M_ξ and M_η. In the Delft3D-Flow manual a more specified description of these terms can be found.

To solve this set of equations, for a limited area type of problem, a set of initial and boundary conditions for water levels and horizontal velocities must be specified.

Boundary conditions

Vertical boundary conditions

In the σ-co-ordinate system, the free surface $(\sigma = 0,\ z = \zeta)$ and the bottom $(\sigma = -1,\ z = -D)$ are σ- co-ordinate surfaces. ω is the vertical velocity relative to the σ-plane. The impermeability of the surface and the bottom is taken into account by prescribing the following kinematic conditions:

$$\omega\big|_{\sigma=-1} = 0 \text{ and } \omega\big|_{\sigma=0} = 0 \tag{A-12}$$

Bed boundary condition

At the seabed, the boundary conditions for the momentum equations are:

$$\frac{\nu_V}{h} \frac{\partial u}{\partial \sigma}\bigg|_{\sigma=-1} = \frac{\tau_{b\xi}}{\rho_0} \tag{A-13}$$

$$\frac{\nu_V}{h} \frac{\partial v}{\partial \sigma}\bigg|_{\sigma=-1} = \frac{\tau_{b\eta}}{\rho_0} \tag{A-14}$$

with $\tau_{b\xi}$ and $\tau_{b\eta}$ the components of the bed stress in ξ- and η-direction, respectively.

The shear stress at the bed induced by a turbulent flow is assumed to be given by a quadratic friction law for both depth-averaged and three-dimensional flow:

$$\vec{\tau}_b = \frac{\rho_0 g}{C_{2D}^2}|U|\vec{U} \quad \text{or} \quad \vec{\tau}_b = \frac{\rho_0 g}{C_{3D}^2}|u_b|\vec{u}_b \tag{A-15}$$

in which U is the magnitude of the depth-averaged horizontal velocity and u_b the magnitude of the horizontal velocity in the first layer just above the bed in three-dimensional flow. Formulations of Chezy, Manning and White Colebrook can be used to specify the bed shear stress for depth-averaged flow. The formulations of Manning and White Colebrook are then transformed into a Chezy expression to suit the given bed shear stress equation (A-15). The Chezy coefficient used in three-dimensional flow is specified as follow:

$$C_{3D} \approx C_{2D} + \frac{\sqrt{g}}{\kappa}\ln\left(\frac{(\Delta z_b/2)}{h}\right) \tag{A-16}$$

The difference between the depth-averaged and three-dimensional Chezy formulations depends thus on the relative thickness of the computational bed layer in Delft3D-Flow.

For calculating the magnitude of the horizontal velocity at the bed in the three-dimensional case, Delft3D-Flow uses the following equation:

$$|u_b| = \frac{u_*}{\kappa}\ln\left(1+\frac{½\Delta z_b}{z_0}\right) \tag{A-17}$$

The contribution of the vertical velocity component to the magnitude of the velocity vector is hereby neglected. The roughness height z_0 depends on the horizontal co-ordinates ξ, η and time t, and can be expressed as:

$$z_0 = \frac{h}{e^{\left(1+\frac{\kappa \cdot C_{2D}}{\sqrt{g}}\right)} - e} \tag{A-18}$$

in which the depth-averaged Chezy value is used and the total water depth, h.

Surface boundary condition
At the free surface the boundary conditions for the momentum equations are:

$$\frac{\nu_V}{h}\frac{\partial u}{\partial \sigma}\bigg|_{\sigma=0} = \frac{|\tau_s|}{\rho_0}\cos(\theta) \tag{A-19}$$

$$\left.\frac{\nu_V}{h}\frac{\partial v}{\partial \sigma}\right|_{\sigma=0} = \frac{|\tau_s|}{\rho_0}\sin(\theta) \tag{A-20}$$

θ is the angle between the wind stress vector and the local direction of the grid-line, η. Without wind, the stress at the free surface is zero. The magnitude of τ_s is defined by equation (2-5). The drag coefficient in here has to be defined by the user and can be a function of the wind speed.

Turbulence closure models

For 3D shallow water flow the stress and diffusion tensor are anisotropic. The horizontal eddy viscosity coefficient ν_H and eddy diffusivity coefficient D_H are much larger than the vertical coefficients. The horizontal coefficients are assumed to be a superposition of three parts: a part due to "2D-turbulence", a part due to "3D-turbulence" and a part due to molecular viscosity. The 2D part is associated with the contribution of horizontal motions and forcings that cannot be resolved by the horizontal grid. The 3D part is referred to as the three-dimensional turbulence and is computed following the turbulence closure model, described in this paragraph. For 2D depth-averaged simulations, the horizontal eddy viscosity and eddy diffusivity coefficient should also contain a contribution to parameterise the net effect of the vertical variation of the horizontal flow.

Delft3D-Flow has no parameterisation for 2D-turbulence yet. The horizontal viscosity coefficient, ν^{2D}, and eddy diffusivity coefficient, D_H, must be specified by the user via the Delft3D-Flow input processor. They are generally needed to damp small-scale noise introduced by the advection terms. They must be chosen dependent on the grid size. The horizontal coefficients are orders of magnitude larger than the vertical coefficients determined by the turbulence closure model specified by the user.

The user can specify four different turbulence closure models to determine the vertical eddy viscosity and the vertical eddy diffusivity coefficient. A choice can be made between a constant coefficient, the Algebraic Eddy viscosity closure Model (AEM), the *k-L* turbulence closure model and the *k-ε* turbulence closure model.

The three models that do not use a constant eddy viscosity are based on the concept of Kolmogorov and Prandtl. According to this concept, the eddy viscosity is related to a characteristic length scale and velocity scale. The eddy viscosity has the following form:

$$\nu_v = c_\mu' L\sqrt{k} \tag{A-21}$$

where:

- c_μ' = a constant determined by calibration, derived from the empirical constant c_μ in the *k-ε* model; $c_\mu' = c_\mu^{1/4}$,
- L = is the mixing length,
- k = is the turbulent kinetic energy.

The turbulence closure models differ in their prescription of the turbulent kinetic energy k, the dissipation rate of turbulent kinetic energy ε, and the mixing length, L.

Algebraic turbulence model
The algebraic eddy viscosity model is a combination of two zero order closure schemes. These models will be denoted by ALG and PML. Both models will be briefly described. The combination of the two models was made to broaden the applicability of the algebraic turbulence closure.

Algebraic closure model (ALG)
In the algebraic closure model ALG a logarithmic velocity profile is assumed. This leads to a linear relation between the turbulent kinetic energy at the bed and the turbulent kinetic energy at the free surface:

$$k = \frac{1}{\sqrt{c_\mu}}\left[\left[u_*^b\right]^2\left(1 - \frac{z+D}{h}\right) + \left[u_*^s\right]^2 \frac{z+D}{h}\right] \tag{A-22}$$

with

c_μ = a constant, $c_\mu \approx 0.09$, calibrated for local-equilibrium shear layers [-]
u_*^s = friction velocity at the free surface, [m/s]
u_*^b = a modified form of the bed friction velocity u_{*b} [m/s]

The turbulent kinetic energy k at the bed and at the free surface is determined on the basis of the shear stresses. The bed friction velocity is determined from the magnitude of the velocity in the first grid point above the bed, under the assumption of a logarithmic velocity profile:

$$u_{*_b} = \frac{|\underline{u}_b|\kappa}{\ln\left(1 + \frac{\Delta z_b}{2z_0}\right)} \tag{A-23}$$

In tidal flows, at slack water the velocities are almost zero near the bed. Higher in the water column, the turbulence intensity may still be large. To avoid a zero eddy viscosity, velocities higher in the water column have to be used in the determination of the bed friction velocity. Under the assumption that the velocity profile is logarithmic in the discrete model for layer with index k:

$$u_{*_k} = \frac{|\underline{u}_k|\kappa}{\ln\left(1 + \frac{z_k + D}{z_0}\right)} \tag{A-24}$$

and the average value is defined as

$$\bar{u}_* = \frac{1}{K}\sum_{k=1}^{K} u_{*k} \tag{A-25}$$

In the linear profile for the turbulence energy (A-22), $u_*^b = \max\left\{\overline{u_*}, u_{*b}\right\}$ is used. The shear velocity at the free surface depends on the wind velocity at 10 m above the free surface

$$\left|\tau_s\right| = \rho_a C_d U_{10}^2 \tag{A-26}$$

In this algebraic turbulence closure model the wind stress and the bed stress affect the eddy viscosity over the total water depth instantaneously. In deep areas this is physically not correct, the turbulent kinetic energy generated at the free surface and at the bed must be transported along the water column by vertical diffusion. This will lead to phase differences in the time-series of the turbulent energy for the different layers.

The mixing length is described by:

$$L = \kappa(z+D)\sqrt{1-\frac{z+D}{h}}F_L(Ri) \tag{A-27}$$

in which $F_L(Ri)$ represents a damping function, which itself, is dependent on the gradient Richardson number Ri [-](see Delft Hydraulics, 1999).

With L [m] given from Equation (A-27) and k [m^2/s^2] from Equation (A-22), the vertical eddy viscosity is known in equation (A-19). The eddy viscosity is parabolic and gives in the case of wind-driven circulation, a double logarithmic vertical velocity profile.

Prandtl's Mixing Length model (PML)
A second algebraic expression for the eddy viscosity is obtained by assuming instantaneous local equilibrium between production and dissipation in the *k-L* model. This closure scheme is known as Prandtl's Mixing Length model (PML). In the production term the horizontal derivatives are left out, because they are small compared to the vertical derivatives. This gives:

$$k = \frac{1}{\sqrt{c_\mu}} L^2 \left[\left(\frac{\partial u}{\partial z}\right)^2 + \left(\frac{\partial v}{\partial z}\right)^2\right] \tag{A-28}$$

The mixing length *L* is again prescribed by Equation (A-27). Note that for a logarithmic velocity profile, without wind, Eq. (A-22) and Eq. (A-28) give the same linear distribution of *k*.

For the turbulence closure scheme ALG, the turbulent kinetic energy over the whole water column is in phase with the bed stress. For the PML model there is a phase difference in *k*, introduced by phase differences in the vertical gradient of the horizontal velocities. The phase differences depend on the total water depth and the eddy viscosity:

$$T \sim \frac{h^2}{\nu_V} \tag{A-29}$$

The PML-model leads to a zero eddy viscosity and eddy diffusivity at the position in the vertical where the vertical gradients of the velocity are zero (e.g. in wind-driven flows). This is physically incorrect.

For robustness, in Delft3D-FLOW the turbulence closure models PML and ALG are combined to one algebraic model denoted as the AEM model. The eddy viscosity is calculated following ALG and PML and the maximum value is taken.

$$\nu_V = \mathrm{MAX}(\nu_{ALG}, \nu_{PML}) \tag{A-30}$$

The eddy diffusivity is derived from the eddy viscosity, using the Prandtl-Schmidt number. Tidal simulations using this parameterisation have been performed for the Irish Sea.

k-L turbulence model

A so-called first order turbulence closure scheme implemented in Delft3D-FLOW is the *k-L* model. In this model the mixing length L is prescribed analytically (Eq. (A-27)). The velocity scale is based on the kinetic energy of turbulent motion. The turbulent kinetic energy k follows from a transport equation that includes an energy dissipation term, a buoyancy term and a production term. The following two assumptions are made: the production, buoyancy and dissipation terms are the dominating terms and the horizontal length scales are larger than the vertical ones (shallow water, boundary layer type of flows). The conservation of the turbulent quantities is less important and the transport equation is implemented in a non-conservation form. The second assumption leads to simplification of the production term. The transport equation for k is as follows:

$$\begin{aligned} &\frac{\partial k}{\partial t} + \frac{u}{\sqrt{G_{\xi\xi}}}\frac{\partial k}{\partial \xi} + \frac{v}{\sqrt{G_{\eta\eta}}}\frac{\partial k}{\partial \eta} + \frac{\omega}{D+\zeta}\frac{\partial k}{\partial \sigma} \\ &\qquad = \frac{1}{(D+\zeta)^2}\frac{\partial}{\partial \sigma}\left(\left(\nu_{mol} + \frac{\nu_{3D}}{\sigma_k}\right)\frac{\partial k}{\partial \sigma}\right) + P_k + B_k - \varepsilon \end{aligned} \tag{A-31}$$

In the production term P_k of turbulent kinetic energy the horizontal gradients of the horizontal velocity and all the gradients of the vertical velocities are neglected. The production term is given by:

$$P_k = \nu_V \frac{1}{(D+\zeta)^2}\left[\left(\frac{\partial u}{\partial \sigma}\right)^2 + \left(\frac{\partial v}{\partial \sigma}\right)^2\right] \tag{A-32}$$

For small scale applications (e.g. simulation of laboratory flume) the user can switch on (option “partial slip”, rough side wall) a more extended production term P_k of turbulent kinetic energy given by:

$$P_k = 2\nu_V \left[\frac{1}{2}\frac{1}{(D+\zeta)^2}\left(\left(\frac{\partial u}{\partial \sigma}\right)^2 + \left(\frac{\partial v}{\partial \sigma}\right)^2\right) + \left(\frac{1}{\sqrt{G_{\xi\xi}}}\left(\frac{\partial u}{\partial \xi}\right)\right)^2 + \frac{1}{2}\left(\frac{1}{\sqrt{G_{\eta\eta}}}\left(\frac{\partial u}{\partial \eta}\right) + \frac{1}{\sqrt{G_{\xi\xi}}}\left(\frac{\partial v}{\partial \xi}\right)\right)^2 + \left(\frac{1}{\sqrt{G_{\eta\eta}}}\left(\frac{\partial v}{\partial \eta}\right)\right)^2 \right] \tag{A-33}$$

In this expression, ν_V is the vertical eddy viscosity, prescribed by Eq. (A-21). In Eq. (A-32) and (A-33) it has been assumed that the gradients of the vertical velocity *w* can be neglected with respect to the gradients of the horizontal velocity components *u* and *v*. The horizontal and vertical (σ-grid) curvature of the grid has also been neglected.

Near the closed walls the normal derivative of the tangential velocity is determined with the law of the wall:

$$\frac{1}{\sqrt{G_{\eta\eta}}}\left(\frac{\partial u}{\partial \eta}\right) = \frac{2u_*}{\kappa\sqrt{G_{\eta\eta}}} \tag{A-34}$$

In stratified flows, turbulent kinetic energy is converted into potential energy. This is represented by a buoyancy flux B_k defined by:

$$B_k = \frac{\nu_V}{\sigma_\rho}\frac{g}{\rho}\frac{1}{D+\zeta}\frac{\partial \rho}{\partial \sigma} \tag{A-35}$$

In the *k-L* model it is assumed that the dissipation ε depends on the mixing length *L* and kinetic turbulent energy *k* according to:

$$\varepsilon = c_D \frac{k\sqrt{k}}{L} \tag{A-36}$$

where c_D is a constant determined by calibration, derived from the constant c_μ in the *k-*ε model; $c_D = c_\mu^{3/4} \approx 0.1925$.

To solve the transport equation, boundary conditions must be specified. A local equilibrium of production and dissipation of kinetic energy is assumed at the bed, which leads to the following Dirichlet boundary condition:

$$k\big|_{\sigma=-1} = \frac{u_{*b}^2}{\sqrt{c_\mu}} \tag{A-37}$$

The friction velocity u_{*b} at the bed is determined from the magnitude of the velocity in the grid point nearest to the bed, under the assumption of a logarithmic velocity profile, see Eq.

(A-17). The bed roughness (roughness length) may be enhanced by the presence of surface waves.

In case of wind forcing, a similar Dirichlet boundary condition is prescribed for the turbulent kinetic energy k at the free surface:

$$k\big|_{\sigma=0} = \frac{\left(u_*^s\right)^2}{\sqrt{c_\mu}} \tag{A-38}$$

In the absence of wind the turbulent kinetic energy k at the surface is set to zero.

At open boundaries the turbulent energy k is computed using the equation for k (A-22) without horizontal advection. For a logarithmic velocity profile this will approximately lead to the following linear distribution based on the shear stress at the bed and at the free surface:

$$k(z) = \frac{1}{\sqrt{c_\mu}}\left[u_{*b}^2\left(1-\frac{z+D}{h}\right) + \left(u_*^s\right)^2\frac{z+D}{h}\right] \tag{A-39}$$

k-ε turbulence model

In the k-ε turbulence model, transport equations must be solved for both the turbulent kinetic energy k and for the energy dissipation ε. The mixing length L is then determined from ε and k according to (A-36):

$$L = c_D\frac{k\sqrt{k}}{\varepsilon} \tag{A-40}$$

In the transport equations the following two assumptions are made:
the production, buoyancy and dissipation terms are the dominating terms
the horizontal length scales are larger than the vertical ones (shallow water, boundary layer type of flows).
Because of the first assumption, the conservation of the turbulent quantities is less important and the transport equation is implemented in a non-conservation form.

The transport equations for k and ε are non-linearly coupled by means of the eddy diffusivity D_V and the dissipation terms. The transport equation for k is already mentioned (equation (A-31)) and the transport equations for ε is given by:

$$\begin{aligned}&\frac{\partial\varepsilon}{\partial t}+\frac{u}{\sqrt{G_{\xi\xi}}}\frac{\partial\varepsilon}{\partial\xi}+\frac{v}{\sqrt{G_{\eta\eta}}}\frac{\partial\varepsilon}{\partial\eta}+\frac{\omega}{D+\zeta}\frac{\partial\varepsilon}{\partial\sigma}\\ &\qquad=\frac{1}{(D+\zeta)^2}\frac{\partial}{\partial\sigma}\left(\left(\nu_{mol}+\frac{\nu_{3D}}{\sigma_\varepsilon}\right)\frac{\partial\varepsilon}{\partial\sigma}\right)+P_\varepsilon+B_\varepsilon-c_{2\varepsilon}\frac{\varepsilon^2}{k}\end{aligned} \tag{A-41}$$

The production term P_k is defined in Eqs. (A-32) and (A-33), the buoyancy term in Eq. (A-35). The production term P_ε and the buoyancy flux B_ε are defined by:

$$P_\varepsilon = c_{1\varepsilon}\frac{\varepsilon}{k}P_k \qquad \text{(A-42)}$$

$$B_\varepsilon = c_{1\varepsilon}\frac{\varepsilon}{k}(1-c_{3\varepsilon})B_k$$

with L prescribed by Eq. (A-40) and the calibration constants by: $c_{1\varepsilon}$=1.44, $c_{2\varepsilon}$=1.92. $c_{3\varepsilon}$=1.0. In Delft3D-FLOW in the ε -equation for stable stratification the buoyancy flux is switched off, so $c_{3\varepsilon}$=1.0 and for unstable stratification the buoyancy flux is switched on $c_{3\varepsilon}$=0.0.

The coefficients of the 3D k-ε turbulence closure model as implemented in Delft3D-Flow are not the same as in the depth-averaged k-ε turbulence closure model, therefore, for depth-averaged simulations, the k-ε turbulence closure model is not available for the user.

The vertical eddy viscosity ν_V is determined by:

$$\nu_V = c_{\mu'}L\sqrt{k} \qquad \text{(A-43)}$$

$$= c_\mu\frac{k^2}{\varepsilon} \quad with \; c_\mu = c_D c_{\mu'}$$

For the transport equation of the turbulent kinetic energy k the same Dirichlet boundary conditions are used as for the k-L model described earlier, see Eq. (A-37) and (A-38). For the transport equation of the dissipation ε, the following boundary condition is used at the bed:

$$\varepsilon|_{\sigma=-1} = \frac{u_{*b}^3}{\kappa\, z_0} \qquad \text{(A-44)}$$

and at the surface the dissipation ε is prescribed by:

$$\varepsilon|_{\sigma=0} = \frac{u_{*_s}^3}{\kappa\,\frac{1}{2}\Delta z_s} \qquad \text{(A-45)}$$

In case of no wind the dissipation ε is set to zero at the free surface.
At open boundaries the energy dissipation ε is computed using Eq. (A-41) without horizontal advection. For a logarithmic velocity profile this will approximately lead to a hyperbolic distribution which is the superposition of two hyperbola, corresponding to a double logarithmic velocity profile, on the basis of the shear stresses at the bed and at the free surface:

$$\varepsilon(z) = \frac{u_{*b}^3}{\kappa(z+D)} + \frac{\left(u_*^s\right)^3}{\kappa(h-z-D)} \qquad \text{(A-46)}$$

where z denotes the vertical co-ordinate.

A.2 Flow-Wave interaction

Soulsby fitted one standard formula to all of the models, each model having its own fitting coefficients. The parameterisation of Soulsby for the time-mean bed stress is of the form

$$\tau_m = y\left(\tau_c + \tau_w\right) \tag{A-47}$$

$$y = x\left(1 + bx^p\left(1-x\right)^q\right) \tag{A-48}$$

and for the maximum bed shear stress:

$$\tau_{\max} = z\left(\tau_c + \tau_w\right) \tag{A-49}$$

$$z = 1 + ax^m\left(1-x\right)^n \tag{A-50}$$

in which a, b, p, q, m and n are parameters, of which the value depends on the friction model which is parameterised, and

$$x = \frac{\tau_c}{\tau_c + \tau_w} \tag{A-51}$$

in which

τ_c	= magnitude of the bed stress due to current alone	[N/m^2]
τ_w	= magnitude of the bed stress for waves alone	[N/m^2]
τ_m	= magnitude of the mean bed stress for combined waves and current	[N/m^2]
$\tau_{\max}$	= magnitude of the maximum bed stress for combined waves and current	[N/m^2]

In the above expressions it is assumed that τ_m and $\tau_{\max}$ have the same direction as τ_c, because the current is dominant.

The bed stress due to the current can be written as:

$$\tau_c = \rho_0 C_z \left|\underline{U}\right|^2 \tag{A-52}$$

in which C_z is the drag coefficient, which is related to the 2D Chézy coefficient:

$$C_z = \frac{g}{C_{2D}^2} \tag{A-53}$$

For 3D simulations the magnitude of the depth-averaged velocity is determined from the velocity near the bed, assuming a logarithmic velocity profile.
The magnitude of the time-averaged bed stress due to waves alone is related to the friction coefficient f_w [-]:

$$\tau_w = \frac{1}{2}\rho_0 f_w \widehat{U}_{orb}^2 \tag{A-54}$$

in which:

f_w = wave friction factor [-]
$\widehat{U}_{orb}$ = amplitude of wave orbital velocity near the bottom [m/s]

Expressions for the parameters *a*, *b*, *p*, *q, m* and *n* are defined by the following formula:

$$a = \left(a_1 + a_2\left|\cos\phi^J\right|\right) + \left(a_3 + a_4\left|\cos\phi^J\right|\right)\log_{10}\left(\frac{f_w}{C_z}\right) \tag{A-55}$$

in which:

C_z = drag coefficient due to current (see Eq. (A-53)) [-]
ϕ = the angle between the current direction and the wave propagation θ_w, relative to a fixed Cartesian axis system, also called wave direction [rad]

The wave direction ϕ is computed in Cartesian co-ordinates by

$$\left|\cos\phi\right| = \frac{\left|\begin{pmatrix} U \\ V \end{pmatrix} \cdot \begin{pmatrix} \cos\theta_w \\ \sin\theta_w \end{pmatrix}\right|}{\sqrt{U^2 + V^2}} \tag{A-56}$$

The wave direction ϕ can also be derived from the components of radiation stress gradients F_x and F_y. In this way, Eq. (A-56) is replaced by

$$\left|\cos\phi\right| = \frac{\left|\begin{pmatrix} U \\ V \end{pmatrix} \cdot \begin{pmatrix} F_x \\ F_y \end{pmatrix}\right|}{\left|\underline{U}\right|\left|\underline{F}\right|} \tag{A-57}$$

The variation of the wave friction factor with relative orbital excursion at the bed under purely oscillatory flow is given by the explicit formula of Swart

$$f_w = \begin{cases} 0.00251\exp\left[5.21\left\{\dfrac{A}{k_s}\right\}^{-0.19}\right] & ;\ \dfrac{\mathrm{A}}{\mathrm{k_s}} > \dfrac{\pi}{2} \\ 0.3 & ;\ \dfrac{\mathrm{A}}{\mathrm{k_s}} \le \dfrac{\pi}{2} \end{cases} \tag{A-58}$$

k_s is the Nikuradse roughness length-scale and A is defined by $\widehat{U}_{orb}/\omega$, in which ω is the wave angular frequency. The above formulation for f_w can also be expressed in terms of the wave period and the bottom roughness length without waves related to the geometrical grain size $z_0 = \frac{k_s}{30}$ [m]:

$$f_w = \begin{cases} 0.00251 \exp\left[14.1\left(A^*\right)^{-0.19}\right] & ;A^* > 30\pi^2 \\ 0.3 & ;A^* \le 30\pi^2 \end{cases} \tag{A-59}$$

with A^* defined by $\widehat{U}_{orb} T / z_0$ [-]

Matching the velocity profile corresponding with the increased mean bed stress τ_m for waves and current, with a logarithmic profile for the mean flow outside the wave boundary layer:

$$\tau_m = \rho_0 \tilde{u}_*^2 \tag{A-60}$$

with $\tilde{u}_*^2$ the shear stress velocity for waves and current and following equation (A-17)

$$|u_b| = \frac{\tilde{u}_*}{\kappa} \ln\left(1 + \frac{1/2\,\Delta z_b}{\tilde{z}_0}\right) \tag{A-61}$$

with $|\underline{u}_b|$ the magnitude of the horizontal velocity in the first layer just above the bed. The increased roughness length for waves and current $\tilde{z}_0$ satisfies:

$$\tilde{z}_0 = \frac{\Delta z_b}{e^{\kappa \frac{|\underline{u}_b|}{\tilde{u}_*}} - 1} \tag{A-62}$$

This increased roughness length is then used in the turbulence closure models.

Stokes-drift

In case of surface waves fluid particles describe an orbital motion. A particle at the top of the orbit beneath a wave crest moves slightly faster in the forward direction than it does in the backward direction beneath a wave trough. The mean drift velocity is a second order quantity in the wave height. The drift leads to additional fluxes in the wave averaged mass continuity equation.

The wave-induced mass fluxes (M_x^S and M_y^S) are found by integration of the components of the Stokes drift (u^S and v^S) over the wave-averaged total water depth:

$$M_x^S = \int_{-D}^{\zeta} \rho_0 u^S dz = \frac{E}{\omega} k_x \tag{A-63}$$

$$M_y^S = \int_{-D}^{\zeta} \rho_0 v^S dz = \frac{E}{\omega} k_y \tag{A-64}$$

with E the wave energy defined as:

$$E = \frac{1}{8} \rho_0 \, g \, H_{rms}^2 \tag{A-65}$$

The velocity can then be computed following:

$$u^S = \frac{M_x^s}{\rho_0 (\zeta + D)} \tag{A-66}$$

$$v^S = \frac{M_y^s}{\rho_0 (\zeta + D)} \tag{A-67}$$

Appendix B Listing of batch files used in case study

B.1 Description of computational method

Start.bat is the batchfile, which starts the computation. It calls for the batchfile ChangeFiles.bat. This batchfile changes values in the '.org' files. '%1' stays for the first column after the string CHANGEFILES so 'A01' and '%2' for the second column, so '1080' for the first line. The first command in ChangeFiles.bat copies FLOWMDF.org to %1.mdf. The command 'MOD -s STARTTIJD %2 %1.mdf' in ChangeFiles.bat changes the string STARTTIJD in %1.mdf (=A01.mdf) by %2 (=1080) for the first time. In this way the strings of FLOWMDF.ORG are all changed by input parameters for Delft3D-Flow. FLOWWAVEMDF.org, MDWAVE.org and MORF.org are thus also copied to an input file with the right extension and then changed with new input parameters. In ChangeFiles.bat, it is seen that first Delft3D-Flow starts and subsequently SWAN. The end of the bat files is reached and the batchfile returns (because of the 'call' statement) to Start.bat. The second line will then be executed. In this way three days were simulated. Beneath, all the input files can be found.

START.BAT

```
call CHANGEFILES A01 1080 1200 Wa9.19961104.180000 1200.wnd 600
copy FlowwaveMDF.org FlowMDF.org
call CHANGEFILES A03 1200 1320 A01.19961104.200000 1320.wnd 660
call CHANGEFILES A05 1320 1440 A03.19961104.220000 1440.wnd 720
call CHANGEFILES A07 1440 1560 A05.19961105.000000 1560.wnd 780
call CHANGEFILES A09 1560 1680 A07.19961105.020000 1680.wnd 840
call CHANGEFILES A11 1680 1800 A09.19961105.040000 1800.wnd 900
call CHANGEFILES A13 1800 1920 A11.19961105.060000 1920.wnd 960
call CHANGEFILES A15 1920 2040 A13.19961105.080000 2040.wnd 1020
call CHANGEFILES A17 2040 2160 A15.19961105.100000 2160.wnd 1080
call CHANGEFILES A19 2160 2280 A17.19961105.120000 2280.wnd 1140
call CHANGEFILES A21 2280 2400 A19.19961105.140000 2400.wnd 1200
call CHANGEFILES A23 2400 2520 A21.19961105.160000 2520.wnd 1260
call CHANGEFILES A25 2520 2640 A23.19961105.180000 2640.wnd 1320
call CHANGEFILES A27 2640 2760 A25.19961105.200000 2760.wnd 1380
call CHANGEFILES A29 2760 2880 A27.19961105.220000 2880.wnd 1440
call CHANGEFILES A31 2880 3000 A29.19961106.000000 3000.wnd 1500
call CHANGEFILES A33 3000 3120 A31.19961106.020000 3120.wnd 1560
call CHANGEFILES A35 3120 3240 A33.19961106.040000 3240.wnd 1620
call CHANGEFILES A37 3240 3360 A35.19961106.060000 3360.wnd 1680
call CHANGEFILES A39 3360 3480 A37.19961106.080000 3480.wnd 1740
call CHANGEFILES A41 3480 3600 A39.19961106.100000 3600.wnd 1800
call CHANGEFILES A43 3600 3720 A41.19961106.120000 3720.wnd 1860
call CHANGEFILES A45 3720 3840 A43.19961106.140000 3840.wnd 1920
call CHANGEFILES A47 3840 3960 A45.19961106.160000 3960.wnd 1980
call CHANGEFILES A49 3960 4080 A47.19961106.180000 4080.wnd 2040
call CHANGEFILES A51 4080 4200 A49.19961106.200000 4200.wnd 2100
call CHANGEFILES A53 4200 4320 A51.19961106.220000 4320.wnd 2160
call CHANGEFILES A55 4320 4440 A53.19961107.000000 4440.wnd 2220
call CHANGEFILES A57 4440 4560 A55.19961107.020000 4560.wnd 2280
call CHANGEFILES A59 4560 4680 A57.19961107.040000 4680.wnd 2340
```

```
call CHANGEFILES A61 4680 4800 A59.19961107.060000 4800.wnd 2400
call CHANGEFILES A63 4800 4920 A61.19961107.080000 4920.wnd 2460
call CHANGEFILES A65 4920 5040 A63.19961107.100000 5040.wnd 2520
call CHANGEFILES A67 5040 5160 A65.19961107.120000 5160.wnd 2580
call CHANGEFILES A69 5160 5280 A67.19961107.140000 5280.wnd 2640
call CHANGEFILES A71 5280 5400 A69.19961107.160000 5400.wnd 2700
```

CHANGEFILES.BAT

```
copy flowrunid.org runid
MOD -s FLOWRUN %1 runid
copy FlowMDF.org %1.mdf

MOD -s STARTTIJD %2 %1.mdf
MOD -s EINDTIJD %3 %1.mdf
MOD -s FLOWRUN %1 %1.mdf
MOD -s RESTARTFILE %4 %1.mdf

copy md-wave.org md-wave.%1
MOD -s WINDINVOERFILE %5 md-wave.%1
MOD -s FLOWRUN %1 md-wave.%1
MOD -s INFOEEN %6 md-wave.%1
copy morf.org morf.%1
MOD -s FLOWRUN %1 morf.%1

Tdatom (STARTS DELFT3D-FLOW)
Trisim  (STARTS DELFT3D-FLOW)

copy C:\delft3d\w32\lib\swan.bat swan.bat
copy C:\delft3d\w32\menu\default\morjob.def morsys.job
echo morf.%1 >>morsys.job
call C:\DELFT3D\W32\MOR\bin\mosyssm2.exe  (STARTS SWAN)
```

FLOWMDF.ORG

```
Ident = #DELFT3D.UI    .03.02 3.34.03#
Runid = #FLOWRUN#
Commnt=
Runtxt= #Andhra Pradesh SSM          #
      #Run 1996                      #
      #Storm Run with final input    #
      #no '                          #
Filcco= #krom9etm.grd#
Fmtcco= #FR#
DxDy  = [.] [.]
Anglat= 17.0000
Grdang= 0.000000
Filgrd= #krom9etm.enc#
Fmtgrd= #FR#
MNgrd = [ ] [ ]
MNKmax= 260 136 1
Thick = 100.000
Fildep= #FinalY.dep  #
Fmtdep= #FR#
Commnt=
Fildry= #newdry.dry  #
Fmtdry= #FR#
Filtd = #Final.thd   #
Fmttd = #FR#
Nambar= #                    #
MNbar = [ ] [ ] # #
MNwlos= [ ] [ ]
Commnt=
Itdate= #1996-11-04#
Tunit = #M#
Tstart= STARTTIJD
Tstop = EINDTIJD
Dt    = 2.00000
Tzone = 0
```

```
Commnt=
Sub1  = #  W #
Sub2  = #   #
Namc1 = #                #
Namc2 = #                #
Namc3 = #                #
Namc4 = #                #
Namc5 = #                #
Wnsvwp= #N#
Filwnd= #UniBckgrd.txt#
Fmtwnd= #FR#
Wndint= #Y#
Commnt=
Restid= #RESTARTFILE#
Commnt=
Filbnd= #curvi8xx.bnd#
Fmtbnd= #FR#
FilbcH= #           #
FmtbcH= #FR#
FilbcT= #           #
FmtbcT= #FR#
Filana= #q3j.bca     #
Filcor= #           #
FilbcC= #           #
FmtbcC= #FR#
Rettis= 0.000000
        0.000000
        0.000000
        0.000000
        0.000000
        0.000000
        0.000000
        0.000000
        0.000000
        0.000000
        0.000000
        0.000000
        0.000000
        0.000000
        0.000000
        0.000000
        0.000000
Rettib= 0.000000
        0.000000
        0.000000
        0.000000
        0.000000
        0.000000
        0.000000
        0.000000
        0.000000
        0.000000
        0.000000
        0.000000
        0.000000
        0.000000
Commnt=
Ag    = 9.81000
Rhow  = 1028.00
Alph0 = [.]
Tempw = 15.0000
Salw  = 31.0000
Rouwav= #           #
Wstres= 0.00250000 0.0000 0.00900 100.000
Rhoa  = 1.00000
Betac = 0.500000
Equili= #N#
Tkemod= #           #
Ktemp = 0
Fclou = 0.000000
Sarea = 0.000000
Filtmp= #           #
Fmttmp= #FR#
Temint= #Y#
Tstmp = [.] [.]
Commnt=
Roumet= #C#
Filrgh= #FinalY.rgh  #
Fmtrgh= #FR#
Xlo   = 0.000000
Filedy= #           #
Vicouv= 1.00000
Dicouv= 10.0000
Vicoww= [.]
Dicoww= [.]
Irov  = 0
Z0v   = [.]
Cmu   = [.]
Cpran = [.]
Commnt=
Iter  =     2
Dryflp= #MAX #
Dryflc= 0.0500000
Dco   = -999.000
Tlfsmo= 360.000
Forfuv= #Y#
Forfww= #N#
Sigcor= #N#
Trasol= #Cyclic-method#
Commnt=
Filsrc= #           #
Fmtsrc= #FR#
Fildis= #           #
```

```
Fmtdis= #FR#
Commnt=                          no. observation
points: 337
Filsta= #Final.obs   #
Fmtsta= #FR#
Tpar  = [.] [.]
XYpar = [.] [.]
Commnt=
Eps   = [.]
Commnt=
Commnt=       no. cross sections: 0
Namcrs= #                  #
MNcrs = [ ] [ ] [ ] [ ]
Commnt=
PMhydr= #YYYYYY#
PMproc= #YYYYYYYYYY#
PMderv= #YYY#
PHhydr= #YYYYYY#
PHproc= #YYYYYYYYYY#
PHderv= #YYY#
PHflux= #YYYY#
SMhydr= #YYYYY#
```

```
SMproc= #YYYYYYYYYY#
SMderv= #YYYYY#
SHhydr= #YYYY#
SHproc= #YYYYYYYYYY#
SHderv= #YYYYY#
SHflux= #YYYY#
Commnt=    attribute file fourier analyzed
Filfou= #          #
Online= #NO #
Prmap = [.]
Prhis = STARTTIJD 0.00000 EINDTIJD
Flmap = STARTTIJD 120.000 EINDTIJD
Flhis = STARTTIJD 10.0000 EINDTIJD
Flpp  = STARTTIJD 120.000 EINDTIJD
Flrst = 120.000000
Commnt=
Filweb= #0411961uur.spw#
Filcio= #coriolis.k9e#
Fillwl= #finalx.wrs#
keva  = 1
Fileva= #bob.eva#
Commnt=
```

FLOWWAVEMDF.ORG

```
Ident = #DELFT3D.UI    .03.02 3.34.03#
Runid = #FLOWRUN#
Commnt=
Runtxt= #Andhra Pradesh SSM          #
      #Run 1996                      #
      #Storm Run with final input    #
      #no '                          #
Filcco= #krom9etm.grd#
Fmtcco= #FR#
DxDy  = [.] [.]
Anglat= 17.0000
Grdang= 0.000000
Filgrd= #krom9etm.enc#
Fmtgrd= #FR#
MNgrd = [ ] [ ]
MNKmax= 260 136 1
Thick = 100.000
Fildep= #FinalY.dep  #
Fmtdep= #FR#
Commnt=
Fildry= #newdry.dry  #
Fmtdry= #FR#
Filtd = #Final.thd   #
Fmttd = #FR#
Nambar= #                  #
MNbar = [ ] [ ] # #
MNwlos= [ ] [ ]
```

```
Commnt=
Itdate= #1996-11-04#
Tunit = #M#
Tstart= STARTTIJD
Tstop = EINDTIJD
Dt    = 2.00000
Tzone = 0
Commnt=
Sub1  = #  W #
Sub2  = #  W#
Namc1 = #                  #
Namc2 = #                  #
Namc3 = #                  #
Namc4 = #                  #
Namc5 = #                  #
Wnsvwp= #N#
Filwnd= #UniBckgrd.txt#
Fmtwnd= #FR#
Wndint= #Y#
Commnt=
Restid= #RESTARTFILE#
Commnt=
Filbnd= #curvi8xx.bnd#
Fmtbnd= #FR#
FilbcH= #          #
FmtbcH= #FR#
FilbcT= #          #
FmtbcT= #FR#
Filana= #q3j.bca     #
```

```
Filcor= #           #
FilbcC= #           #
FmtbcC= #FR#
Rettis= 0.000000
        0.000000
        0.000000
        0.000000
        0.000000
        0.000000
        0.000000
        0.000000
        0.000000
        0.000000
        0.000000
        0.000000
        0.000000
        0.000000
        0.000000
        0.000000
        0.000000
Rettib= 0.000000
        0.000000
        0.000000
        0.000000
        0.000000
        0.000000
        0.000000
        0.000000
        0.000000
        0.000000
        0.000000
        0.000000
        0.000000
        0.000000
        0.000000
        0.000000
        0.000000
        0.000000
Commnt=
Ag    = 9.81000
Rhow  = 1028.00
Alph0 = [.]
Tempw = 15.0000
Salw  = 31.0000
Rouwav= #FR84#
Wstres= 0.00250000 0.000 0.009000 100.000
Rhoa  = 1.00000
Betac = 0.500000
Equili= #N#
Tkemod= #           #
Ktemp = 0
Fclou = 0.000000
Sarea = 0.000000
Filtmp= #           #
Fmttmp= #FR#
Temint= #Y#
Tstmp = [.] [.]
Commnt=
Roumet= #C#
Filrgh= #FinalY.rgh  #
Fmtrgh= #FR#
Xlo   = 0.000000
Filedy= #           #
Vicouv= 1.00000
Dicouv= 10.0000
Vicoww= [.]
Dicoww= [.]
Irov  = 0
Z0v   = [.]
Cmu   = [.]
Cpran = [.]
Commnt=
Iter  =     2
Dryflp= #MAX #
Dryflc= 0.0500000
Dco   = -999.000
Tlfsmo= 360.000
Forfuv= #Y#
Forfww= #N#
Sigcor= #N#
Trasol= #Cyclic-method#
Commnt=
Filsrc= #           #
Fmtsrc= #FR#
Fildis= #           #
Fmtdis= #FR#
Commnt=   no. observation points: 337
Filsta= #Final.obs   #
Fmtsta= #FR#
Tpar  = [.] [.]
XYpar = [.] [.]
Commnt=
Eps   = [.]
Commnt=
Commnt=          no. cross sections: 0
Namcrs= #                #
MNcrs = [ ] [ ] [ ] [ ]
Commnt=
PMhydr= #YYYYYY#
PMproc= #YYYYYYYYYY#
PMderv= #YYY#
PHhydr= #YYYYYY#
PHproc= #YYYYYYYYYY#
PHderv= #YYY#
PHflux= #YYYY#
SMhydr= #YYYYY#
SMproc= #YYYYYYYYYY#
```

```
SMderv= #YYYYY#
SHhydr= #YYYY#
SHproc= #YYYYYYYYYY#
SHderv= #YYYYY#
SHflux= #YYYY#
Commnt=   attribute file fourier analyzed
Filfou= #          #
Online= #NO #
Prmap = [.]
Prhis = STARTTIJD 0.00000 EINDTIJD
Flmap = STARTTIJD 120.000 EINDTIJD
```

```
Flhis = STARTTIJD 10.0000 EINDTIJD
Flpp  = STARTTIJD 120.000 EINDTIJD
Flrst = 120.000000
Commnt=
Filweb= #0411961uur.spw#
Filcio= #coriolis.k9e#
Fillwl= #finalx.wrs#
keva  = 1
Fileva= #bob.eva#
Commnt=
```

```
MDWAVE.ORG

md-wave.FLOWRUN  Generated by
Delft3D-WAVE IP Version 4.86
*
* -- HISWA input ------------------------------
*
* -------------------- Group 1 --------------------
* SWMOR
 .TRUE.
* SWBOT
 .TRUE.
*
* -------------------- Group 2 --------------------
* SWWLT
 .TRUE.
*
* -------------------- Group 3 --------------------
* SWUVT
 .TRUE.
* SWUVI
 .FALSE.
*
* -------------------- Group 4 --------------------
* SWWAV
 .TRUE.
* SWFLUX
 .FALSE.
* CORHT
 .FALSE.
* SWOUT
 .TRUE.
*
* -------------------- Group 5 --------------------
* CURVI (=SWWAV)
 .TRUE.
*
* Flow grid description
  'krom9etm.grd'
*
```

```
* Output grid description (dummy if
SWOUT=FALSE)
* computational grid #1
*MXR! MYR!  DX  DY ALFORI  XORI YORI
-1  -1  -999.99 -999.99 -999.99 -999.99 -999.99
*
* ==== Tidal info ====
*
* number of tide steps (Ntide)
  2
*   tscale = 120.00
*   time              water level   Ux      Vy
    INFORMATIE          0.00    0.00    0.00
*   INFORMATIE2         0.00    0.00    0.00

* ========= Hiswa input =========
*
* project name
  ''
* project number
  ''
* 3 lines scenario description
  ''
  ''
  ''
* ----- Numerical and test parameters ------
* itest  itrace
     0      0
* power     pca     dis
  5.00    1.10    3.00
*   cdn     cdd
  0.50    0.50
*
*-------------------------------------------------
*  Wind
*      Two input items for constant wind field
(vel. + dir.)
*   or Four input items (vel. + dir. are dummy)
for variable wind
*      field, file name and grid choice, if Grid is
'dif' then record
```

```
*      XW, YW etc. must be specified
*-------------------------------------------------
*Velocity     direction     File-name
Grid
*          (wind-field with     'bot' - as bottom
*            wx and wy)          'dif' - different
  30.00  270.00  'WINDINVOERFILE'   'bot'
*
* ------- nested computations ----------
* Nnest
  1
*
* ----------------- bottom grids ------------------
*    xp    yp    alp     mx     my    dx     dy
   0.00    0.00  0.0  258  134    50.00   100.00
*
* -------------- file names and FAC -------------
--
* Bottom    Current   FAC
'FinalY.dep' 'Current1'   1.00
*
* -------------- computational grids --------------
* xclen     yclen    sector     mxc       myc
* mdc       xpc      ypc        alpc
*
  10000.00   10000.00     120.0     258     134
      12       0.00       0.00     0.0
*
* ----------------- coefficients ------------------
* level   negmes   interp
   0.00       0       1
* maxerr     grav     rho   inrhog
      2   9.8100  1025.0       1
*
* -------- up-wave boundary definition -------
* Nop   Gamma0
    1     3.30
*     Y     Tpeak    Hsig     Dir     Ms
      0   1.00000   0.000     0.0    4.0
*
*-----------------------------------------
*  Dissipation coefficients
*  Six input items for constant friction field or
*  eight input items for variable friction field,
if Grid is 'dif'
*  then record XF  YF etc must be specified.
*-------------------------------------------------
* GAMS   GAMD   ALFA   CFW   CFC
FREQ    File-name      Grid
*                                friction  'bot' - as
bottom
*                                field     'dif' -
different
  0.80   1.00   1.00   0.0100   0.0050  .FALSE.
*
*-------------------------------------------------
* Side boundary conditions in overall
computation
*-------------------------------------------------
* Boundary Left ('inc'  or 'ref' + coeff.)
   'inc'
* Boundary Right ('inc'  or 'ref' + coeff.)
   'inc'
*
* -------------------- nest data ------------------
* nest name   file name  Inest
*
*-------------------------------------------------
*  Obstacles
*     Number of obstacles
              0
*
*-------------------------------------------------
*  Output Curves
*     Number of curves
              0
*
* ----------- end of HISWA input -----------
*  Swan run
 .TRUE.
*
*******************************
*
* -- SWAN input -------------------------
*
*  Set commands
*
*  North
*  []
   90
*
*  Minimum depth
*  []
   0.05
*
*  Convention:
*  Carnaut = .true.  : cartesian convention
*          = .false. : nautical convention
*  Carnaut
*  (.true.) / (.false.)
   .false.
*
*  Setup (as computed by SWAN):
*  Setup = .true.  : setup activated
*        = .false. : no setup
*  Setup
```

```
*  (.true.) / (.false.)
   .false.
*
*  Forces on bases of
*  Swdiss = .true.  : wave energy dissipation
rate
*         = .false. : radiation stresses
*  Swdiss
*  (.true.) / (.false.)
   .true.
*
*  Spectral resolution for every nest: 1 =
circle, 2 = sector
*  flow   fhigh  msc   mdc   C/s    dir1     dir2
   0.04    1       18      72      1       0       0
*
*  Parameter for reading bottom file
*  Idla
   4
* ------------------------------------------------
*  Additional parameters for regular grid
*
*  Number of exception values regular grid:
*  Nexv
   0
*
*  Excval
*  []
   0
* ------------------------------------------------
*  Curvilinear grid
*
*  Compgrid curvilinear:
*  Curli = .true.  : curvilinear compgrid
*  Curli = .false. : rectilinear compgrid
*  Curli
*  (.true.) / (.false.)
   .true.
*
*  If compgrid is curvilinear, then give
characteristics for reading from file.
*  If not, give dummy values.
*
*  Characteristics for reading from file
*  idla    nhedf    nhedvec
   4       0        1
*
*  filename
*  curlif
   'flow2swan.grd'
*
*  Curvilinear bottom, current, waterlevel,
friction:
*     .true.  : yes
*     .false. : no
*
*  clbot    clcur    clwin    clwat    clfric
*  no/yes   no/yes   no/yes   no/yes   no/yes
   .true.   .true.   .true.   .true.   .true.
*
*  Give exception values.
*  Dummy (-99.99) if there are no exception
values.
*
*  Number of exception values curvilinear grid:
*  nexcc
   0
*  xexcval   yexcval
   0    0
* ------------------------------------------------
*  number of boundaries
   0
* ------------------------------------------------
*  Physics
*  Formulation generation:
*             0 = off,  1 = first,     2 = second,   3 =
third
*
*Breaking: 0 = off, 1 = constant,  2 = variable
*
*  Friction:    0 = off,  1 = Jonswap,   2 =
Collins,  3 = Madsen
*
*  Triads:      0 = off,  1 = on
*
*  Deactivate:
*  Physics     : windgrowth, whitecapping,
quadruplets
*             0 = off,  1 = on
*  Wave prop.  : refraction, phase shift
*             0 = off,  1 = on
* ------------------------------------------------
*  Gen
*  0,1,2,3
   2
*
*  Break         Coefficients
*  0/1           []          []
   1             1           0.73
*
*  Fric          Coefficient
*  0/1/2/3       []
   1             0.067
*
*  Triad         Coefficients [default values]
*  0/1           [0.25         2.5]
```

```
  1          0.1          2.2
*  Windgrowth  Wcap   Quad   Refrac   Fshift
*  0/1         0/1         0/1         0/1         0/1
   1           1           1           1           1
* ------------------------------------------------
*  Numerical accuracy coefficients (default
values):
*  drel        dhabs      dtabs      npnts      itermx
   0.02        0.02        0.02        98          30
* ------------------------------------------------
*  Compute/no compute
*  comp
   1
* ------------------------------------------------
```

```
*  Output requests
*  if points == (.true.) : generate output for
locations
*           == (.false.): no output for locations
*
*  points
*  (.true.)/(.false.)
   .false.
*
*  Output at compgrid: 0 = no,  1 = yes
*
*  dep      dir      hs       tp       tm01     mesh
*  0/1      0/1      0/1      0/1      0/1      0/1
   0        0        0        0        0        0
```

MORF.ORG

```
*
* case   label   labw   labr
  'FLOWRUN' ''    ''   ''
* initp
  0
* ito1      ito2
  19961104  000000
* tima   tscale
  0      120.00
* nback
  0
* pointer sequence
* ninpfi
  1
* iproc  ivers  md-file
  1      3      'md-wave.FLOWRUN'
* Flow tidal period (expressed in tscale)
  999999
* process tree
* norder     ndproc
  1          1
* child-parent relations
* child    parent
  1        2
* controls
* i        nctr     itelcm   xtelm
  1        1        0        0.000000
* ntimin1  ntimin2  ntimin3  ntimin4
  1        1        3        0
* subprocesses
* ife      k        l        m        n
  1        3        0        0        0
* time intervals
  1        0        0
```

Appendix C Case study results

C.1 Stricken areas in the Bay of Bengal

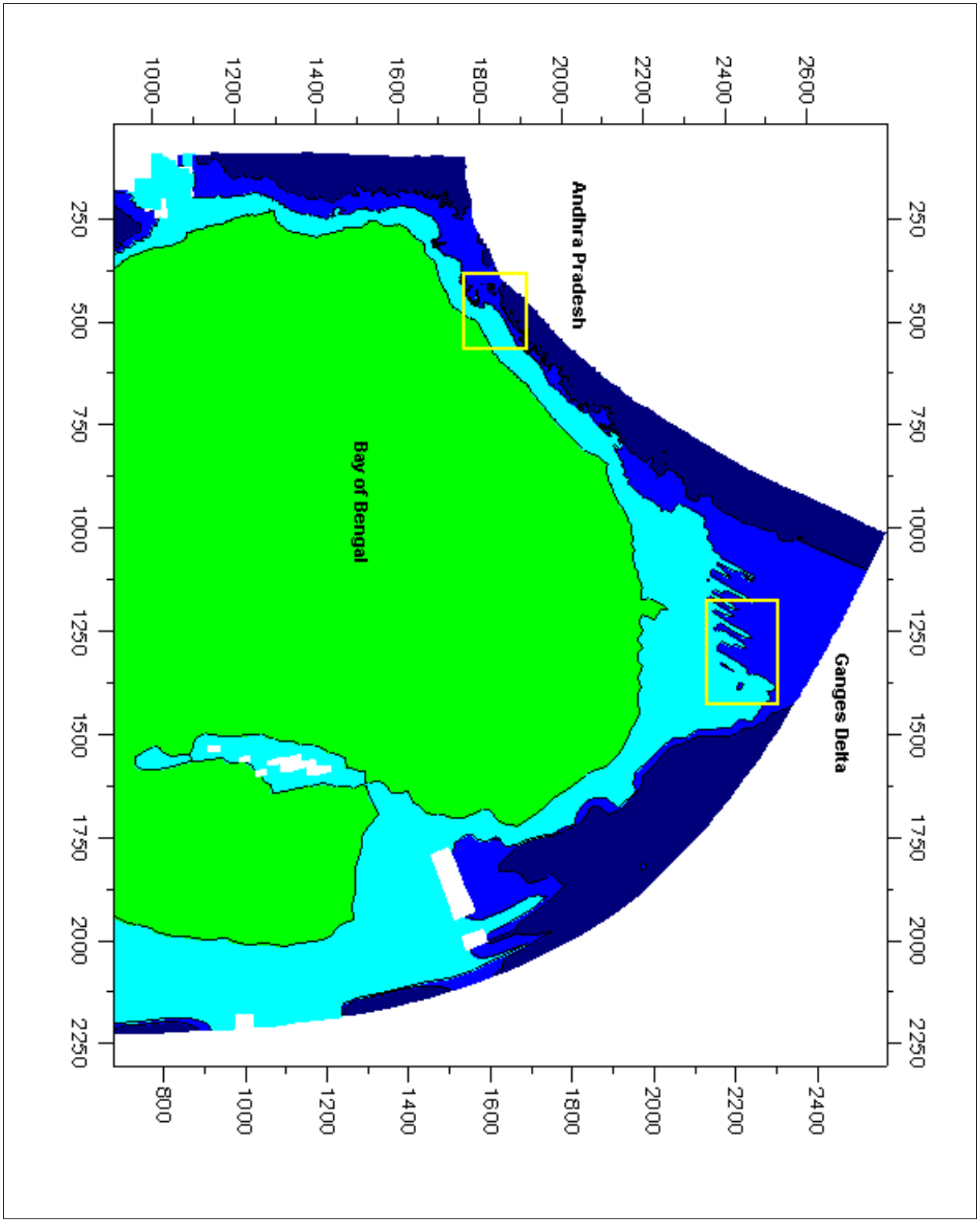

Figure C-1: Overview of Bay of Bengal including the selected areas

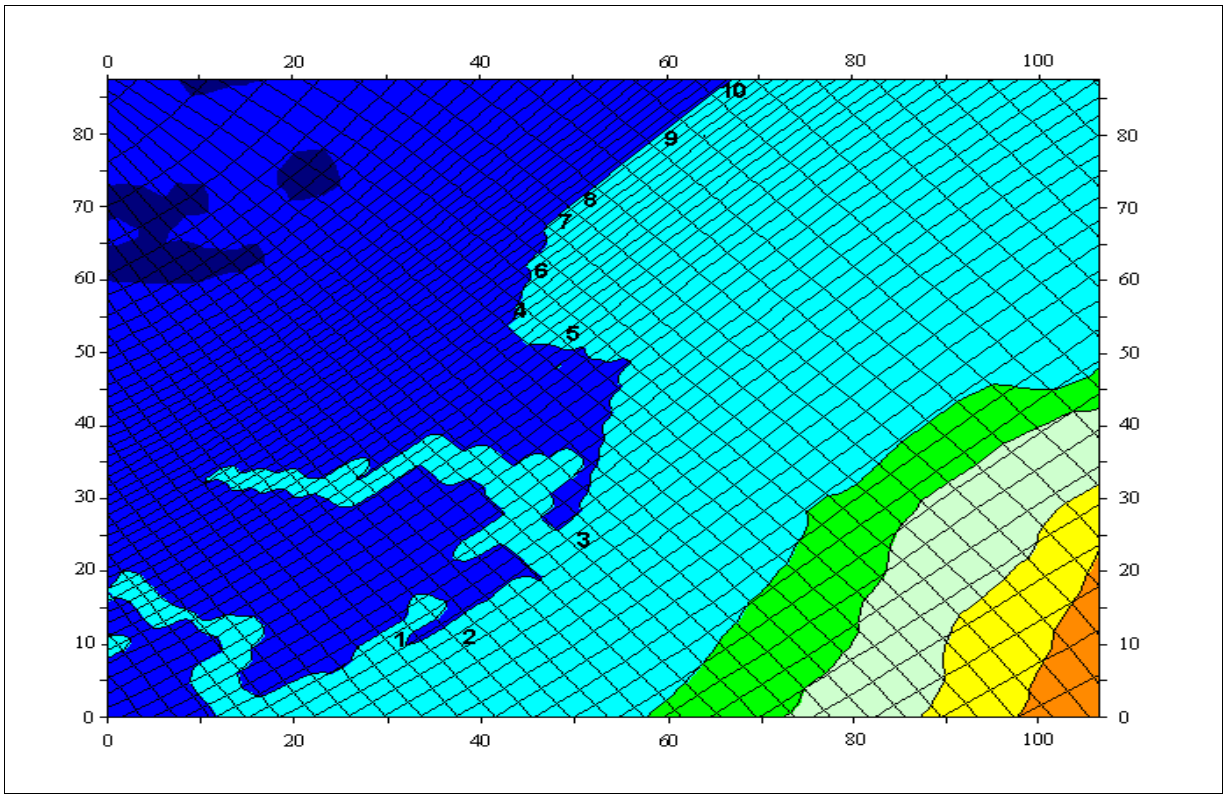

Figure C-2: Andhra Pradesh selected area

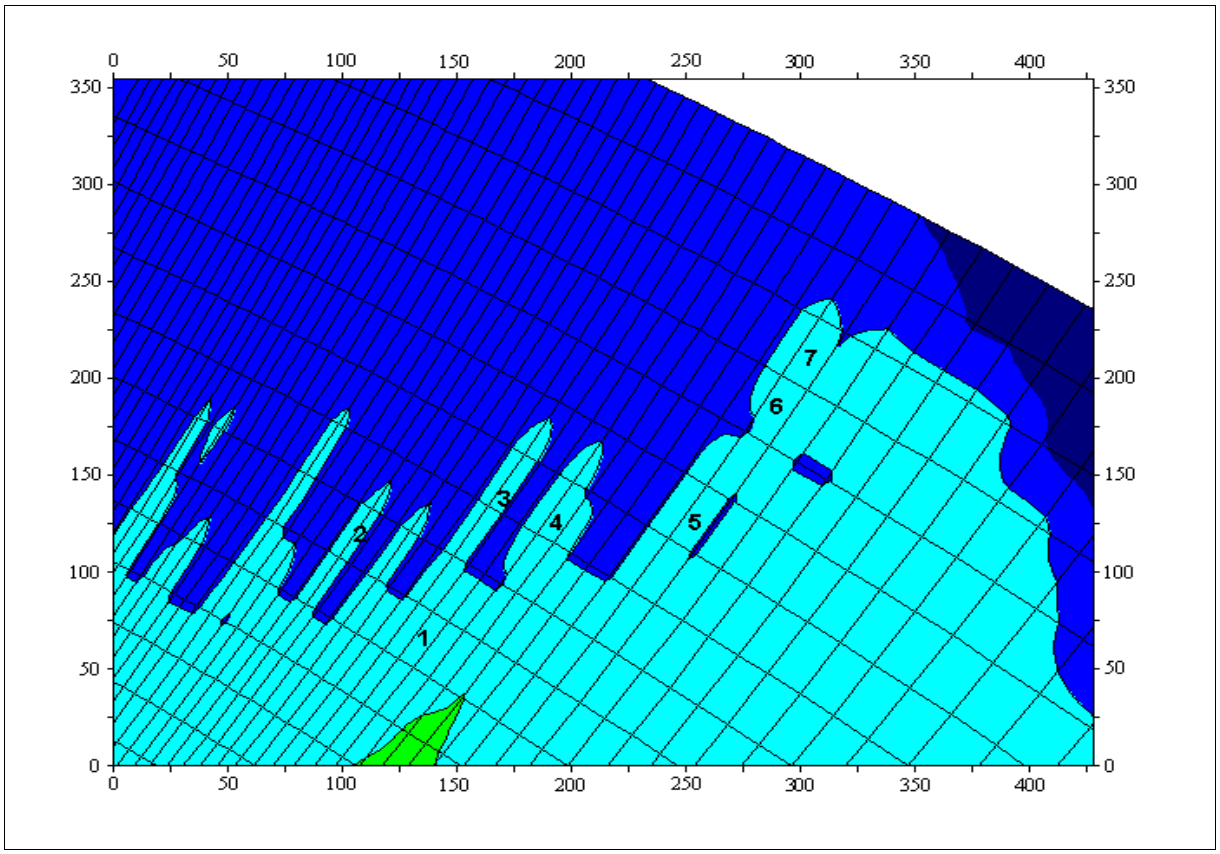

Figure C-3: Ganges Delta selected area

C.2 Water level registration at Andhra Pradesh

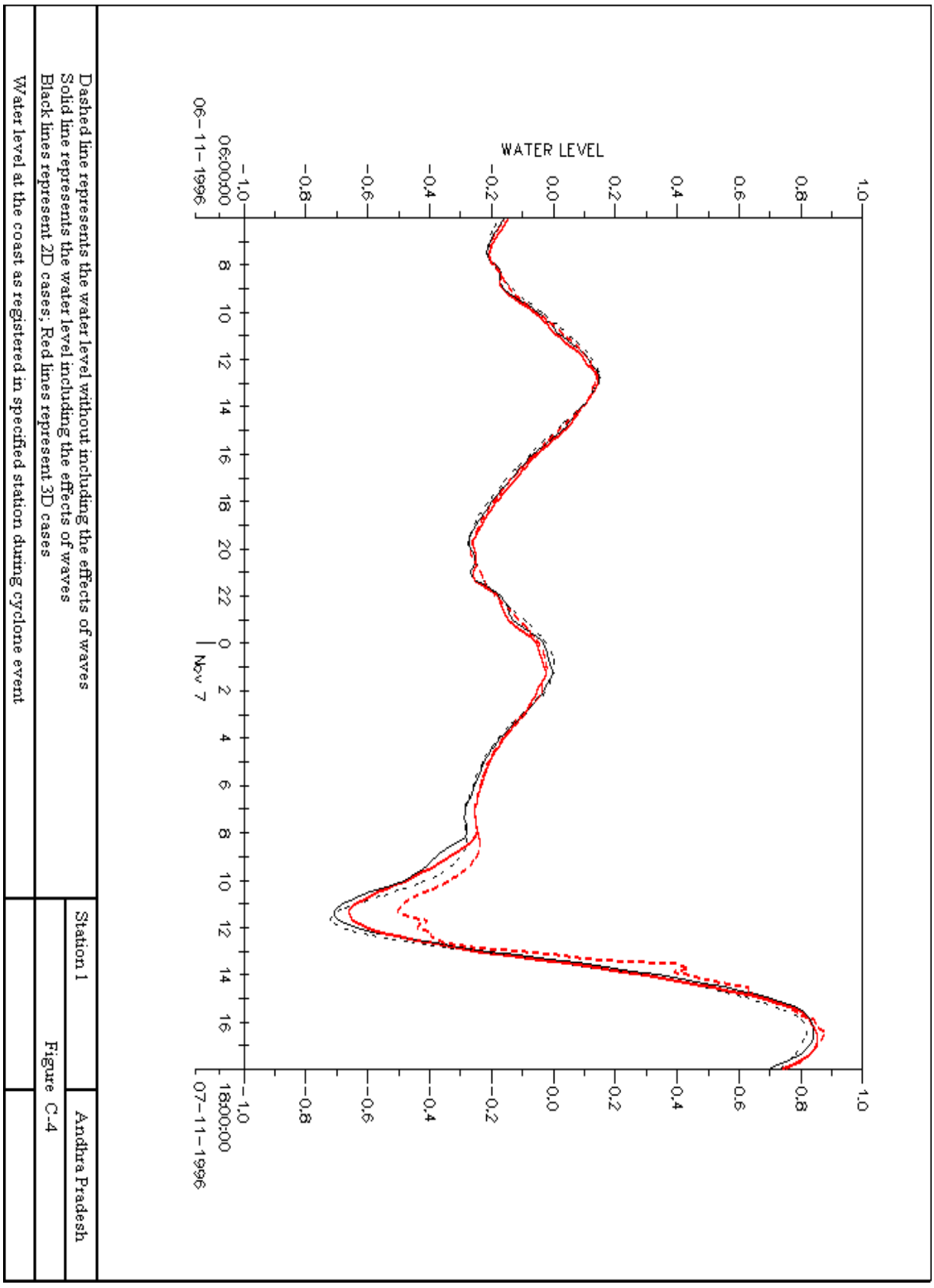

Dashed line represents the water level without including the effects of waves
Solid line represents the water level including the effects of waves
Black lines represent 2D cases; Red lines represent 3D cases

Station 1 | Andhra Pradesh

Figure C-4

Water level at the coast as registered in specified station during cyclone event

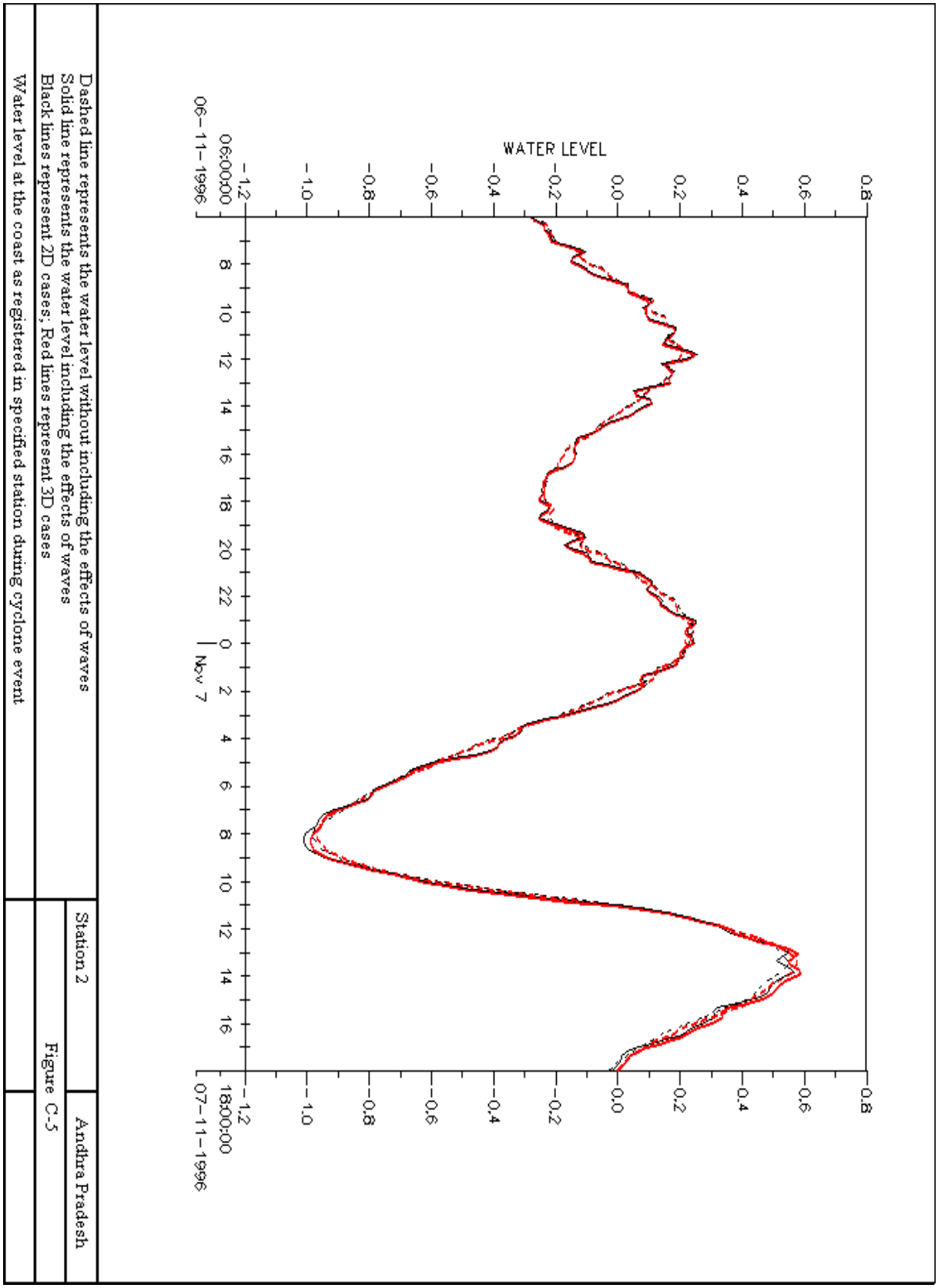

Dashed line represents the water level without including the effects of waves
Solid line represents the water level including the effects of waves
Black lines represent 2D cases; Red lines represent 3D cases

Station 2 — Andhra Pradesh

Figure C-5

Water level at the coast as registered in specified station during cyclone event

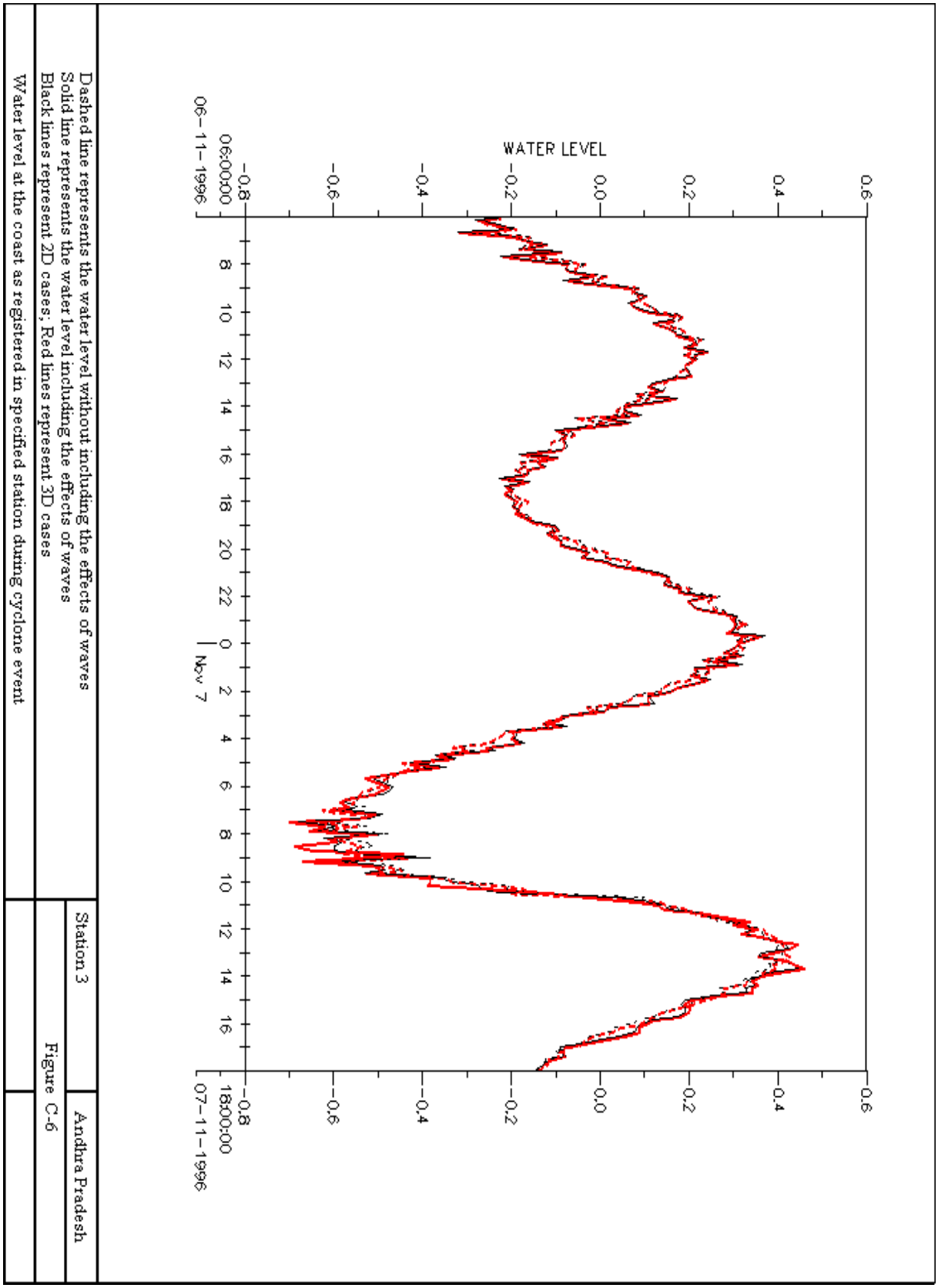

Dashed line represents the water level without including the effects of waves
Solid line represents the water level including the effects of waves
Black lines represent 2D cases; Red lines represent 3D cases

Water level at the coast as registered in specified station during cyclone event

Station 3

Andhra Pradesh

Figure C-6

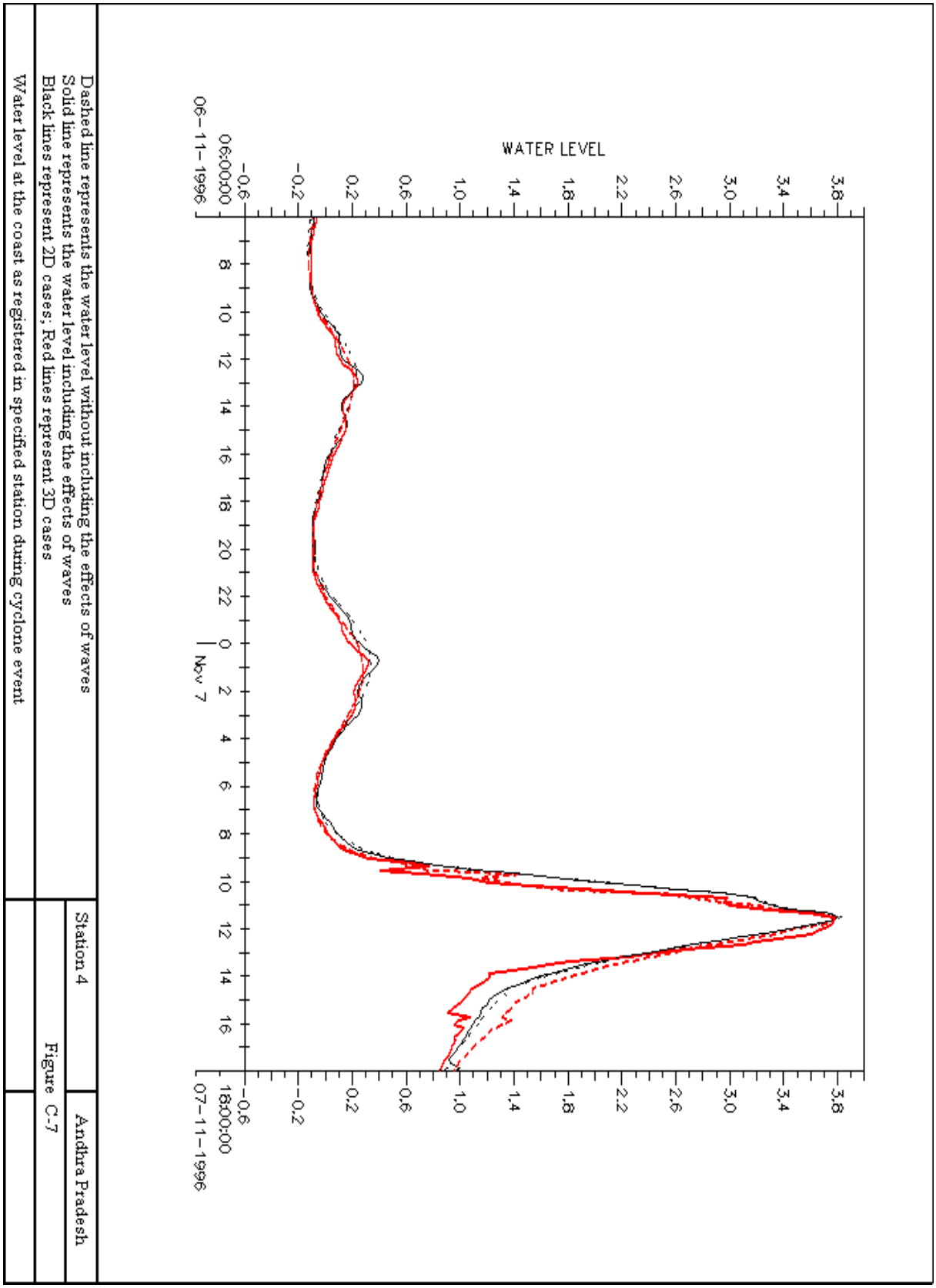

Dashed line represents the water level without including the effects of waves
Solid line represents the water level including the effects of waves
Black lines represent 2D cases; Red lines represent 3D cases

Station 4 | Andhra Pradesh

Figure C-7

Water level at the coast as registered in specified station during cyclone event

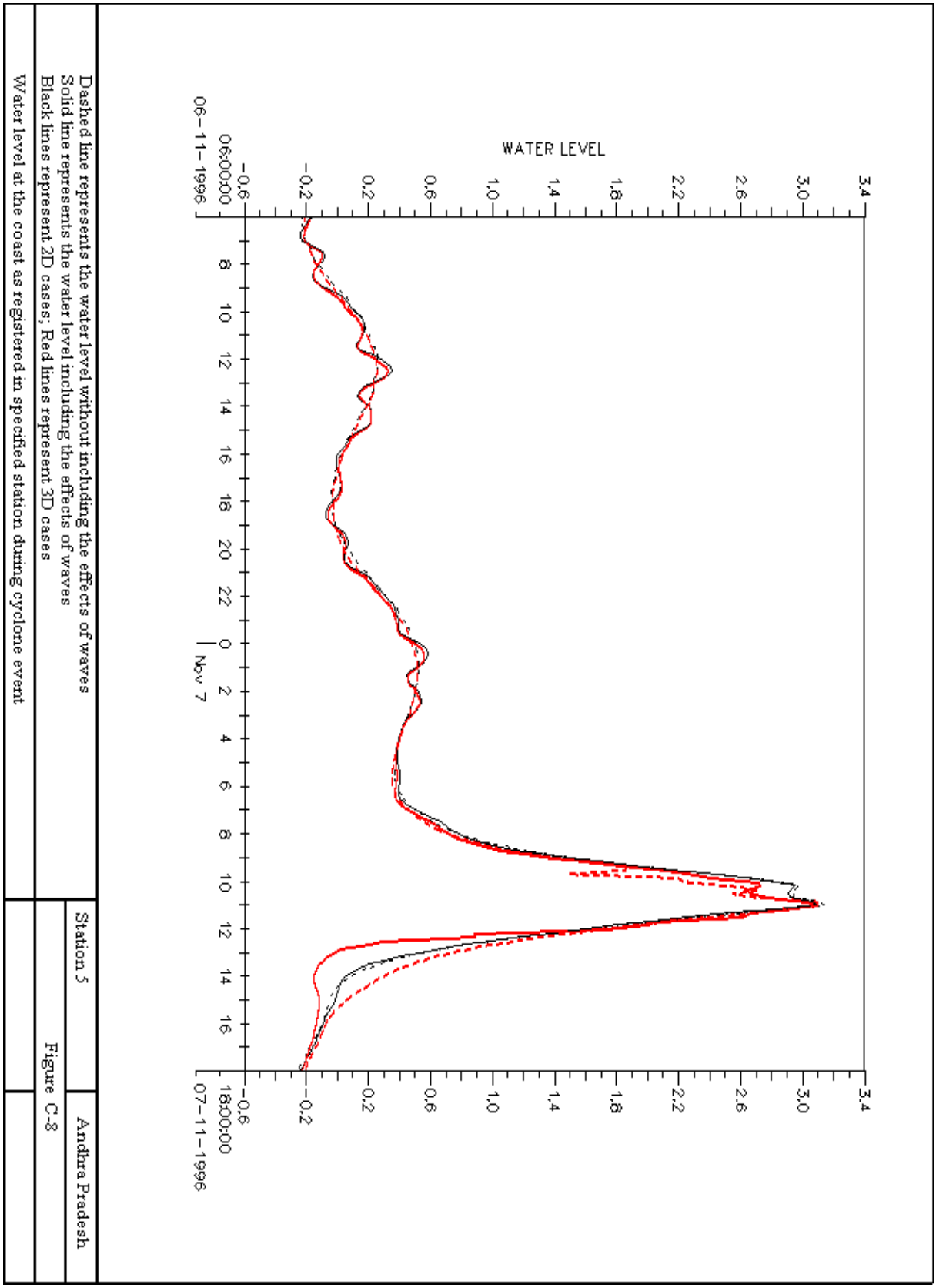

Dashed line represents the water level without including the effects of waves
Solid line represents the water level including the effects of waves
Black lines represent 2D cases; Red lines represent 3D cases

Water level at the coast as registered in specified station during cyclone event

Station 3 — Andhra Pradesh

Figure C-8

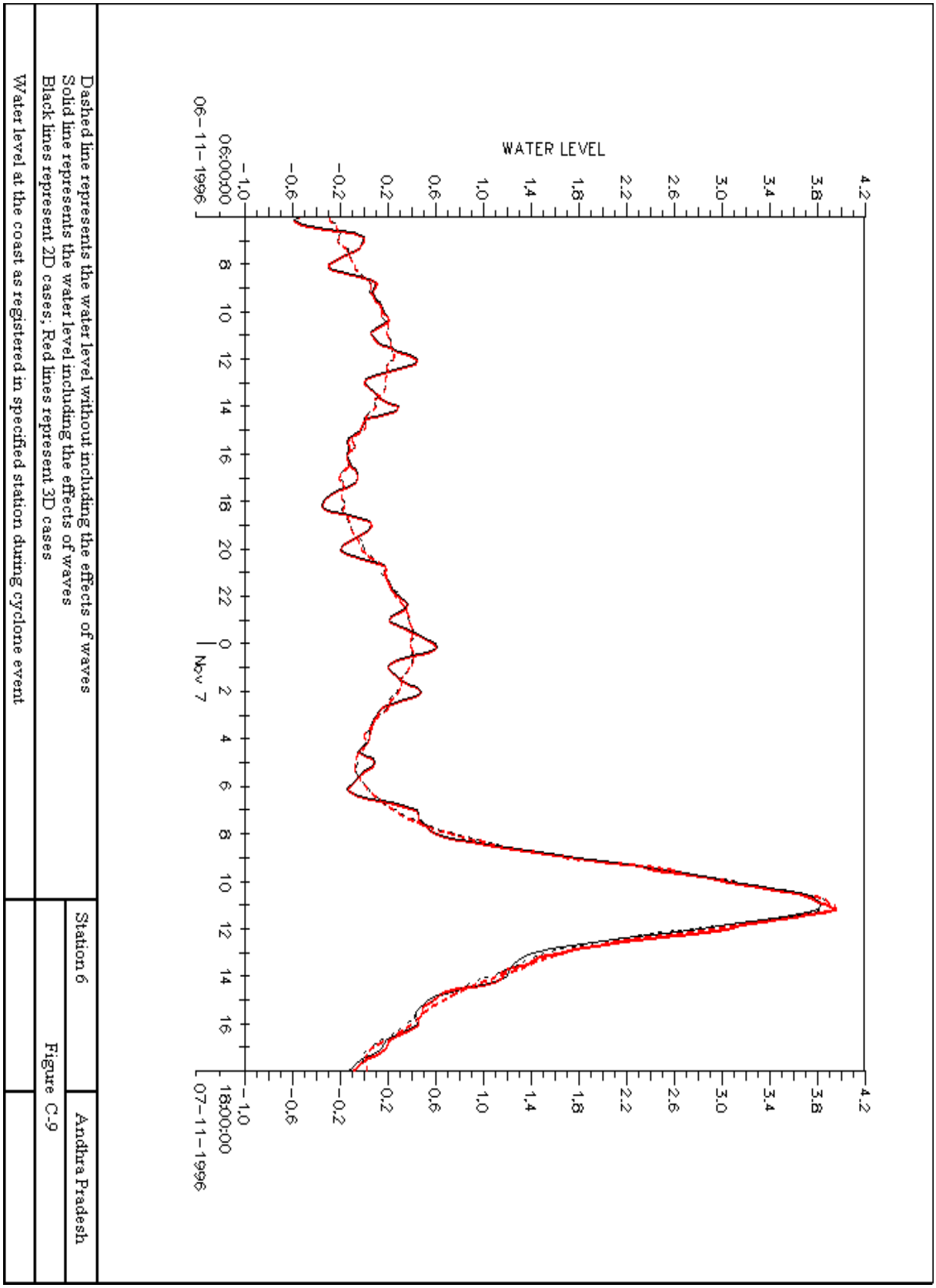

Dashed line represents the water level without including the effects of waves
Solid line represents the water level including the effects of waves
Black lines represent 2D cases; Red lines represent 3D cases

Station 6 — Andhra Pradesh

Figure C-9

Water level at the coast as registered in specified station during cyclone event

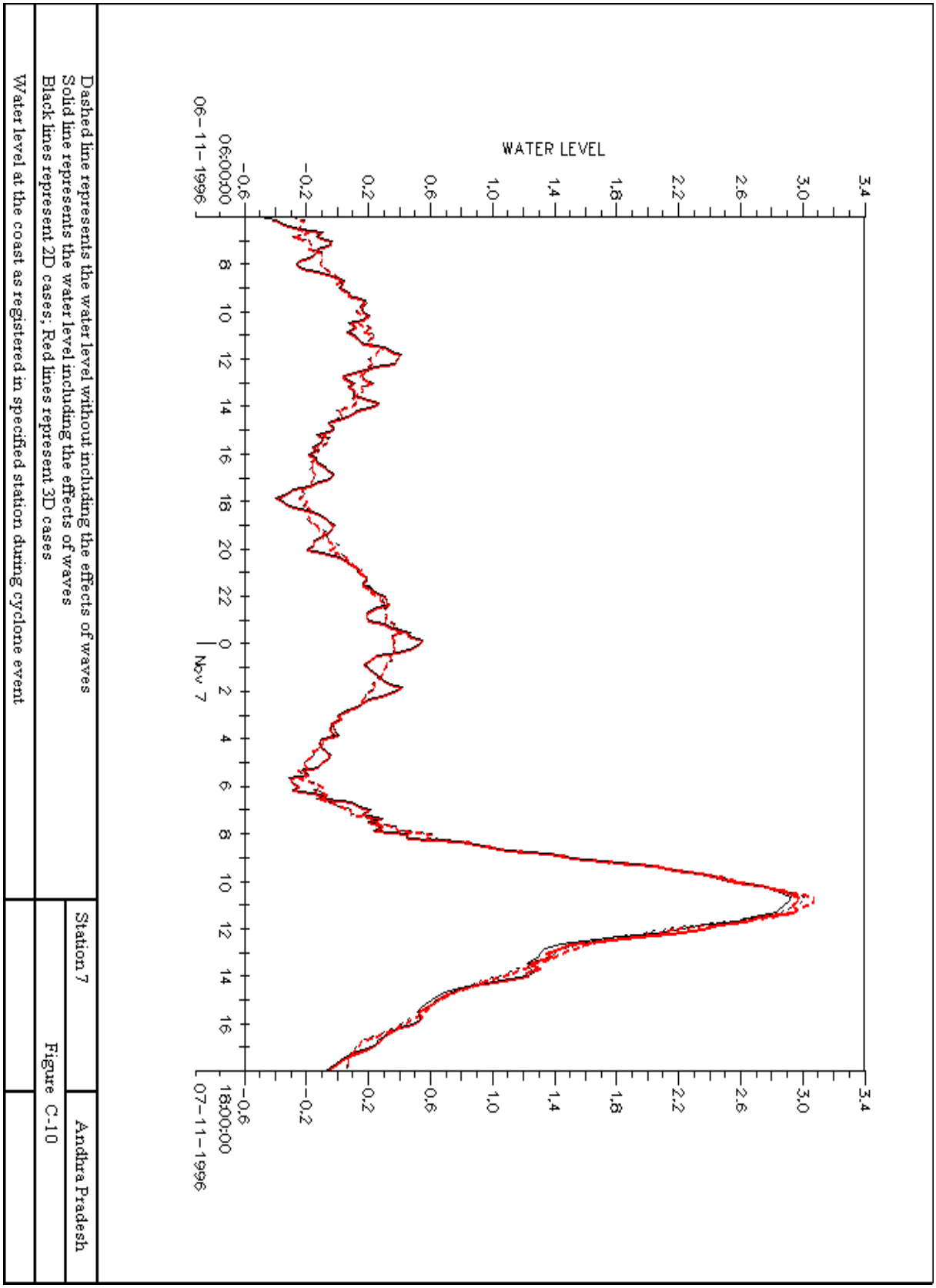

Dashed line represents the water level without including the effects of waves
Solid line represents the water level including the effects of waves
Black lines represent 2D cases; Red lines represent 3D cases

Station 7 | Andhra Pradesh

Figure C-10

Water level at the coast as registered in specified station during cyclone event

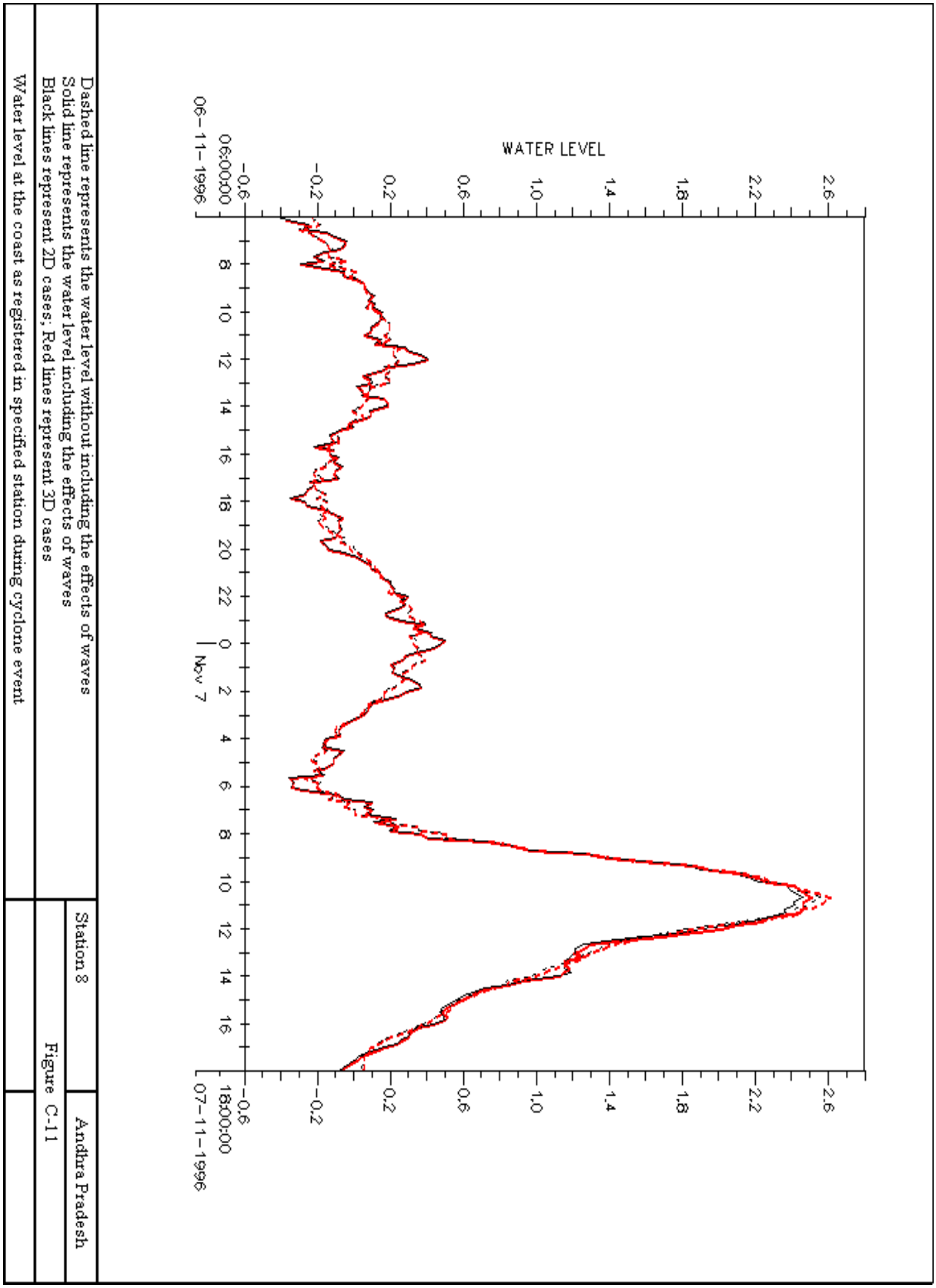

Dashed line represents the water level without including the effects of waves
Solid line represents the water level including the effects of waves
Black lines represent 2D cases; Red lines represent 3D cases

Station 8 — Andhra Pradesh

Figure C-11

Water level at the coast as registered in specified station during cyclone event

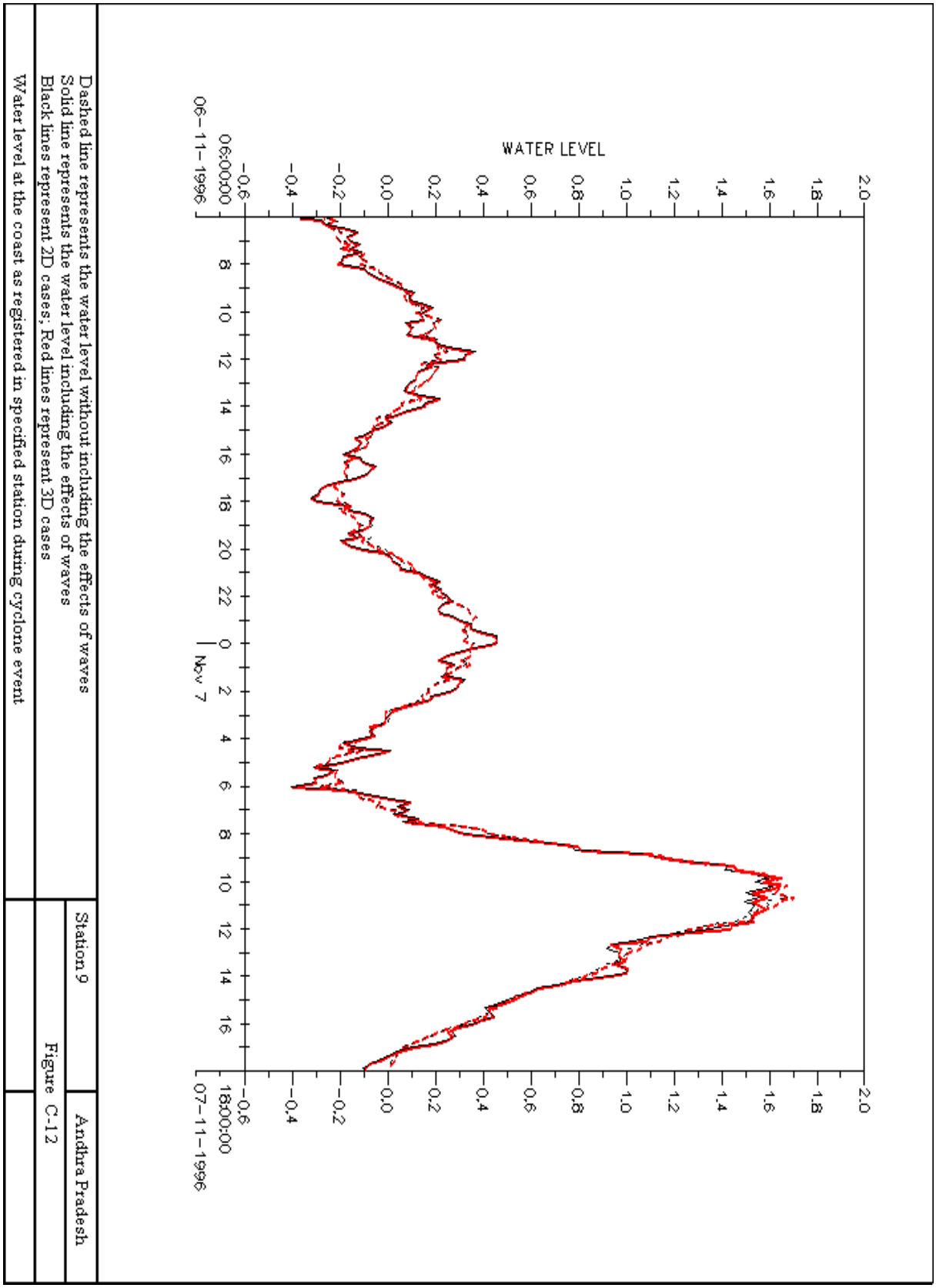

Dashed line represents the water level without including the effects of waves
Solid line represents the water level including the effects of waves
Black lines represent 2D cases; Red lines represent 3D cases

Station 9 | Andhra Pradesh

Figure C-12

Water level at the coast as registered in specified station during cyclone event

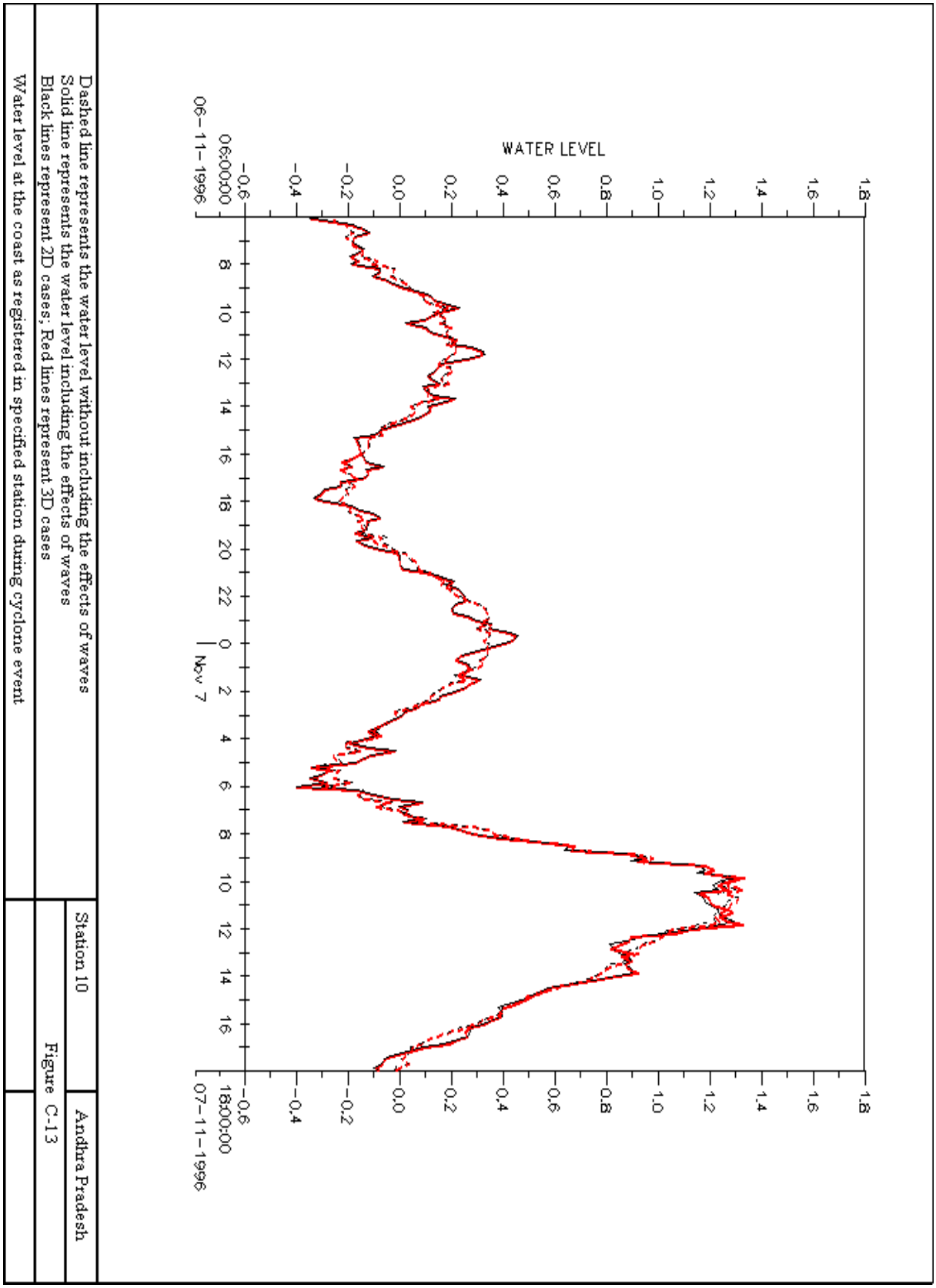

Dashed line represents the water level without including the effects of waves
Solid line represents the water level including the effects of waves
Black lines represent 2D cases; Red lines represent 3D cases

Station 10 | Andhra Pradesh

Figure C-13

Water level at the coast as registered in specified station during cyclone event

C.3 Water level registration at Ganges Delta

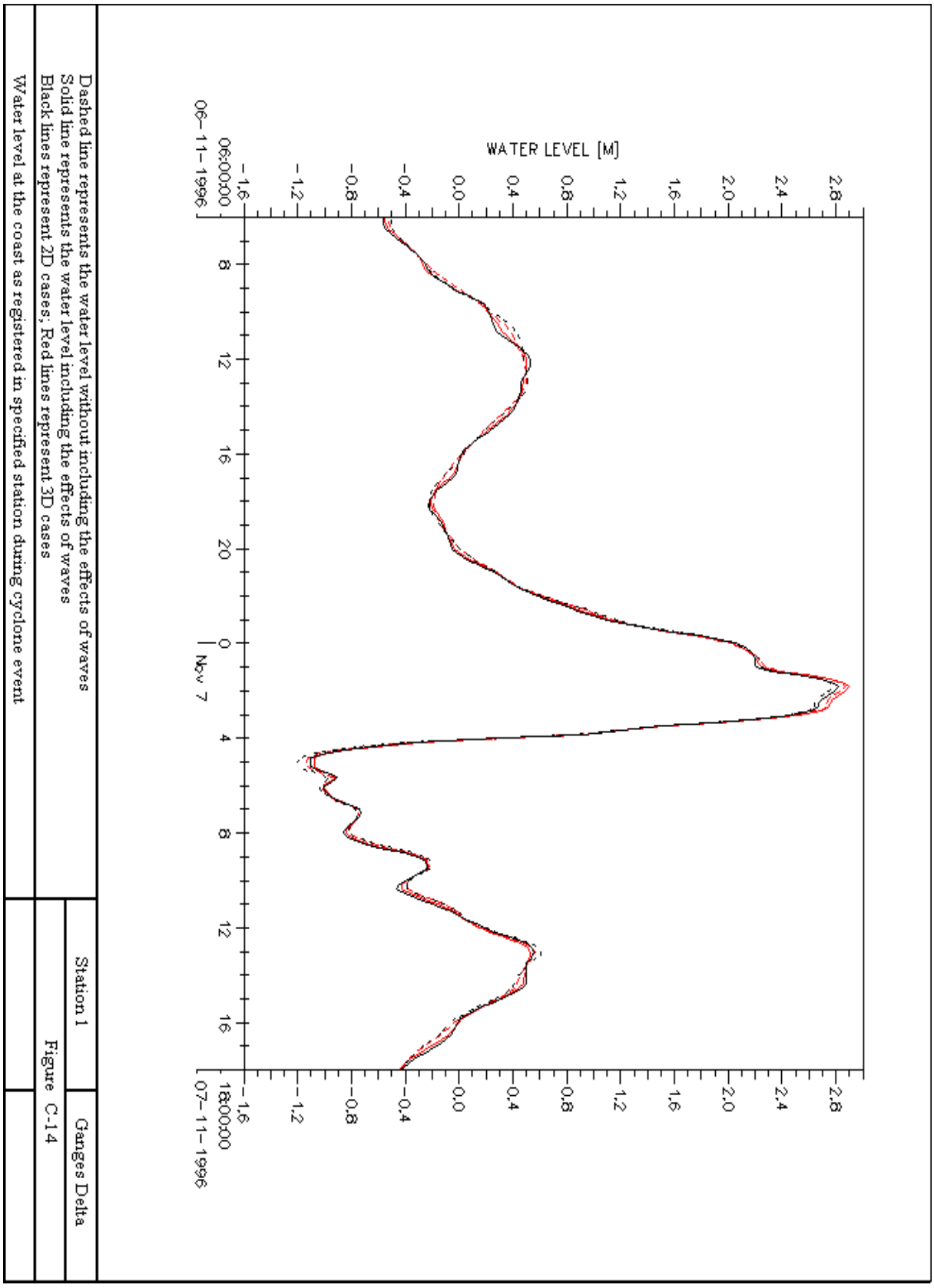

Dashed line represents the water level without including the effects of waves
Solid line represents the water level including the effects of waves
Black lines represent 2D cases; Red lines represent 3D cases

Station 1 | Ganges Delta

Figure C-14

Water level at the coast as registered in specified station during cyclone event

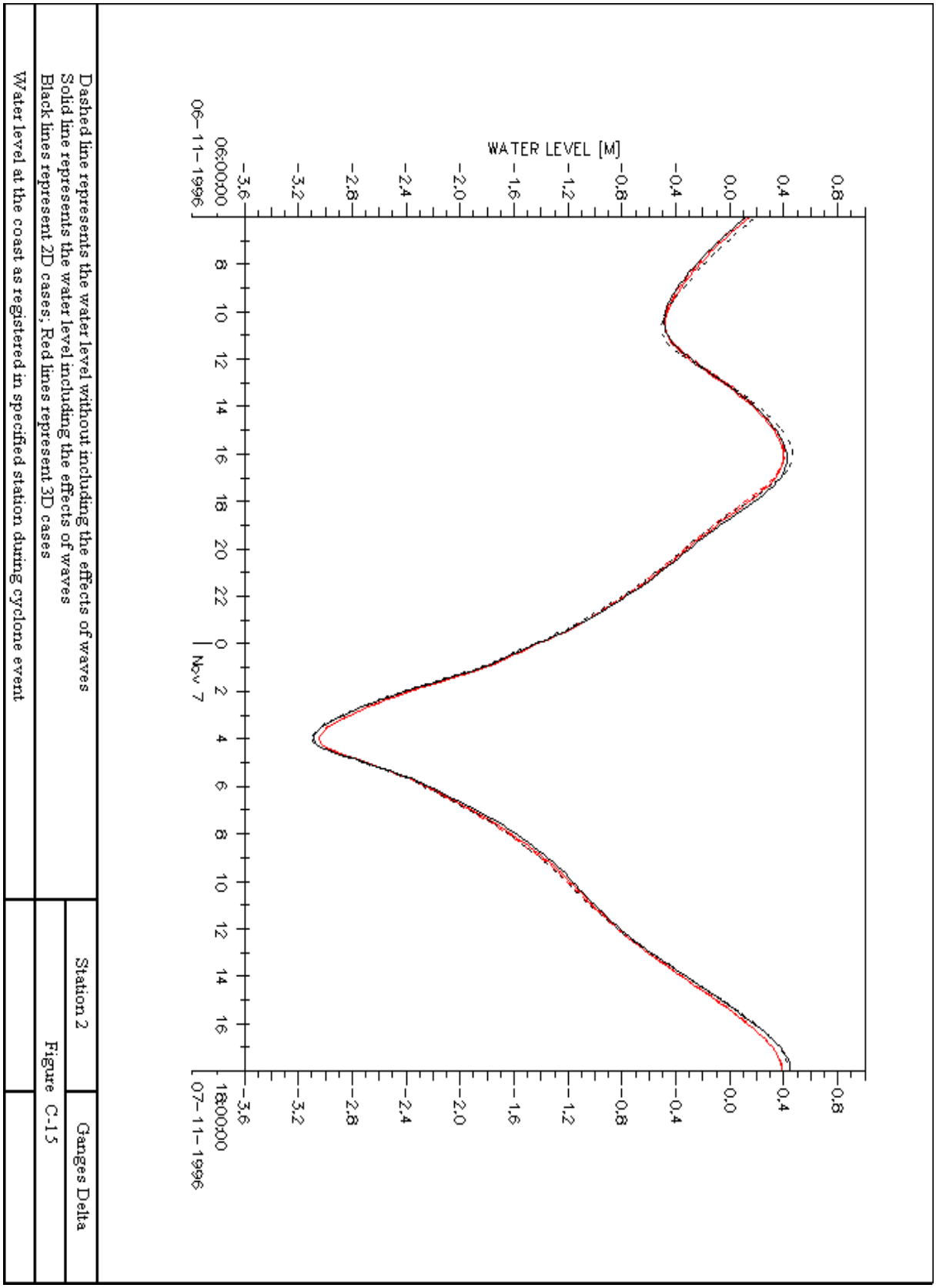

Dashed line represents the water level without including the effects of waves
Solid line represents the water level including the effects of waves
Black lines represent 2D cases; Red lines represent 3D cases

Station 2 | Ganges Delta

Figure C-15

Water level at the coast as registered in specified station during cyclone event

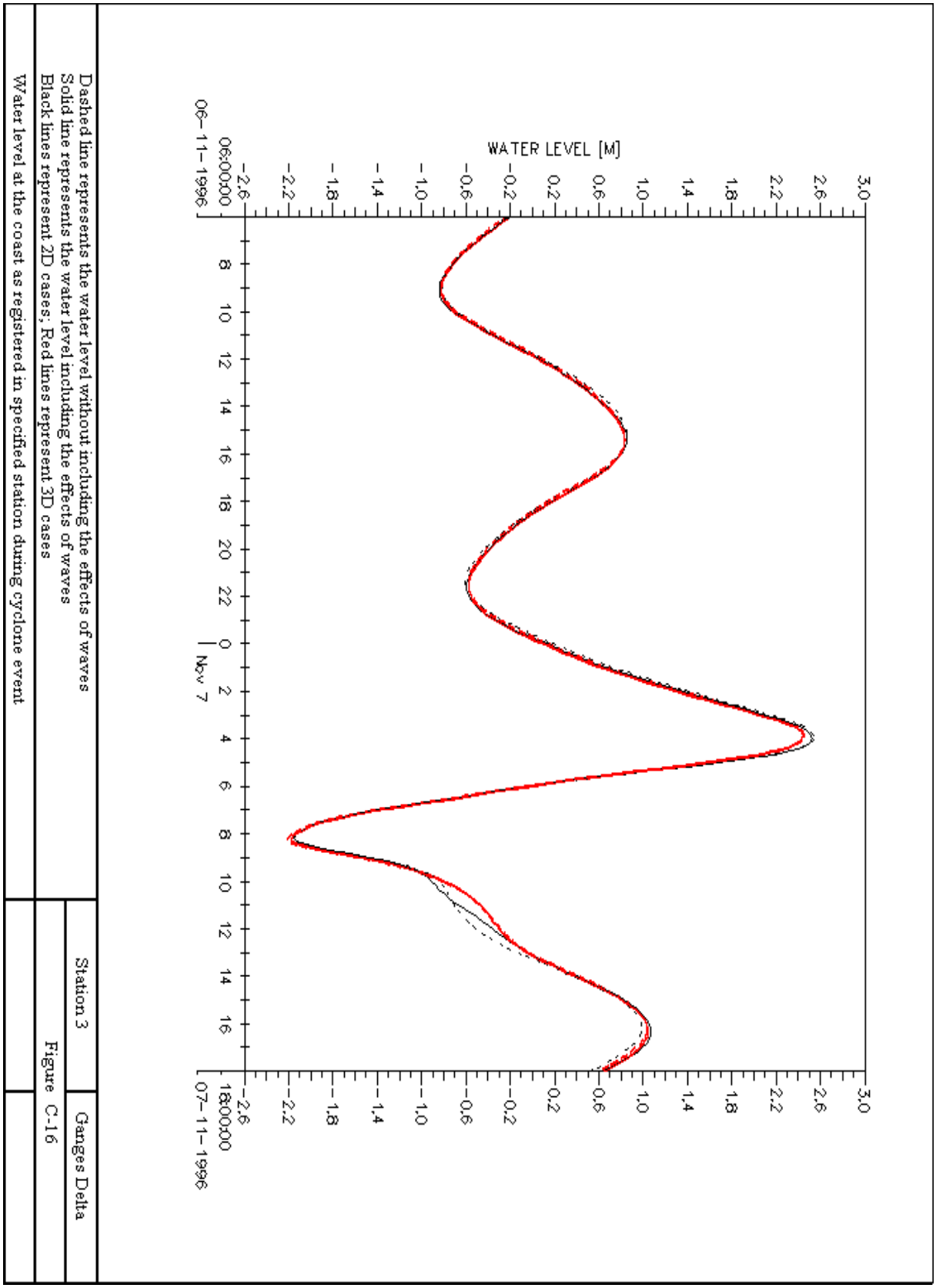

Dashed line represents the water level without including the effects of waves
Solid line represents the water level including the effects of waves
Black lines represent 2D cases; Red lines represent 3D cases

Station 3 | Ganges Delta

Figure C-16

Water level at the coast as registered in specified station during cyclone event

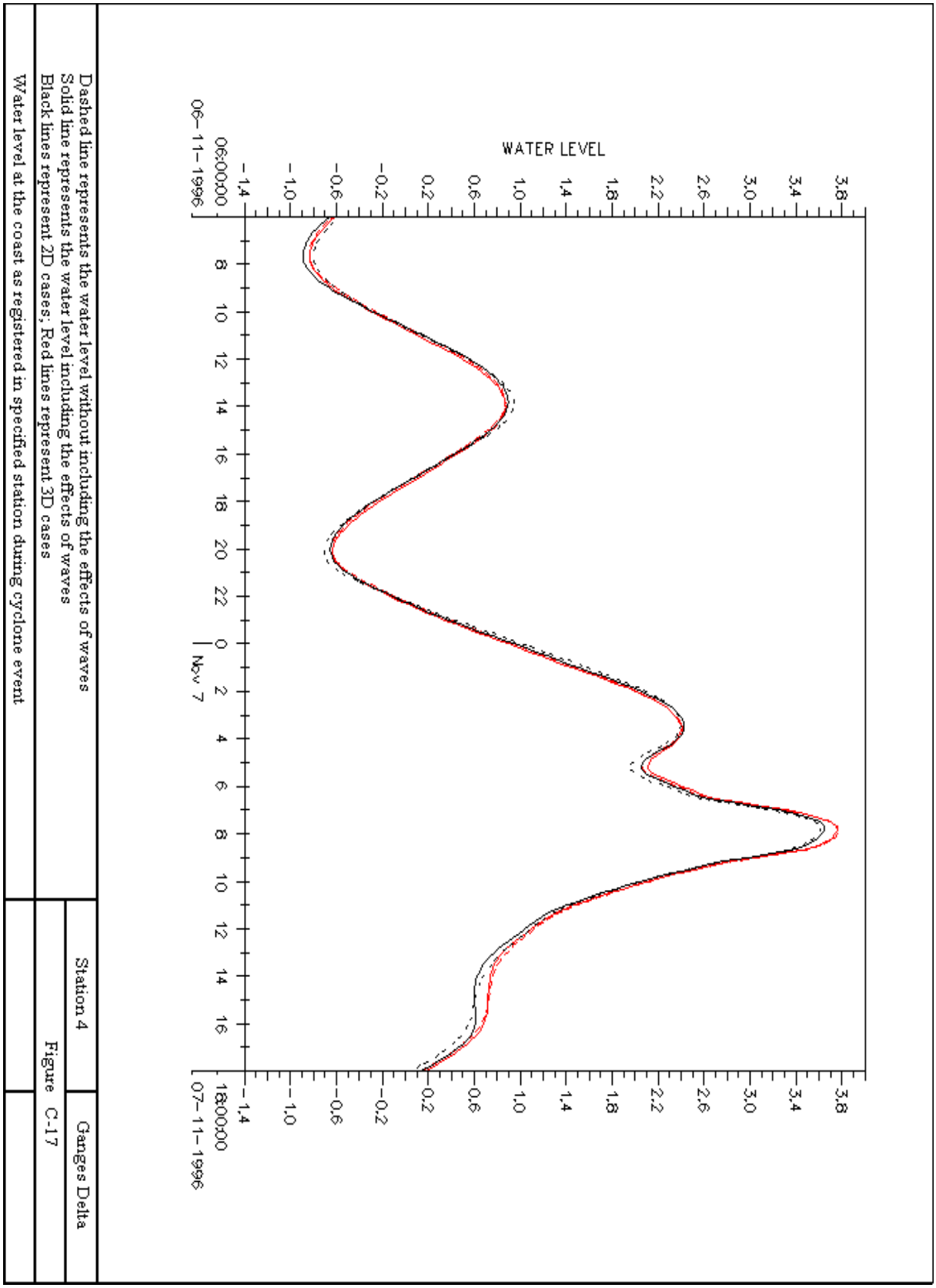

Dashed line represents the water level without including the effects of waves
Solid line represents the water level including the effects of waves
Black lines represent 2D cases; Red lines represent 3D cases

Station 4 | Ganges Delta

Figure C-17

Water level at the coast as registered in specified station during cyclone event

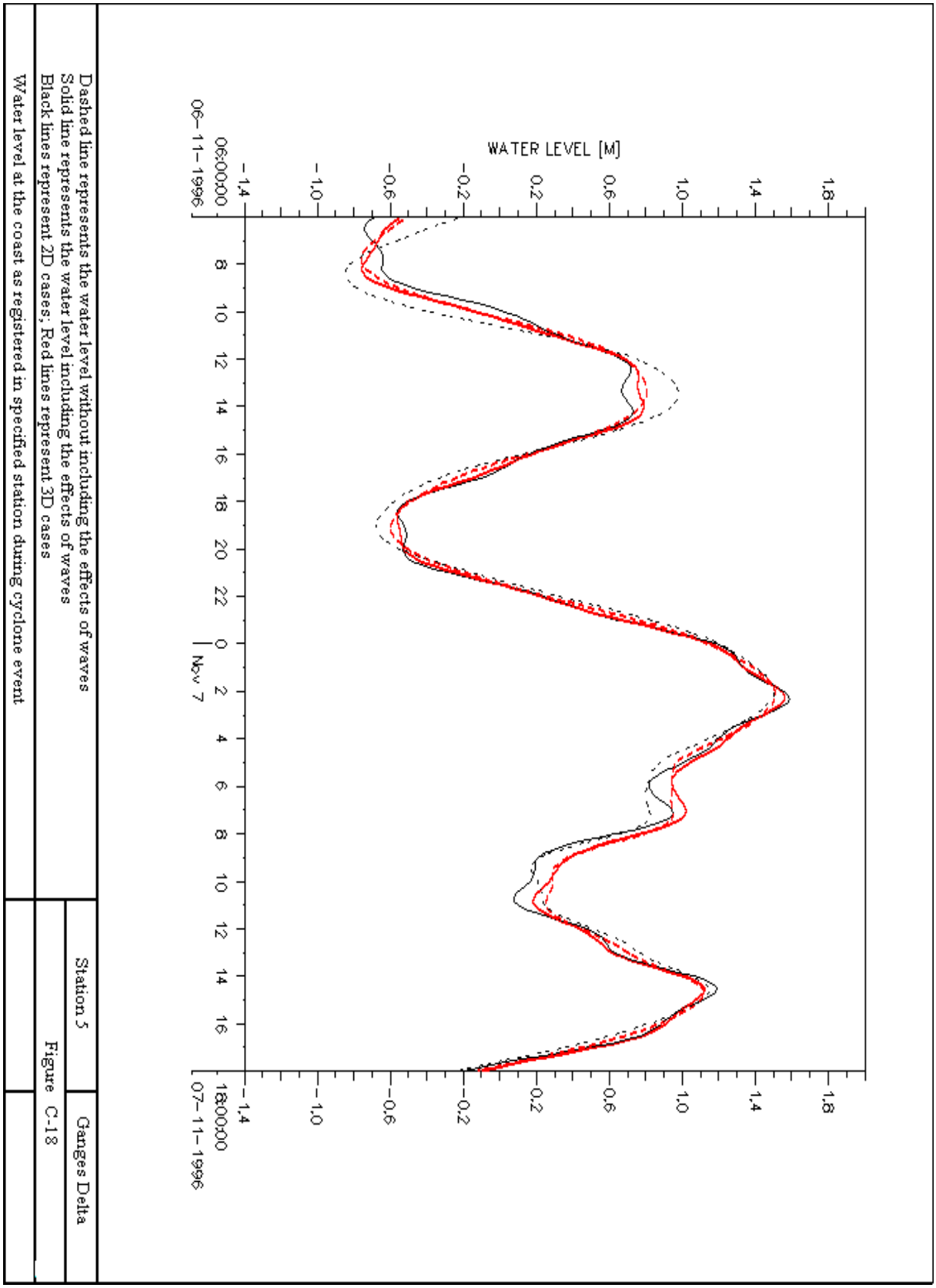

Dashed line represents the water level without including the effects of waves
Solid line represents the water level including the effects of waves
Black lines represent 2D cases; Red lines represent 3D cases

Station 5 | Ganges Delta

Figure C-18

Water level at the coast as registered in specified station during cyclone event

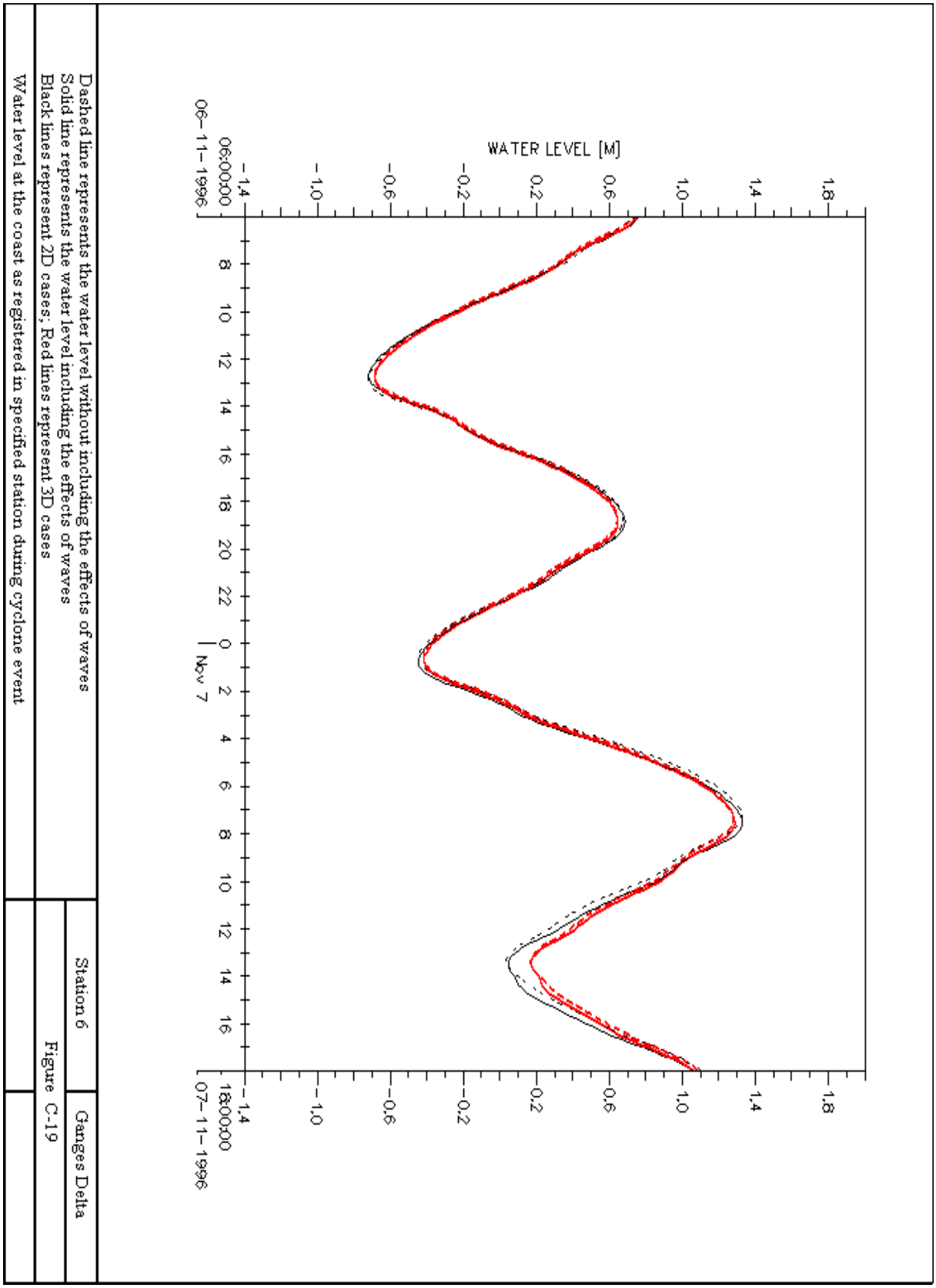

Dashed line represents the water level without including the effects of waves
Solid line represents the water level including the effects of waves
Black lines represent 2D cases; Red lines represent 3D cases

Station 6 | Ganges Delta

Figure C-19

Water level at the coast as registered in specified station during cyclone event

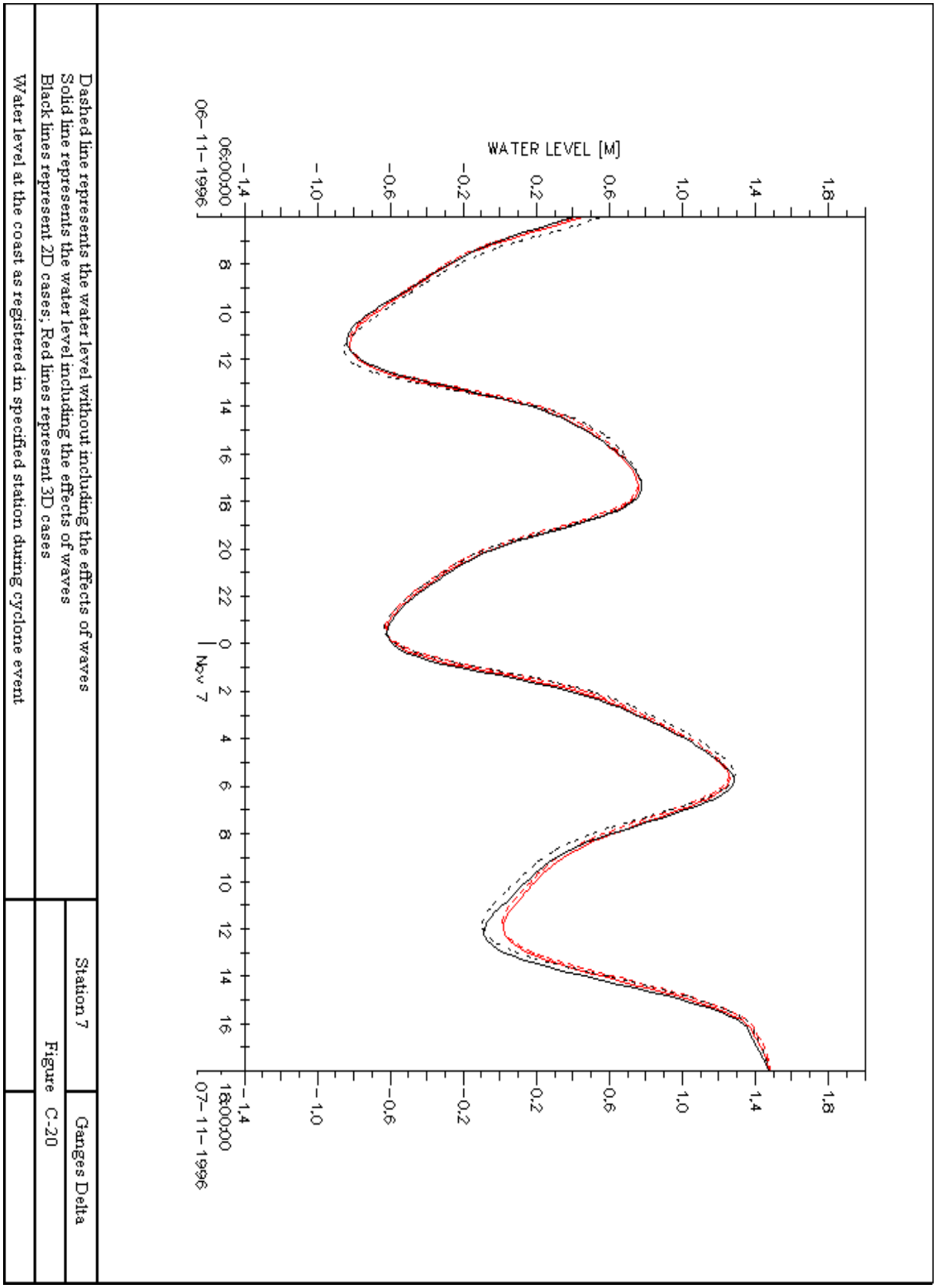

Dashed line represents the water level without including the effects of waves
Solid line represents the water level including the effects of waves
Black lines represent 2D cases; Red lines represent 3D cases

Station 7 | Ganges Delta

Figure C-20

Water level at the coast as registered in specified station during cyclone event

C.4 Water level set-up due to waves in 2D Andhra Pradesh case

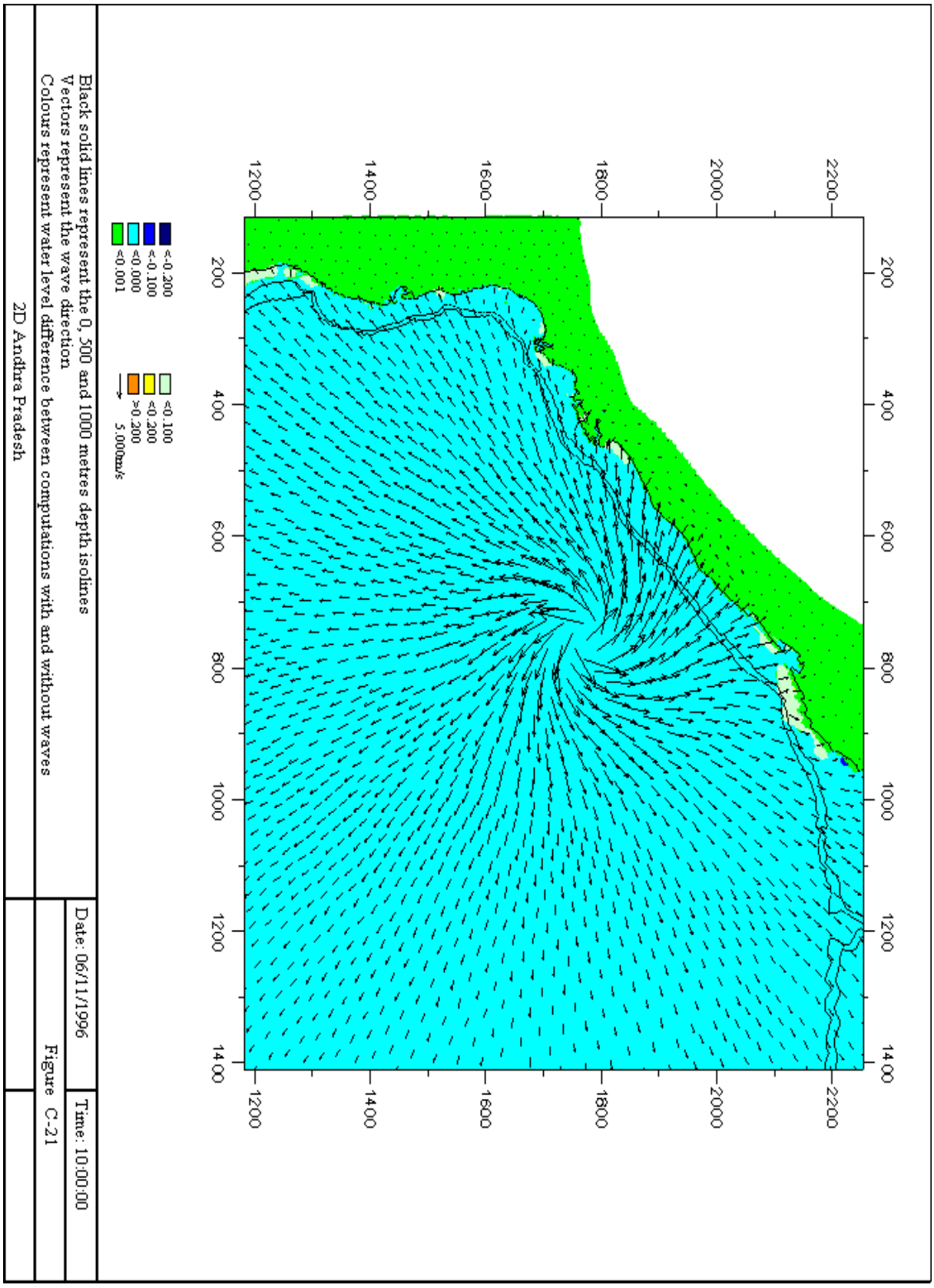

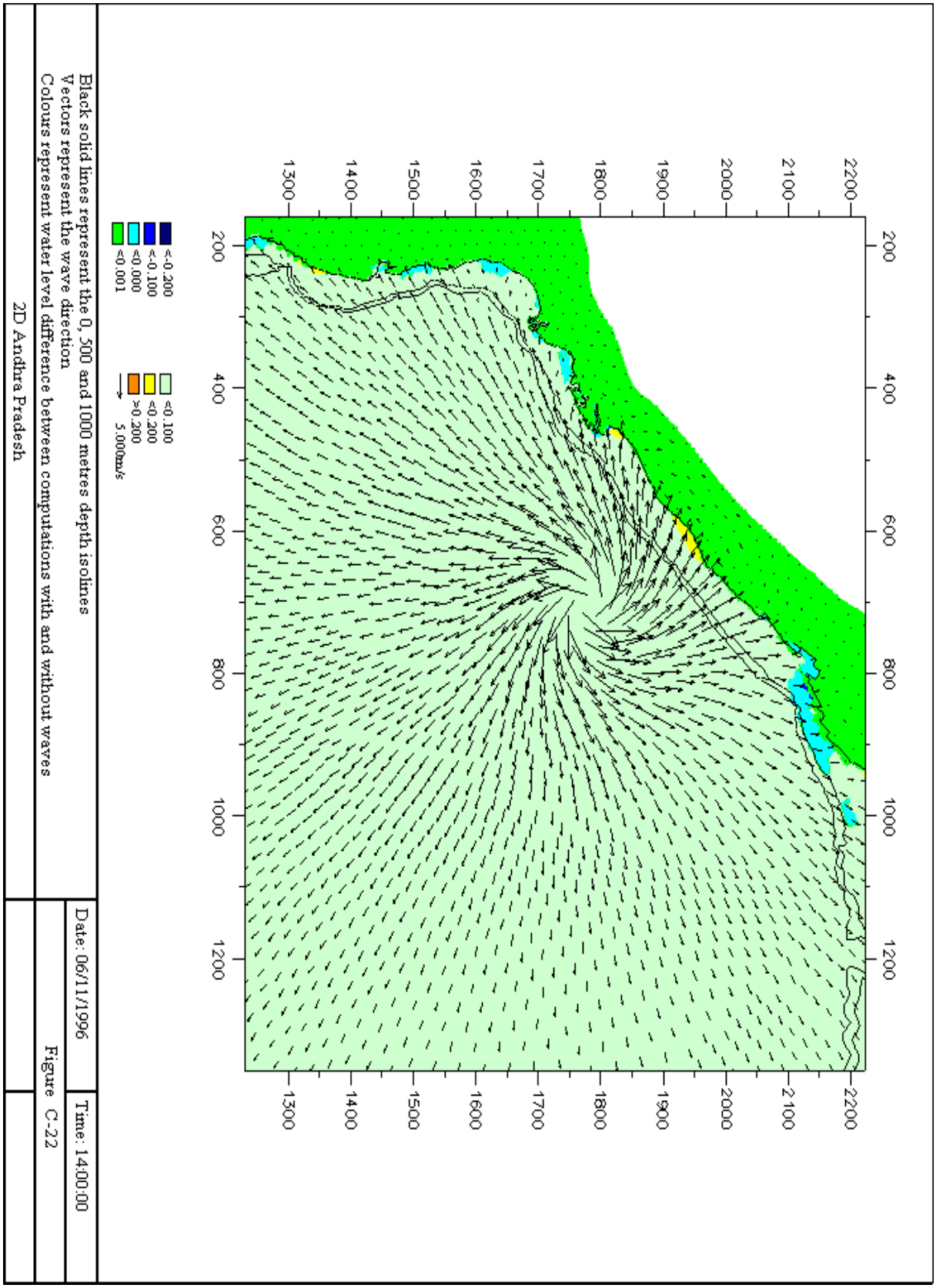
Black solid lines represent the 0, 500 and 1000 metres depth isolines
Vectors represent the wave direction
Colours represent water level difference between computations with and without waves
2D Andhra Pradesh
Date: 06/11/1996
Time: 14:00:00
Figure C-22
<-0.200
<-0.100
<0.000
<0.001
<0.100
<0.200
>0.200
5.000m/s

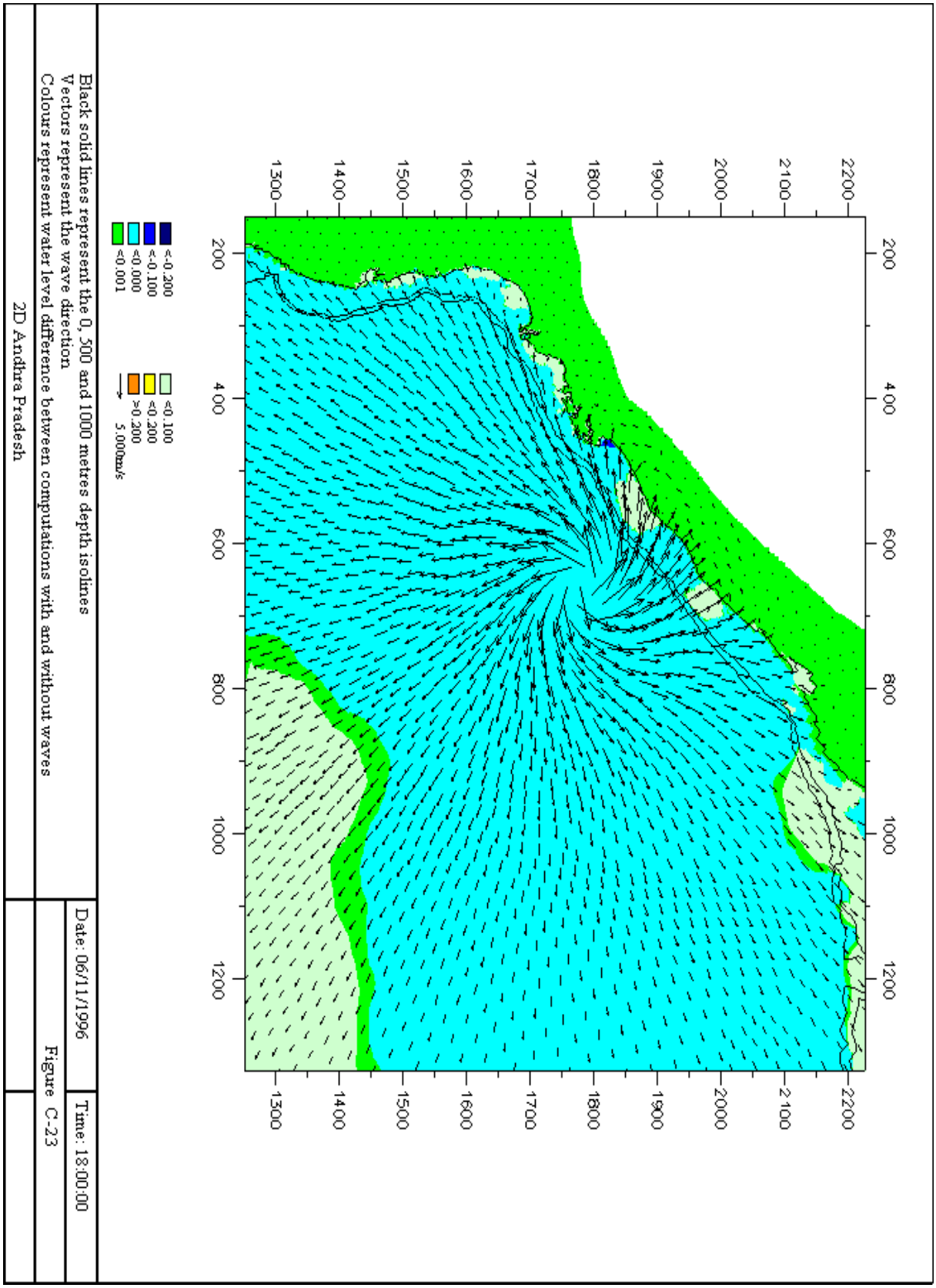
Black solid lines represent the 0, 500 and 1000 metres depth isolines
Vectors represent the wave direction
Colours represent water level difference between computations with and without waves
2D Andhra Pradesh
Date: 06/11/1996
Time: 18:00:00
Figure C-23
<-0.200
<-0.100
<0.000
<0.001
<0.100
<0.200
>0.200
5.000m/s

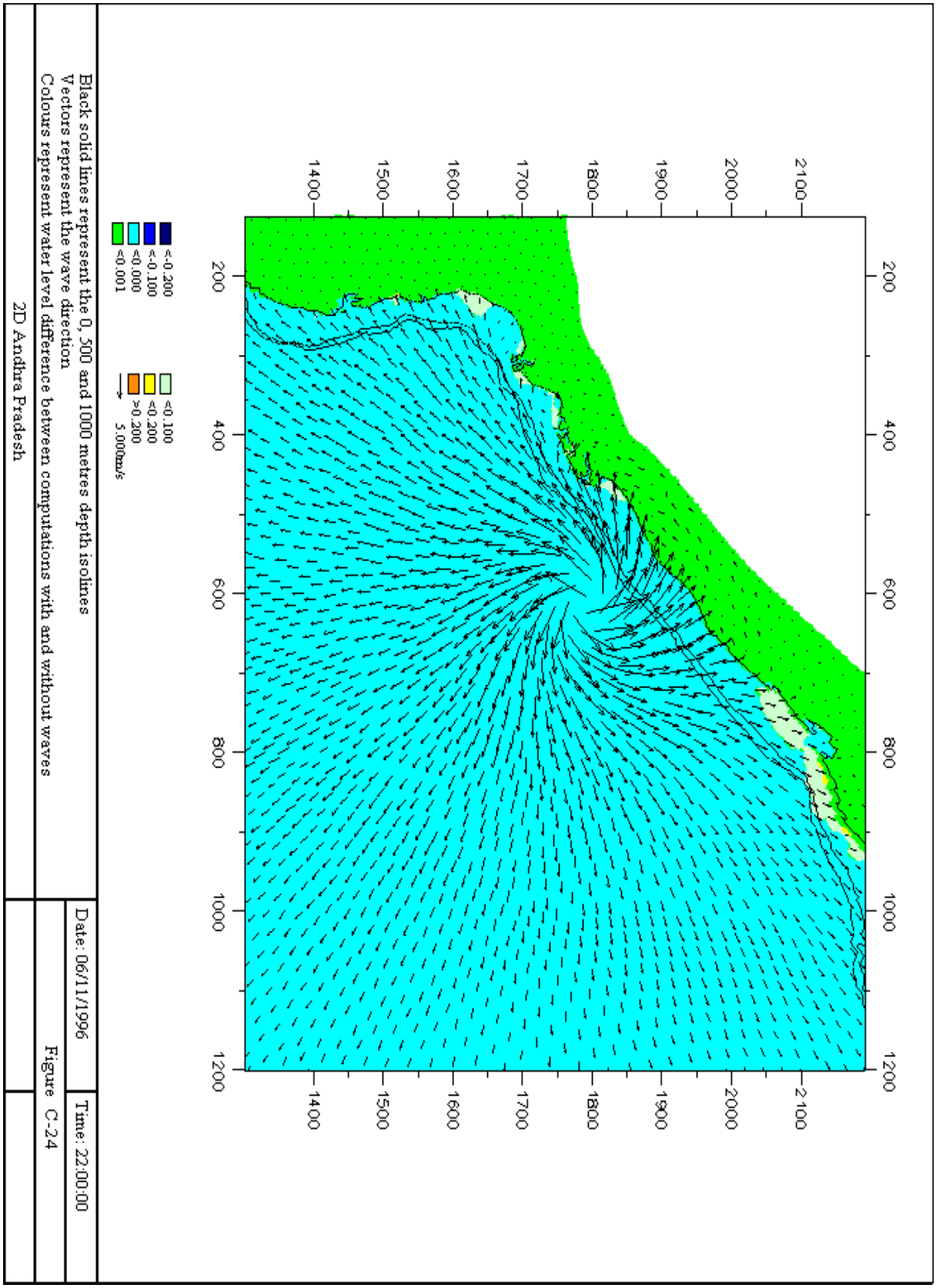
Black solid lines represent the 0, 500 and 1000 metres depth isolines
Vectors represent the wave direction
Colours represent water level difference between computations with and without waves
2D Andhra Pradesh
Date: 06/11/1996
Time: 22:00:00
Figure C-24
<-0.200
<-0.100
<0.000
<0.001
<0.100
<0.200
>0.200
5.000m/s

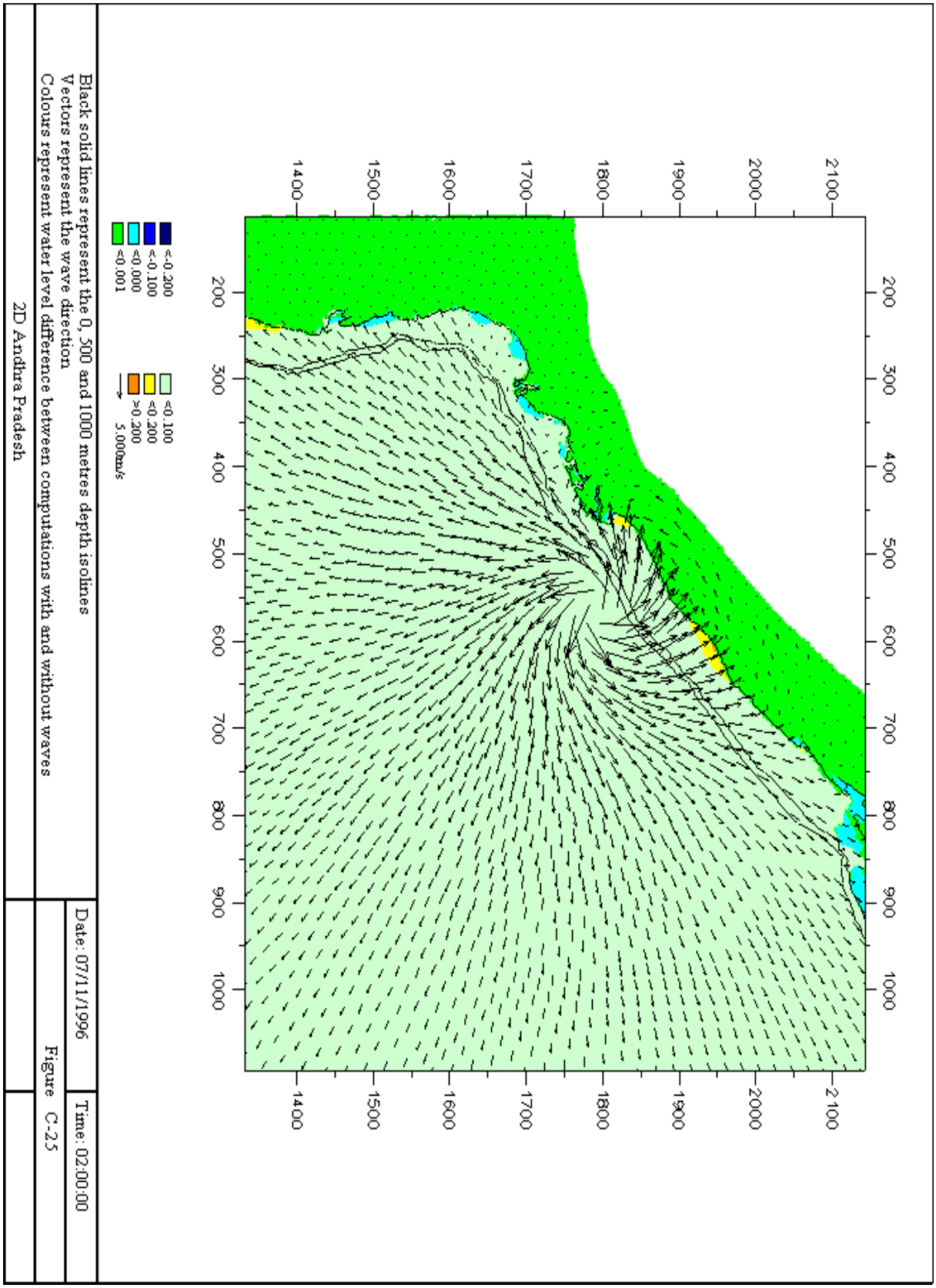
Black solid lines represent the 0, 500 and 1000 metres depth isolines
Vectors represent the wave direction
Colours represent water level difference between computations with and without waves
2D Andhra Pradesh
Date: 07/11/1996
Time: 02:00:00
Figure C-25
<-0.200
<-0.100
<0.000
<0.001
<0.100
<0.200
>0.200
5.000m/s

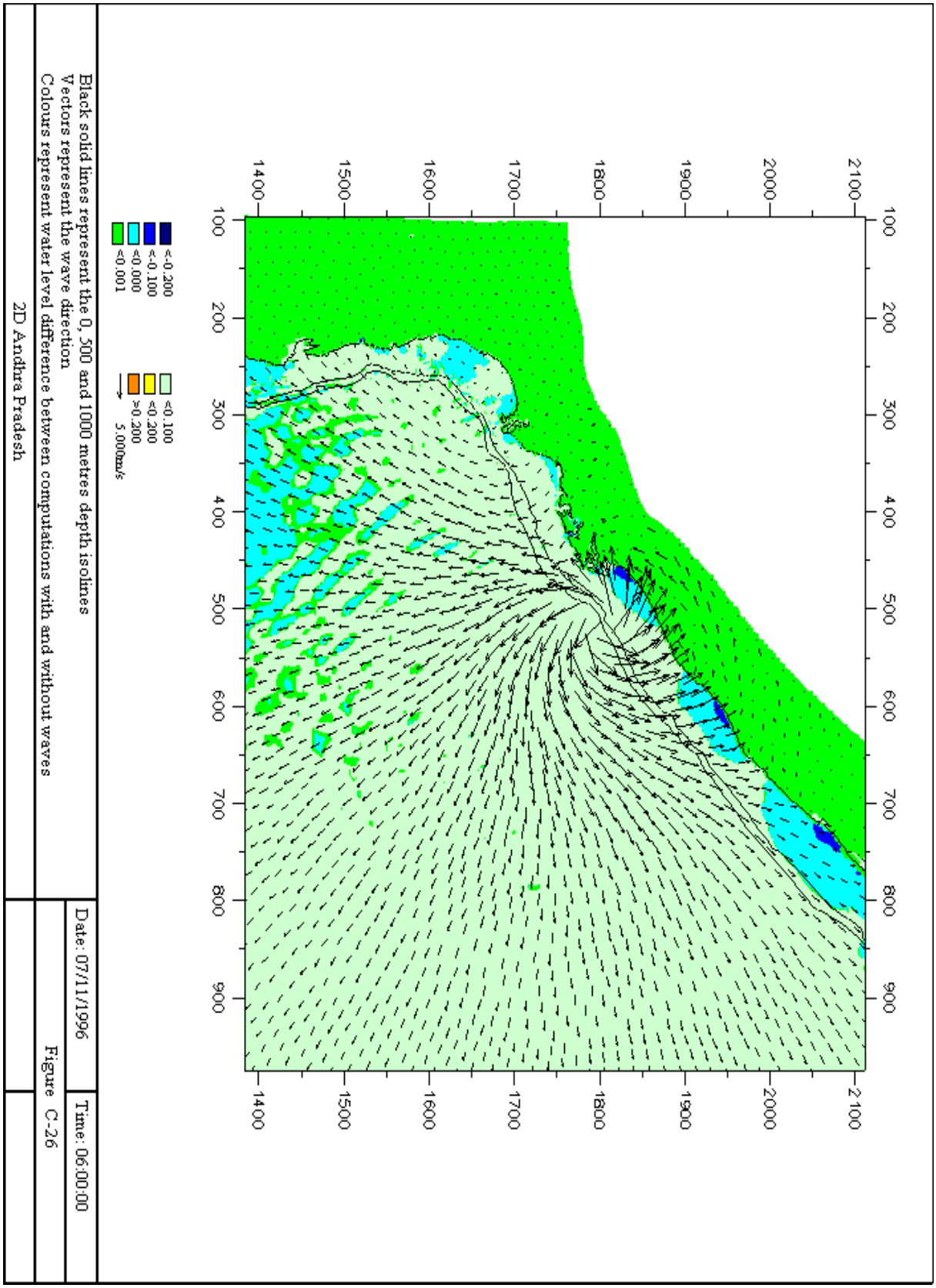
Black solid lines represent the 0, 500 and 1000 metres depth isolines
Vectors represent the wave direction
Colours represent water level difference between computations with and without waves
2D Andhra Pradesh
Date: 07/11/1996
Time: 06:00:00
Figure C-26
<-0.200
<-0.100
<0.000
<0.001
<0.100
<0.200
>0.200
5.000m/s

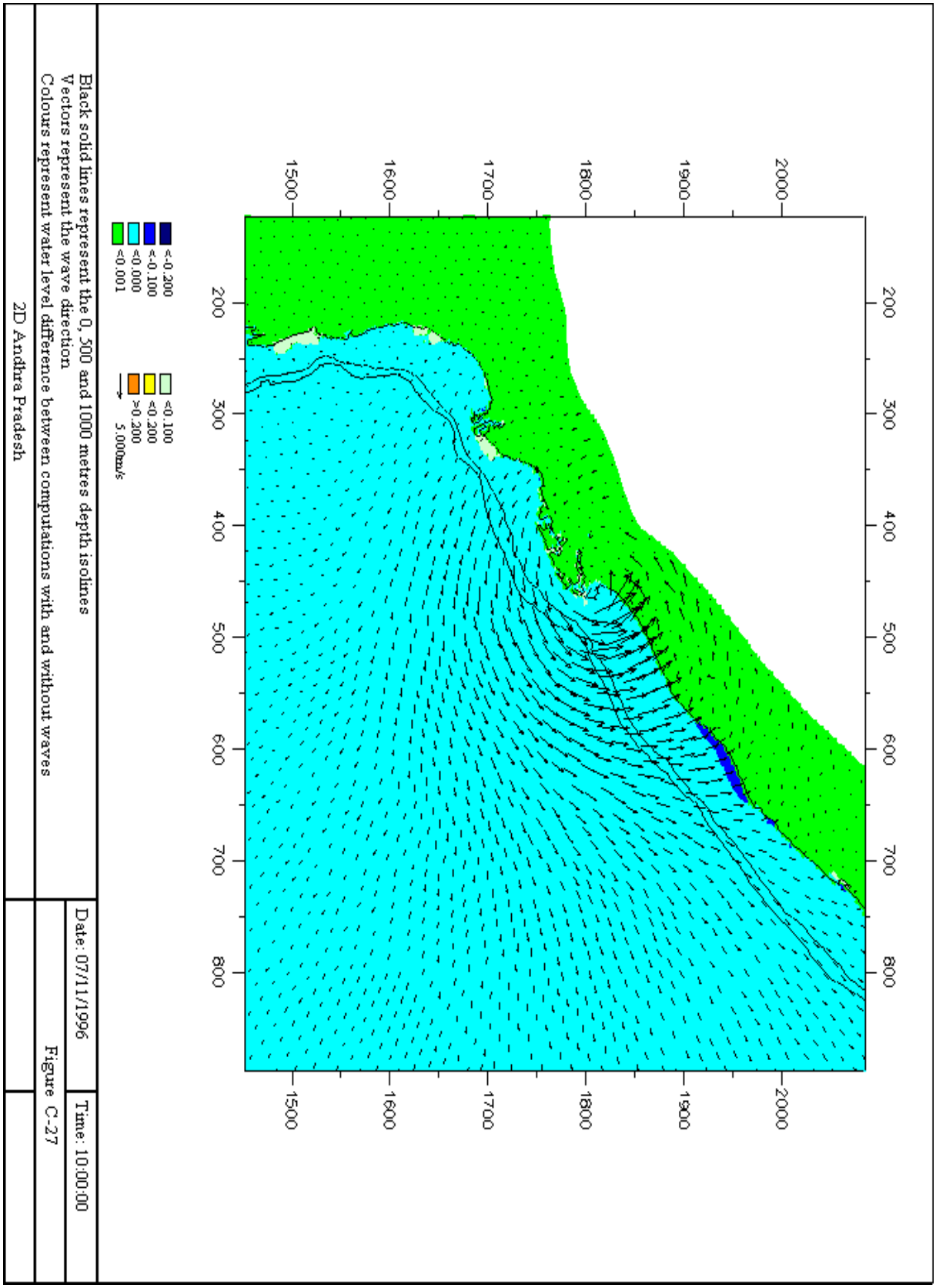
Black solid lines represent the 0, 500 and 1000 metres depth isolines
Vectors represent the wave direction
Colours represent water level difference between computations with and without waves
2D Andhra Pradesh
Date: 07/11/1996
Time: 10:00:00
Figure C-27
<-0.200
<-0.100
<0.000
<0.001
<0.100
<0.200
>0.200
5.000m/s
200
300
400
500
600
700
800
1500
1600
1700
1800
1900
2000

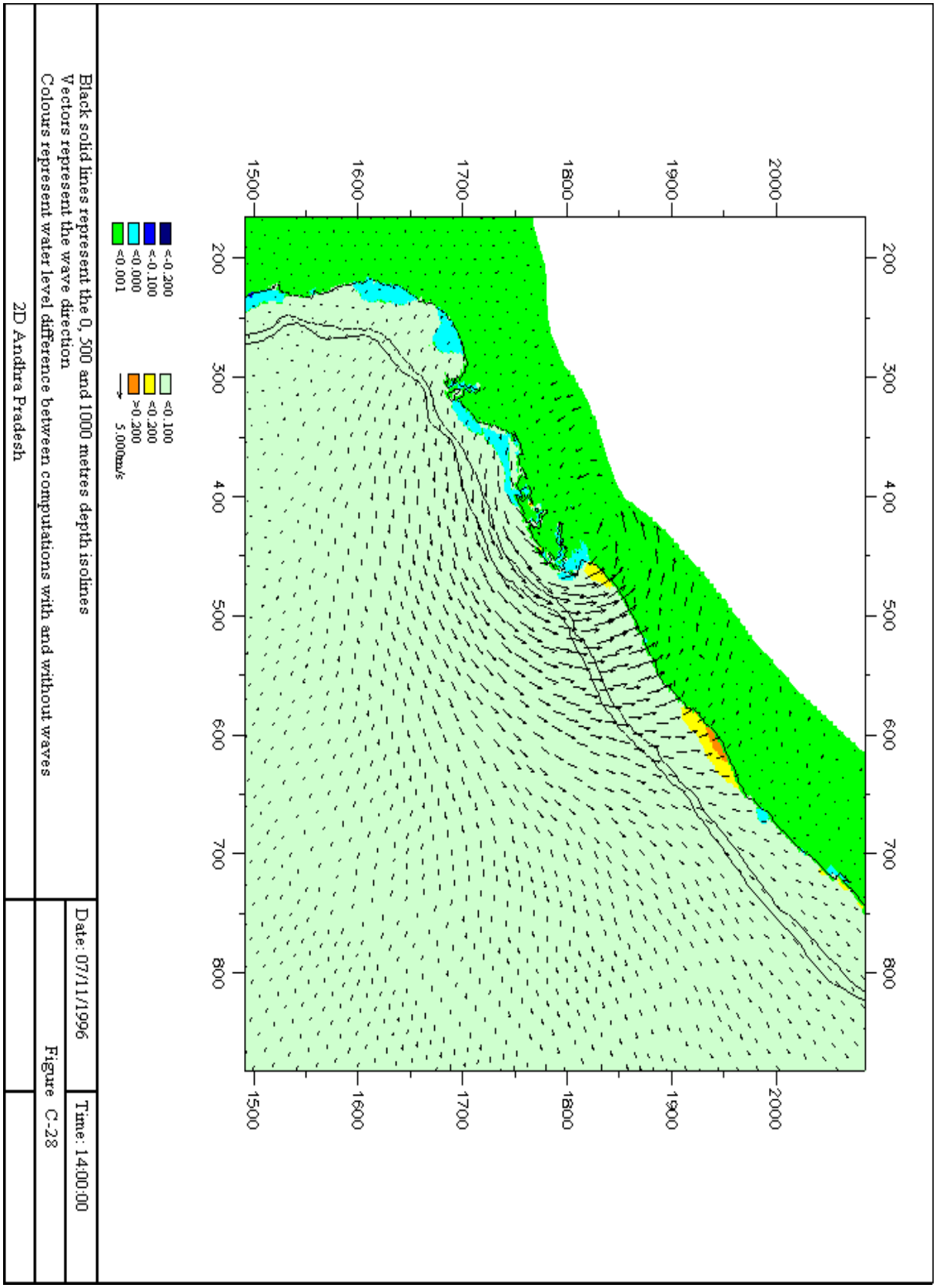
Black solid lines represent the 0, 500 and 1000 metres depth isolines
Vectors represent the wave direction
Colours represent water level difference between computations with and without waves
2D Andhra Pradesh
Date: 07/11/1996
Time: 14:00:00
Figure C-28
<-0.200
<-0.100
<0.000
<0.001
<0.100
<0.200
>0.200
5.000m/s
200
300
400
500
600
700
800
1500
1600
1700
1800
1900
2000

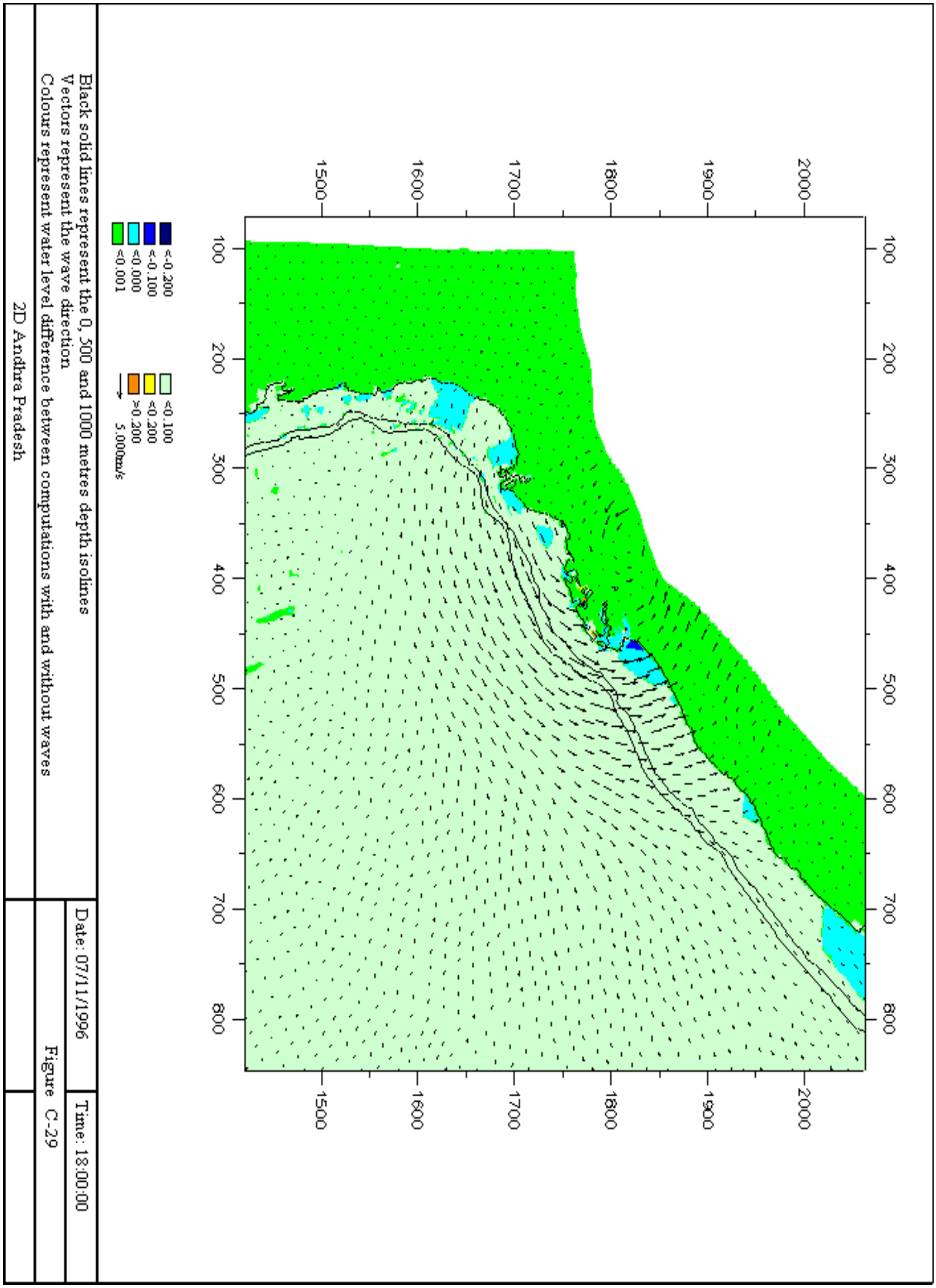
Black solid lines represent the 0, 500 and 1000 metres depth isolines
Vectors represent the wave direction
Colours represent water level difference between computations with and without waves
2D Andhra Pradesh
Date: 07/11/1996
Time: 18:00:00
Figure C-29
<-0.200
<-0.100
<0.000
<0.001
<0.100
<0.200
>0.200
5.000m/s
100
200
300
400
500
600
700
800
1500
1600
1700
1800
1900
2000

C.5 Wave height and Dissipation for 2D Andhra Pradesh case

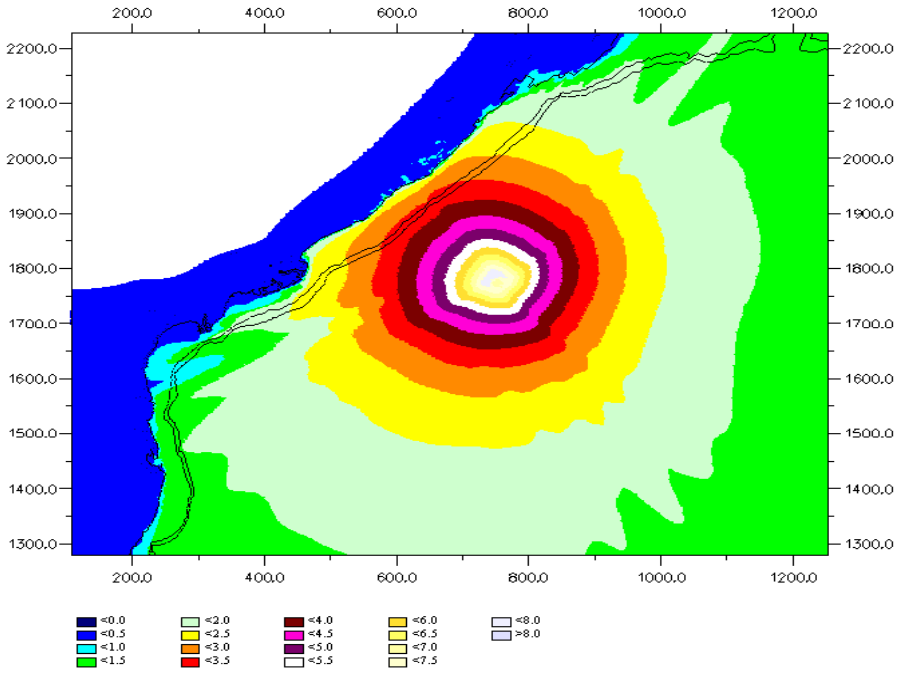

Colours represent the root mean square wave height [m] The solid lines represent the 0, 500 and 1000 metres depth isolines	Date: 06/11/1996	Time: 10:00:00
	Figure C-30	
2D Andhra Pradesh		

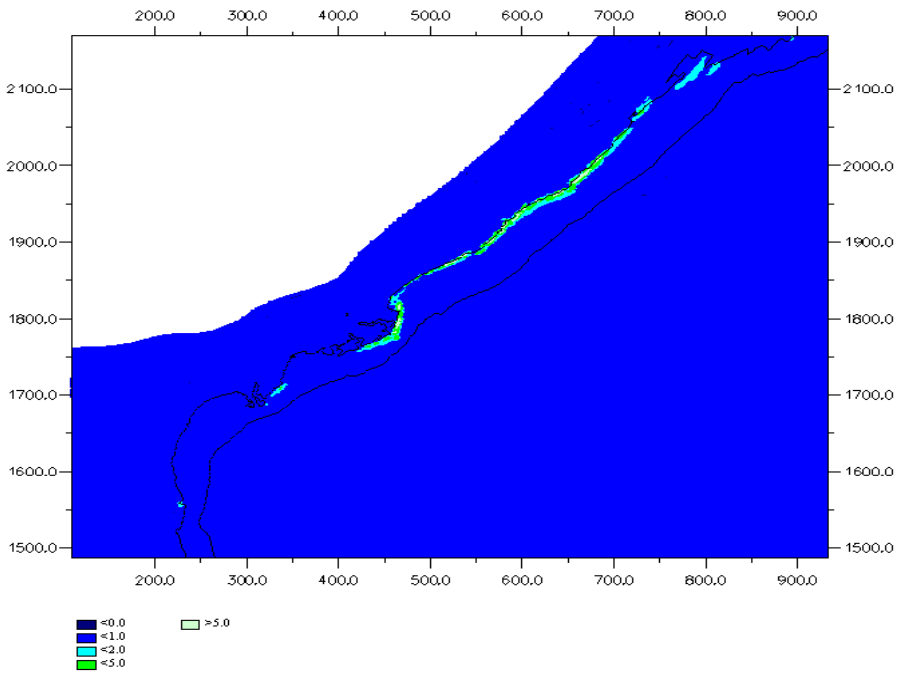

Colours represent the dissipation of energy Solid lines represent a water depth of 0 and 500 metres	Date: 06/11/1996	Time: 10:00:00
	Figure C-31	
2D Andhra Pradesh		

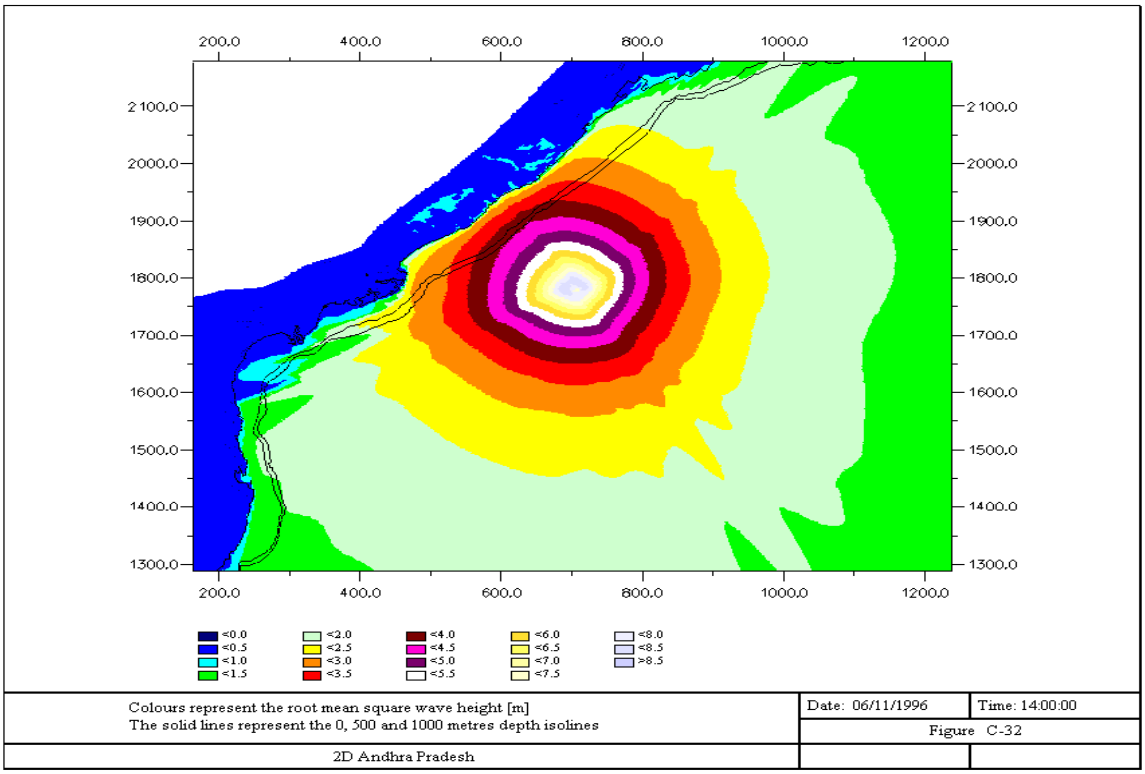

Colours represent the root mean square wave height [m] The solid lines represent the 0, 500 and 1000 metres depth isolines	Date: 06/11/1996	Time: 14:00:00
	Figure C-32	
2D Andhra Pradesh		

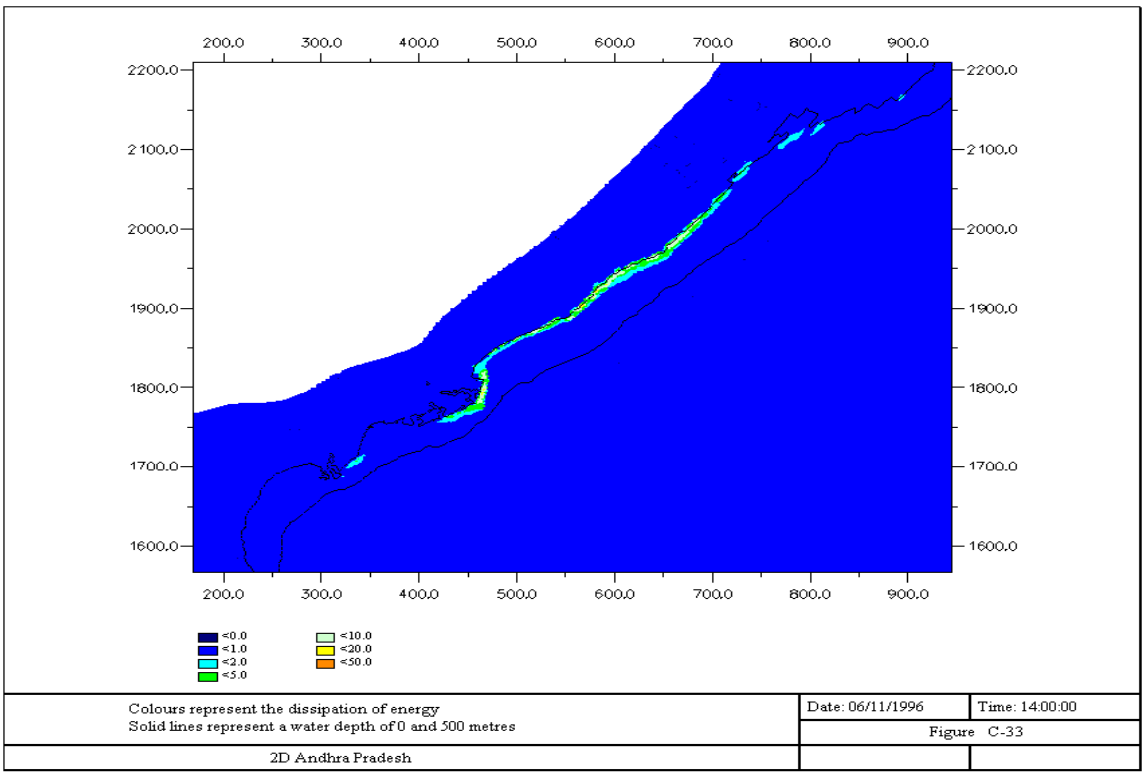

Colours represent the dissipation of energy Solid lines represent a water depth of 0 and 500 metres	Date: 06/11/1996	Time: 14:00:00
	Figure C-33	
2D Andhra Pradesh		

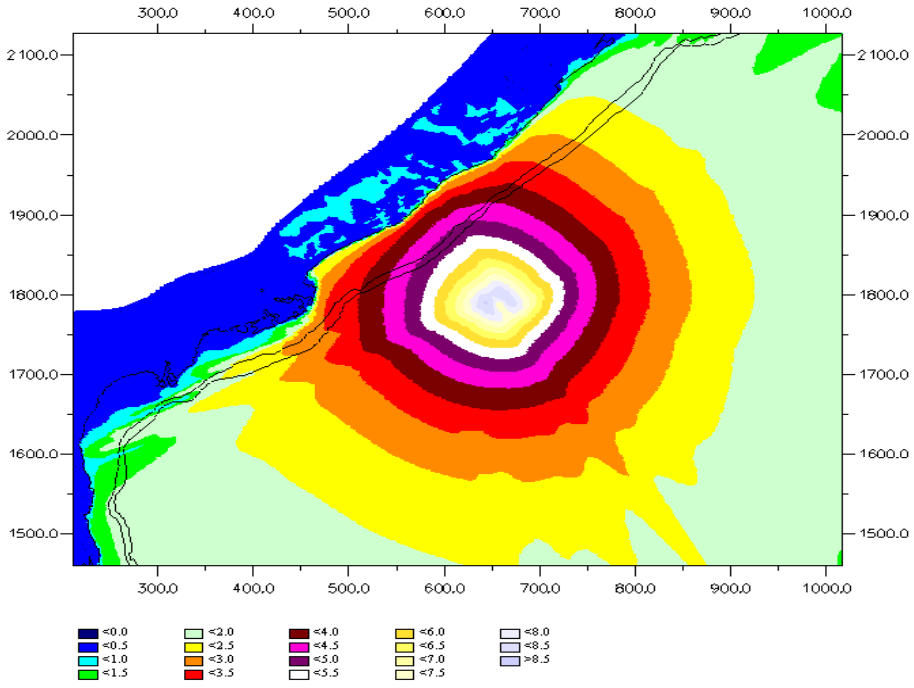

Colours represent the root mean square wave height [m] The solid lines represent the 0, 500 and 1000 metres depth isolines	Date: 06/11/1996	Time: 18:00:00
	Figure C-34	
2D Andhra Pradesh		

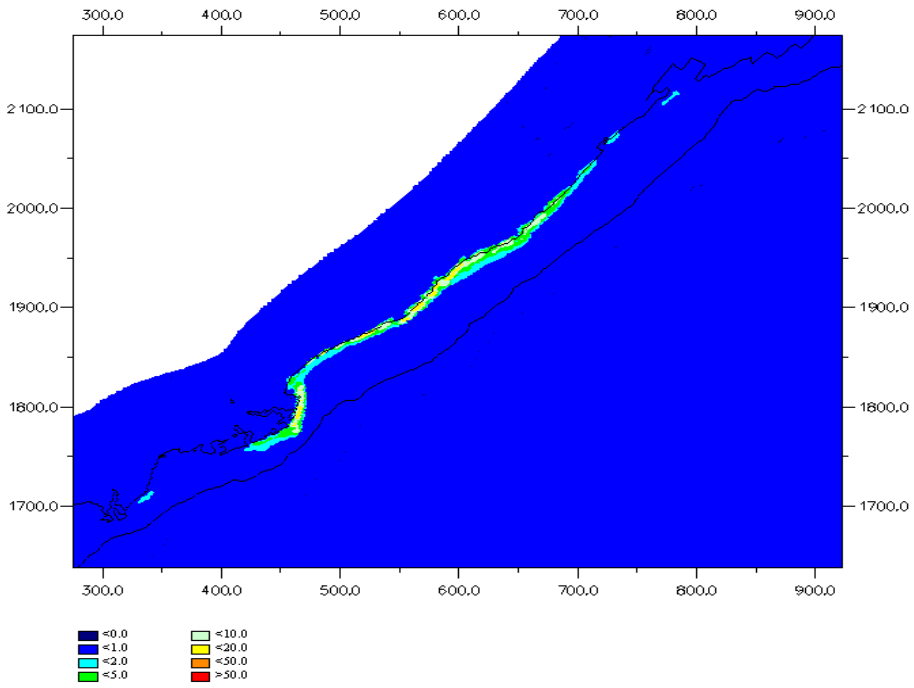

Colours represent the dissipation of energy Solid lines represent a water depth of 0 and 500 metres	Date: 06/11/1996	Time: 18:00:00
	Figure C-35	
2D Andhra Pradesh		

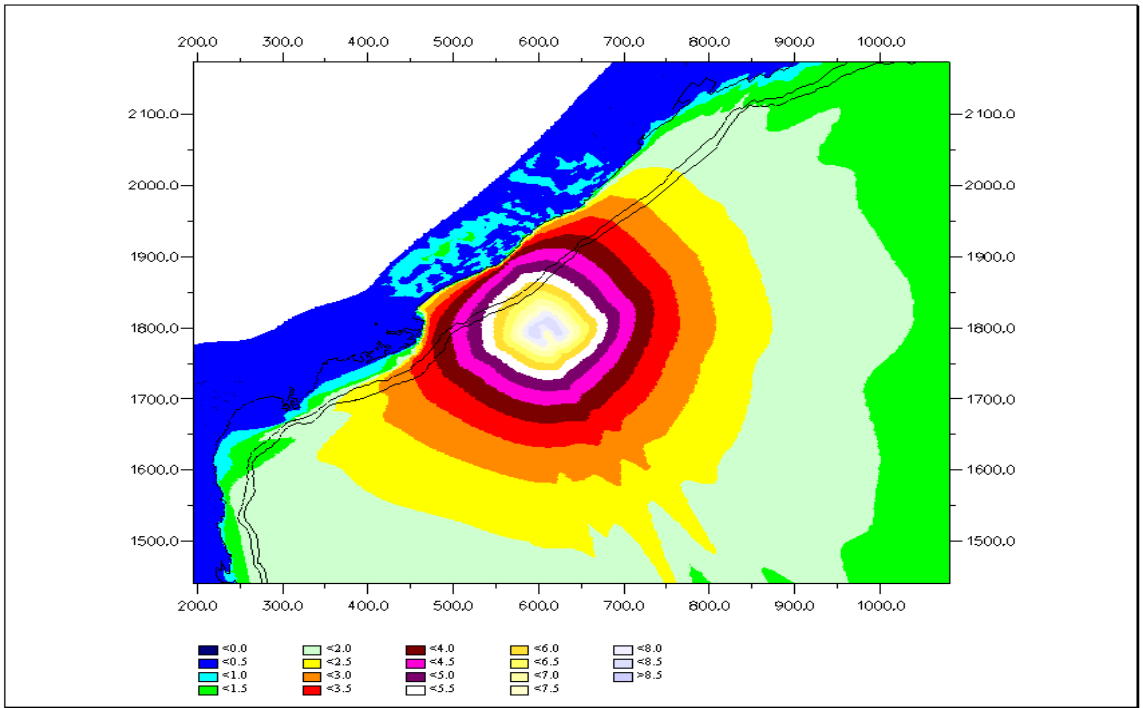

Colours represent the root mean square wave height [m] The solid lines represent the 0, 500 and 1000 metres depth isolines	Date: 06/11/1996	Time: 22:00:00
	Figure C-36	
2D Andhra Pradesh		

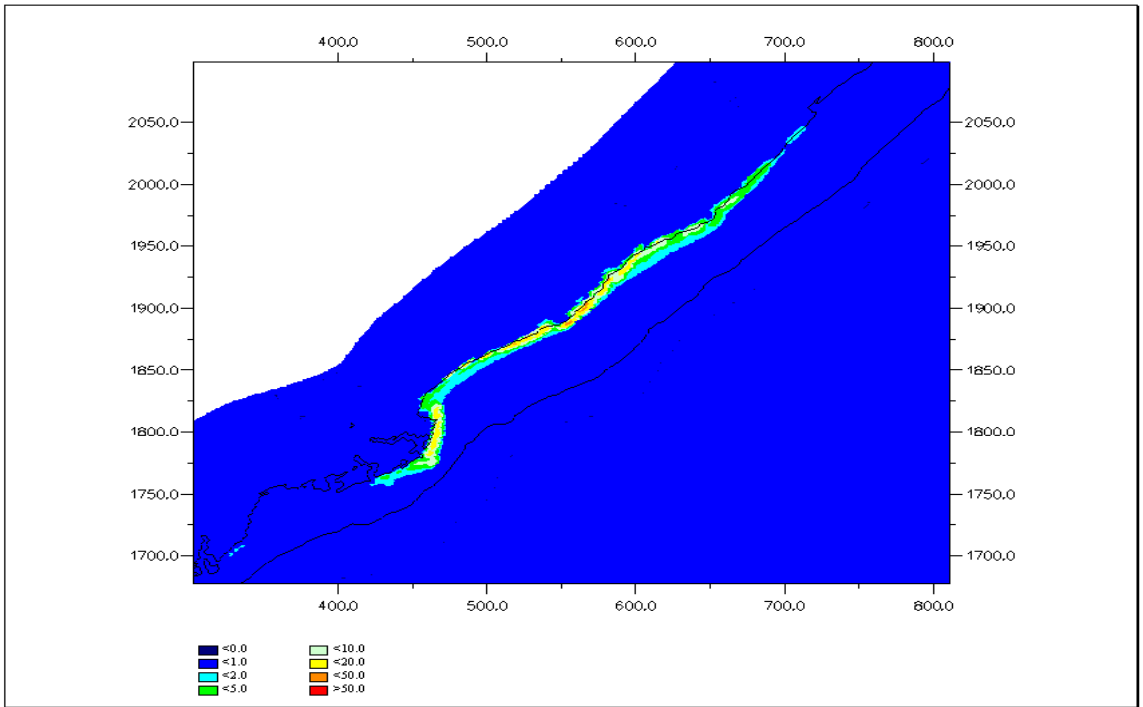

Colours represent the dissipation of energy Solid lines represent a water depth of 0 and 500 metres	Date: 06/11/1996	Time: 22:00:00
	Figure C-37	
2D Andhra Pradesh		

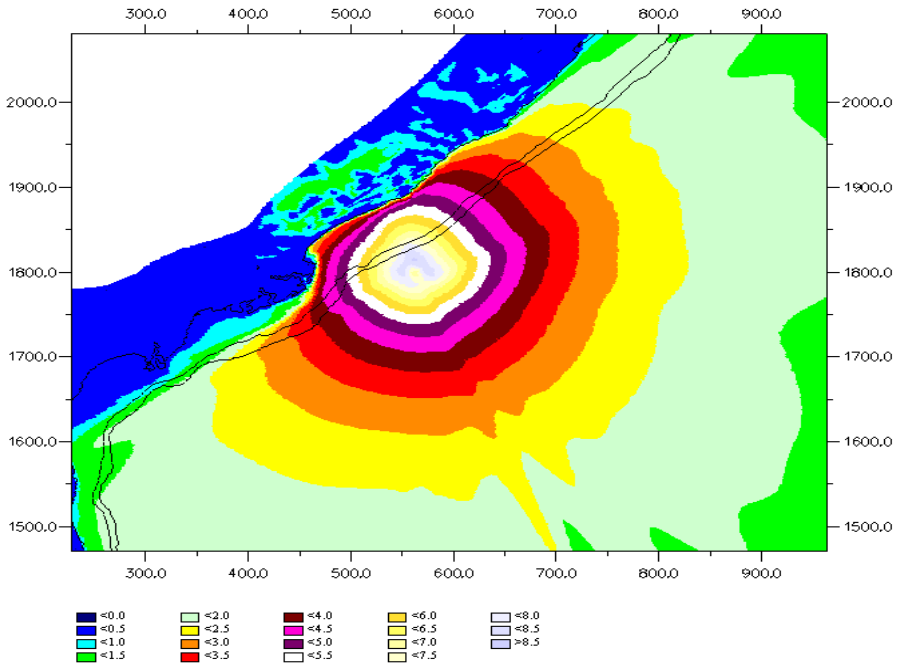

Colours represent the root mean square wave height [m] The solid lines represent the 0, 500 and 1000 metres depth isolines	Date: 07/11/1996	Time: 02:00:00
	Figure C-38	
2D Andhra Pradesh		

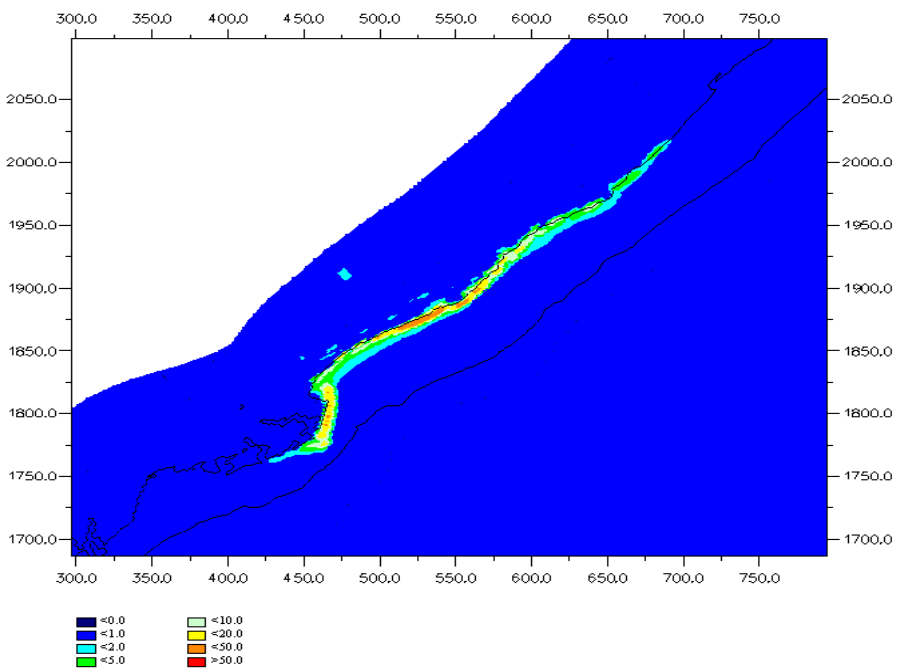

Colours represent the dissipation of energy Solid lines represent a water depth of 0 and 500 metres	Date: 07/11/1996	Time: 02:00:00
	Figure C-39	
2D Andhra Pradesh		

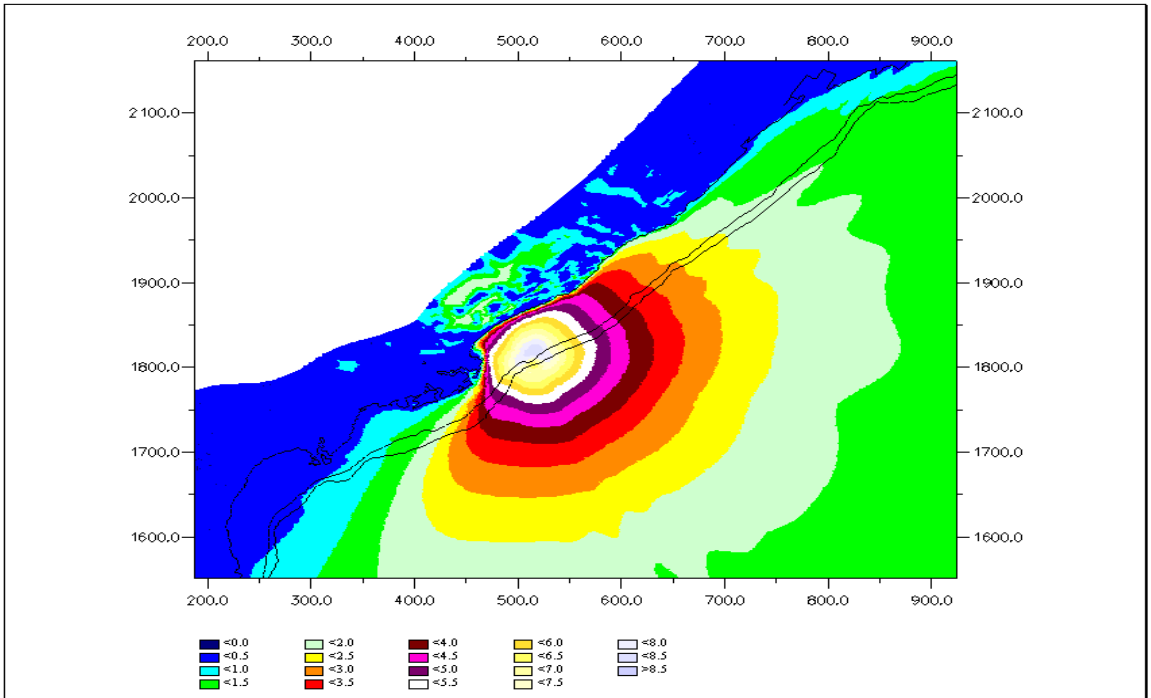

Colours represent the root mean square wave height [m] The solid lines represent the 0, 500 and 1000 metres depth isolines	Date: 07/11/1996	Time: 06:00:00
	Figure C-40	
2D Andhra Pradesh		

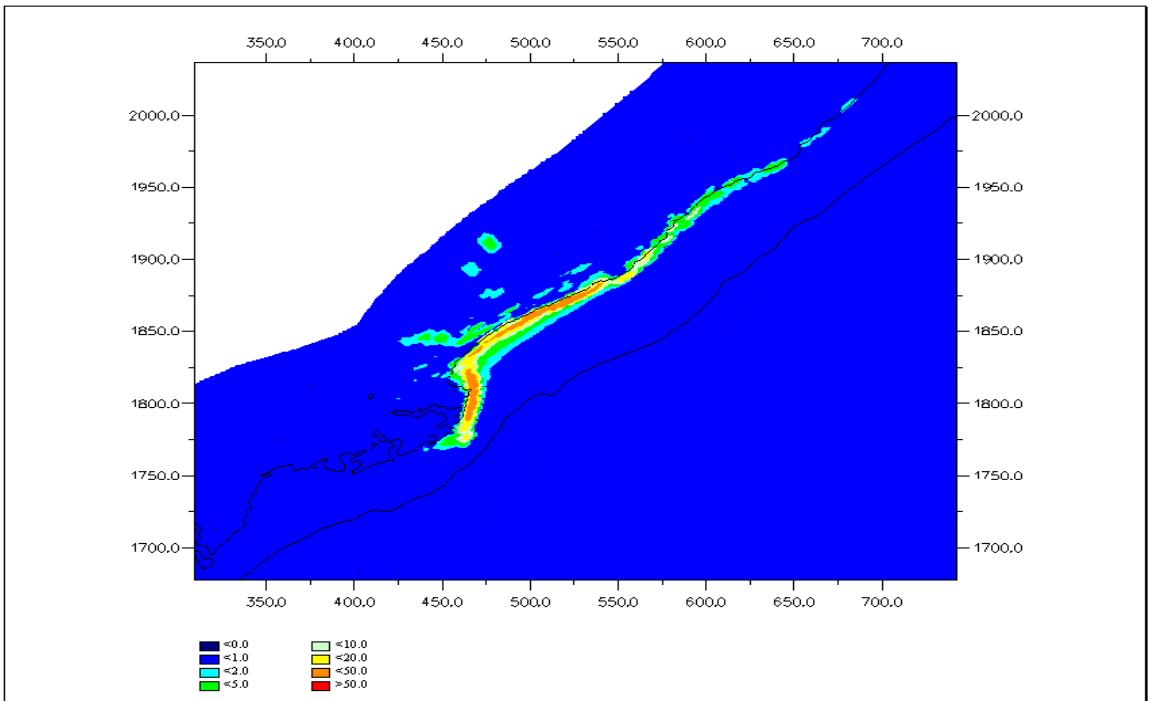

Colours represent the dissipation of energy Solid lines represent a water depth of 0 and 500 metres	Date: 07/11/1996	Time: 06:00:00
	Figure C-41	
2D Andhra Pradesh		

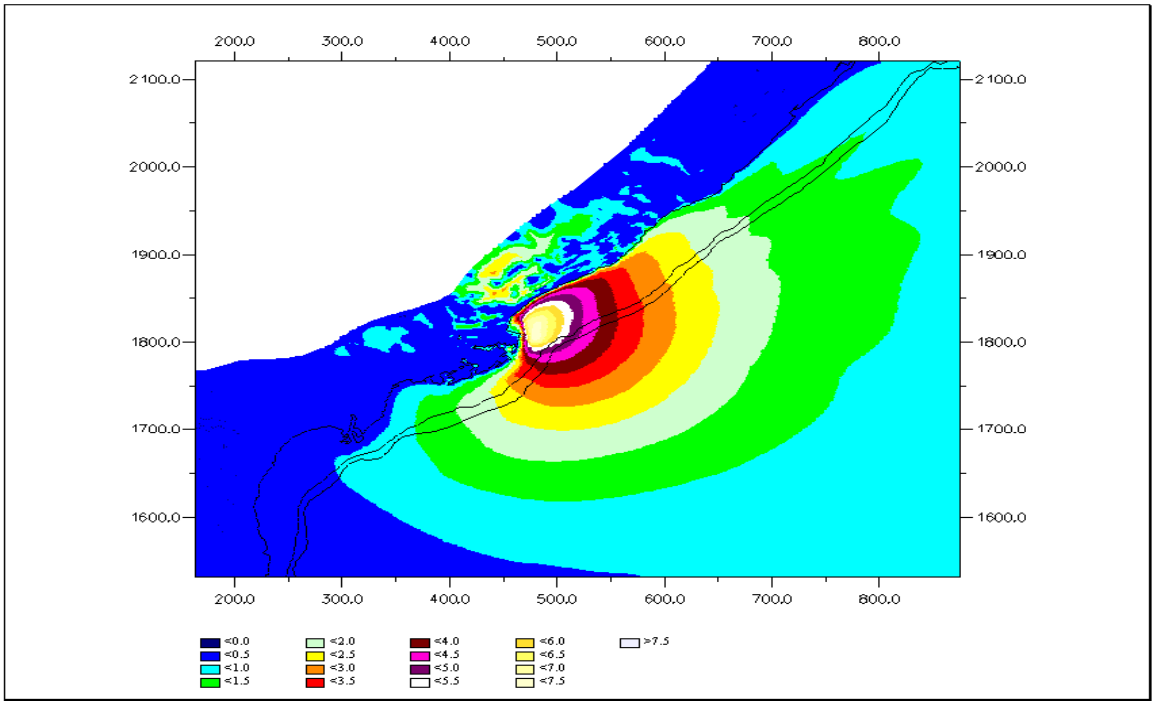

Colours represent the root mean square wave height [m] The solid lines represent the 0, 500 and 1000 metres depth isolines	Date: 07/11/1996	Time: 10:00:00
	Figure C-42	
2D Andhra Pradesh		

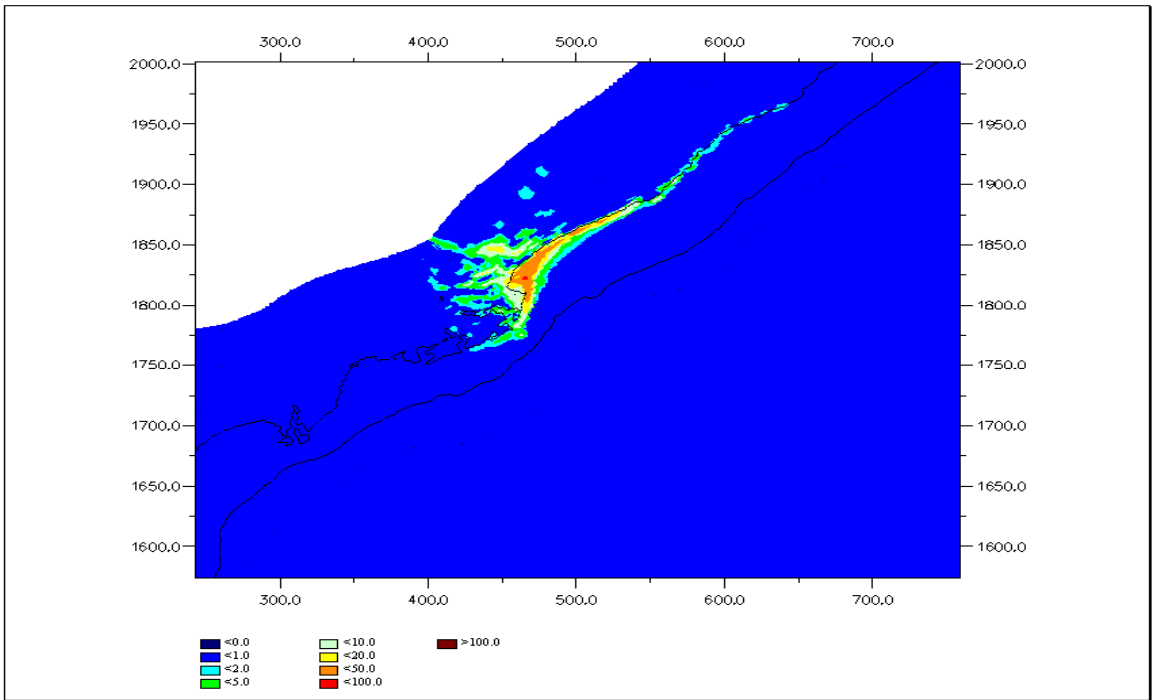

Colours represent the dissipation of energy Solid lines represent a water depth of 0 and 500 metres	Date: 07/11/1996	Time: 10:00:00
	Figure C-43	
2D Andhra Pradesh		

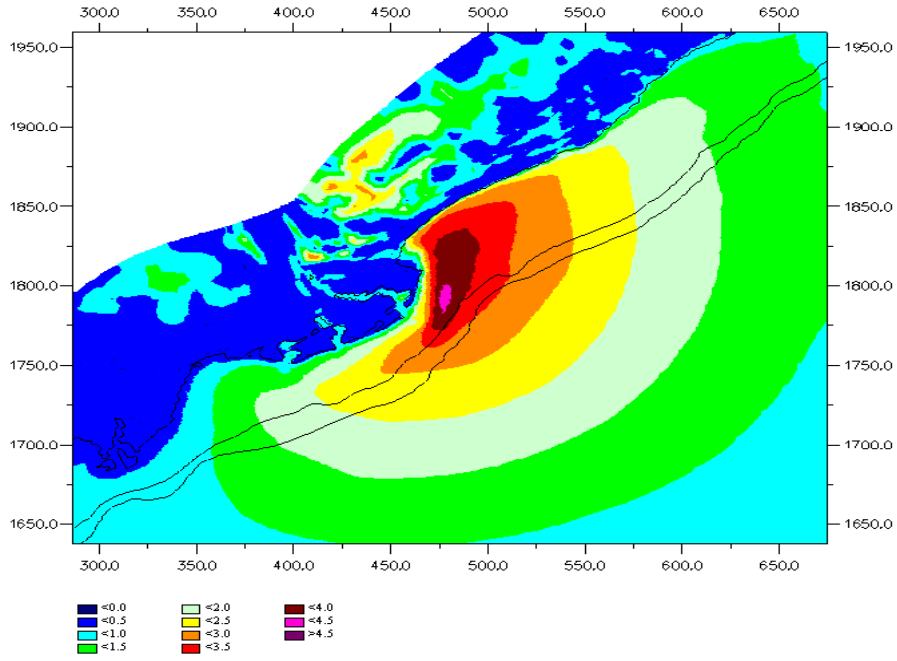

Colours represent the root mean square wave height [m] The solid lines represent the 0, 500 and 1000 metres depth isolines	Date: 07/11/1996	Time: 14:00:00
	Figure C-44	
2D Andhra Pradesh		

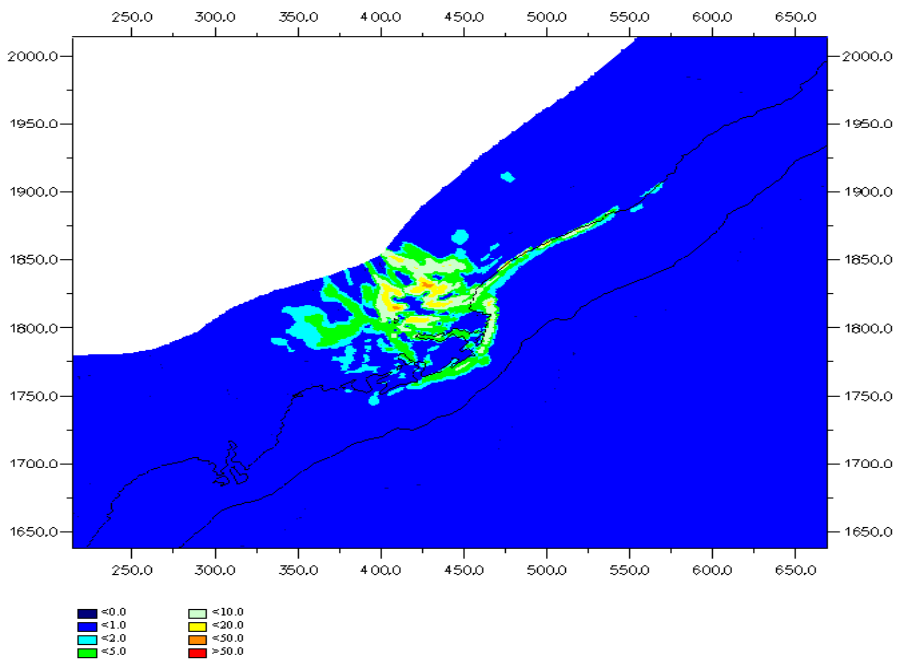

Colours represent the dissipation of energy Solid lines represent a water depth of 0 and 500 metres	Date: 07/11/1996	Time: 14:00:00
	Figure C-45	
2D Andhra Pradesh		

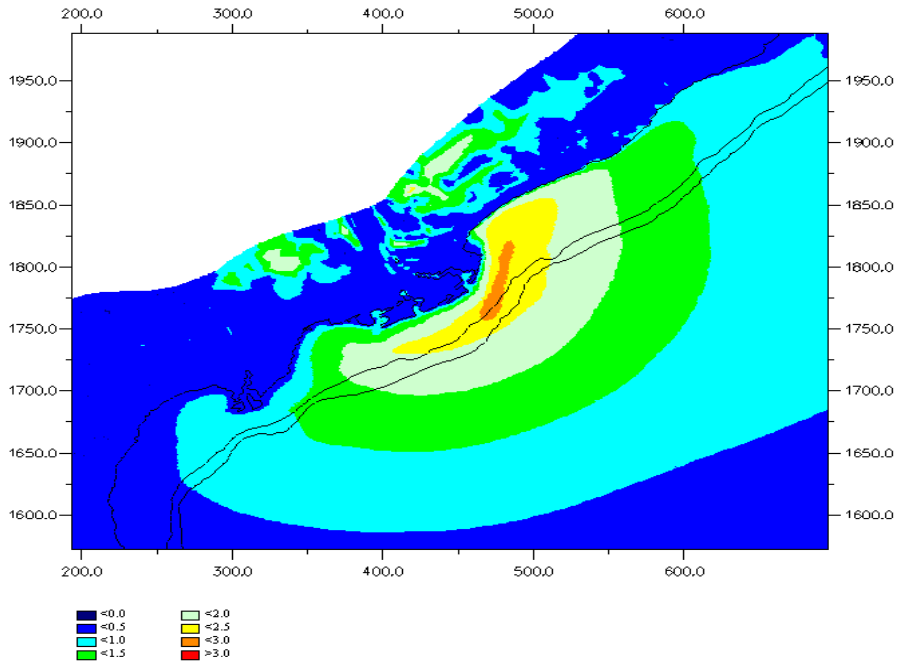

Colours represent the root mean square wave height [m] The solid lines represent the 0, 500 and 1000 metres depth isolines	Date: 07/11/1996	Time: 18:00:00
	Figure C-46	
2D Andhra Pradesh		

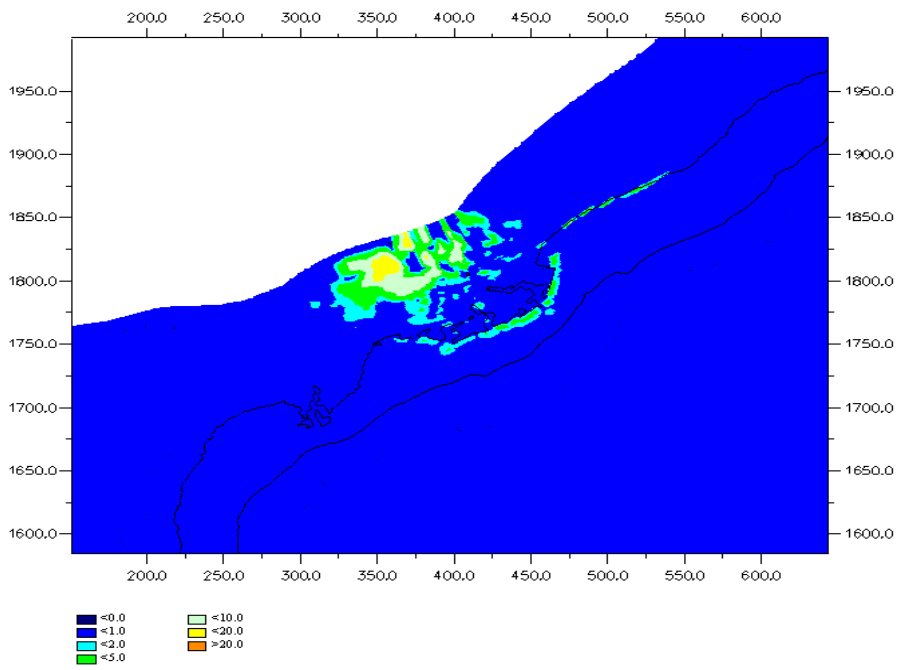

Colours represent the dissipation of energy Solid lines represent a water depth of 0 and 500 metres	Date: 07/11/1996	Time: 18:00:00
	Figure C-47	
2D Andhra Pradesh		

C.6 Water level set-up due to waves in 3D Andhra Pradesh case

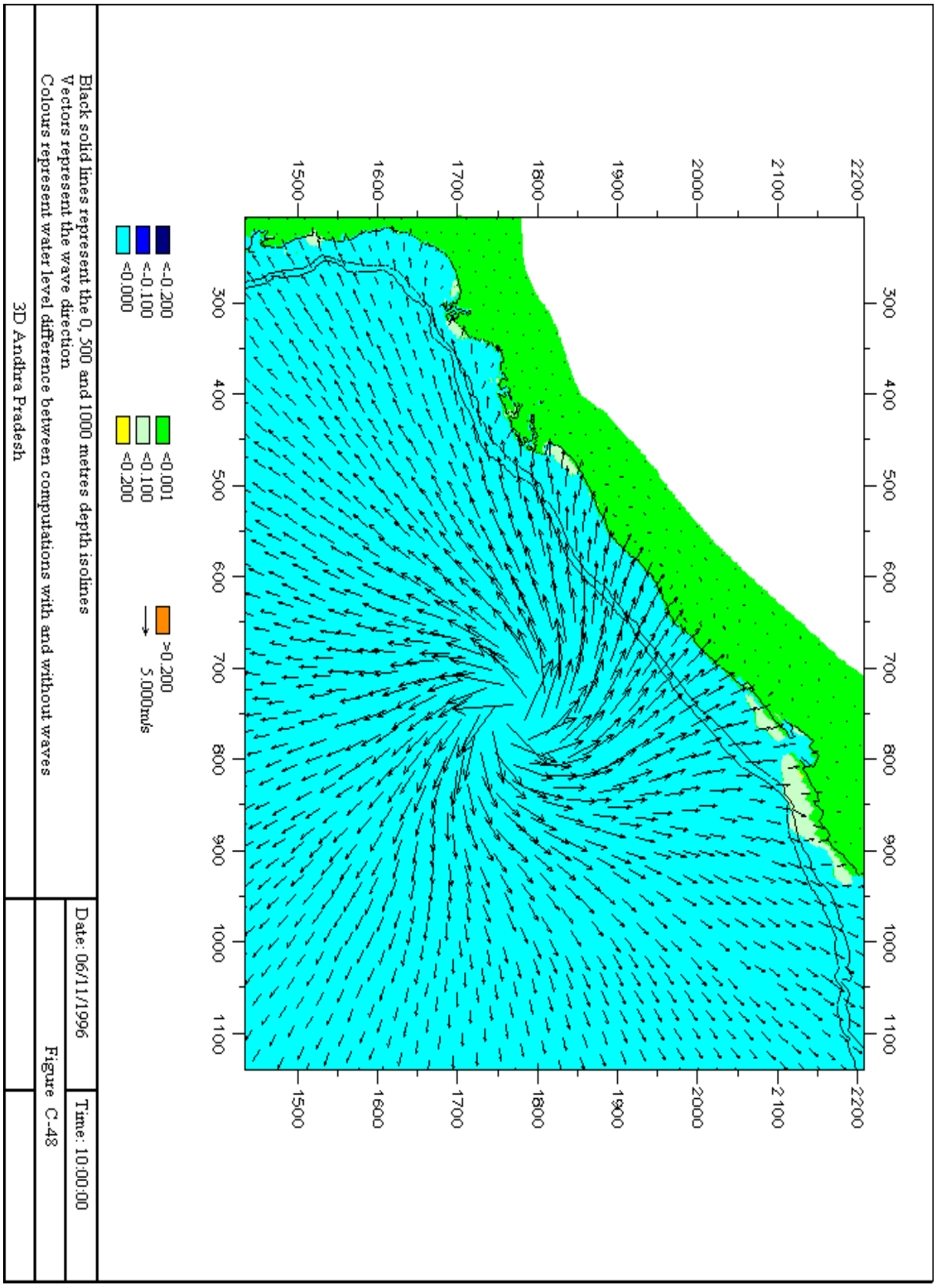

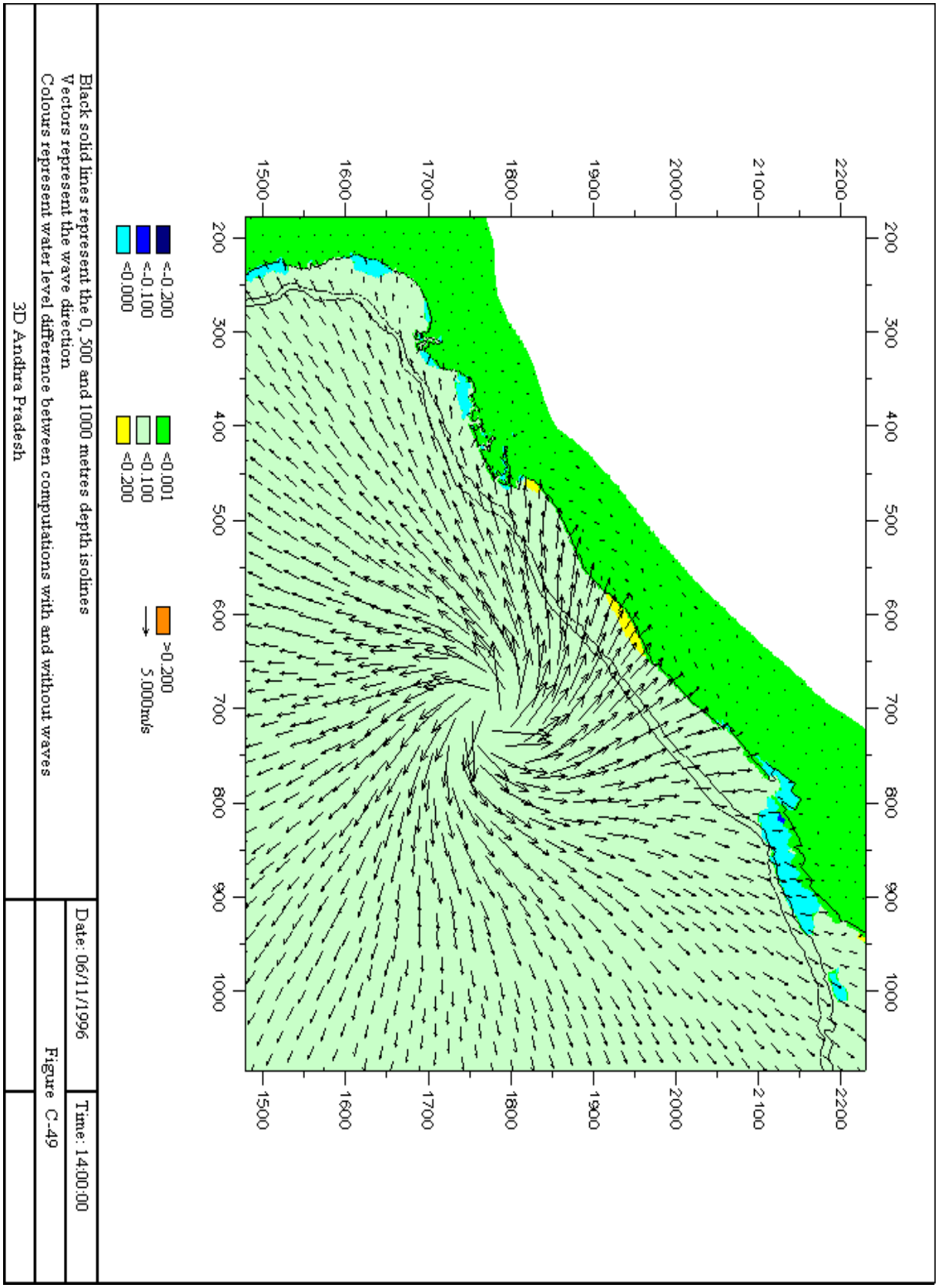
Black solid lines represent the 0, 500 and 1000 metres depth isolines
Vectors represent the wave direction
Colours represent water level difference between computations with and without waves
3D Andhra Pradesh
Date: 06/11/1996
Time: 14:00:00
Figure C-49
<-0.200
<-0.100
<0.000
<0.001
<0.100
<0.200
>0.200
5.000m/s

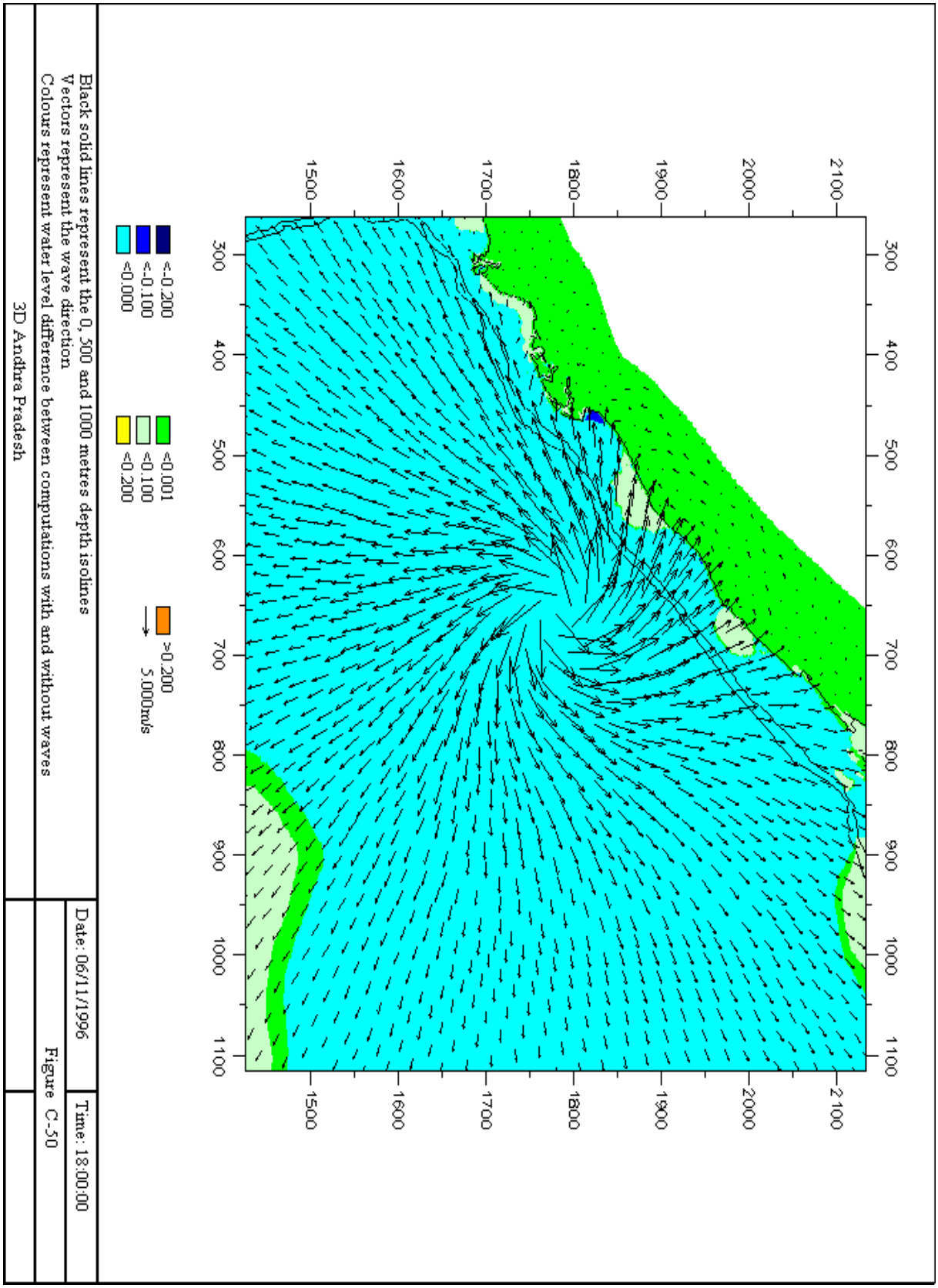
Black solid lines represent the 0, 500 and 1000 metres depth isolines
Vectors represent the wave direction
Colours represent water level difference between computations with and without waves
3D Andhra Pradesh
Date: 06/11/1996
Time: 18:00:00
Figure C-50
<-0.200
<-0.100
<0.000
<0.001
<0.100
<0.200
>0.200
5.000m/s

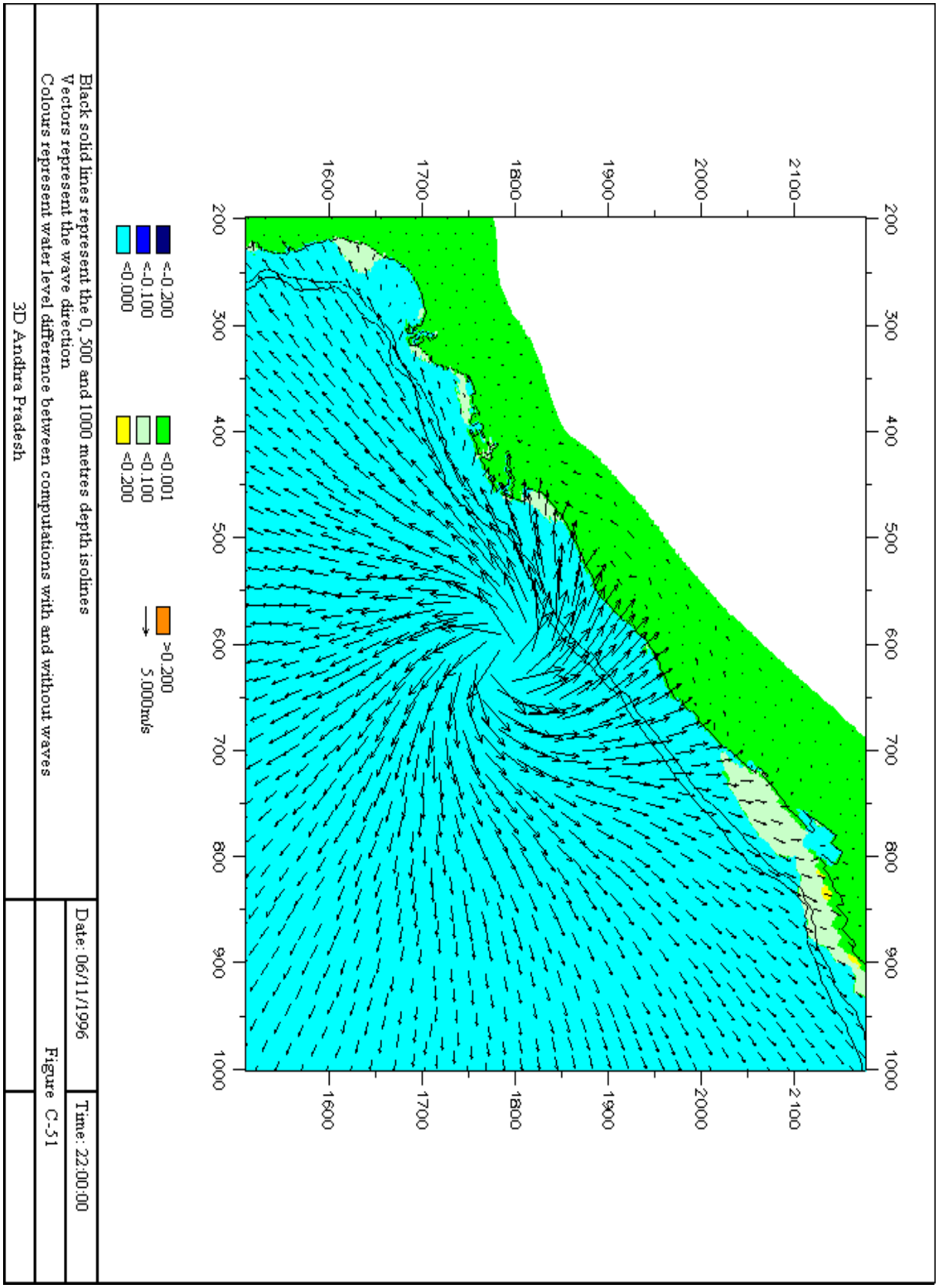
Black solid lines represent the 0, 500 and 1000 metres depth isolines
Vectors represent the wave direction
Colours represent water level difference between computations with and without waves
3D Andhra Pradesh
Date: 06/11/1996
Time: 22:00:00
Figure C-51
<-0.200
<-0.100
<0.000
<0.001
<0.100
<0.200
>0.200
5.000m/s

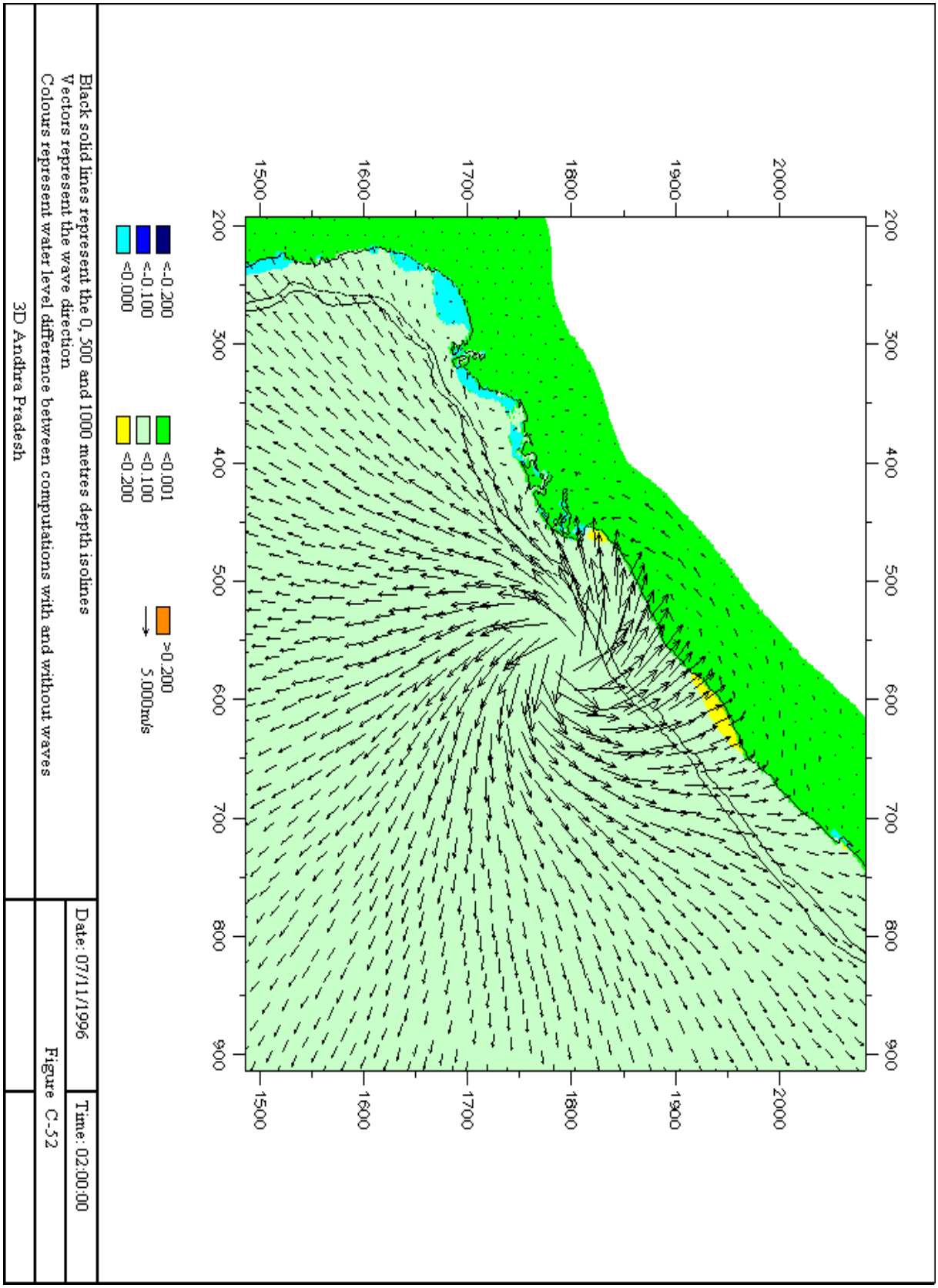
Black solid lines represent the 0, 500 and 1000 metres depth isolines
Vectors represent the wave direction
Colours represent water level difference between computations with and without waves
3D Andhra Pradesh
Date: 07/11/1996
Time: 02:00:00
Figure C-52
<-0.200
<-0.100
<0.000
<0.001
<0.100
<0.200
>0.200
5.000m/s
200
300
400
500
600
700
800
900
1500
1600
1700
1800
1900
2000

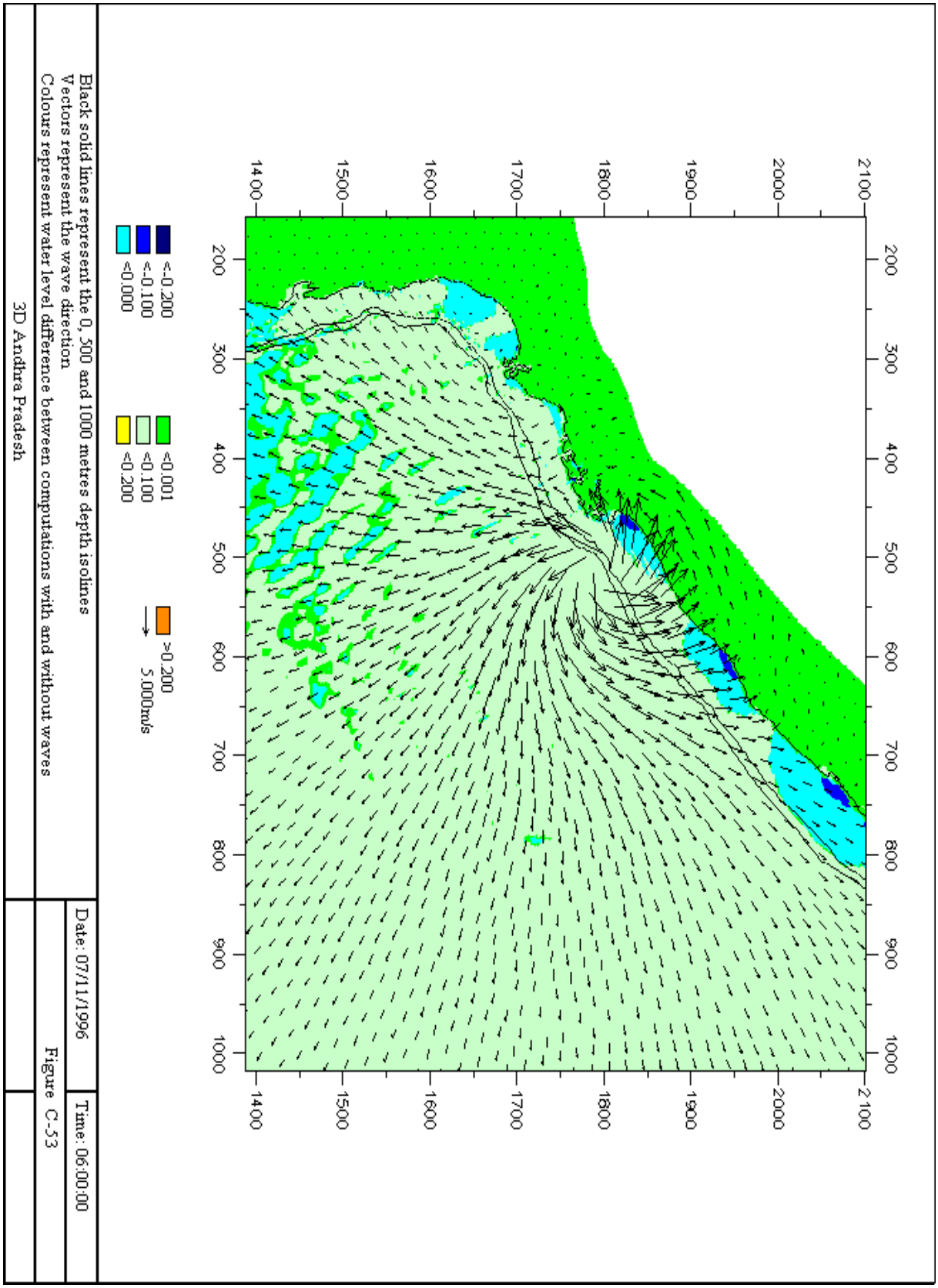
Black solid lines represent the 0, 500 and 1000 metres depth isolines
Vectors represent the wave direction
Colours represent water level difference between computations with and without waves
3D Andhra Pradesh
Date: 07/11/1996
Time: 06:00:00
Figure C-53
<-0.200
<-0.100
<0.000
<0.001
<0.100
<0.200
>0.200
5.000m/s

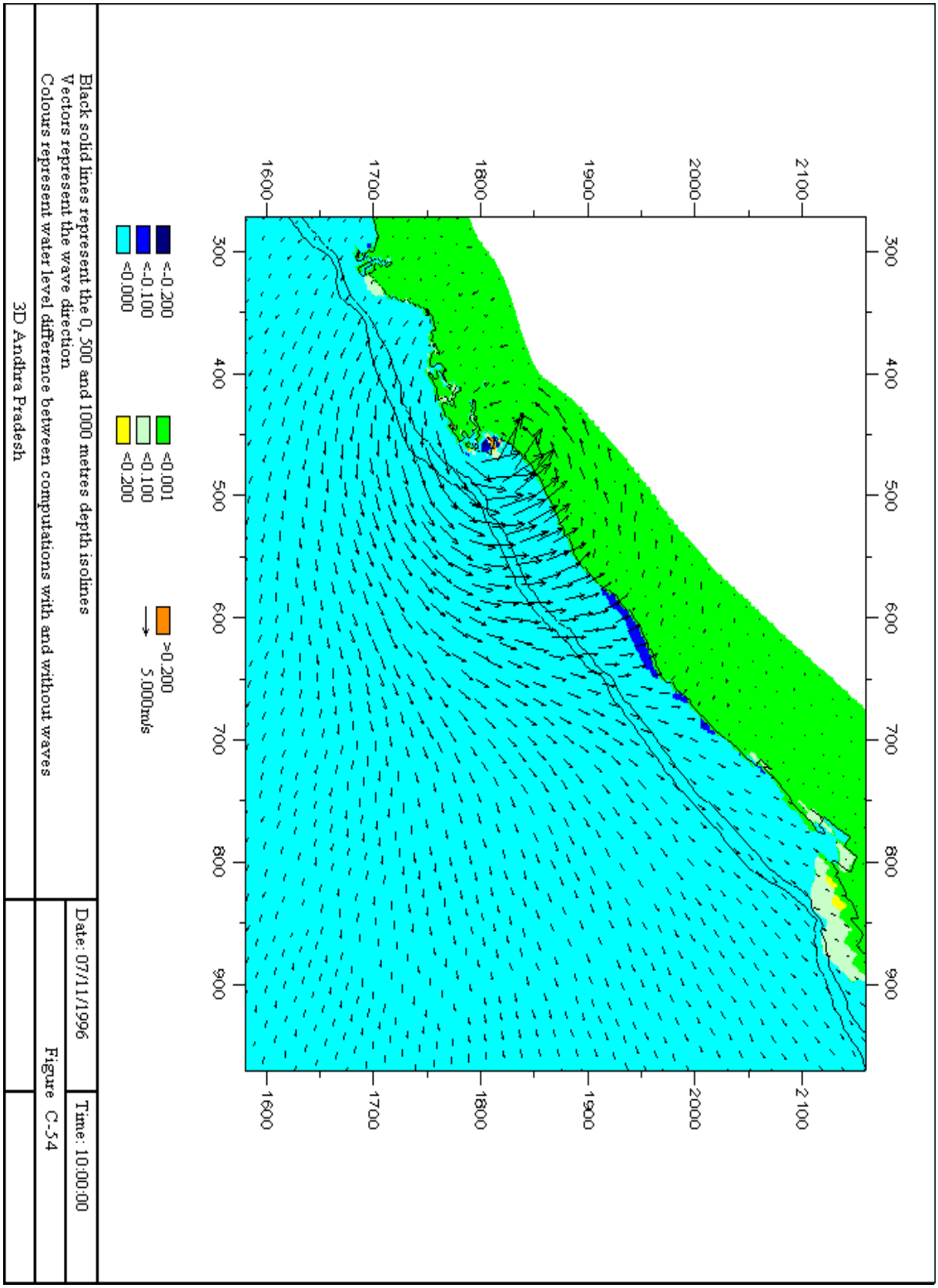
Black solid lines represent the 0, 500 and 1000 metres depth isolines
Vectors represent the wave direction
Colours represent water level difference between computations with and without waves
3D Andhra Pradesh
Date: 07/11/1996
Time: 10:00:00
Figure C-54
<-0.200
<-0.100
<0.000
<0.001
<0.100
<0.200
>0.200
5.000m/s
300
400
500
600
700
800
900
1600
1700
1800
1900
2000
2100

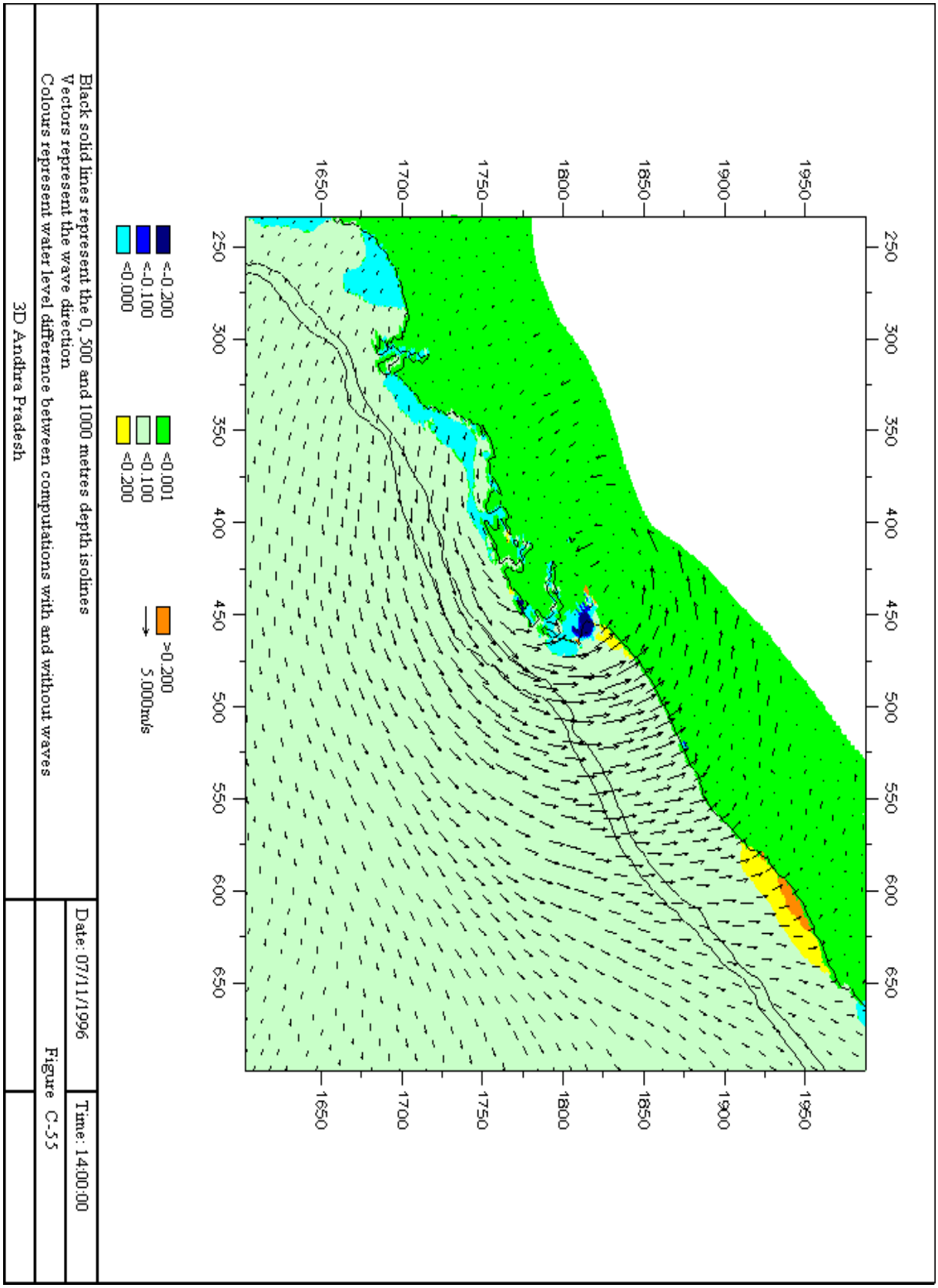
Black solid lines represent the 0, 500 and 1000 metres depth isolines
Vectors represent the wave direction
Colours represent water level difference between computations with and without waves
3D Andhra Pradesh
Date: 07/11/1996
Time: 14:00:00
Figure C-55
<-0.200
<-0.100
<0.000
<0.001
<0.100
<0.200
>0.200
5.000m/s

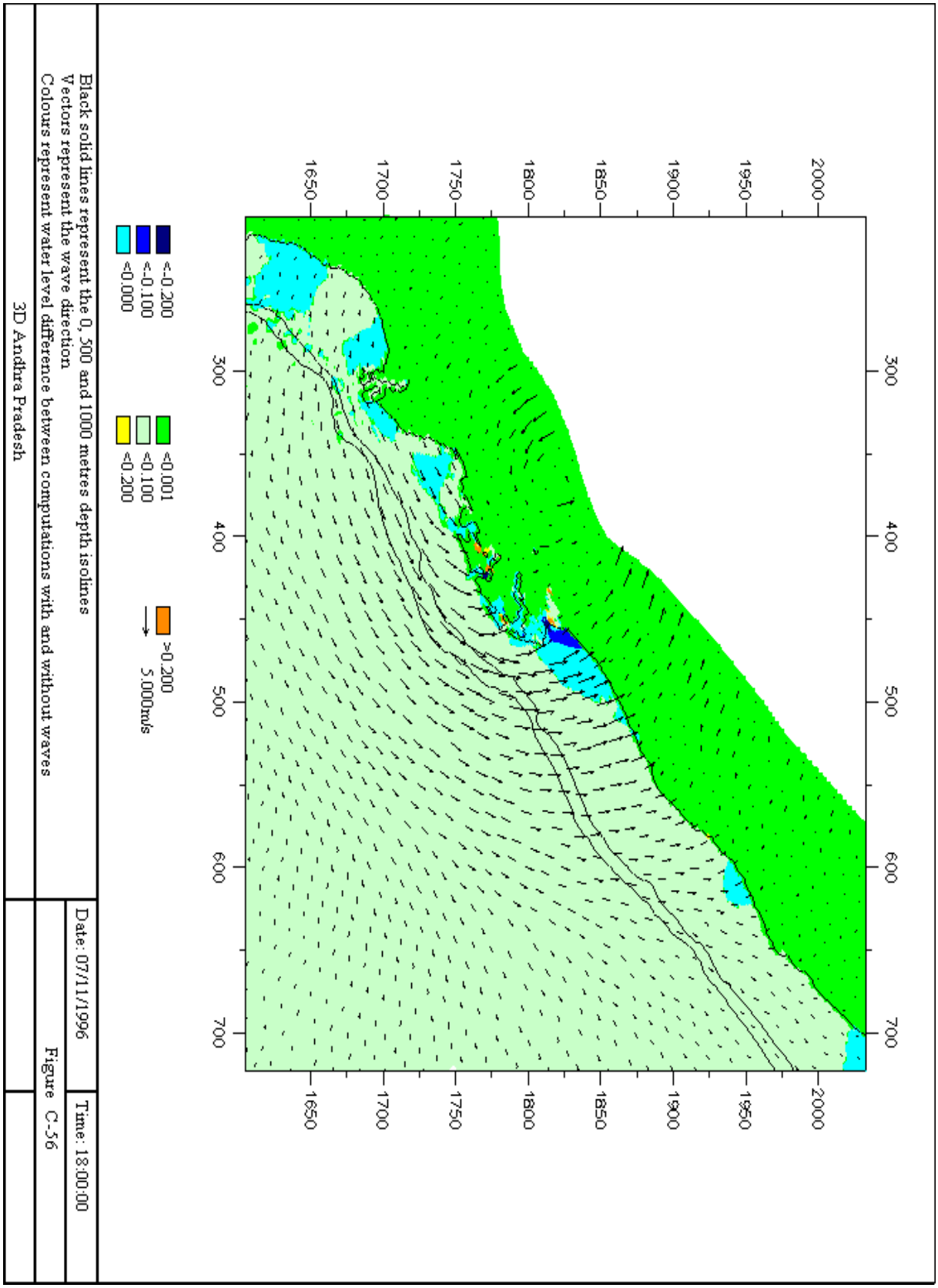
Black solid lines represent the 0, 500 and 1000 metres depth isolines
Vectors represent the wave direction
Colours represent water level difference between computations with and without waves
3D Andhra Pradesh
Date: 07/11/1996
Time: 18:00:00
Figure C-56
<-0.200
<-0.100
<0.000
<0.001
<0.100
<0.200
>0.200
5.000m/s
300
400
500
600
700
1650
1700
1750
1800
1850
1900
1950
2000

C.7 Wave height and Dissipation for 3D Andhra Pradesh case

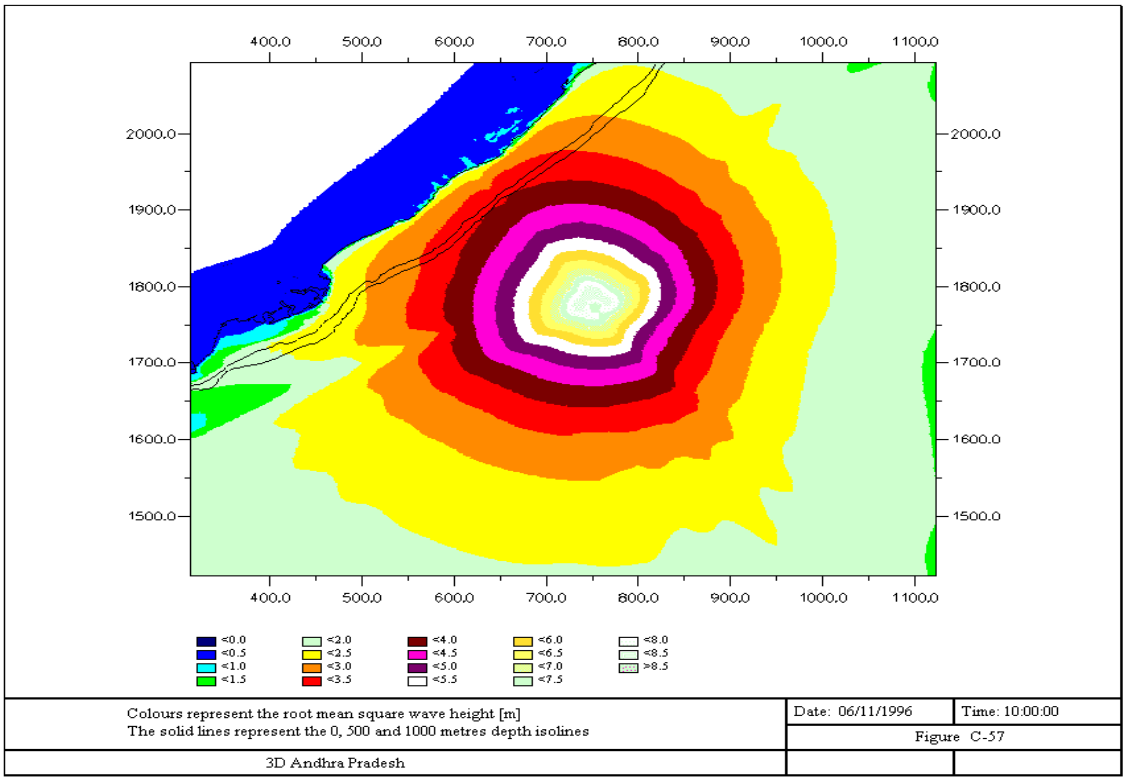

Colours represent the root mean square wave height [m] The solid lines represent the 0, 500 and 1000 metres depth isolines	Date: 06/11/1996	Time: 10:00:00
	Figure C-57	
3D Andhra Pradesh		

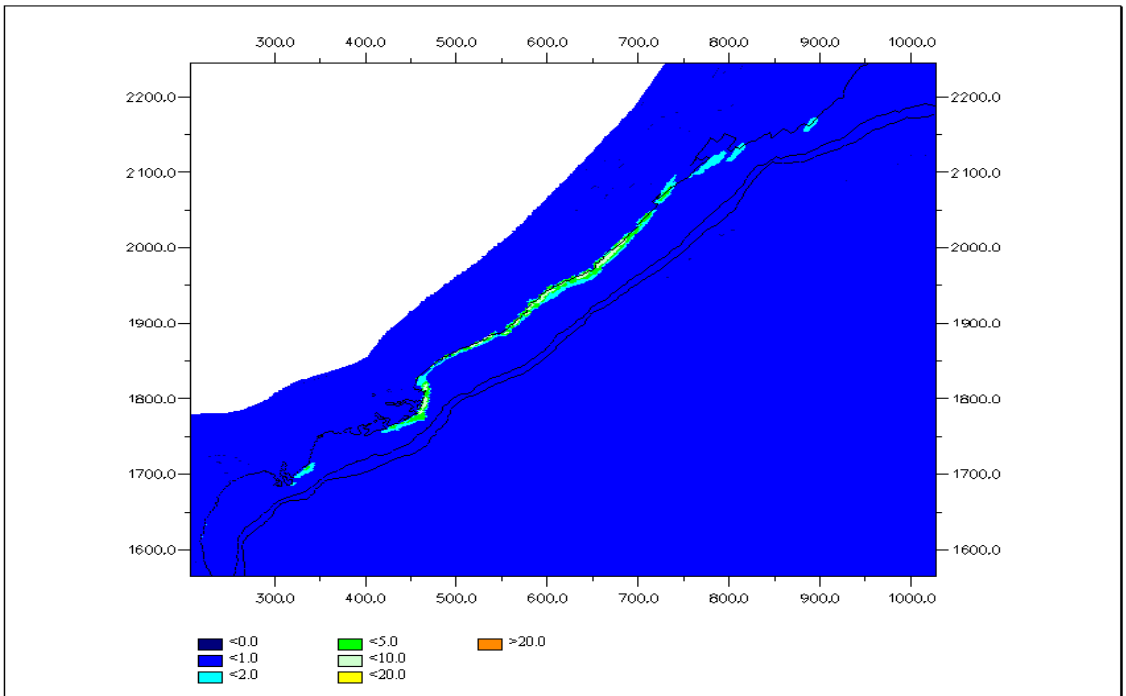

Colours represent the dissipation of energy Solid lines represent the 0, 500 and 1000 metres water depth isolines	Date: 06/11/1996	Time: 10:00:00
	Figure C-58	
3D Andhra Pradesh		

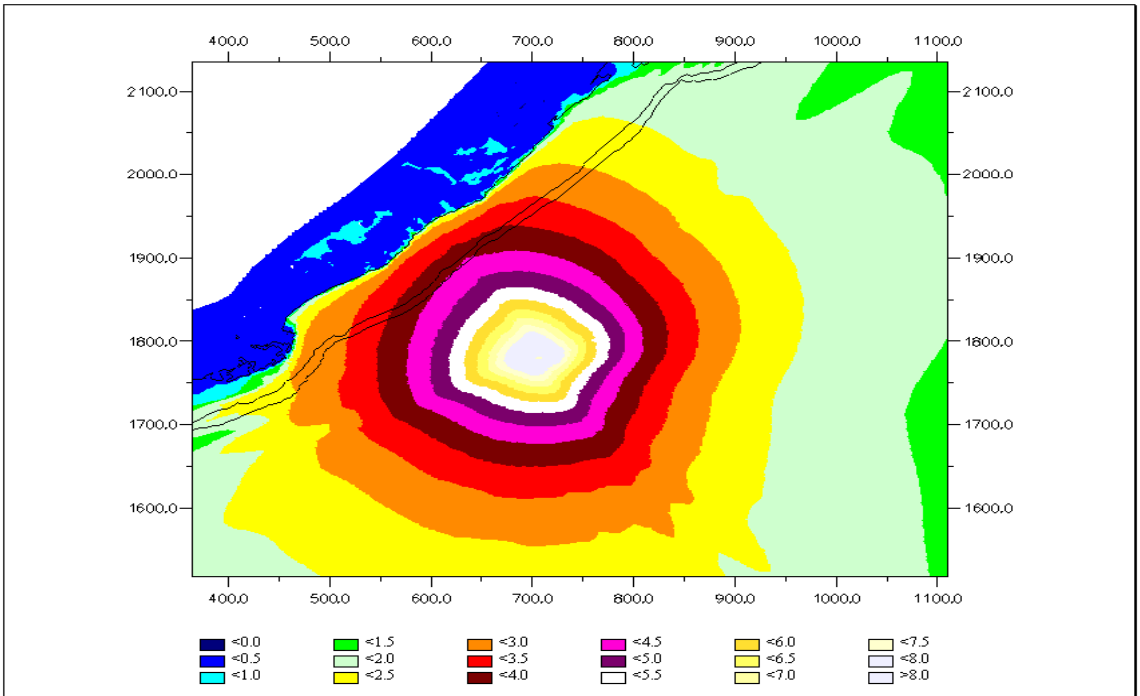

Colours represent the root mean square wave height [m] The solid lines represent the 0, 500 and 1000 metres depth isolines	Date: 06/11/1996	Time: 14:00:00
	Figure C-59	
3D Andhra Pradesh		

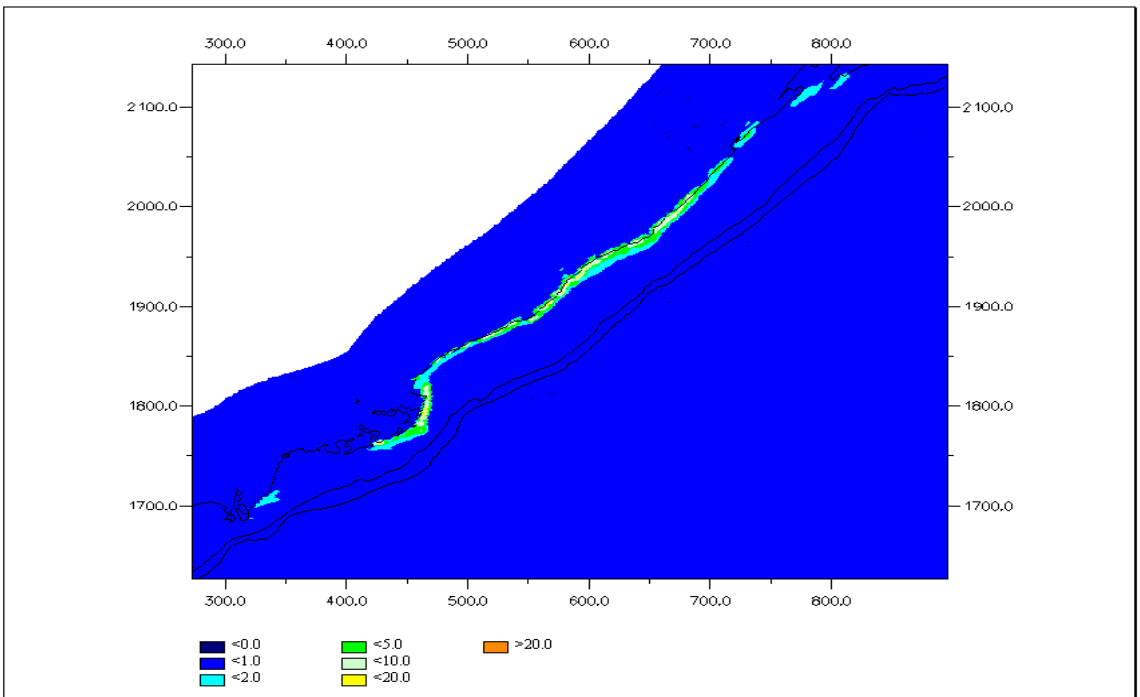

Colours represent the dissipation of energy Solid lines represent the 0, 500 and 1000 metres water depth isolines	Date: 06/11/1996	Time: 14:00:00
	Figure C-60	
3D Andhra Pradesh		

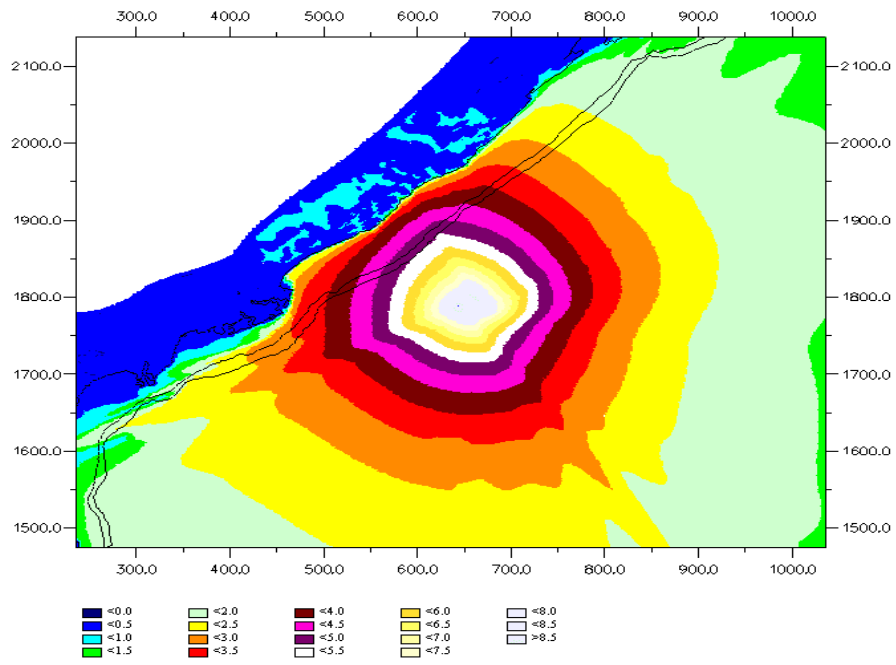

Colours represent the root mean square wave height [m] The solid lines represent the 0, 500 and 1000 metres depth isolines	Date: 06/11/1996	Time: 18:00:00
	Figure C-61	
3D Andhra Pradesh		

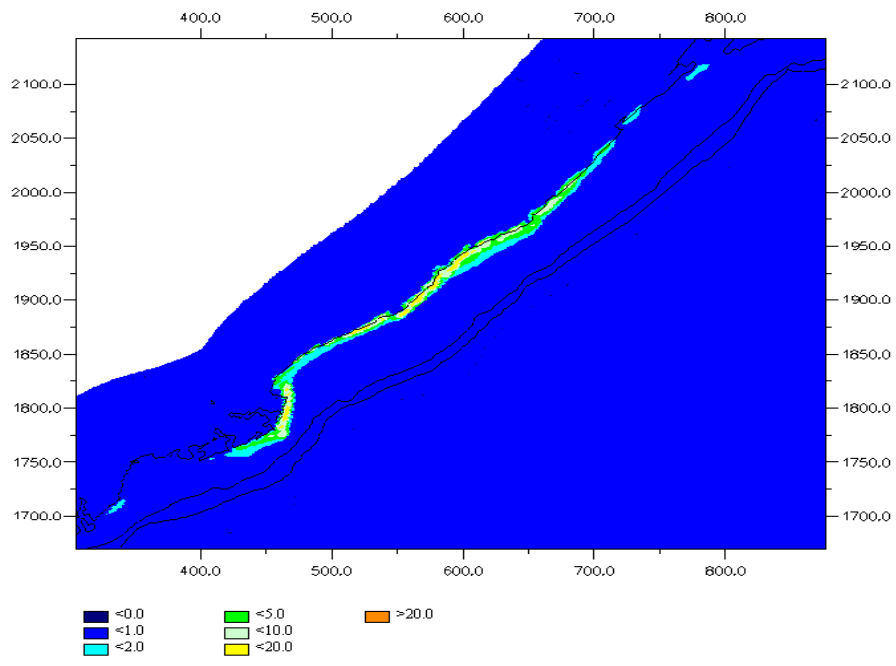

Colours represent the dissipation of energy Solid lines represent the 0, 500 and 1000 metres water depth isolines	Date: 06/11/1996	Time: 18:00:00
	Figure C-62	
3D Andhra Pradesh		

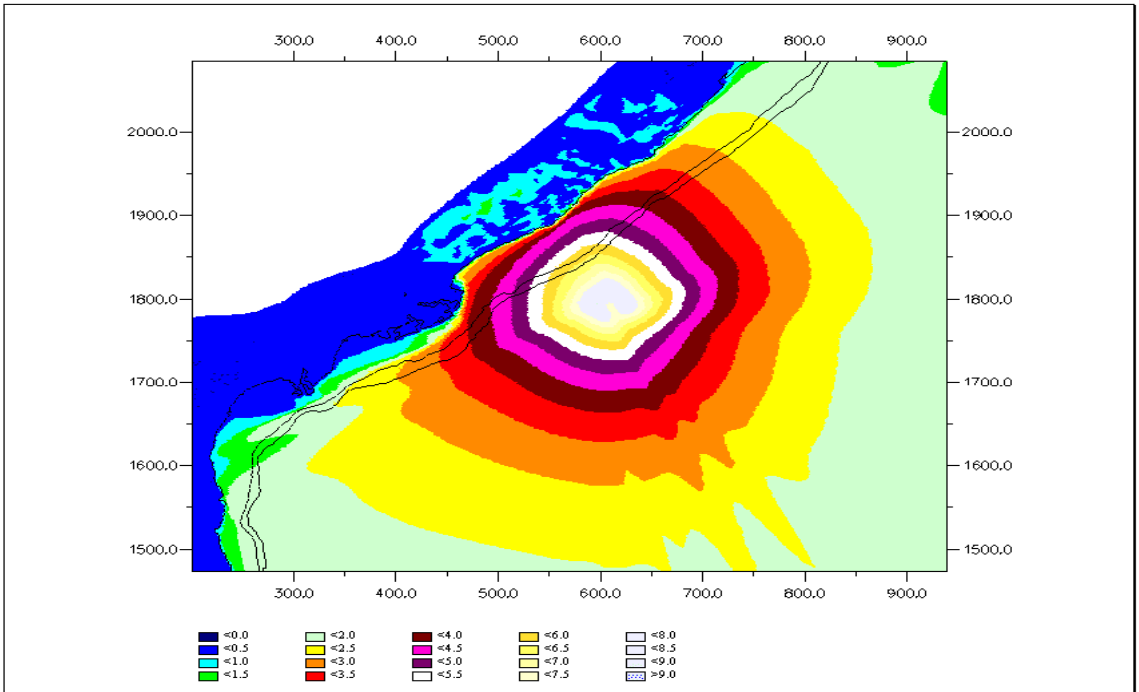

Colours represent the root mean square wave height [m] The solid lines represent the 0, 500 and 1000 metres depth isolines	Date: 06/11/1996	Time: 22:00:00
	Figure C-63	
3D Andhra Pradesh		

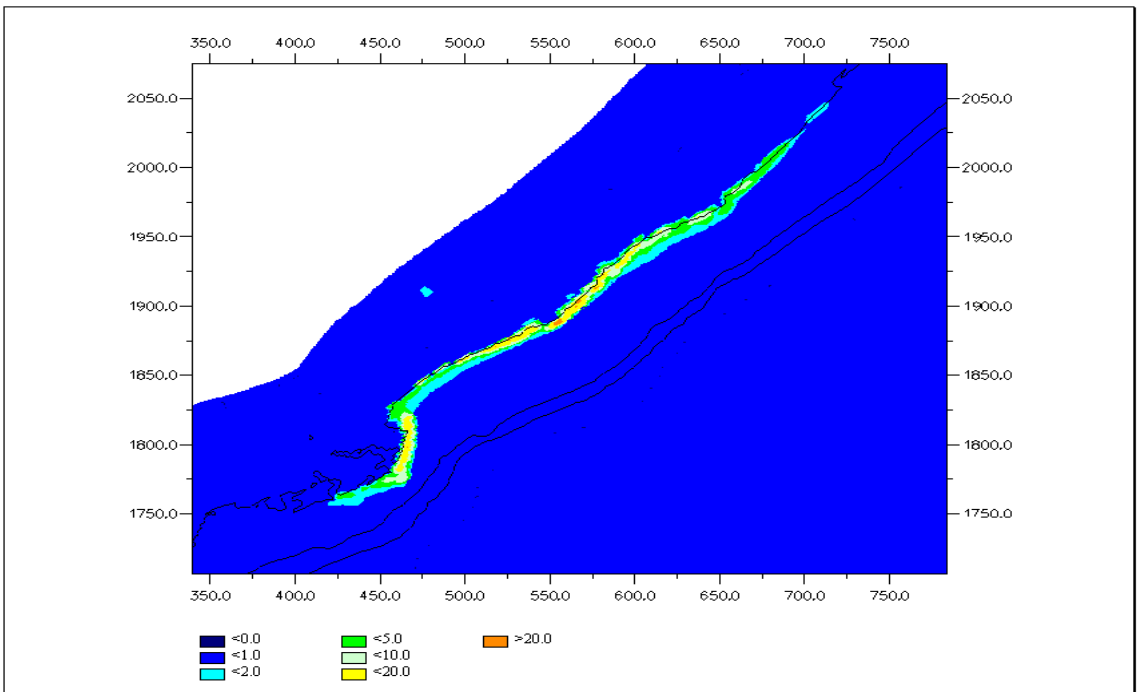

Colours represent the dissipation of energy Solid lines represent the 0, 500 and 1000 metres water depth isolines	Date: 06/11/1996	Time: 22:00:00
	Figure C-64	
3D Andhra Pradesh		

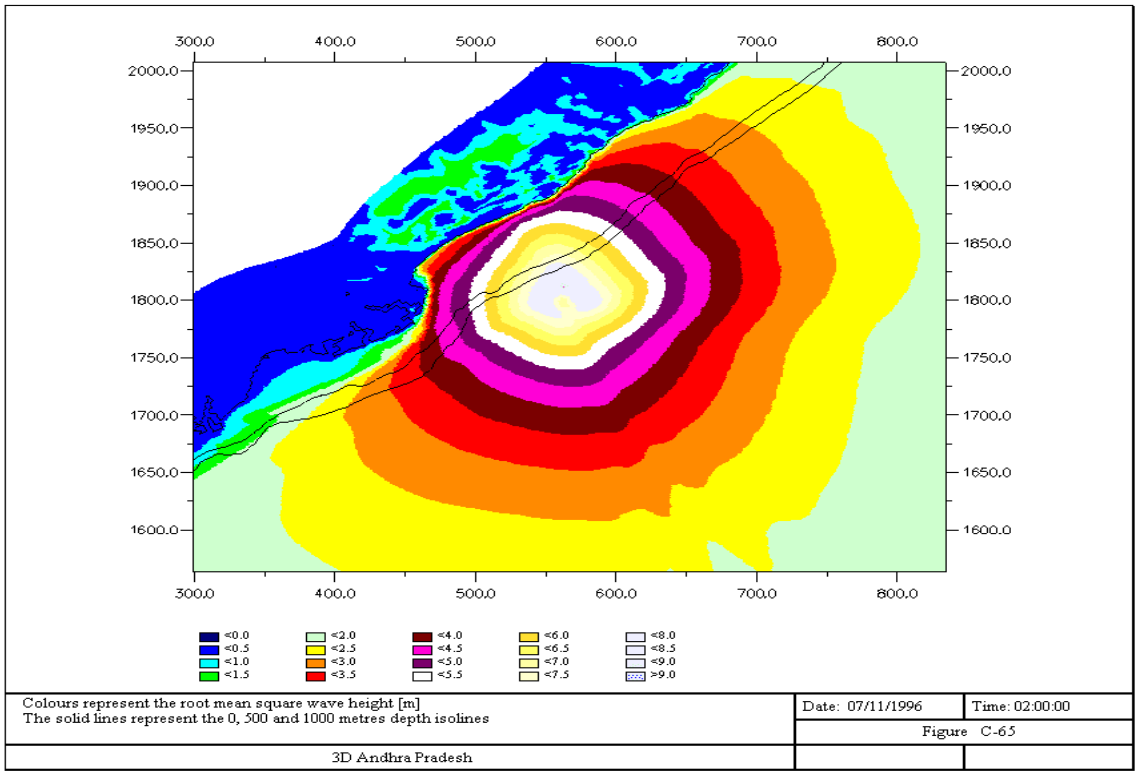

Colours represent the root mean square wave height [m]
The solid lines represent the 0, 500 and 1000 metres depth isolines

Date: 07/11/1996 Time: 02:00:00

Figure C-65

3D Andhra Pradesh

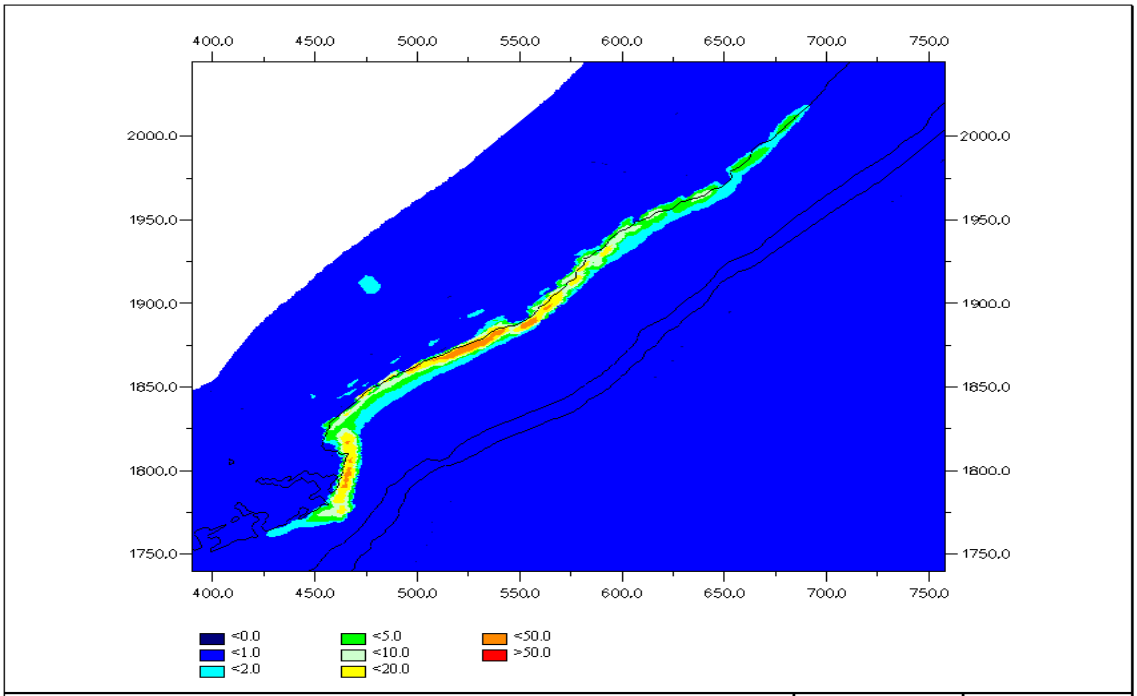

Colours represent the dissipation of energy
Solid lines represent the 0, 500 and 1000 metres water depth isolines

Date: 07/11/1996 Time: 02:00:00

Figure C-66

3D Andhra Pradesh

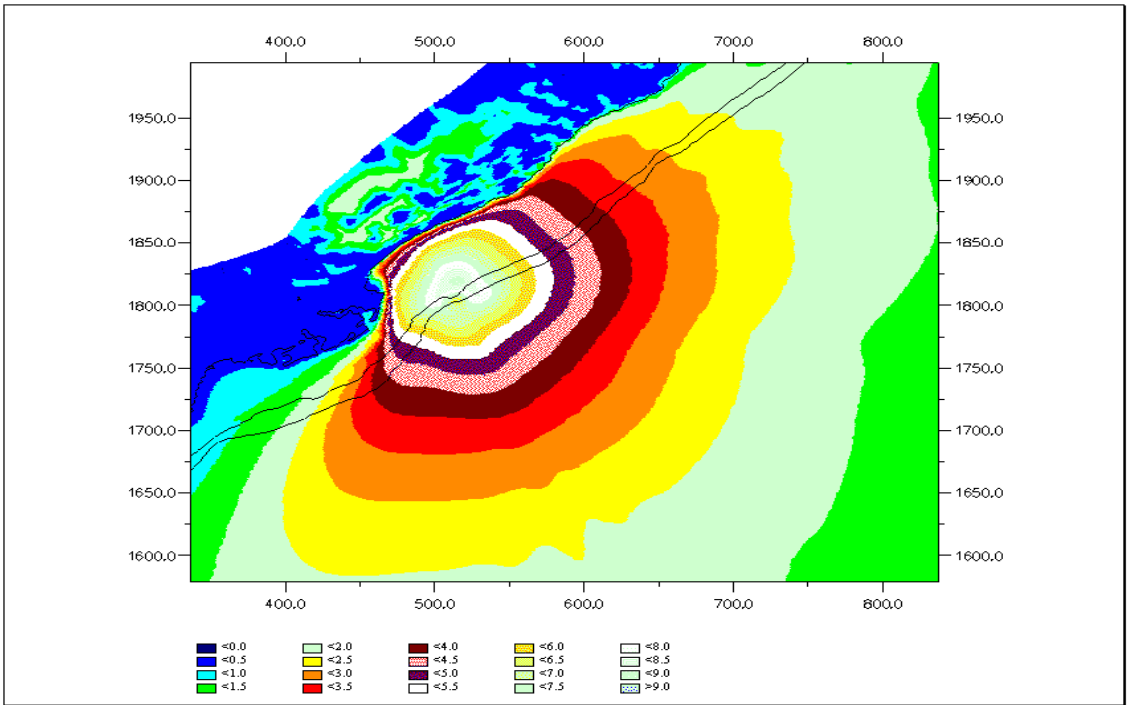

Colours represent the root mean square wave height [m] The solid lines represent the 0, 500 and 1000 metres depth isolines	Date: 07/11/1996	Time: 06:00:00
	Figure C-67	
3D Andhra Pradesh		

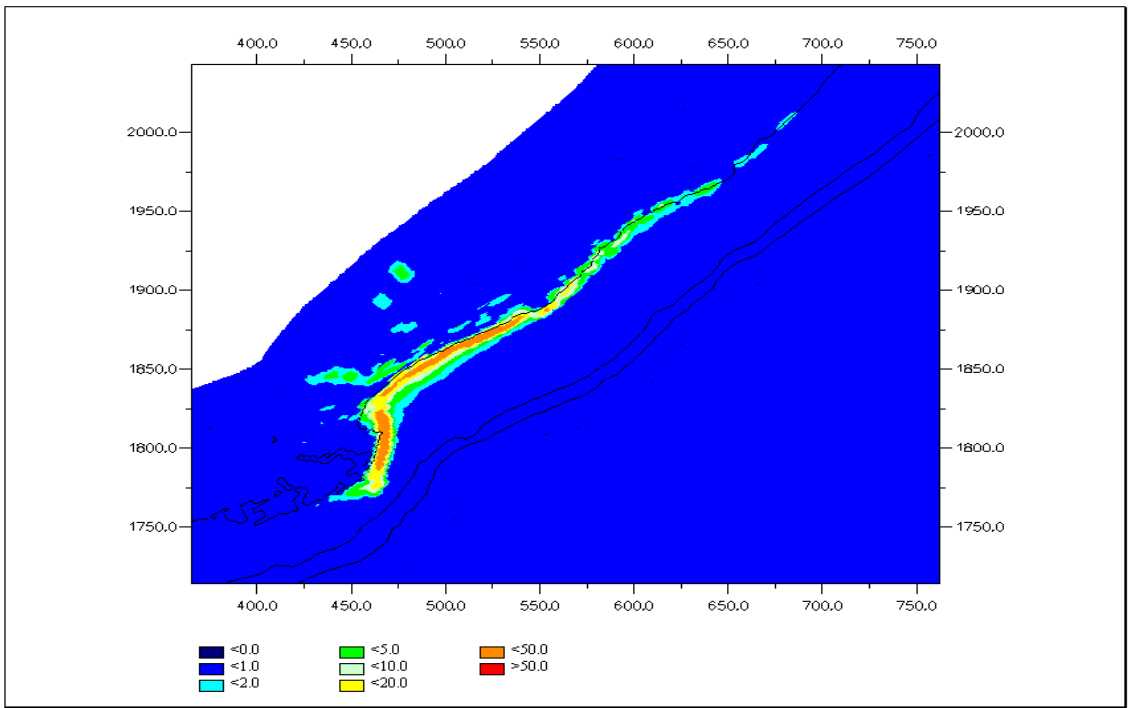

Colours represent the dissipation of energy Solid lines represent the 0, 500 and 1000 metres water depth isolines	Date: 07/11/1996	Time: 06:00:00
	Figure C-68	
3D Andhra Pradesh		

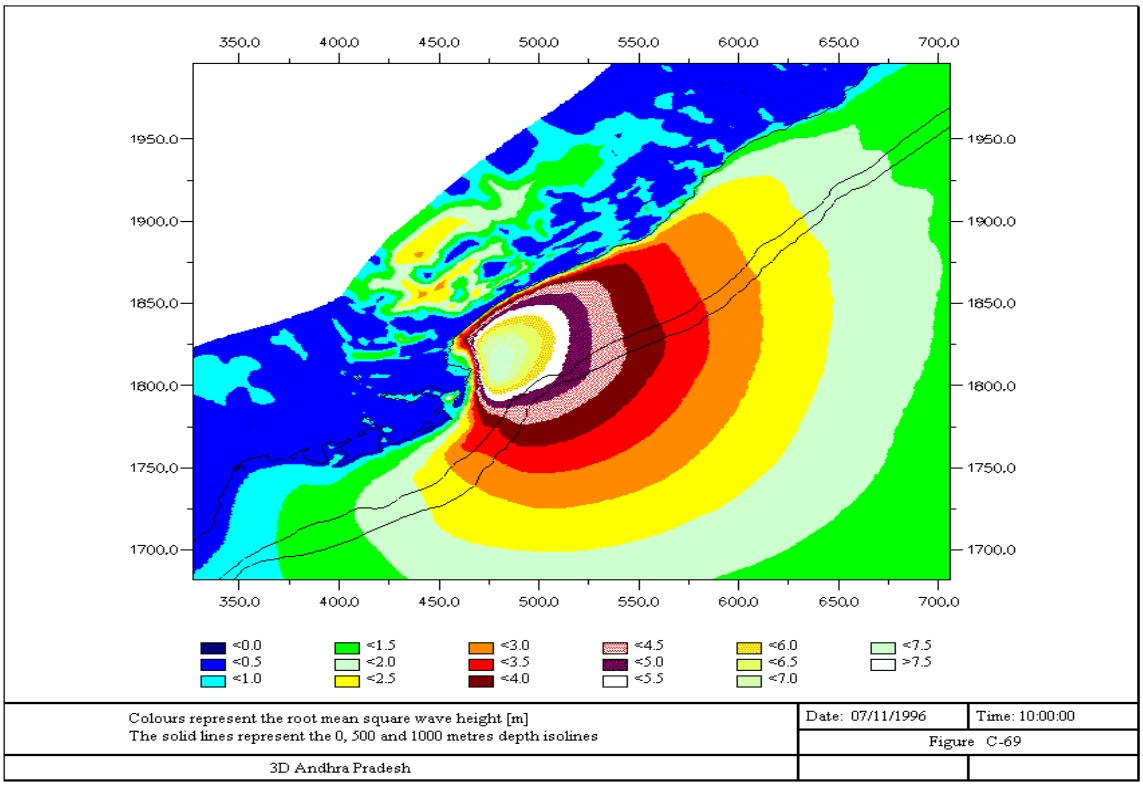

Colours represent the root mean square wave height [m] The solid lines represent the 0, 500 and 1000 metres depth isolines	Date: 07/11/1996	Time: 10:00:00
	Figure C-69	
3D Andhra Pradesh		

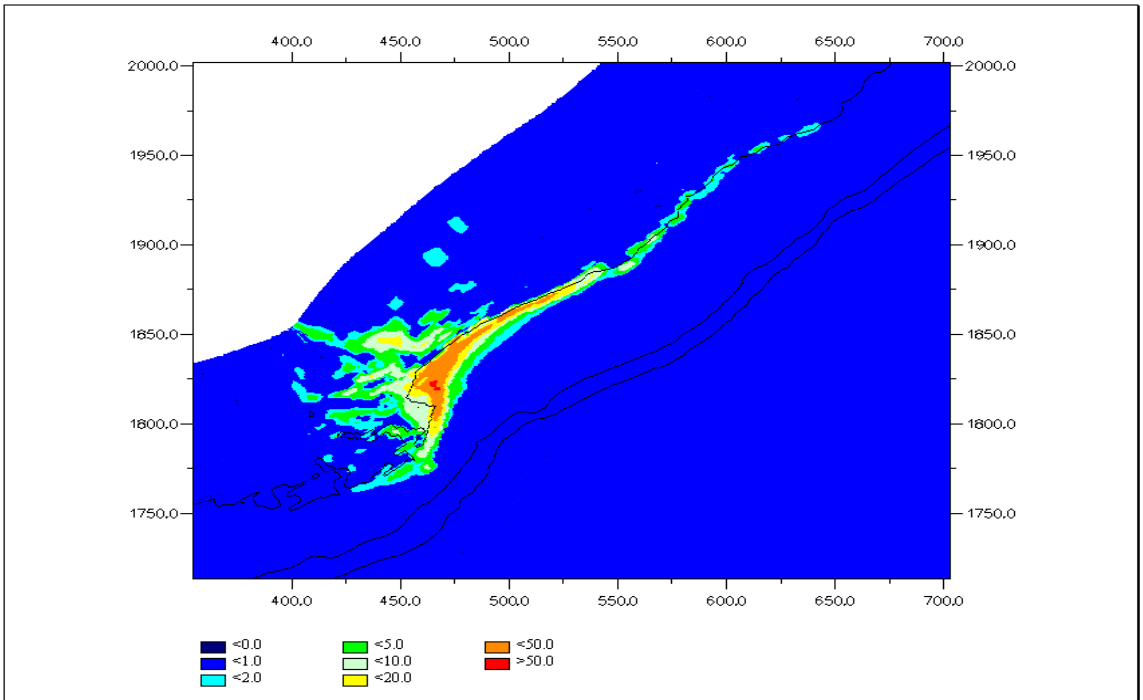

Colours represent the dissipation of energy Solid lines represent the 0, 500 and 1000 metres water depth isolines	Date: 07/11/1996	Time: 10:00:00
	Figure C-70	
3D Andhra Pradesh		

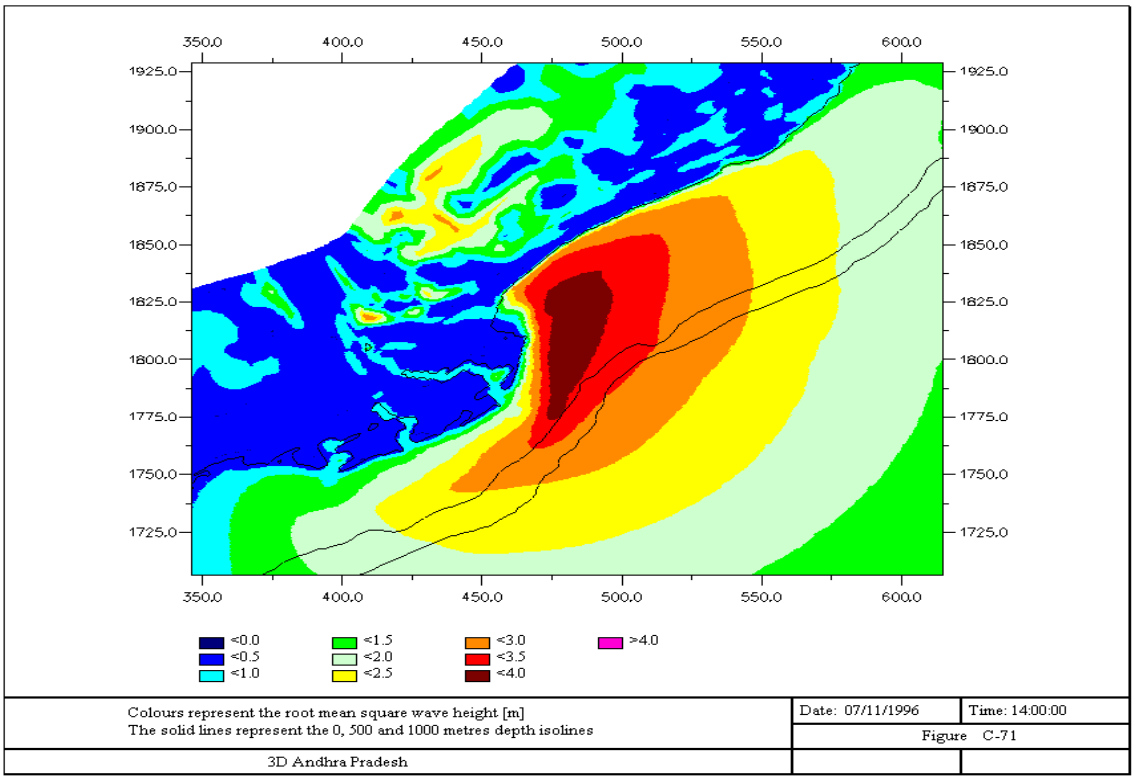

Colours represent the root mean square wave height [m] The solid lines represent the 0, 500 and 1000 metres depth isolines	Date: 07/11/1996	Time: 14:00:00
	Figure C-71	
3D Andhra Pradesh		

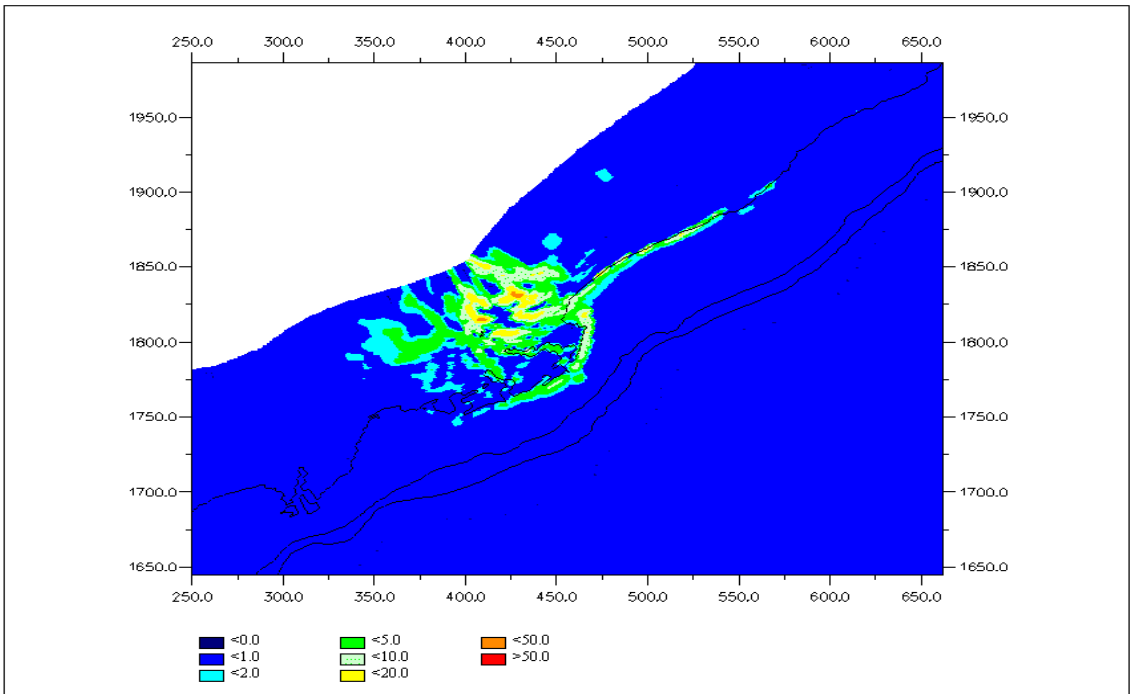

Colours represent the dissipation of energy Solid lines represent the 0, 500 and 1000 metres water depth isolines	Date: 07/11/1996	Time: 14:00:00
	Figure C-72	
3D Andhra Pradesh		

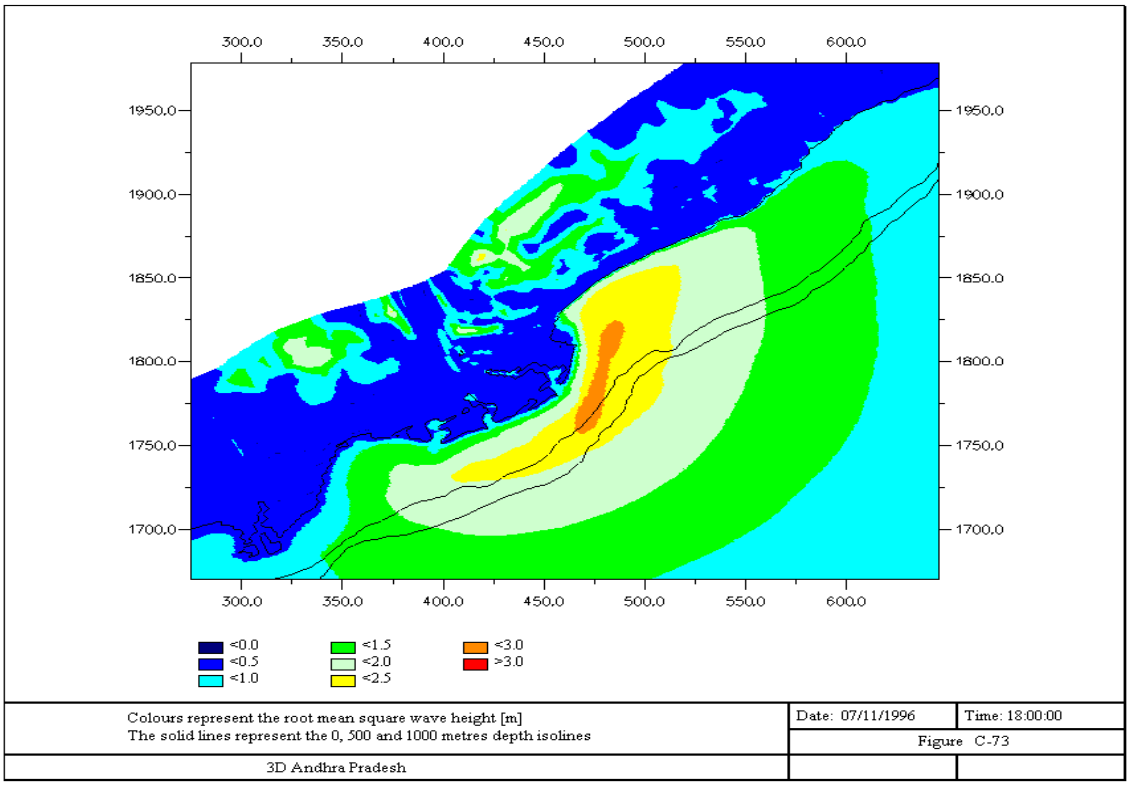

Colours represent the root mean square wave height [m] The solid lines represent the 0, 500 and 1000 metres depth isolines	Date: 07/11/1996	Time: 18:00:00
	Figure C-73	
3D Andhra Pradesh		

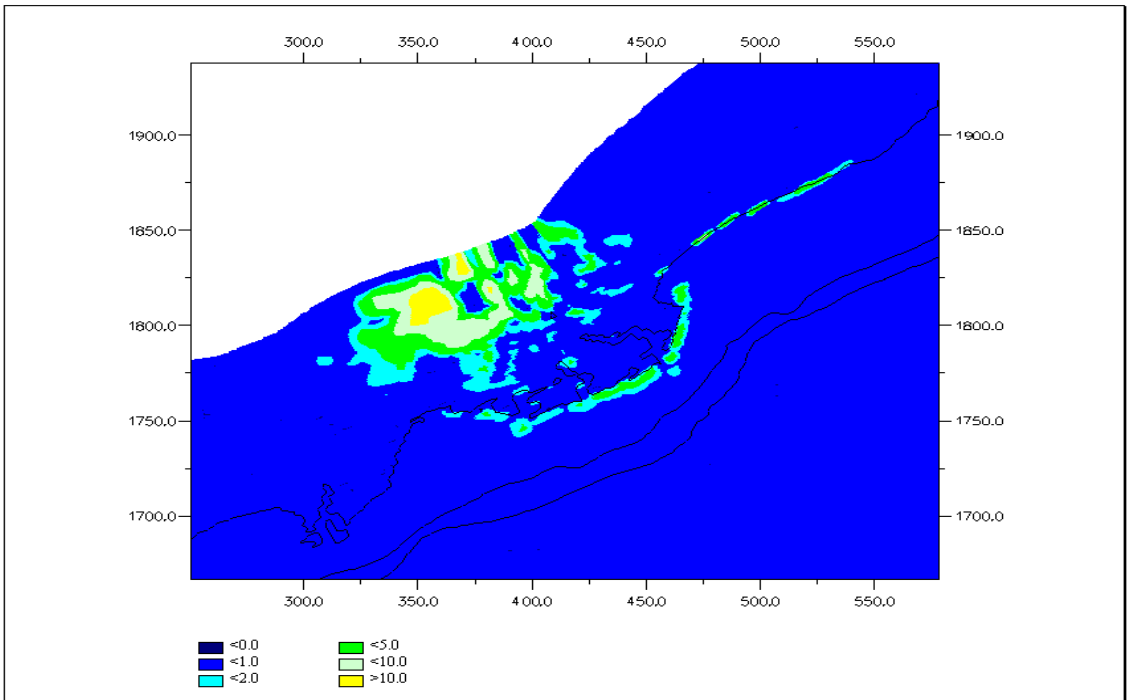

Colours represent the dissipation of energy Solid lines represent the 0, 500 and 1000 metres water depth isolines	Date: 07/11/1996	Time: 18:00:00
	Figure C-74	
3D Andhra Pradesh		

C.8 Water level set-up due to waves in 2D Ganges Delta case

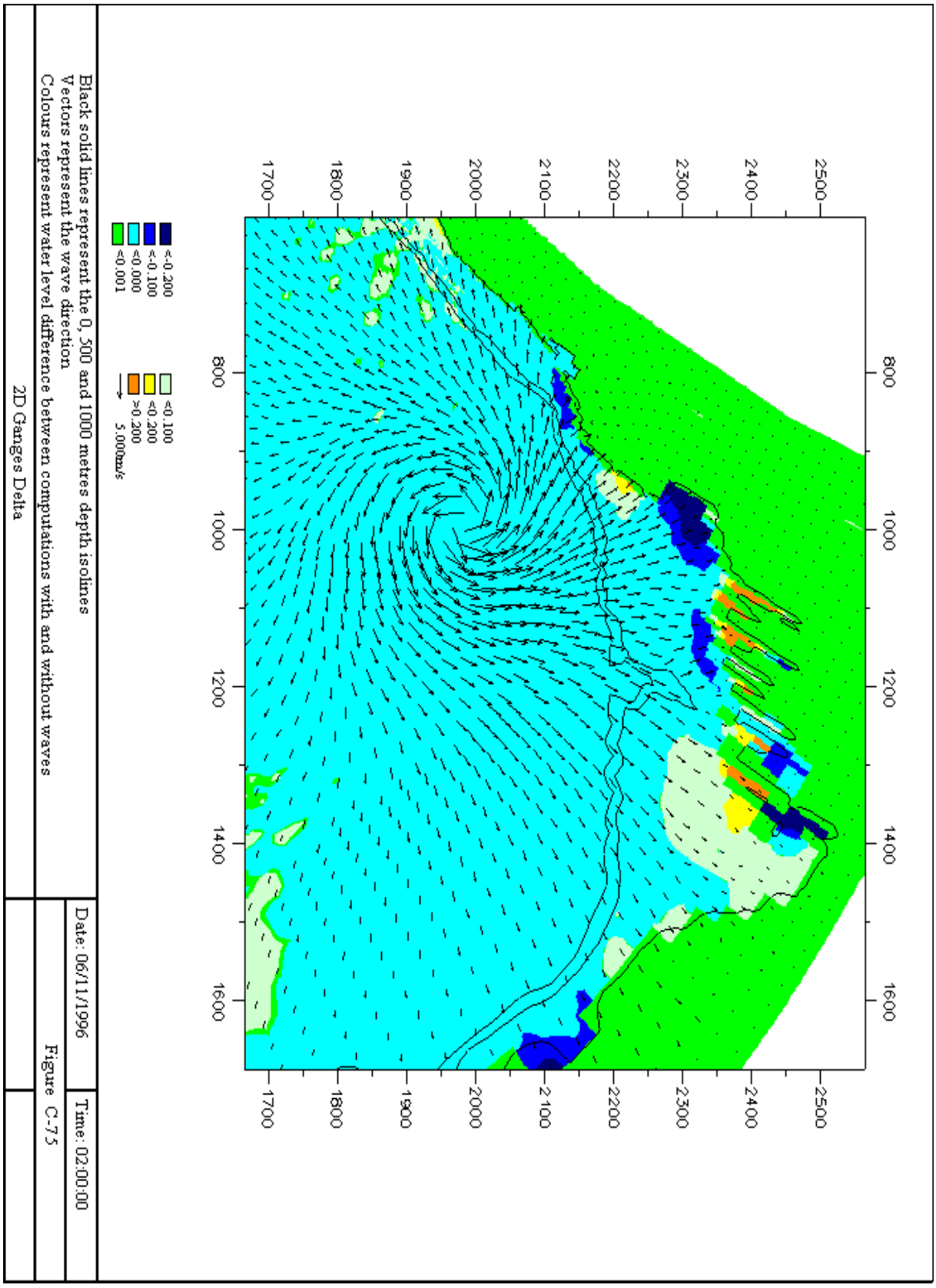

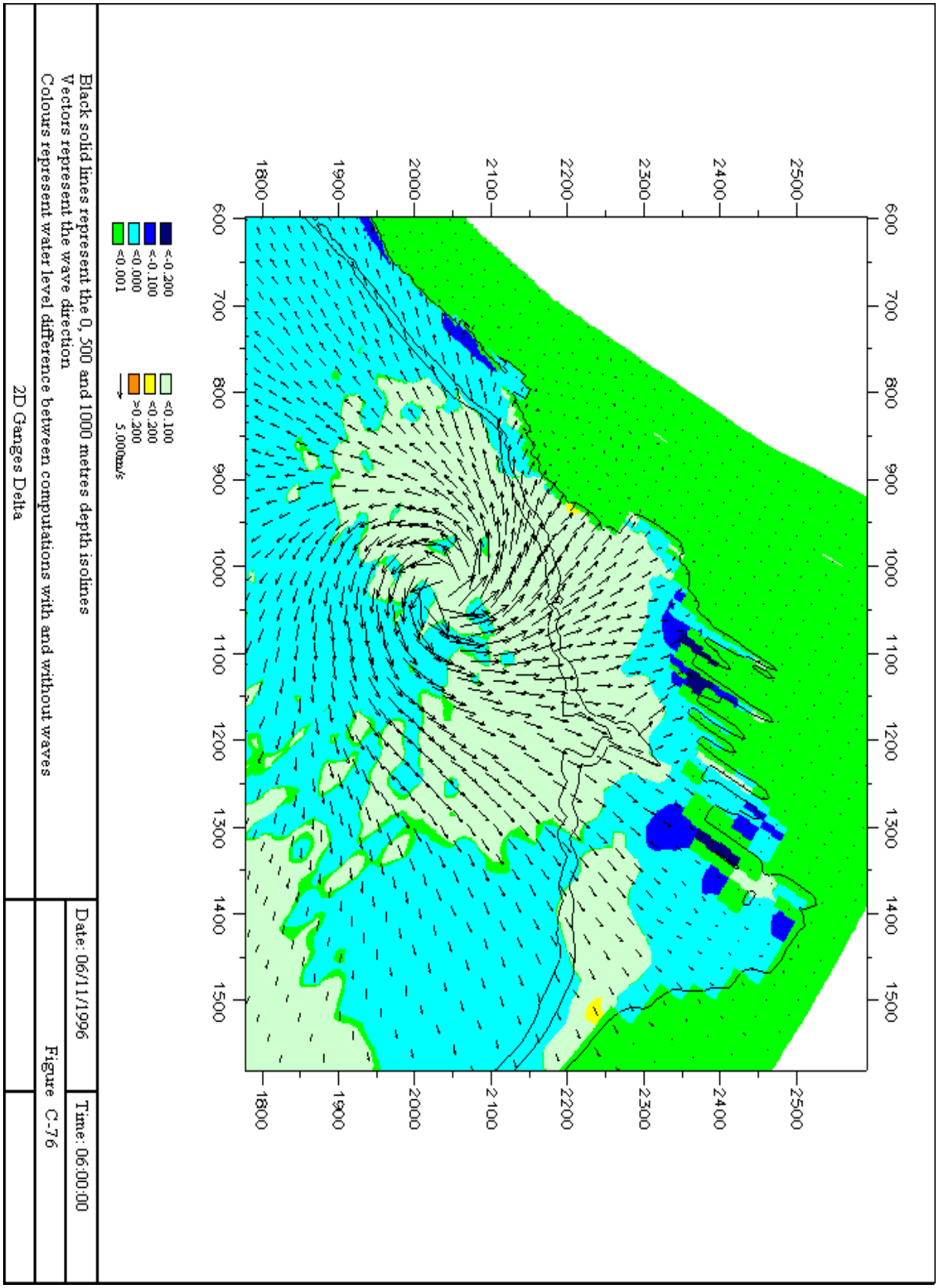
Black solid lines represent the 0, 500 and 1000 metres depth isolines
Vectors represent the wave direction
Colours represent water level difference between computations with and without waves
2D Ganges Delta
Date: 06/11/1996
Time: 06:00:00
Figure C-76
<-0.200
<-0.100
<0.000
<0.001
<0.100
<0.200
>0.200
5.000m/s

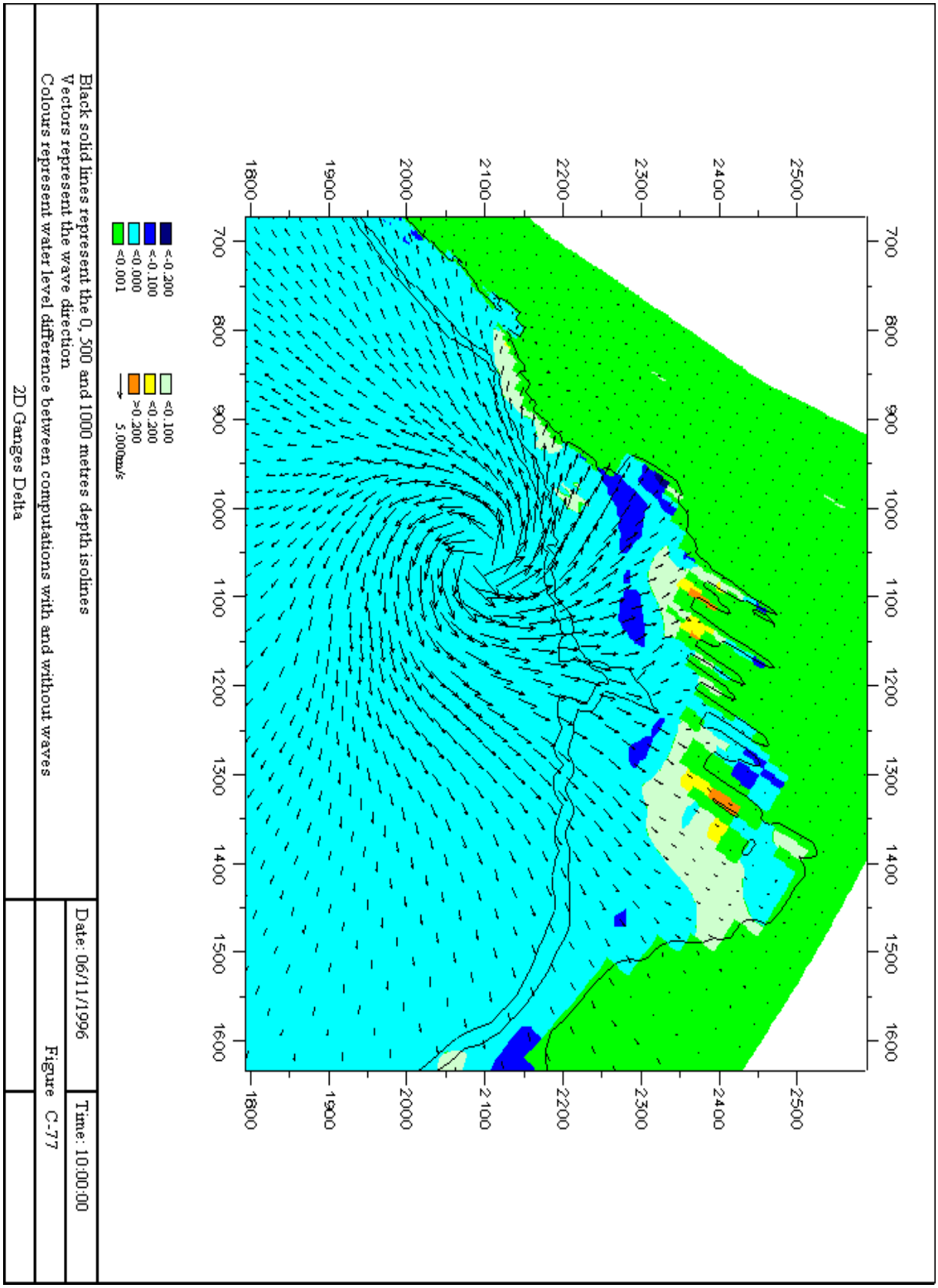
Black solid lines represent the 0, 500 and 1000 metres depth isolines
Vectors represent the wave direction
Colours represent water level difference between computations with and without waves
2D Ganges Delta
Date: 06/11/1996
Time: 10:00:00
Figure C-77
<-0.200
<-0.100
<0.000
<0.001
<0.100
<0.200
>0.200
5.000m/s

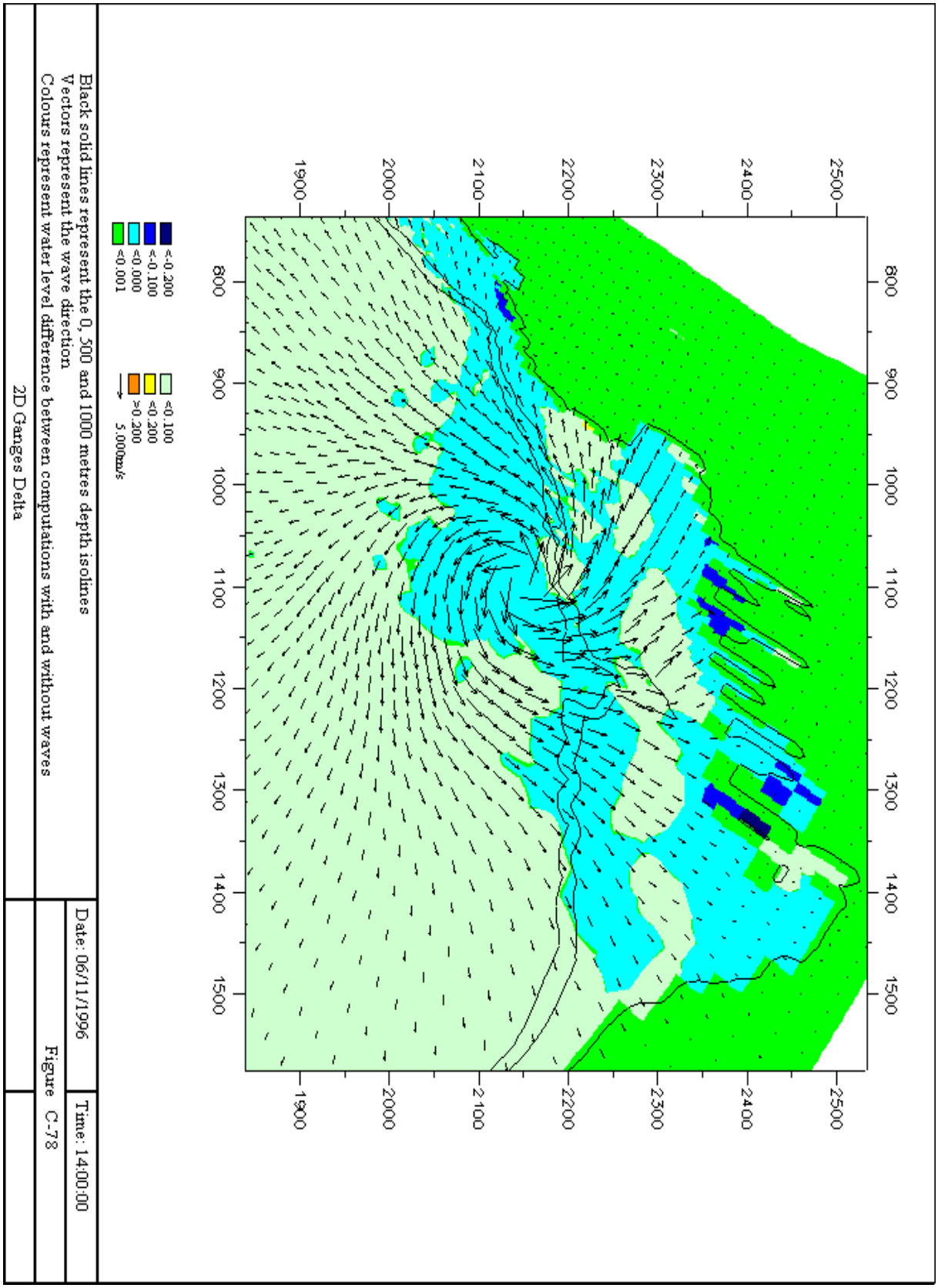
Black solid lines represent the 0, 500 and 1000 metres depth isolines
Vectors represent the wave direction
Colours represent water level difference between computations with and without waves
2D Ganges Delta
Date: 06/11/1996
Time: 14:00:00
Figure C-78
<-0.200
<-0.100
<0.000
<0.001
<0.100
<0.200
>0.200
5.000m/s

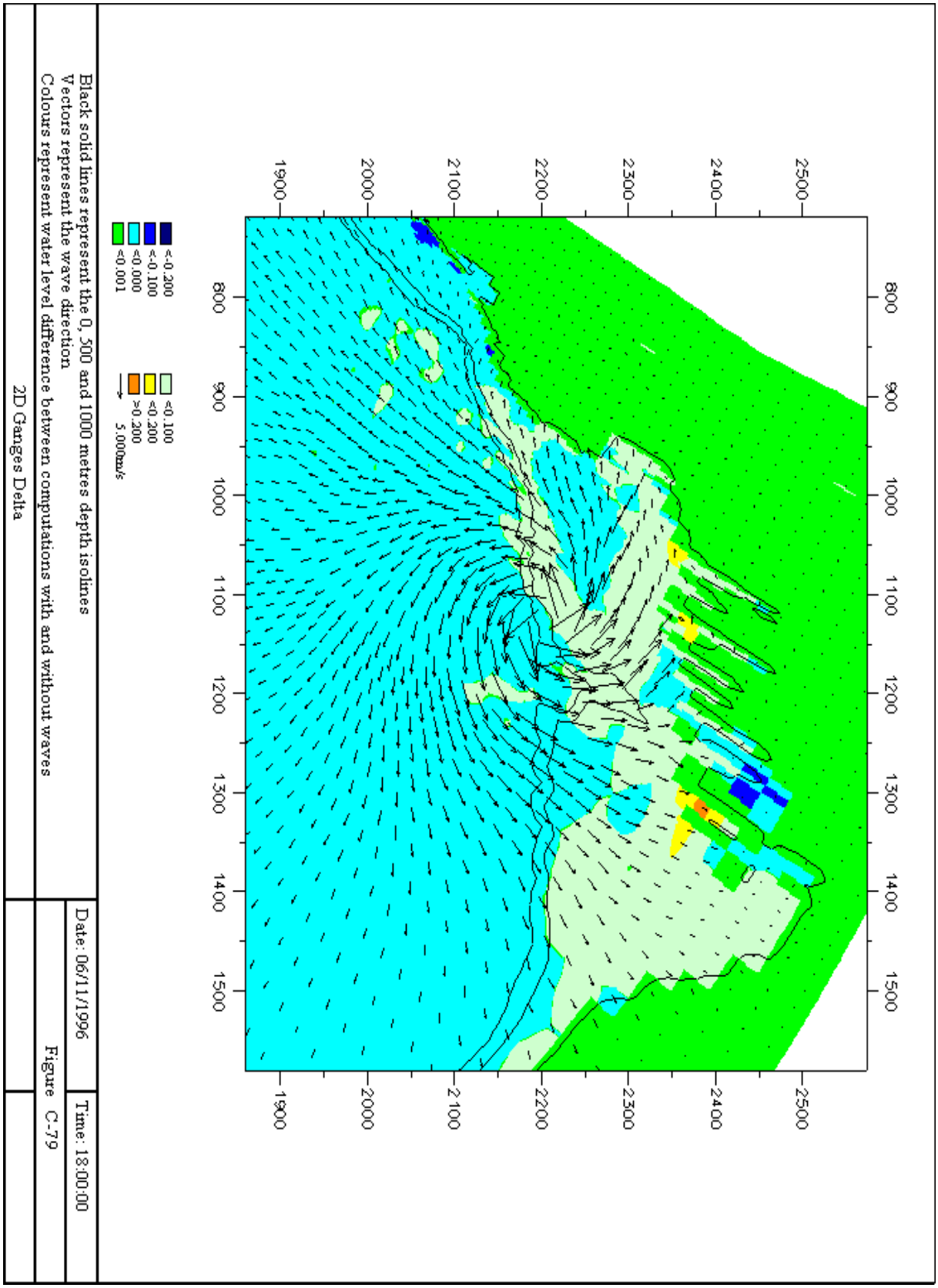
Black solid lines represent the 0, 500 and 1000 metres depth isolines
Vectors represent the wave direction
Colours represent water level difference between computations with and without waves
2D Ganges Delta
Date: 06/11/1996
Time: 18:00:00
Figure C-79
<-0.200
<-0.100
<0.000
<0.001
<0.100
<0.200
>0.200
5.000m/s
800
900
1000
1100
1200
1300
1400
1500
1900
2000
2100
2200
2300
2400
2500

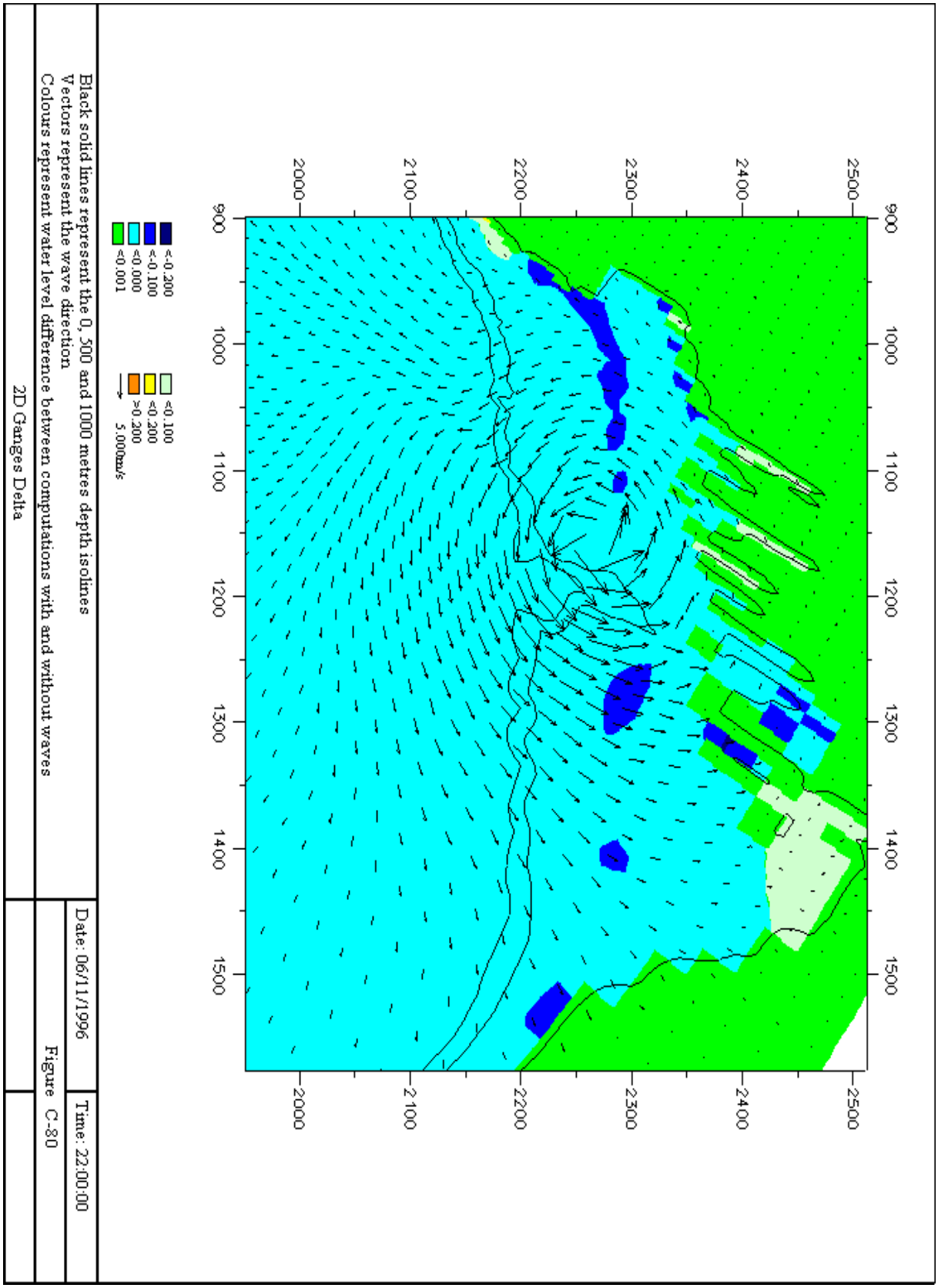
Black solid lines represent the 0, 500 and 1000 metres depth isolines
Vectors represent the wave direction
Colours represent water level difference between computations with and without waves
2D Ganges Delta
Date: 06/11/1996
Time: 22:00:00
Figure C-80
<-0.200
<-0.100
<0.000
<0.001
<0.100
<0.200
>0.200
5.000m/s
900
1000
1100
1200
1300
1400
1500
2000
2100
2200
2300
2400
2500

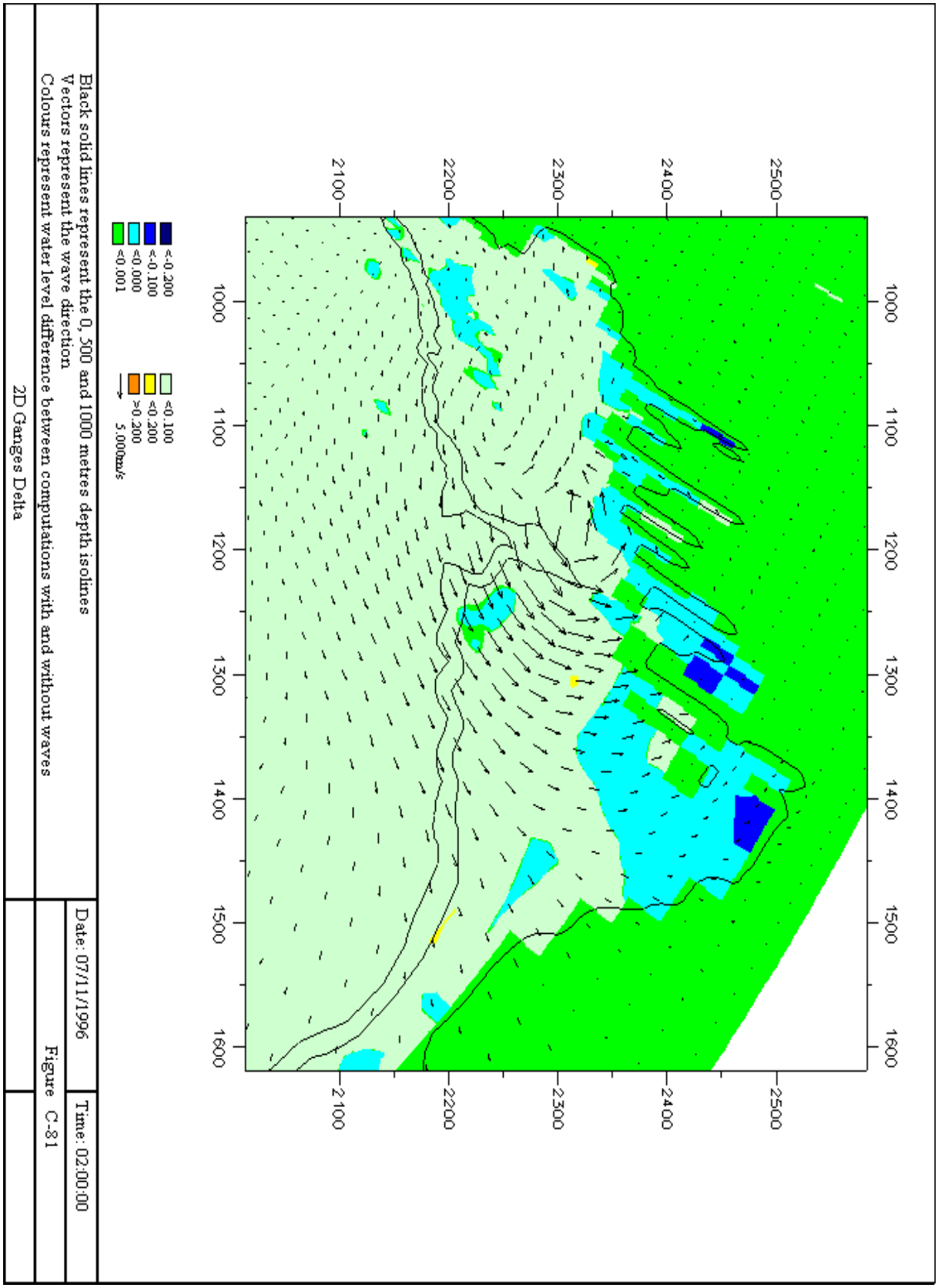
1000
1100
1200
1300
1400
1500
1600
2100
2200
2300
2400
2500
<-0.200
<-0.100
<0.000
<0.001
<0.100
<0.200
>0.200
5.000m/s
Black solid lines represent the 0, 500 and 1000 metres depth isolines
Vectors represent the wave direction
Colours represent water level difference between computations with and without waves
2D Ganges Delta
Date: 07/11/1996
Time: 02:00:00
Figure C-81

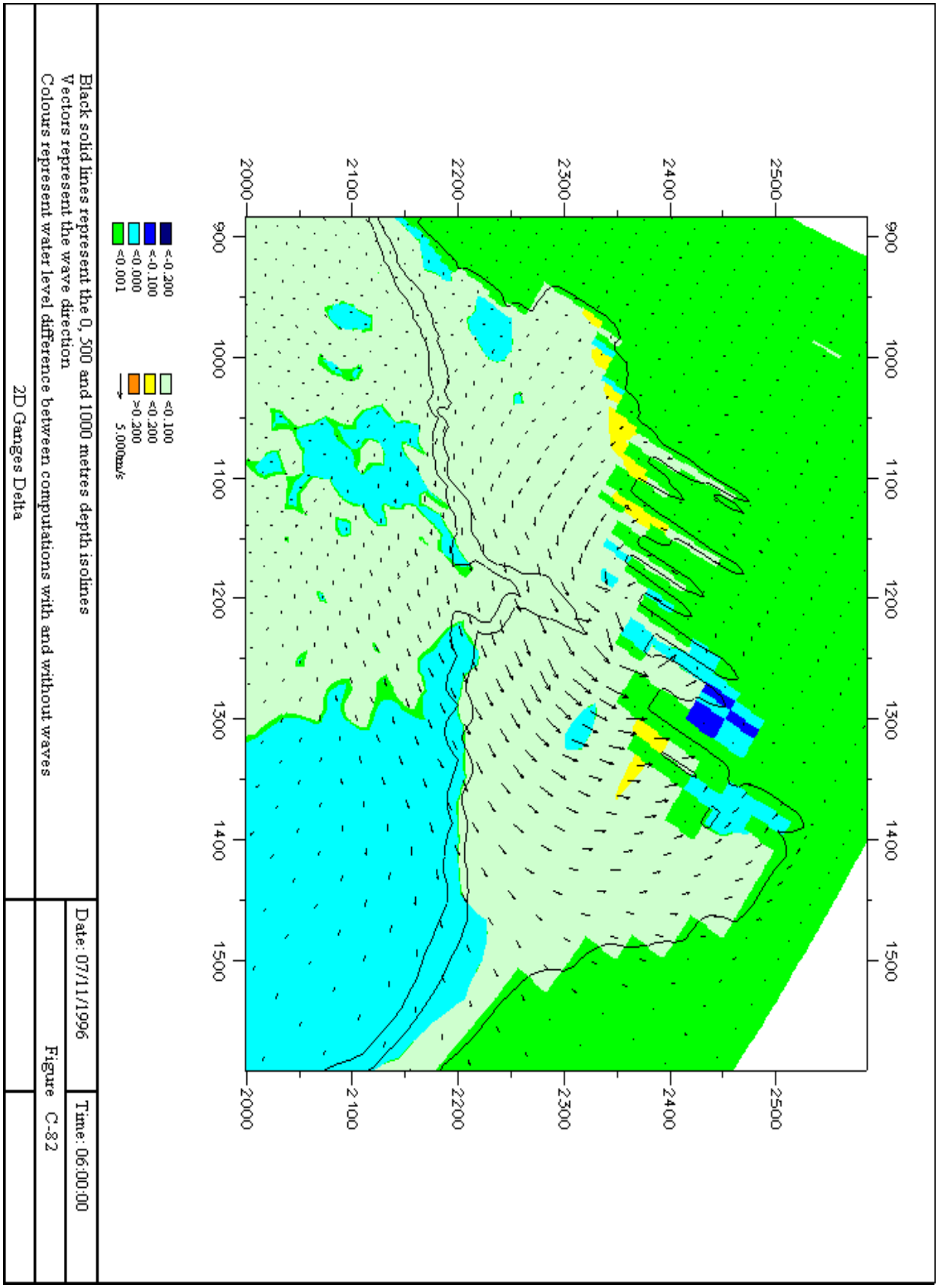
Black solid lines represent the 0, 500 and 1000 metres depth isolines
Vectors represent the wave direction
Colours represent water level difference between computations with and without waves
2D Ganges Delta
Date: 07/11/1996
Time: 06:00:00
Figure C-82
<-0.200
<-0.100
<0.000
<0.001
<0.100
<0.200
>0.200
5.000m/s
900
1000
1100
1200
1300
1400
1500
2000
2100
2200
2300
2400
2500

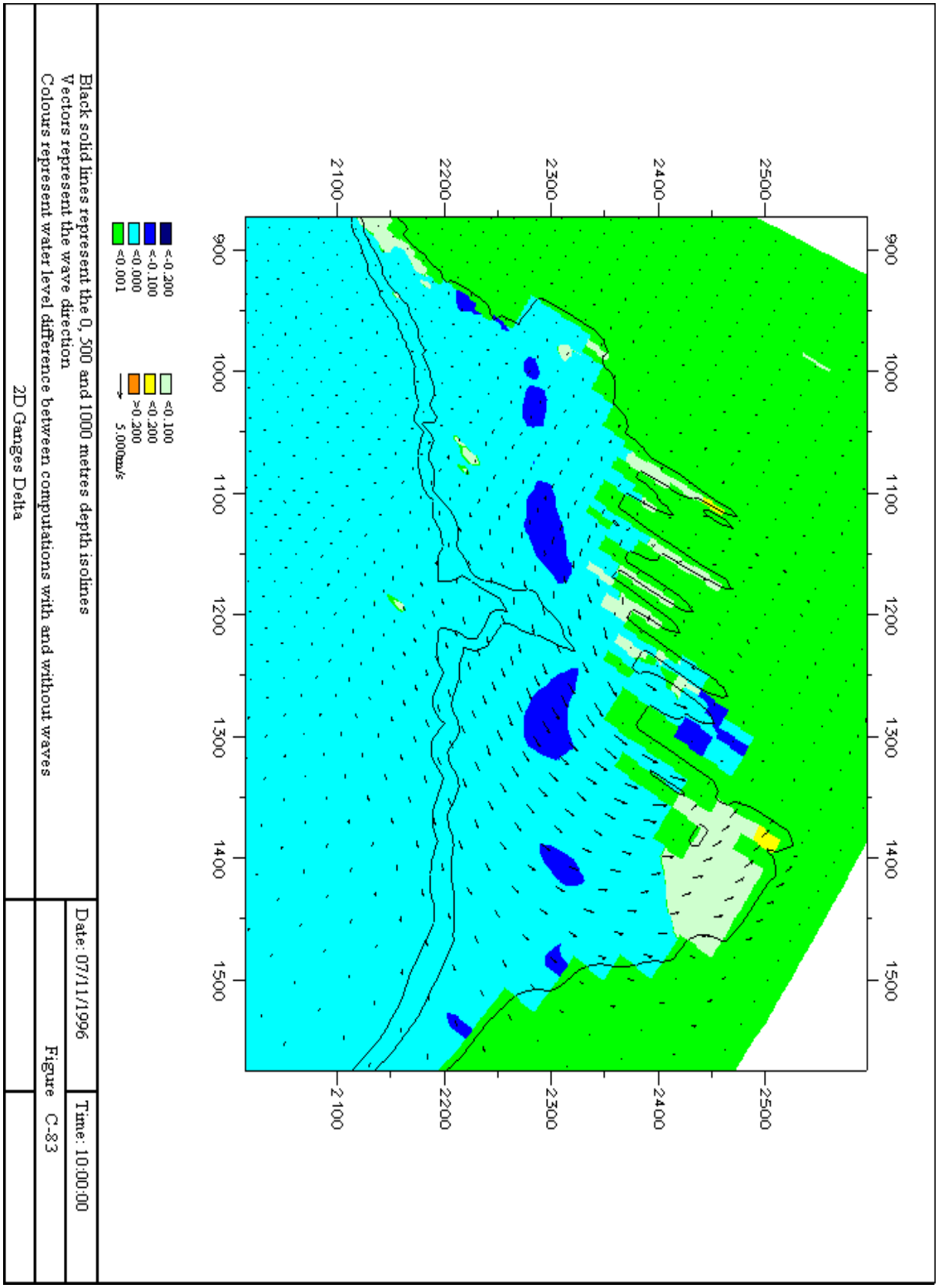
Black solid lines represent the 0, 500 and 1000 metres depth isolines
Vectors represent the wave direction
Colours represent water level difference between computations with and without waves
2D Ganges Delta
Date: 07/11/1996
Time: 10:00:00
Figure C-83
<-0.200
<-0.100
<0.000
<0.001
<0.100
<0.200
>0.200
5.000m/s
900
1000
1100
1200
1300
1400
1500
2100
2200
2300
2400
2500

C.9 Wave height and Dissipation for 2D Ganges Delta case

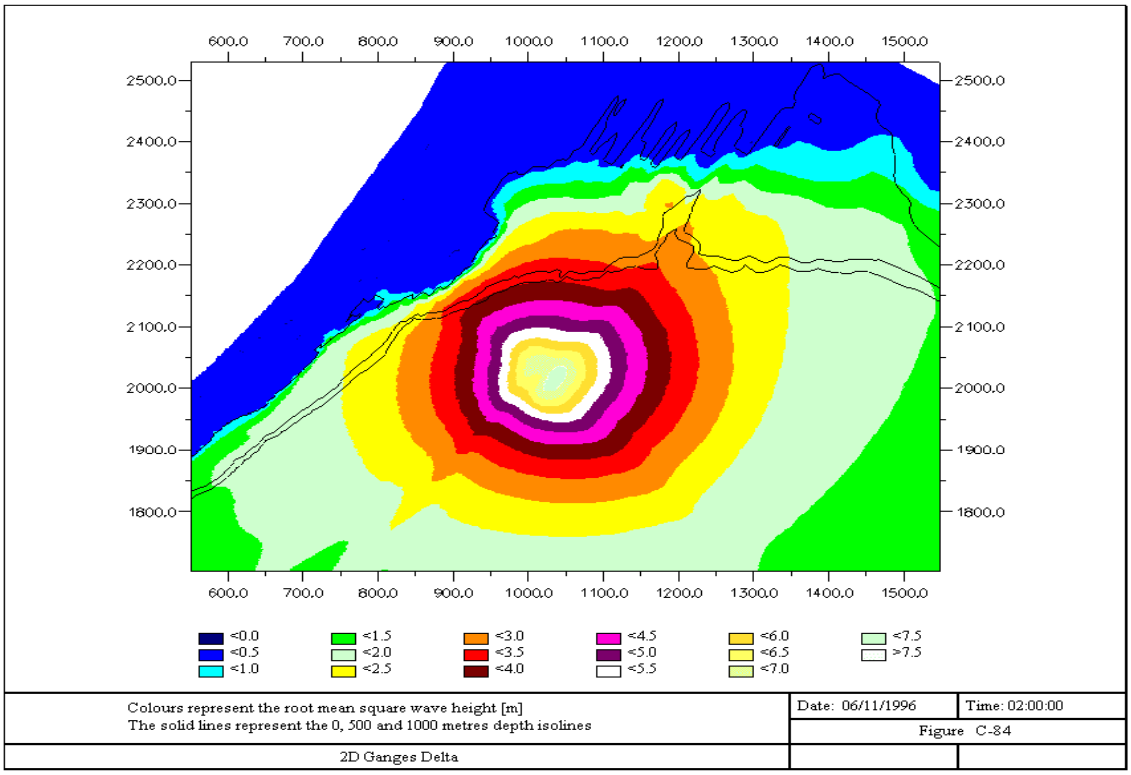

Colours represent the root mean square wave height [m] The solid lines represent the 0, 500 and 1000 metres depth isolines	Date: 06/11/1996	Time: 02:00:00
	Figure C-84	
2D Ganges Delta		

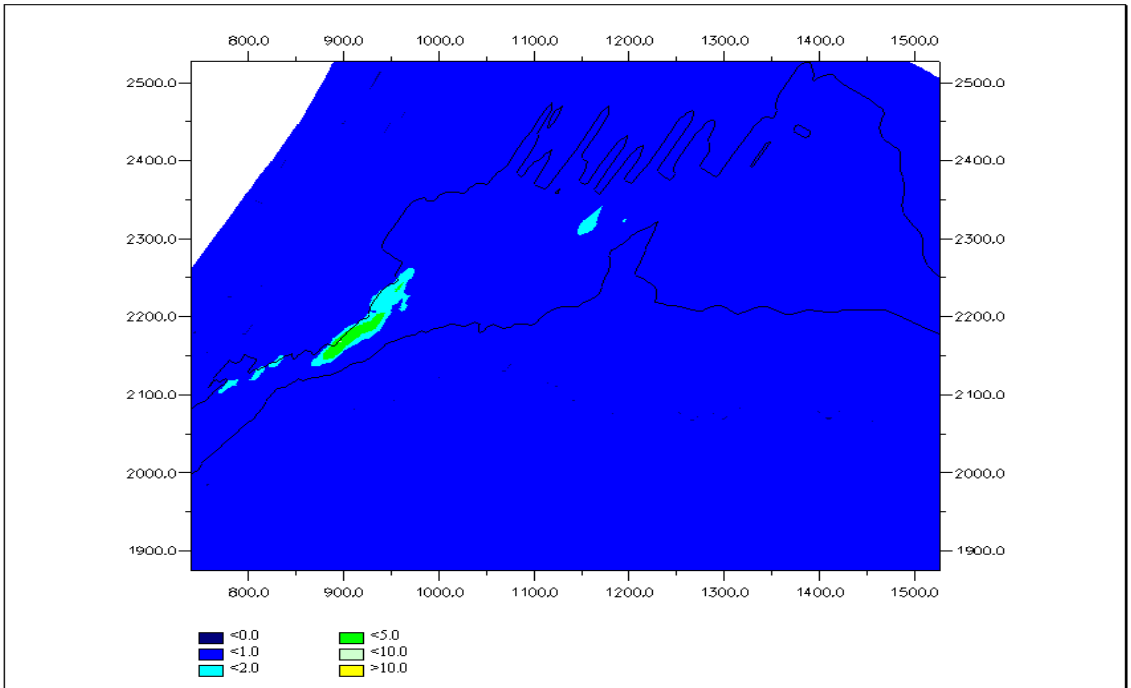

Colours represent the dissipation of energy Solid lines represent a water depth of 0 and 500 metres	Date: 06/11/1996	Time: 02:00:00
	Figure C-85	
2D Ganges Delta		

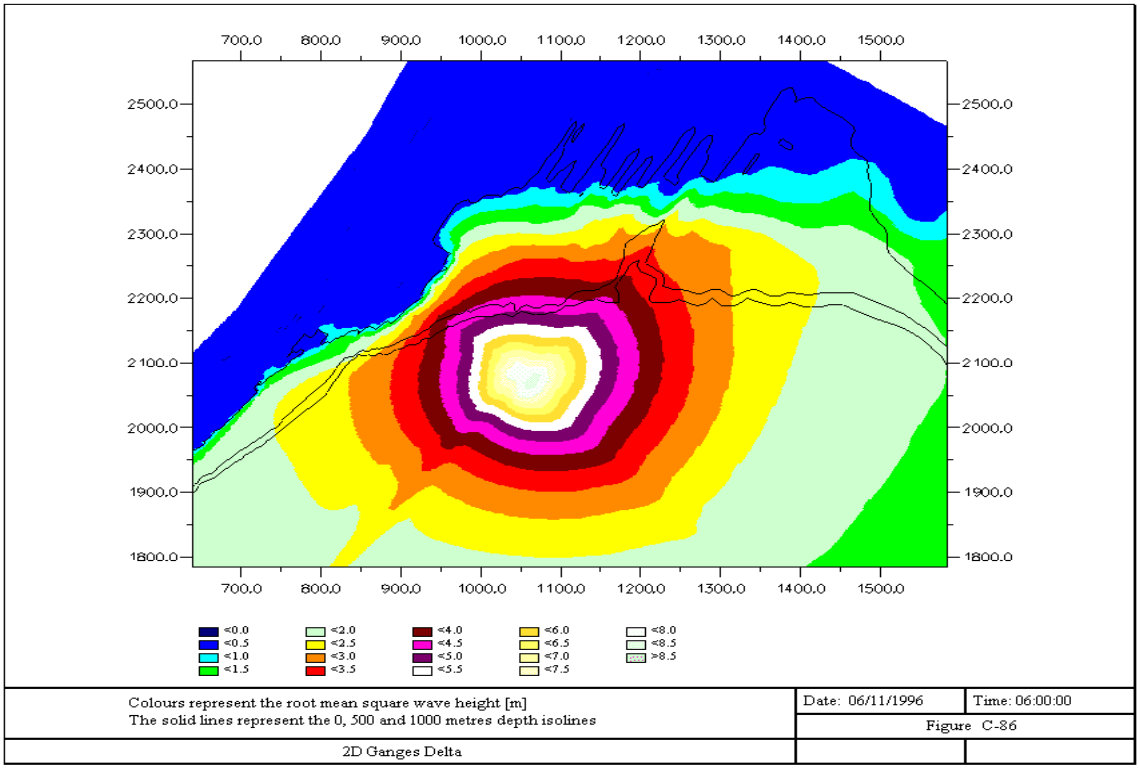

Colours represent the root mean square wave height [m] The solid lines represent the 0, 500 and 1000 metres depth isolines	Date: 06/11/1996	Time: 06:00:00
	Figure C-86	
2D Ganges Delta		

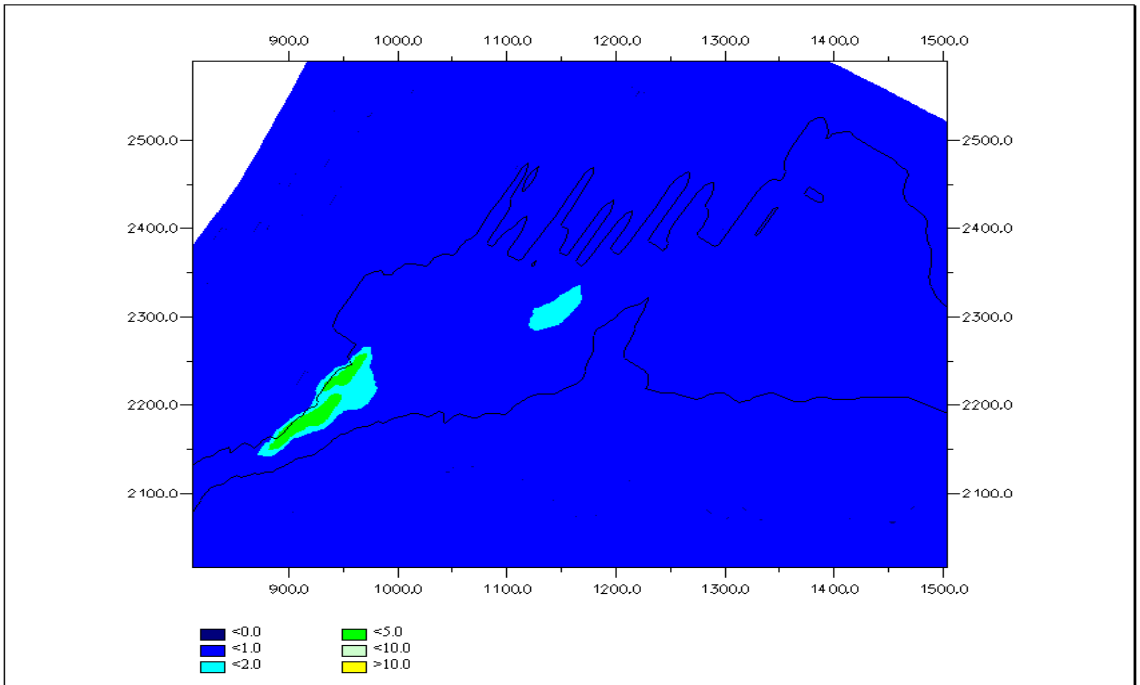

Colours represent the dissipation of energy Solid lines represent a water depth of 0 and 500 metres	Date: 06/11/1996	Time: 06:00:00
	Figure C-87	
2D Ganges Delta		

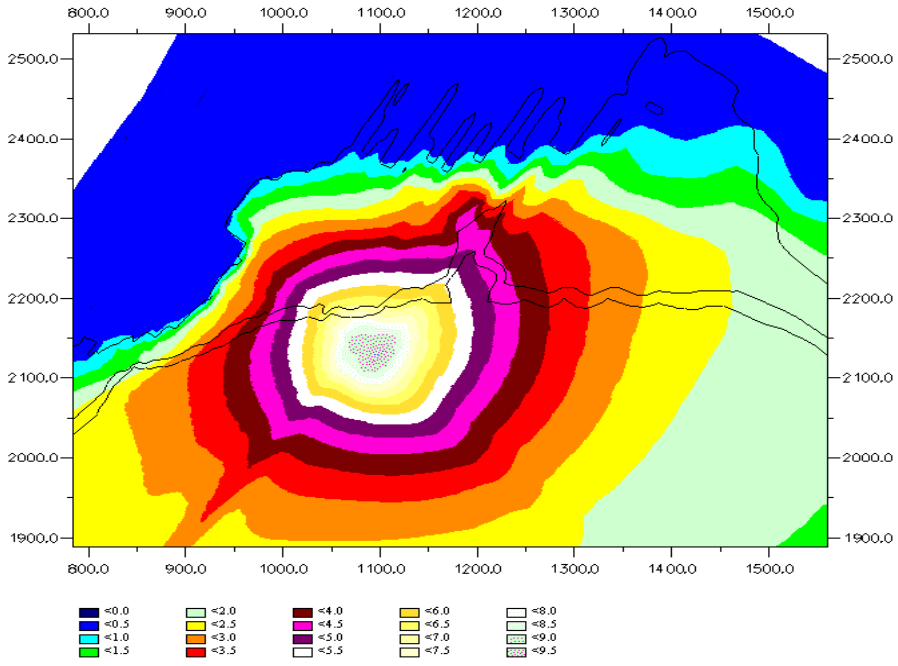

Colours represent the root mean square wave height [m] The solid lines represent the 0, 500 and 1000 metres depth isolines	Date: 06/11/1996	Time: 10:00:00
	Figure C-88	
2D Ganges Delta		

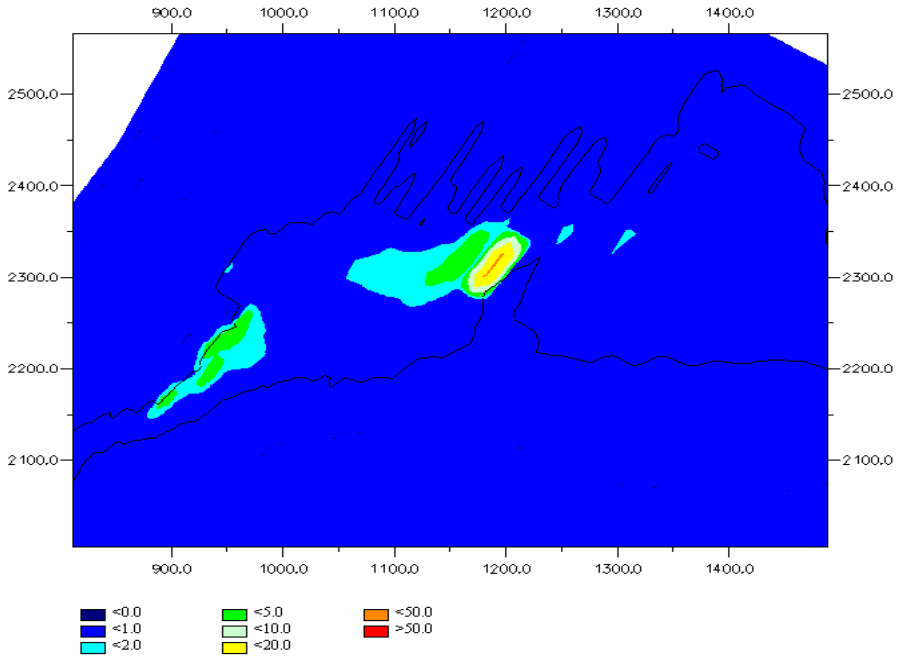

Colours represent the dissipation of energy Solid lines represent a water depth of 0 and 500 metres	Date: 06/11/1996	Time: 10:00:00
	Figure C-89	
2D Ganges Delta		

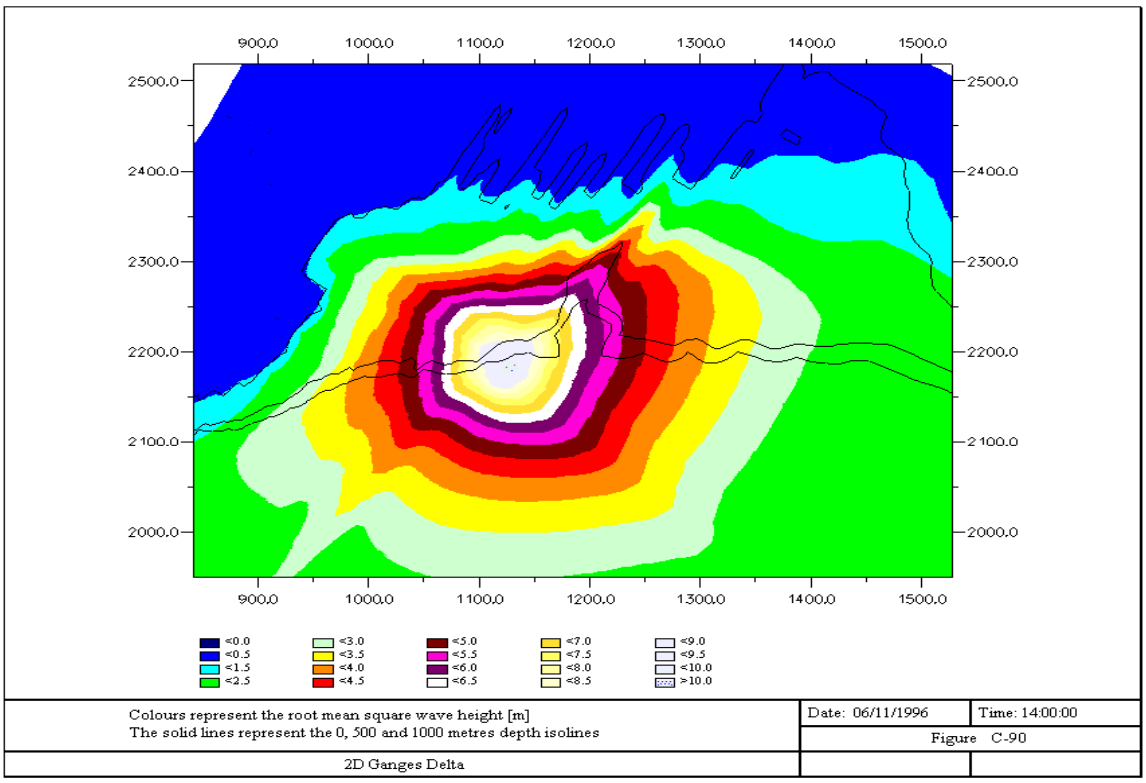

Colours represent the root mean square wave height [m] The solid lines represent the 0, 500 and 1000 metres depth isolines	Date: 06/11/1996	Time: 14:00:00
	Figure C-90	
2D Ganges Delta		

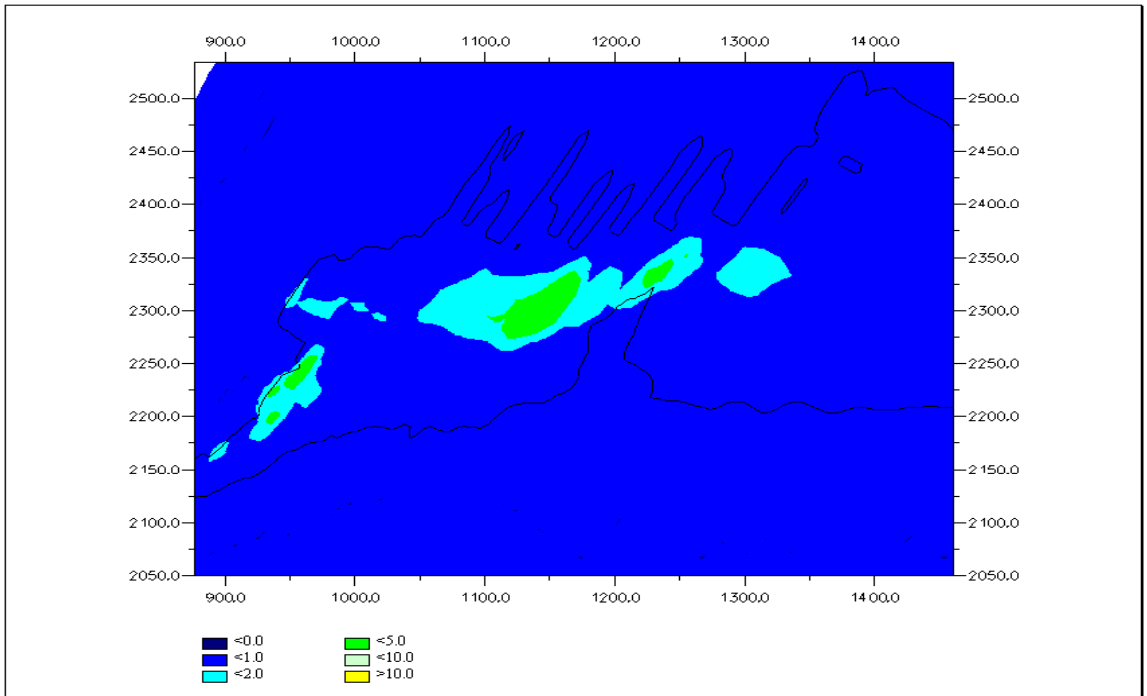

Colours represent the dissipation of energy Solid lines represent a water depth of 0 and 500 metres	Date: 06/11/1996	Time: 14:00:00
	Figure C-91	
2D Ganges Delta		

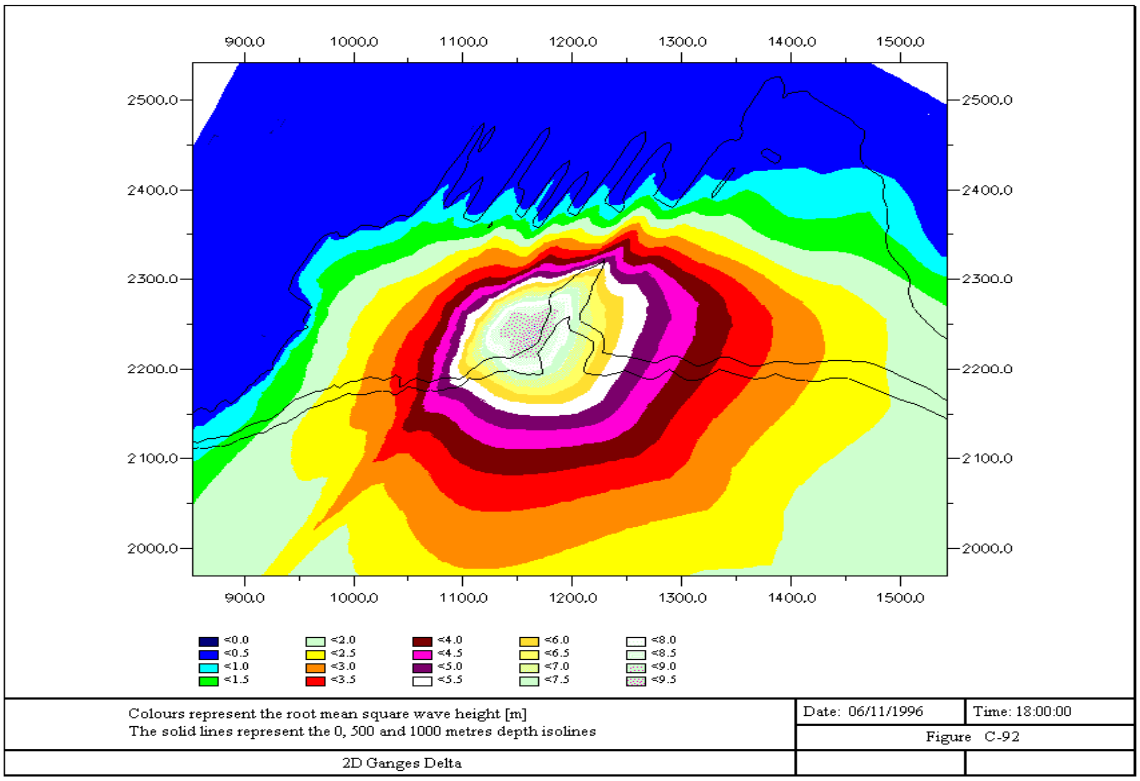

Colours represent the root mean square wave height [m] The solid lines represent the 0, 500 and 1000 metres depth isolines	Date: 06/11/1996	Time: 18:00:00
	Figure C-92	
2D Ganges Delta		

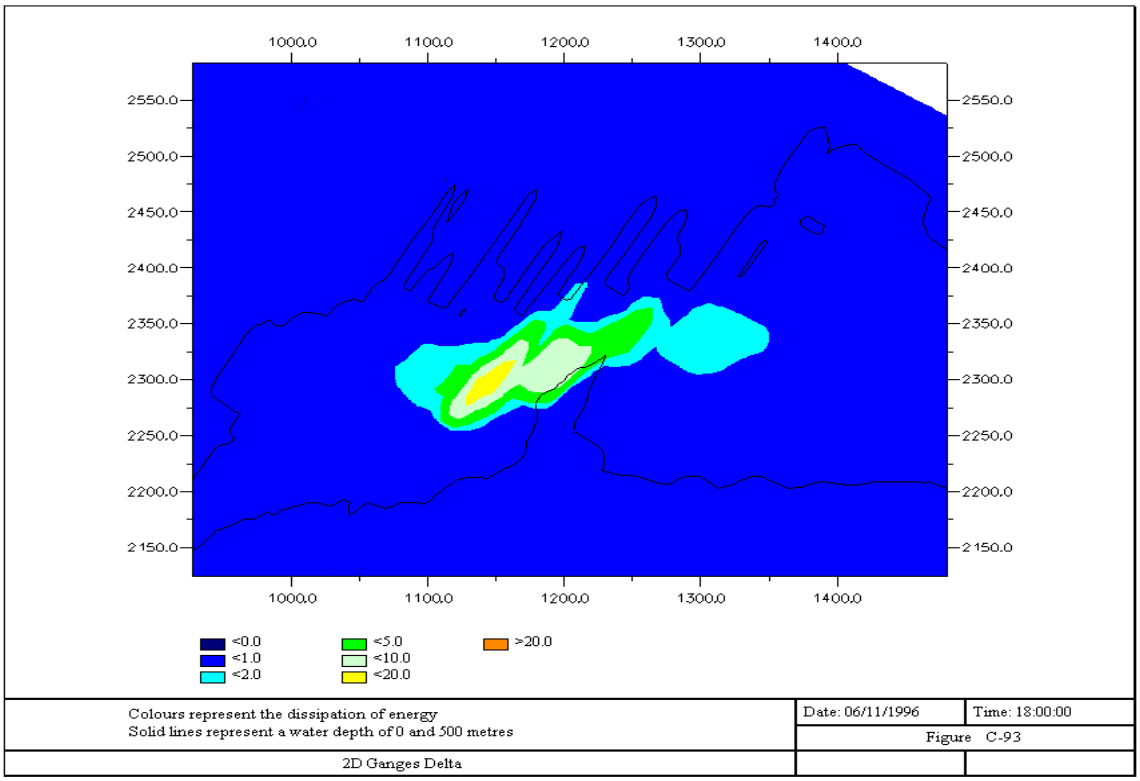

Colours represent the dissipation of energy Solid lines represent a water depth of 0 and 500 metres	Date: 06/11/1996	Time: 18:00:00
	Figure C-93	
2D Ganges Delta		

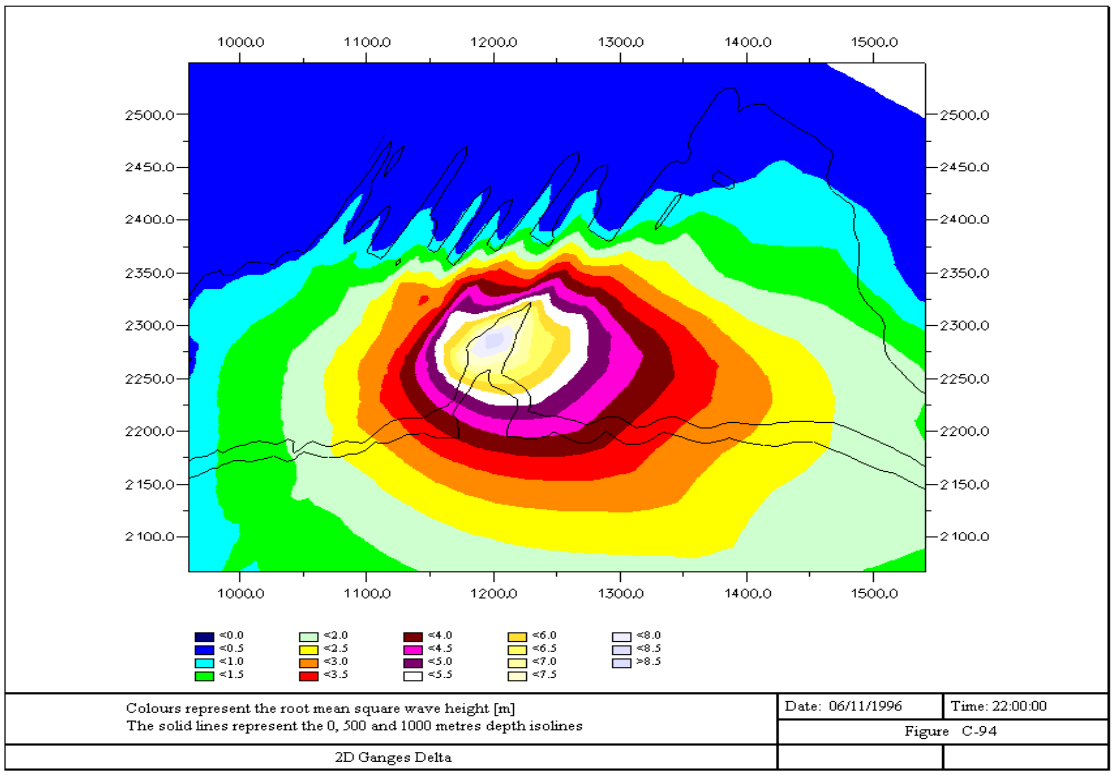

Colours represent the root mean square wave height [m] The solid lines represent the 0, 500 and 1000 metres depth isolines	Date: 06/11/1996	Time: 22:00:00
	Figure C-94	
2D Ganges Delta		

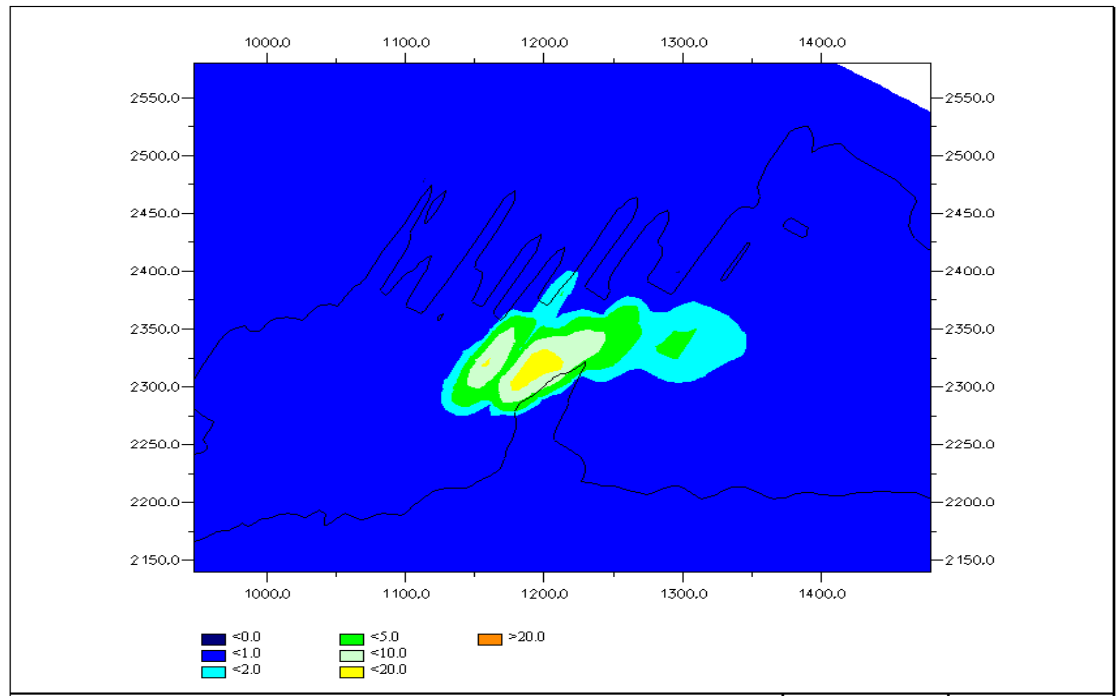

Colours represent the dissipation of energy Solid lines represent a water depth of 0 and 500 metres	Date: 06/11/1996	Time: 22:00:00
	Figure C-95	
2D Ganges Delta		

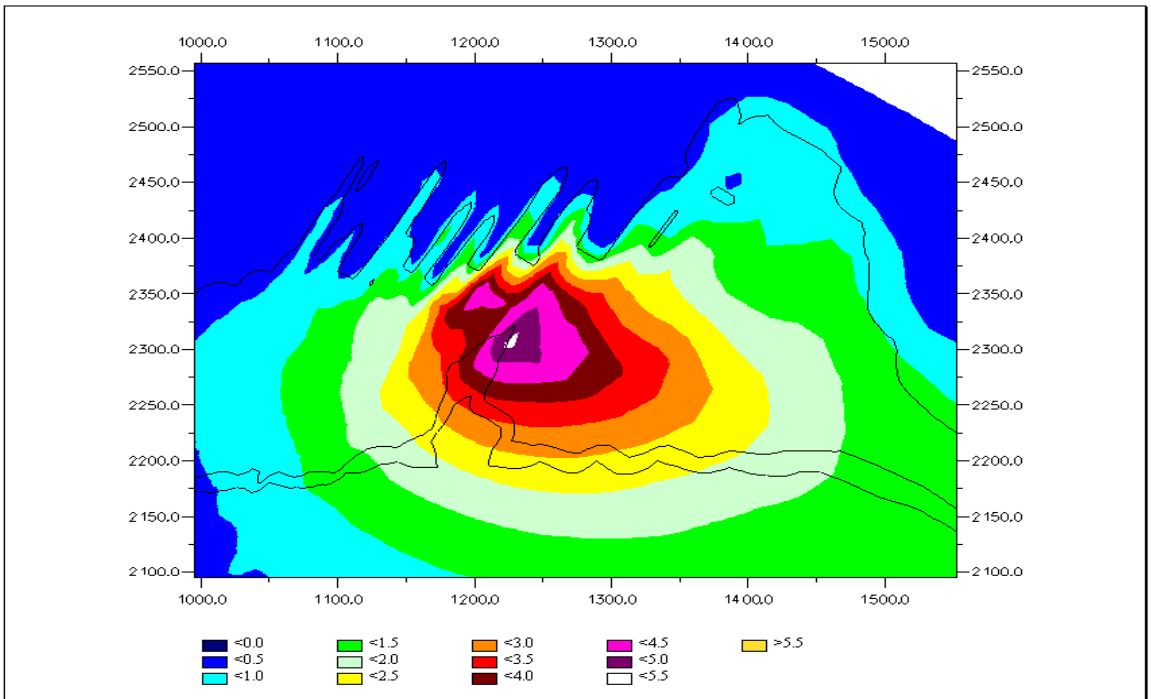

Colours represent the root mean square wave height [m]
The solid lines represent the 0, 500 and 1000 metres depth isolines

Date: 07/11/1996 Time: 02:00:00

Figure C-96

2D Ganges Delta

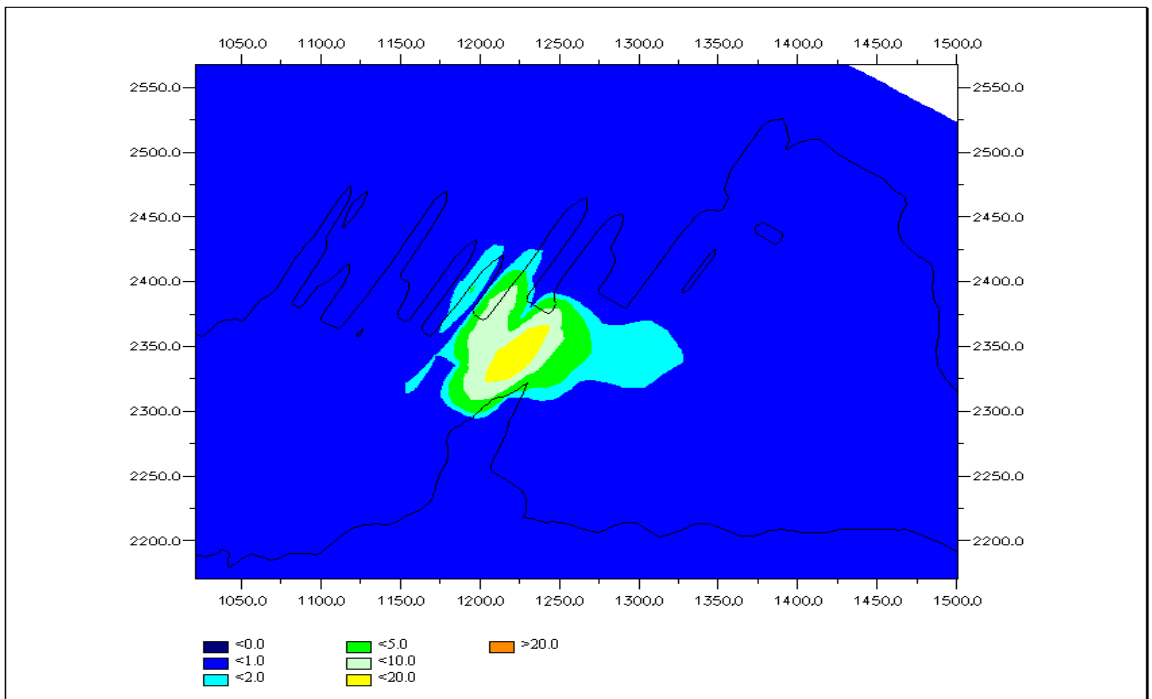

Colours represent the dissipation of energy
Solid lines represent a water depth of 0 and 500 metres

Date: 07/11/1996 Time: 02:00:00

Figure C-97

2D Ganges Delta

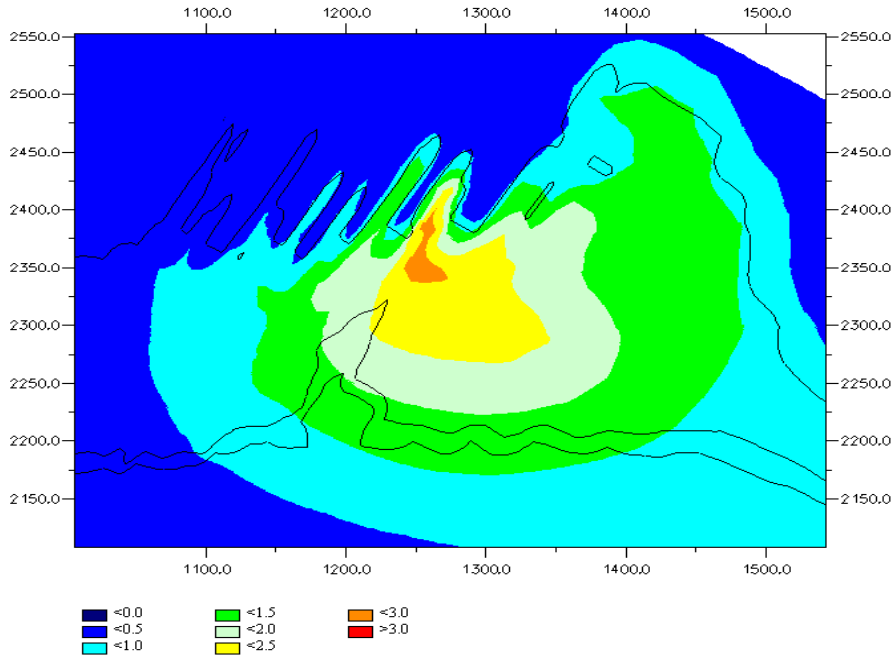

Colours represent the root mean square wave height [m] The solid lines represent the 0, 500 and 1000 metres depth isolines	Date: 07/11/1996	Time: 06:00:00
	Figure C-98	
2D Ganges Delta		

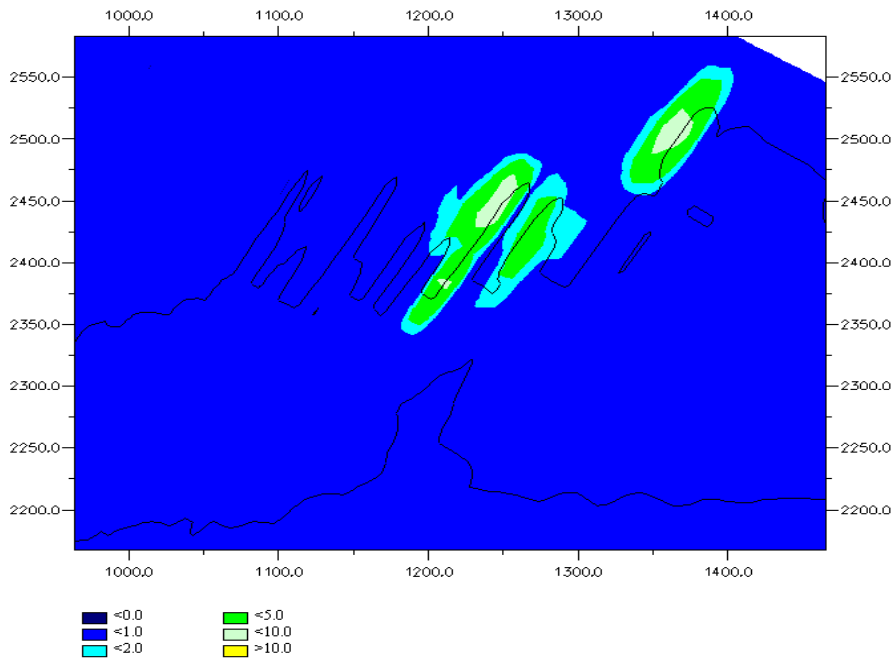

Colours represent the dissipation of energy Solid lines represent a water depth of 0 and 500 metres	Date: 07/11/1996	Time: 06:00:00
	Figure C-99	
2D Ganges Delta		

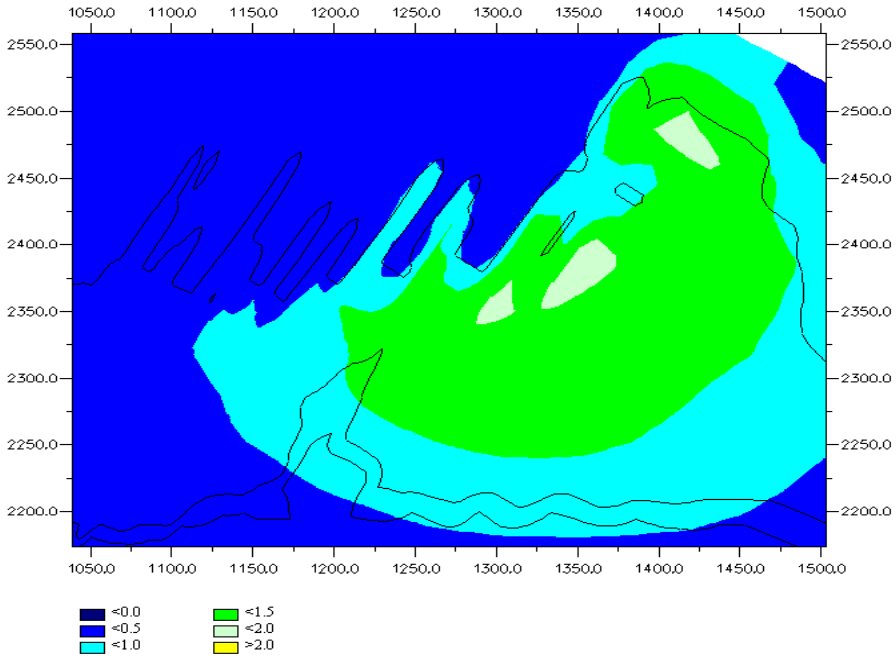

Colours represent the root mean square wave height [m] The solid lines represent the 0, 500 and 1000 metres depth isolines	Date: 07/11/1996	Time: 10:00:00
	Figure C-100	
2D Ganges Delta		

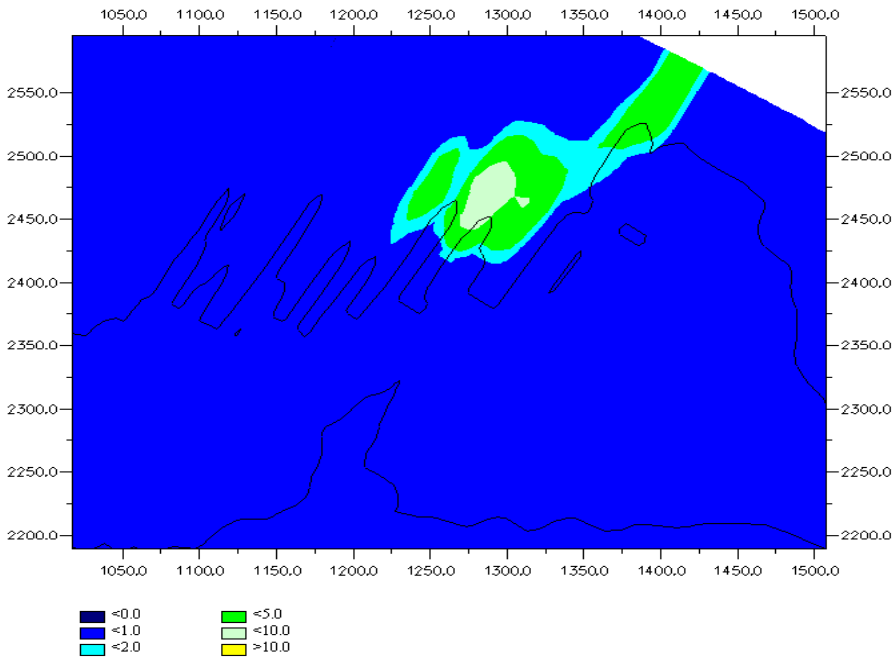

Colours represent the dissipation of energy Solid lines represent a water depth of 0 and 500 metres	Date: 07/11/1996	Time: 10:00:00
	Figure C-101	
2D Ganges Delta		

C.10 Water level set-up due to waves in 3D Ganges Delta case

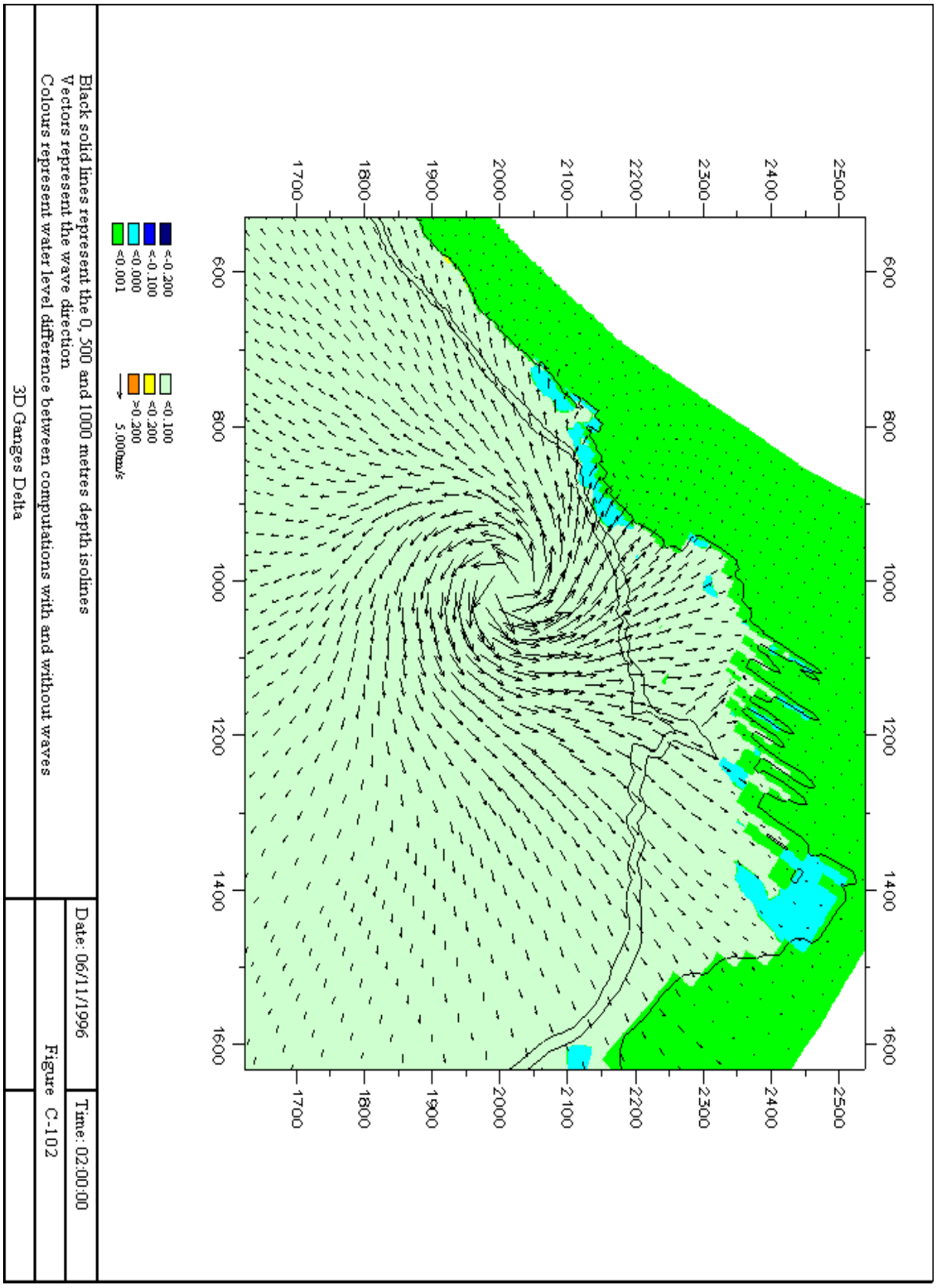

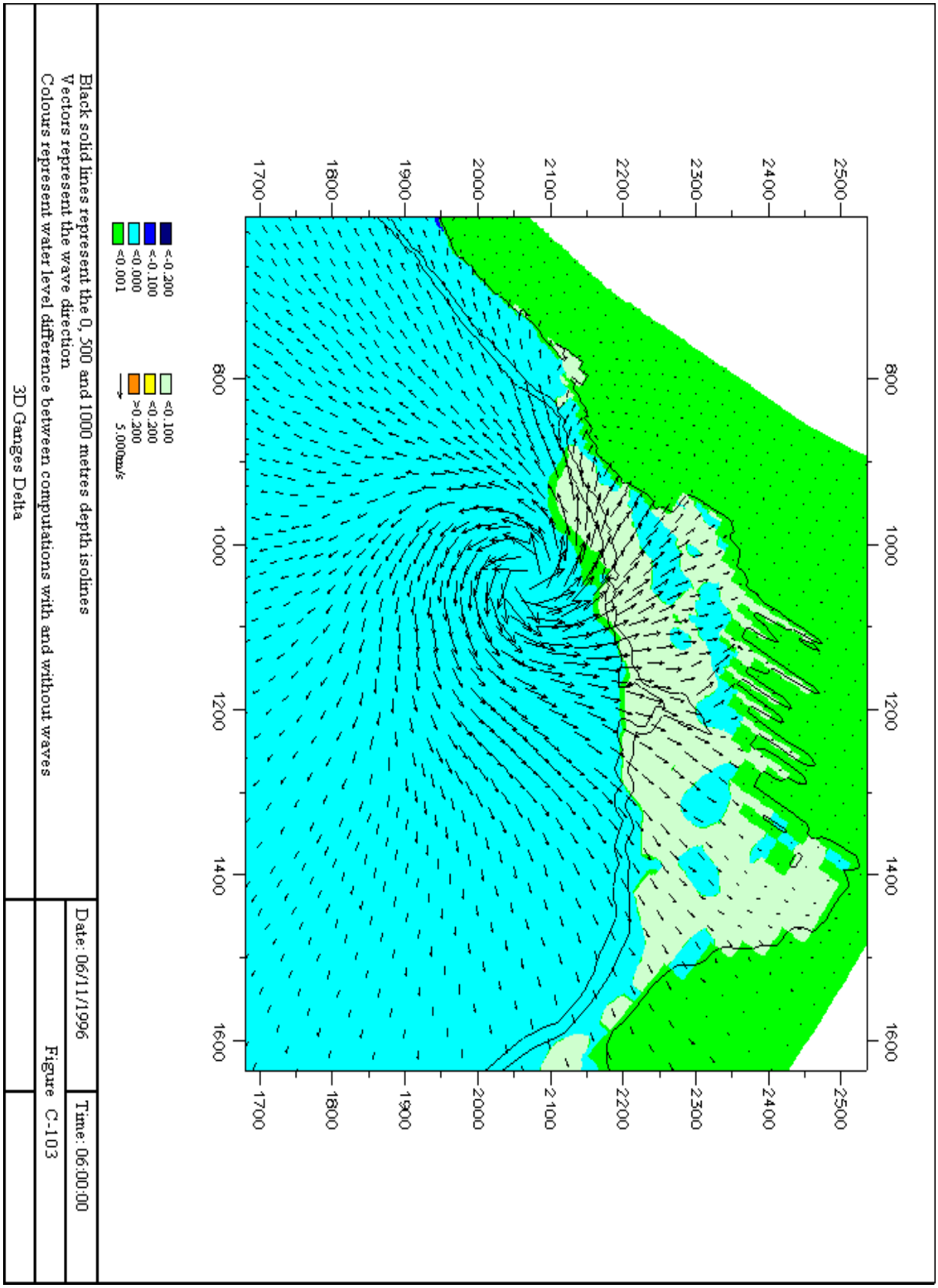
Black solid lines represent the 0, 500 and 1000 metres depth isolines
Vectors represent the wave direction
Colours represent water level difference between computations with and without waves
3D Ganges Delta
Date: 06/11/1996
Time: 06:00:00
Figure C-103
<-0.200
<-0.100
<0.000
<0.001
<0.100
<0.200
>0.200
5.000m/s
2500
2400
2300
2200
2100
2000
1900
1800
1700
800
1000
1200
1400
1600

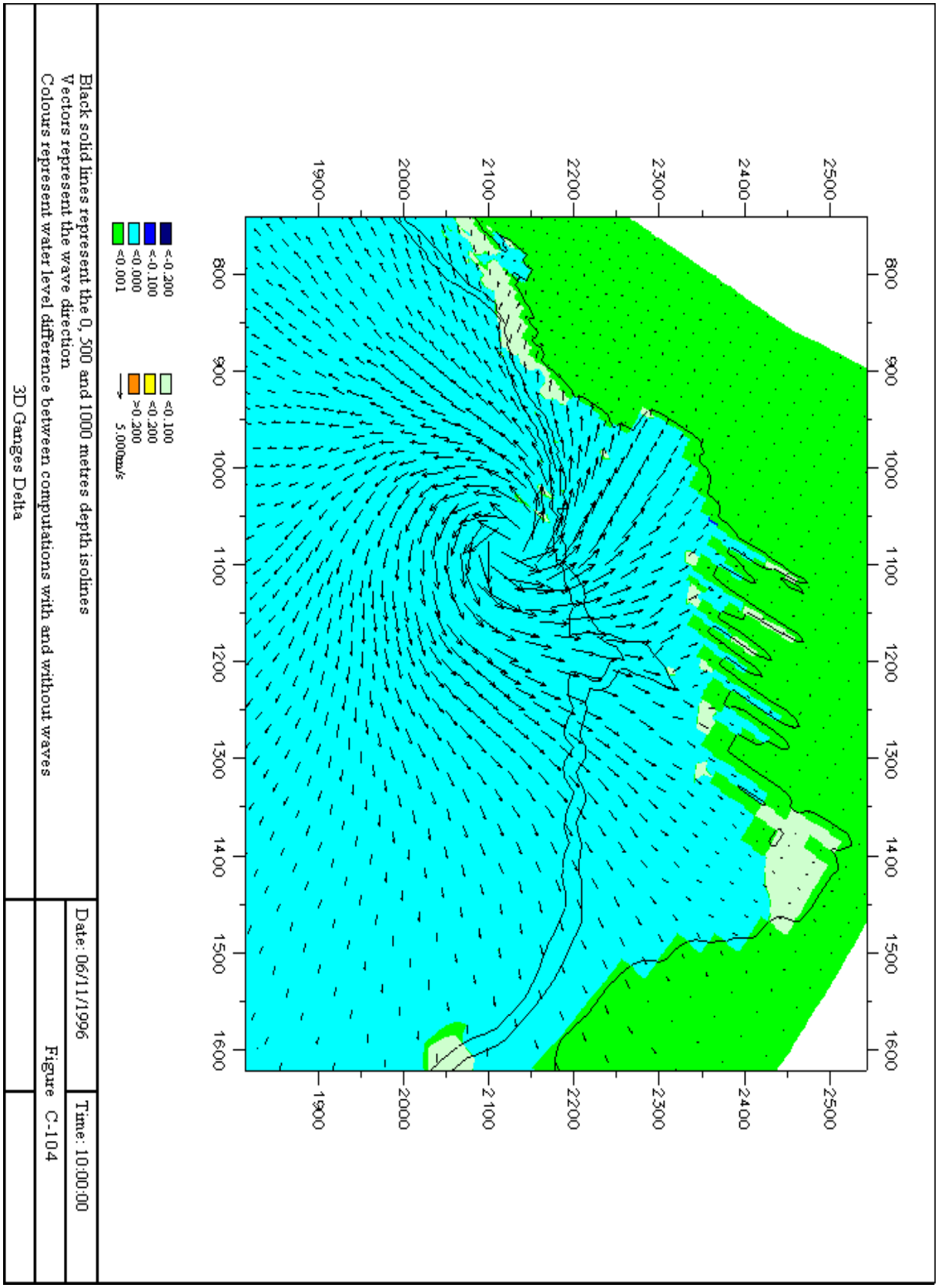
Black solid lines represent the 0, 500 and 1000 metres depth isolines
Vectors represent the wave direction
Colours represent water level difference between computations with and without waves
3D Ganges Delta
Date: 06/11/1996
Time: 10:00:00
Figure C-104
<-0.200
<-0.100
<0.000
<0.001
<0.100
<0.200
>0.200
5.000m/s

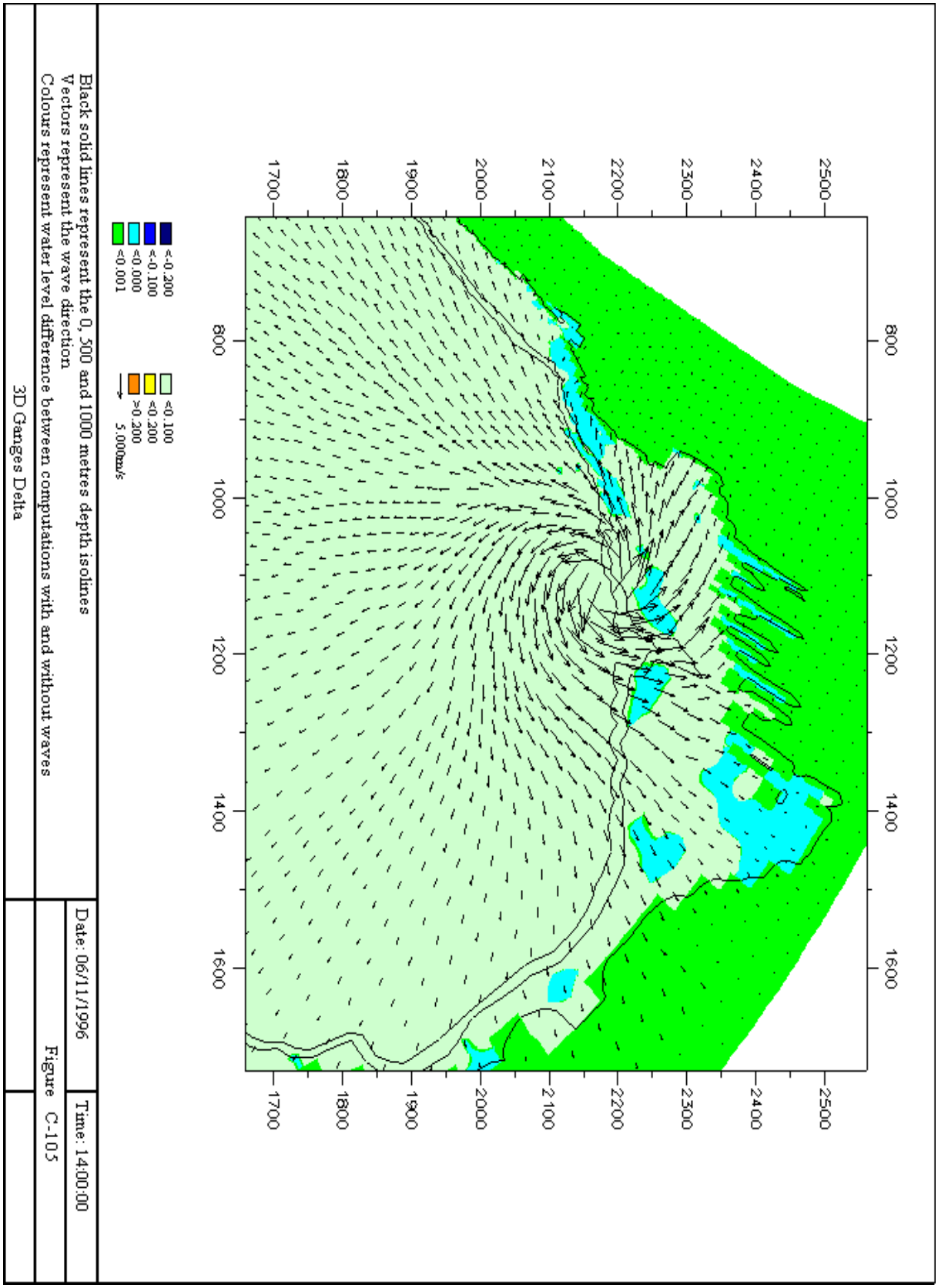
Black solid lines represent the 0, 500 and 1000 metres depth isolines
Vectors represent the wave direction
Colours represent water level difference between computations with and without waves
3D Ganges Delta
Date: 06/11/1996
Time: 14:00:00
Figure C-105
<-0.200
<-0.100
<0.000
<0.001
<0.100
<0.200
>0.200
5.000m/s
800
1000
1200
1400
1600
1700
1800
1900
2000
2100
2200
2300
2400
2500

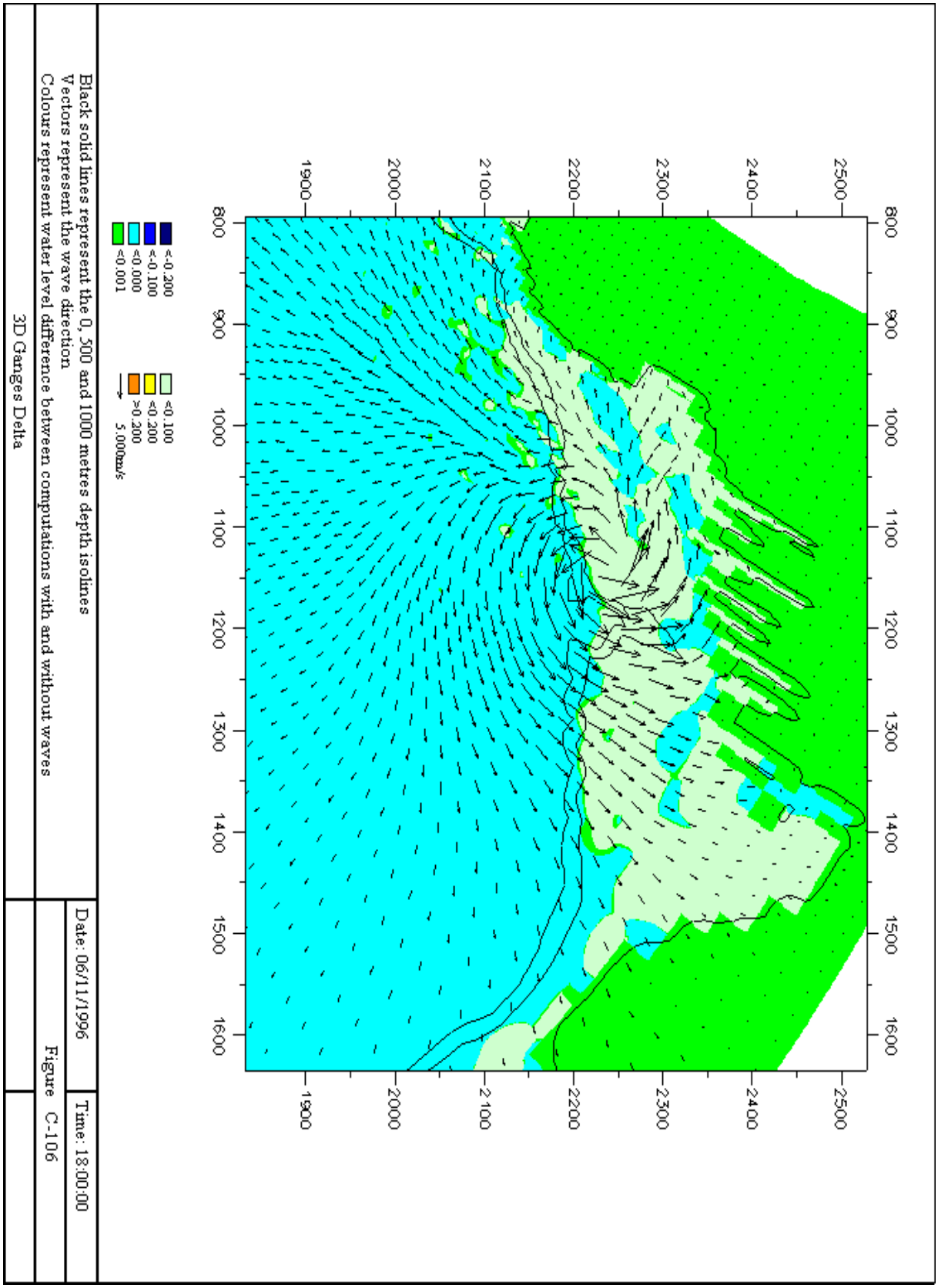
Black solid lines represent the 0, 500 and 1000 metres depth isolines
Vectors represent the wave direction
Colours represent water level difference between computations with and without waves
3D Ganges Delta
Date: 06/11/1996
Time: 18:00:00
Figure C-106
<-0.200
<-0.100
<0.000
<0.001
<0.100
<0.200
>0.200
5.000m/s

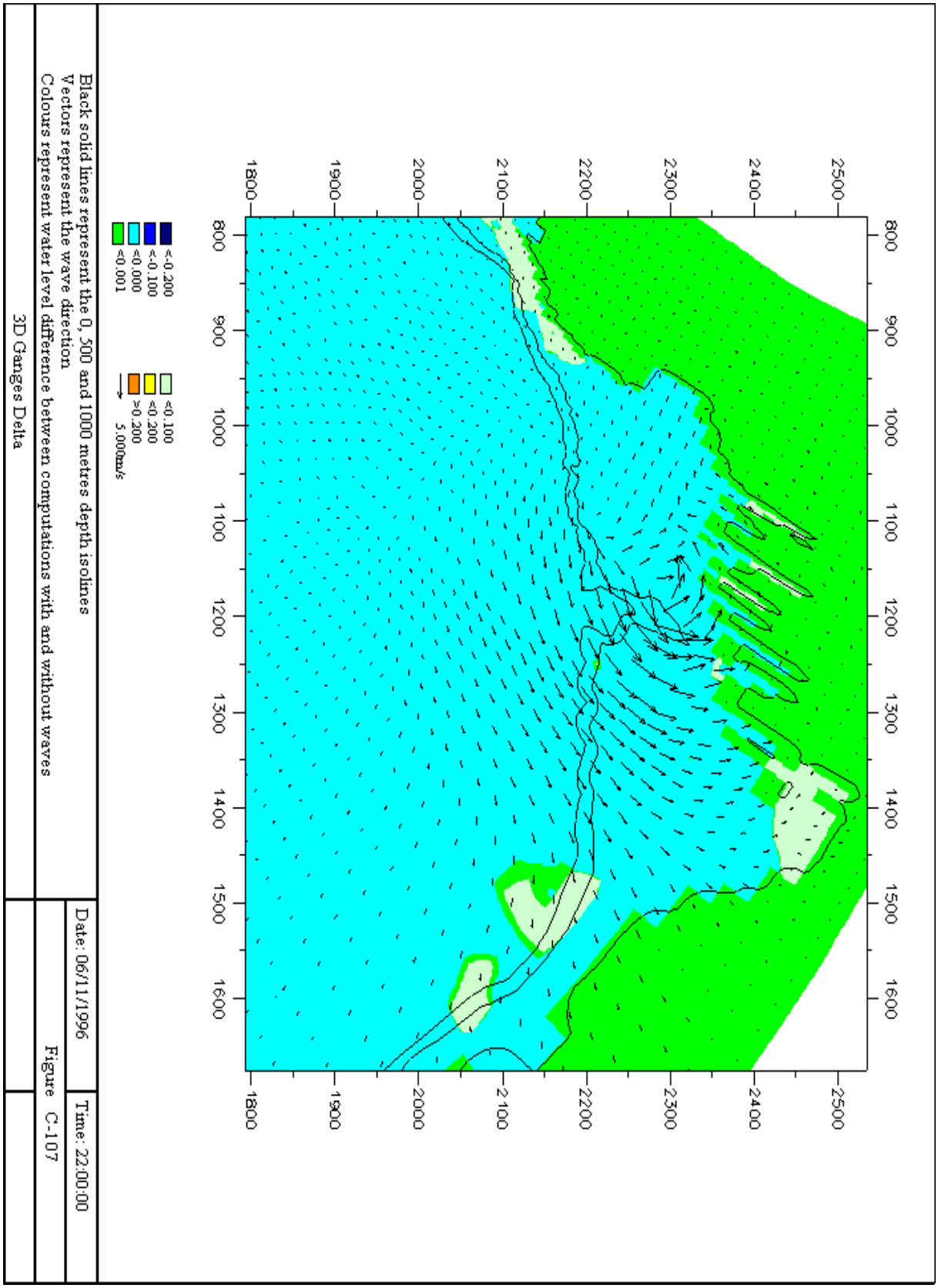
Black solid lines represent the 0, 500 and 1000 metres depth isolines
Vectors represent the wave direction
Colours represent water level difference between computations with and without waves
3D Ganges Delta
Date: 06/11/1996
Time: 22:00:00
Figure C-107
<-0.200
<-0.100
<0.000
<0.001
<0.100
<0.200
>0.200
5.000m/s

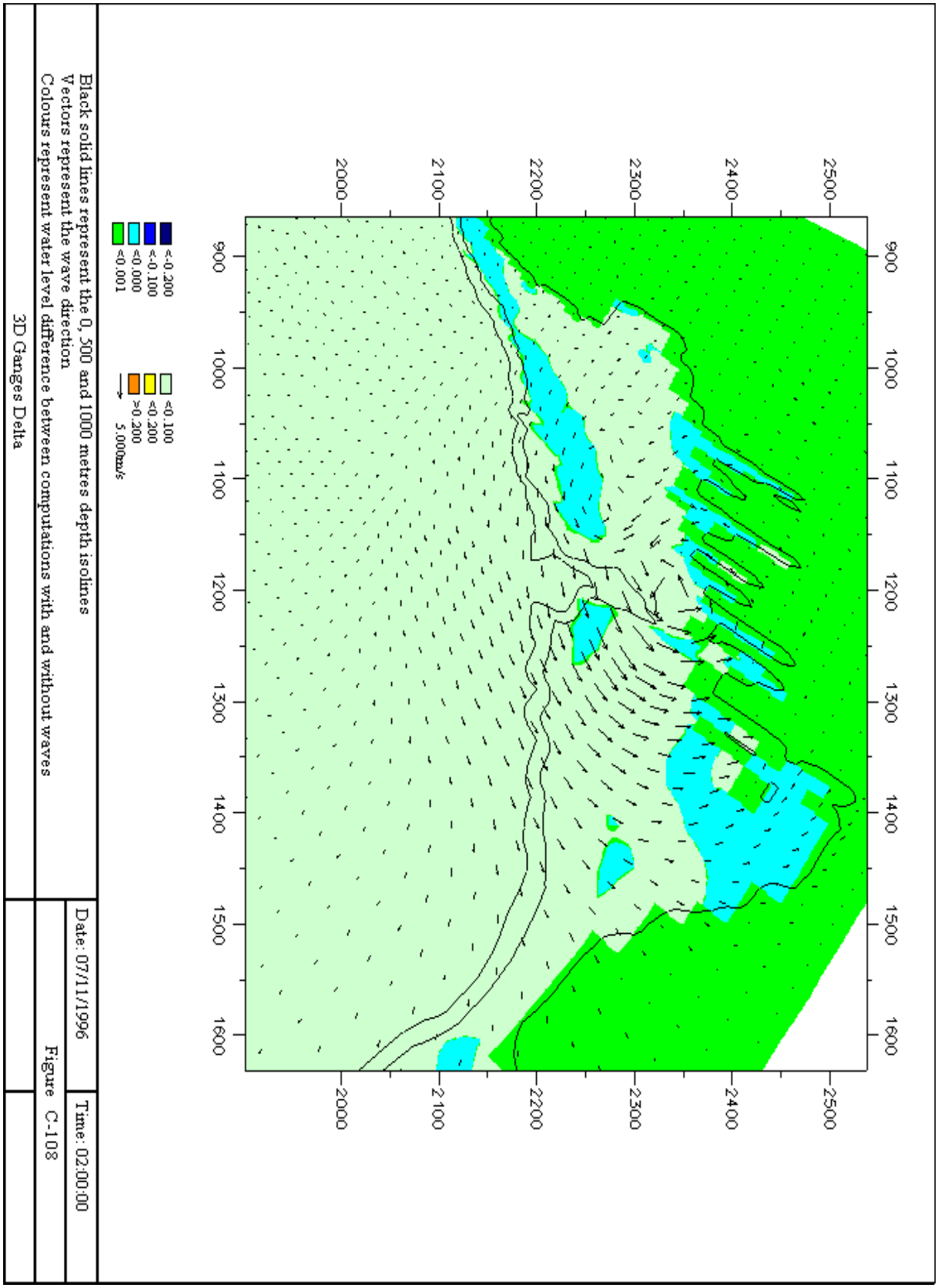
Black solid lines represent the 0, 500 and 1000 metres depth isolines
Vectors represent the wave direction
Colours represent water level difference between computations with and without waves
3D Ganges Delta
Date: 07/11/1996
Time: 02:00:00
Figure C-108
<-0.200
<-0.100
<0.000
<0.001
<0.100
<0.200
>0.200
5.000m/s
2500
2400
2300
2200
2100
2000
900
1000
1100
1200
1300
1400
1500
1600

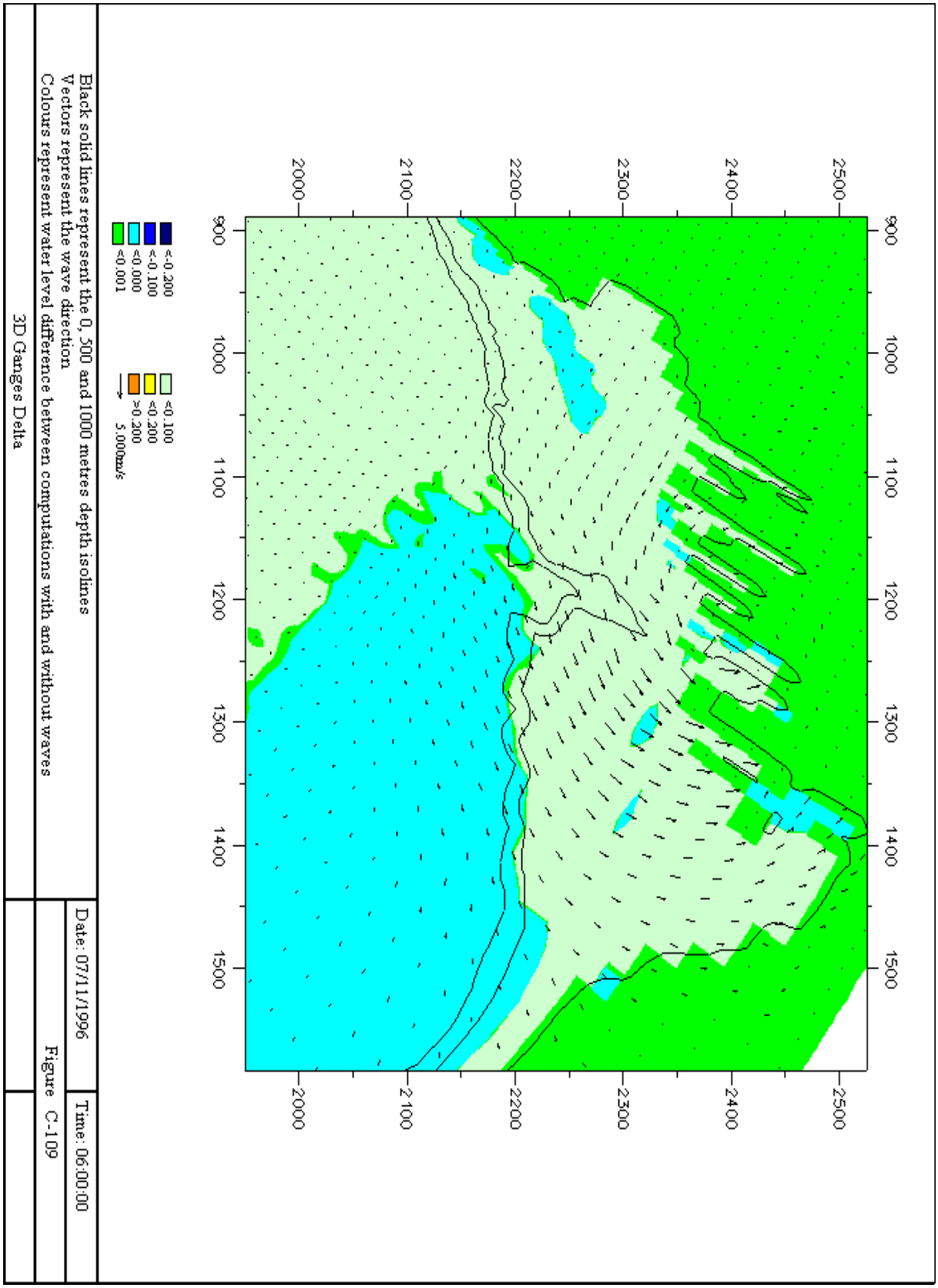
900
1000
1100
1200
1300
1400
1500
2000
2100
2200
2300
2400
2500
<-0.200
<-0.100
<0.000
<0.001
<0.100
<0.200
>0.200
5.000m/s
Black solid lines represent the 0, 500 and 1000 metres depth isolines
Vectors represent the wave direction
Colours represent water level difference between computations with and without waves
3D Ganges Delta
Date: 07/11/1996
Time: 06:00:00
Figure C-109

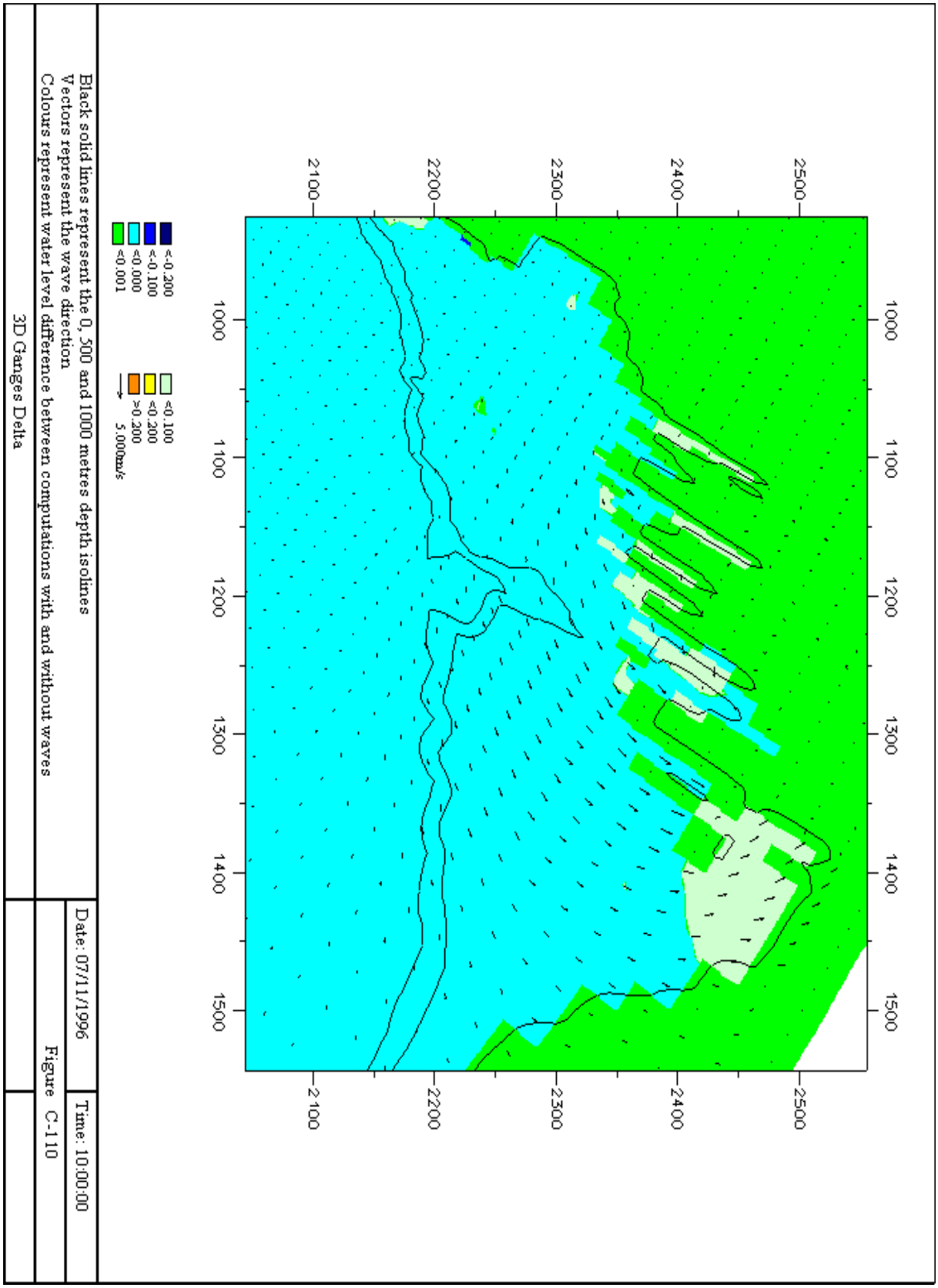
1000
1100
1200
1300
1400
1500
2100
2200
2300
2400
2500
<-0.200
<-0.100
<0.000
<0.001
<0.100
<0.200
>0.200
5.000m/s
Black solid lines represent the 0, 500 and 1000 metres depth isolines
Vectors represent the wave direction
Colours represent water level difference between computations with and without waves
3D Ganges Delta
Date: 07/11/1996
Time: 10:00:00
Figure C-110

C.11 Wave height and Dissipation for 3D Ganges Delta case

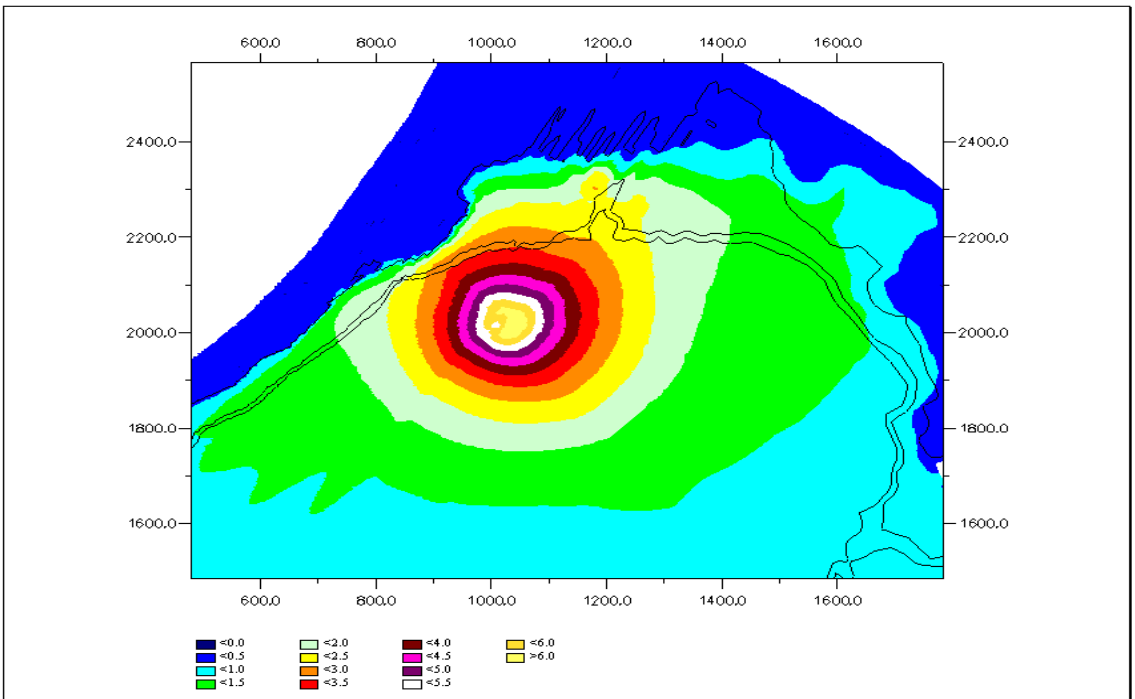

Colours represent the root mean square wave height [m] The solid lines represent the 0, 500 and 1000 metres depth isolines	Date: 06/11/1996	Time: 02:00:00
	Figure C-111	
3D Ganges Delta		

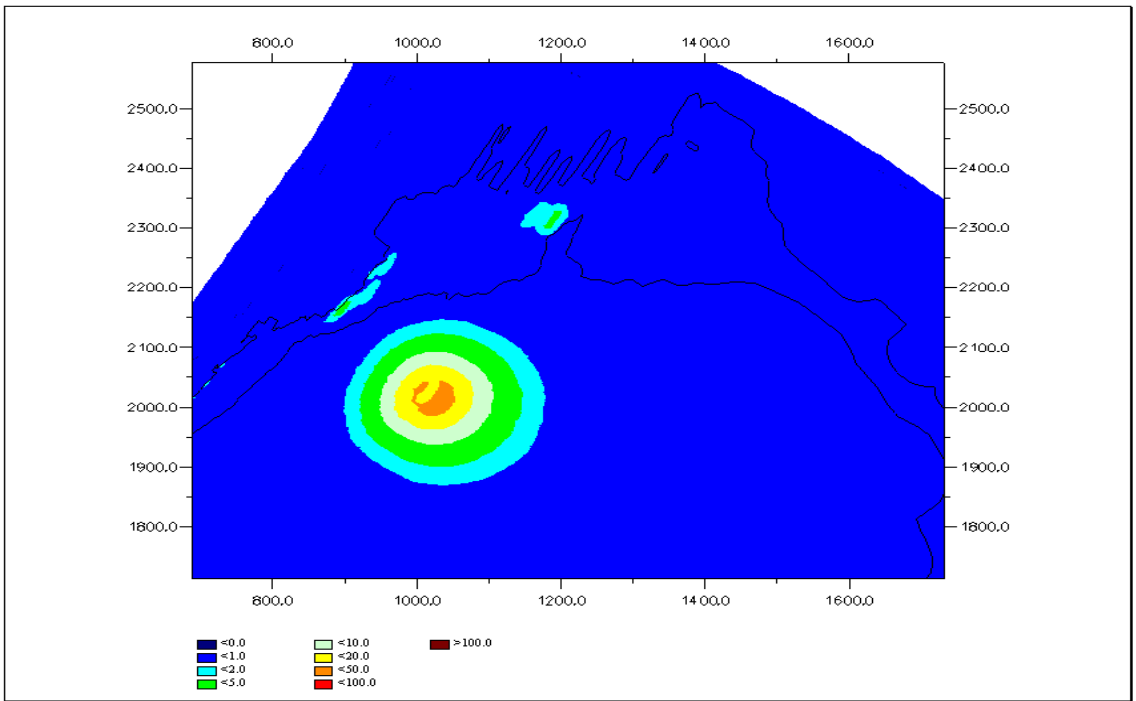

Colours represent the dissipation of energy Solid lines represent a water depth of 0 and 500 metres	Date: 06/11/1996	Time: 02:00:00
	Figure C-112	
3D Ganges Delta		

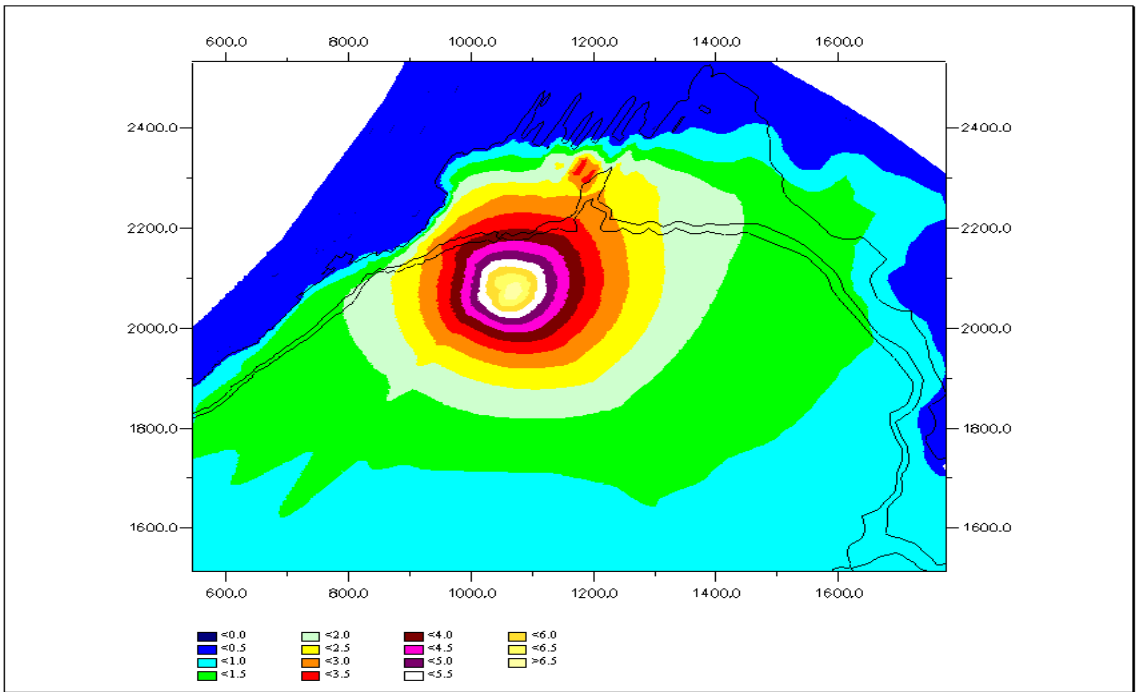

Colours represent the root mean square wave height [m] The solid lines represent the 0, 500 and 1000 metres depth isolines	Date: 06/11/1996	Time: 06:00:00
	Figure C-113	
3D Ganges Delta		

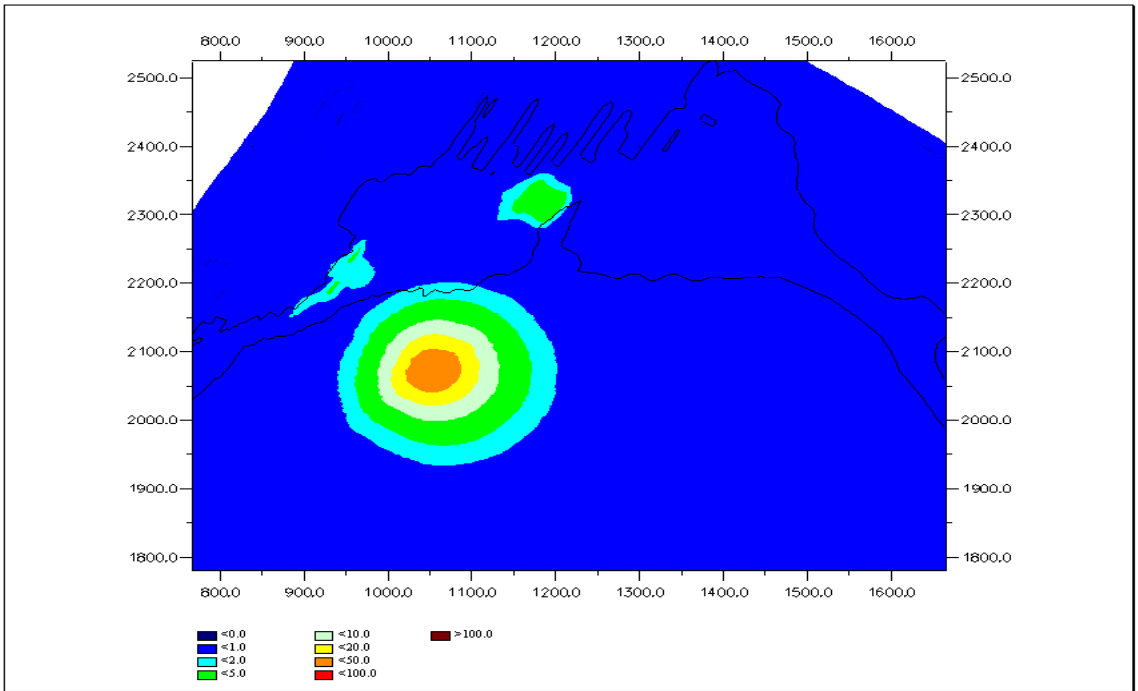

Colours represent the dissipation of energy Solid lines represent a water depth of 0 and 500 metres	Date: 06/11/1996	Time: 06:00:00
	Figure C-114	
3D Ganges Delta		

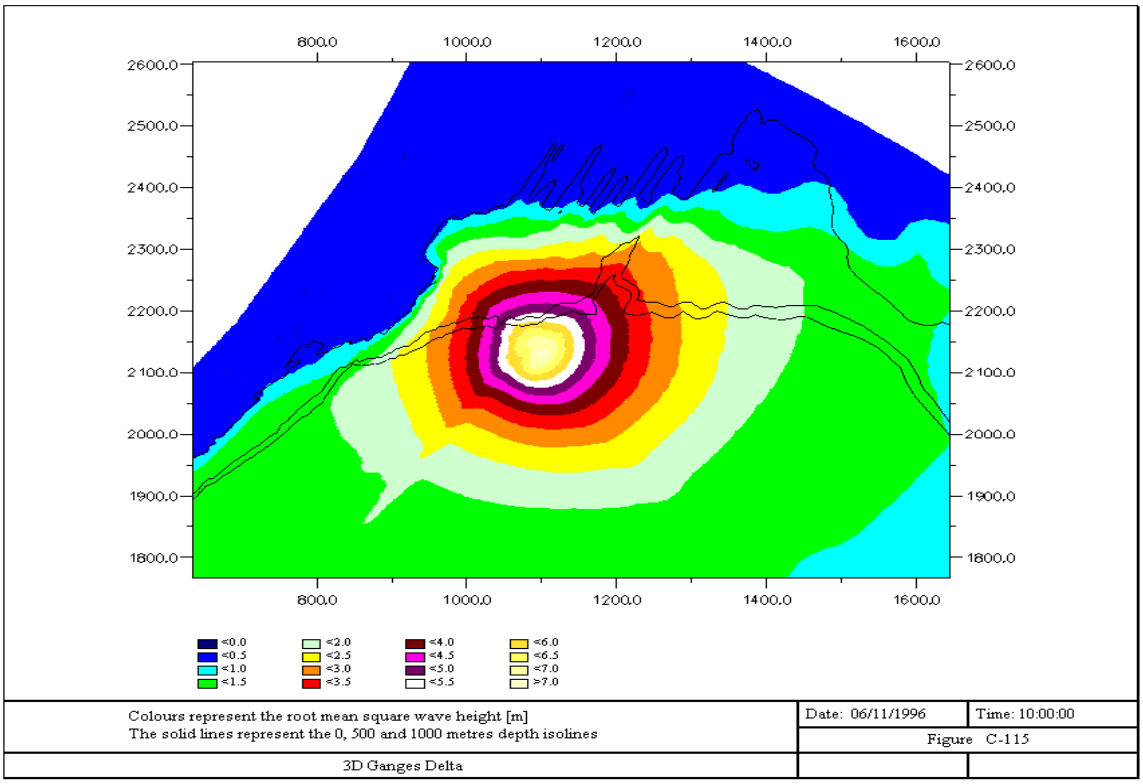

Colours represent the root mean square wave height [m] The solid lines represent the 0, 500 and 1000 metres depth isolines	Date: 06/11/1996	Time: 10:00:00
	Figure C-115	
3D Ganges Delta		

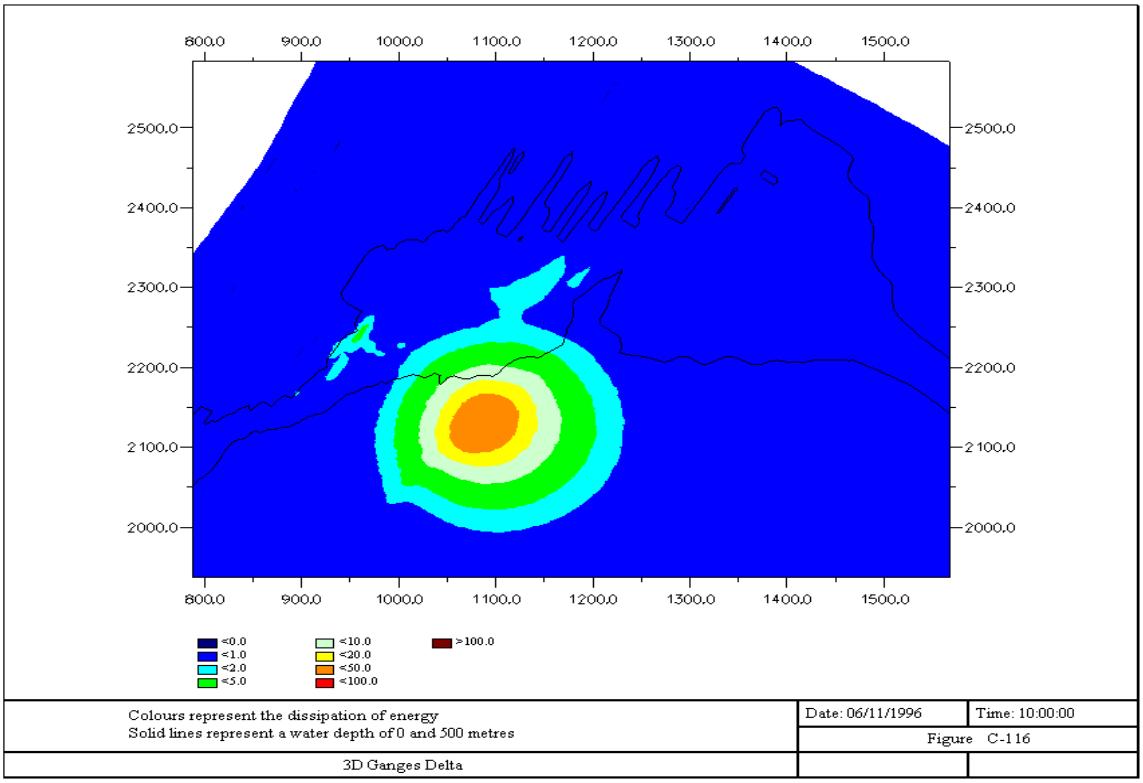

Colours represent the dissipation of energy Solid lines represent a water depth of 0 and 500 metres	Date: 06/11/1996	Time: 10:00:00
	Figure C-116	
3D Ganges Delta		

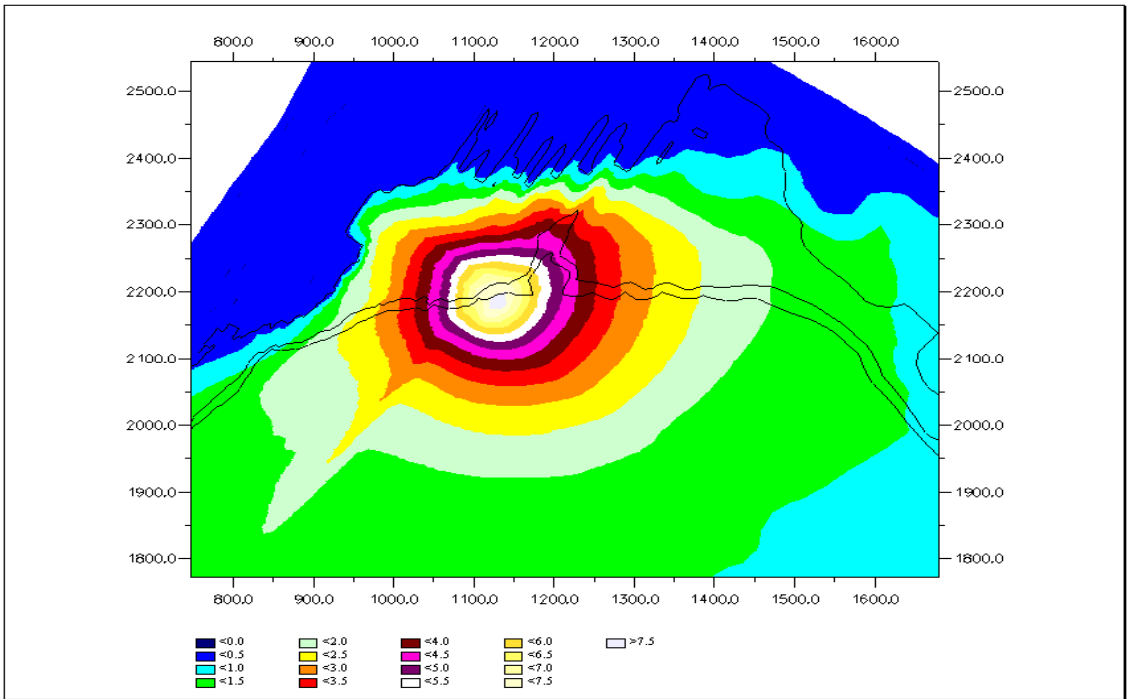

Colours represent the root mean square wave height [m] The solid lines represent the 0, 500 and 1000 metres depth isolines	Date: 06/11/1996	Time: 14:00:00
	Figure C-117	
3D Ganges Delta		

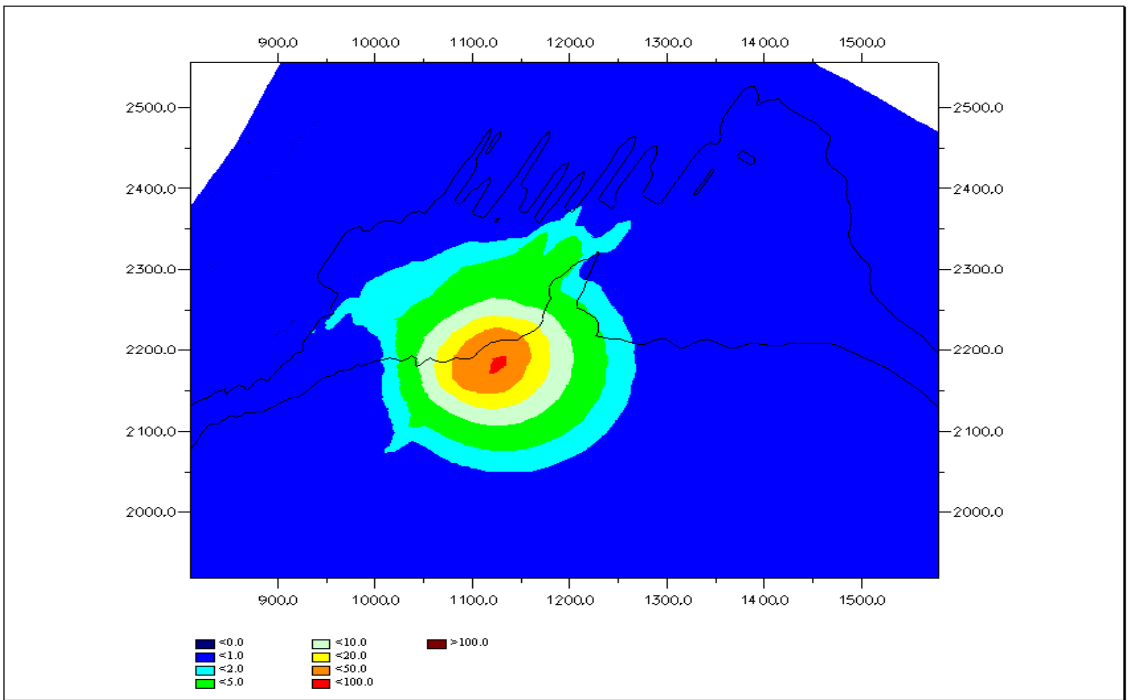

Colours represent the dissipation of energy Solid lines represent a water depth of 0 and 500 metres	Date: 06/11/1996	Time: 14:00:00
	Figure C-118	
3D Ganges Delta		

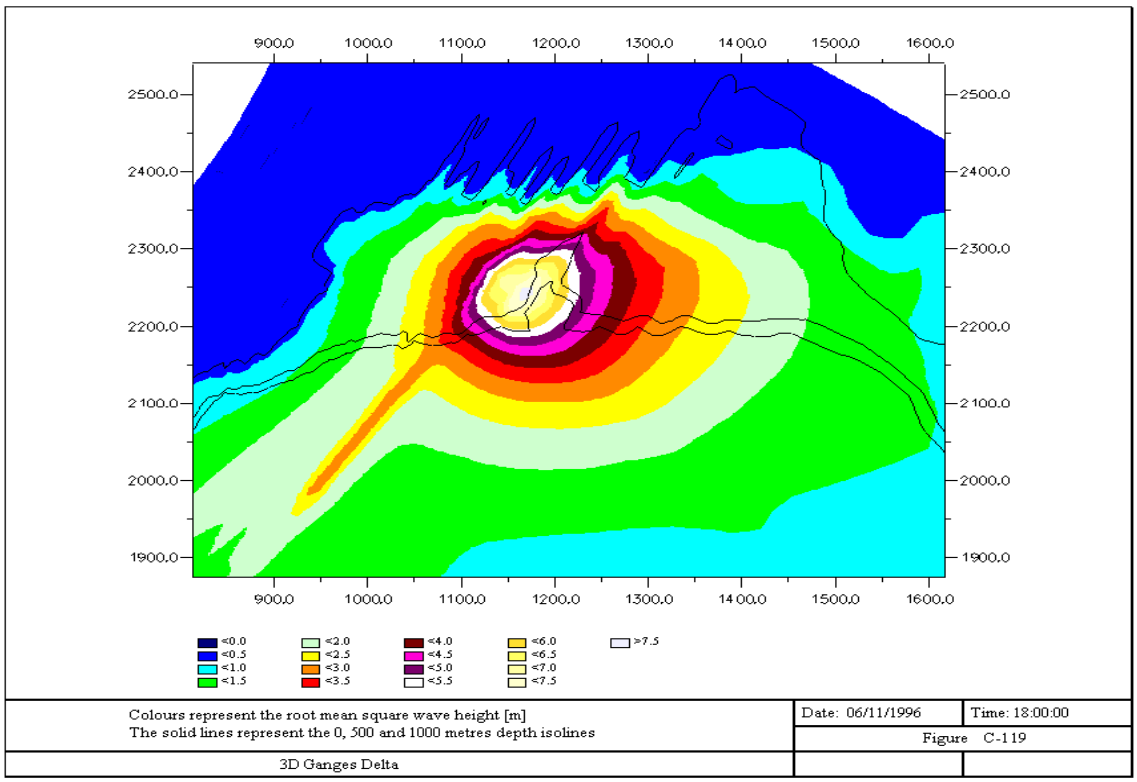

Colours represent the root mean square wave height [m] The solid lines represent the 0, 500 and 1000 metres depth isolines	Date: 06/11/1996	Time: 18:00:00
	Figure C-119	
3D Ganges Delta		

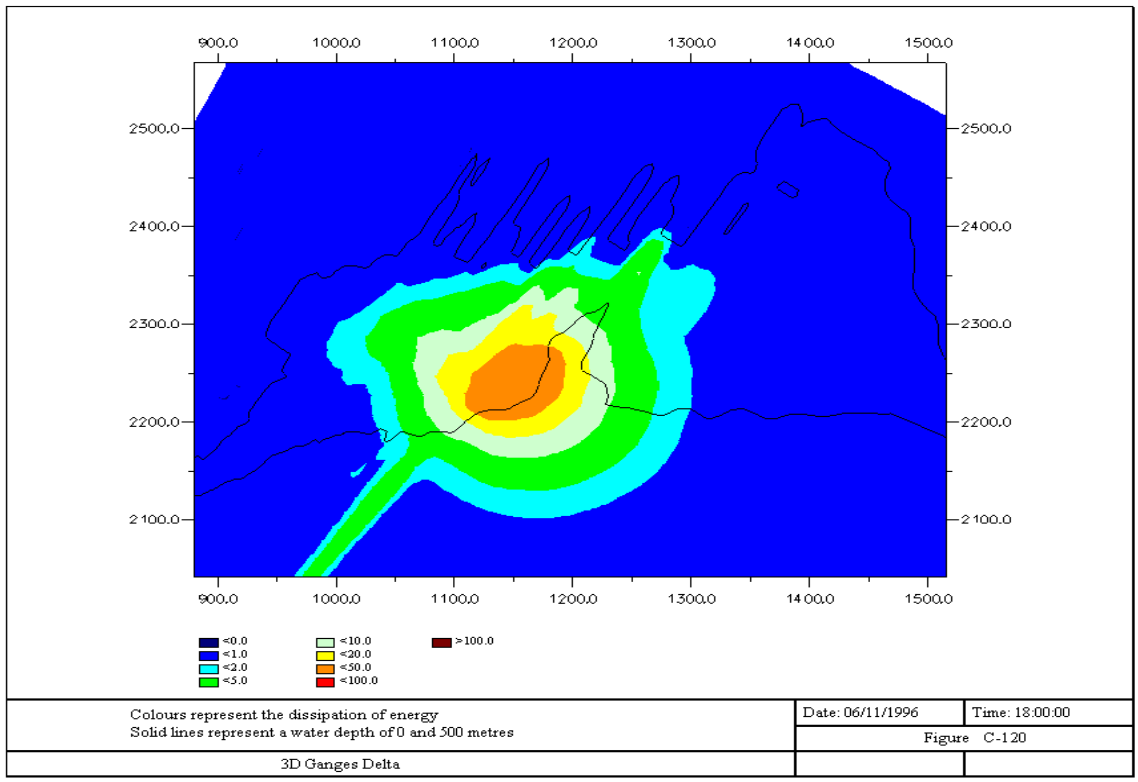

Colours represent the dissipation of energy Solid lines represent a water depth of 0 and 500 metres	Date: 06/11/1996	Time: 18:00:00
	Figure C-120	
3D Ganges Delta		

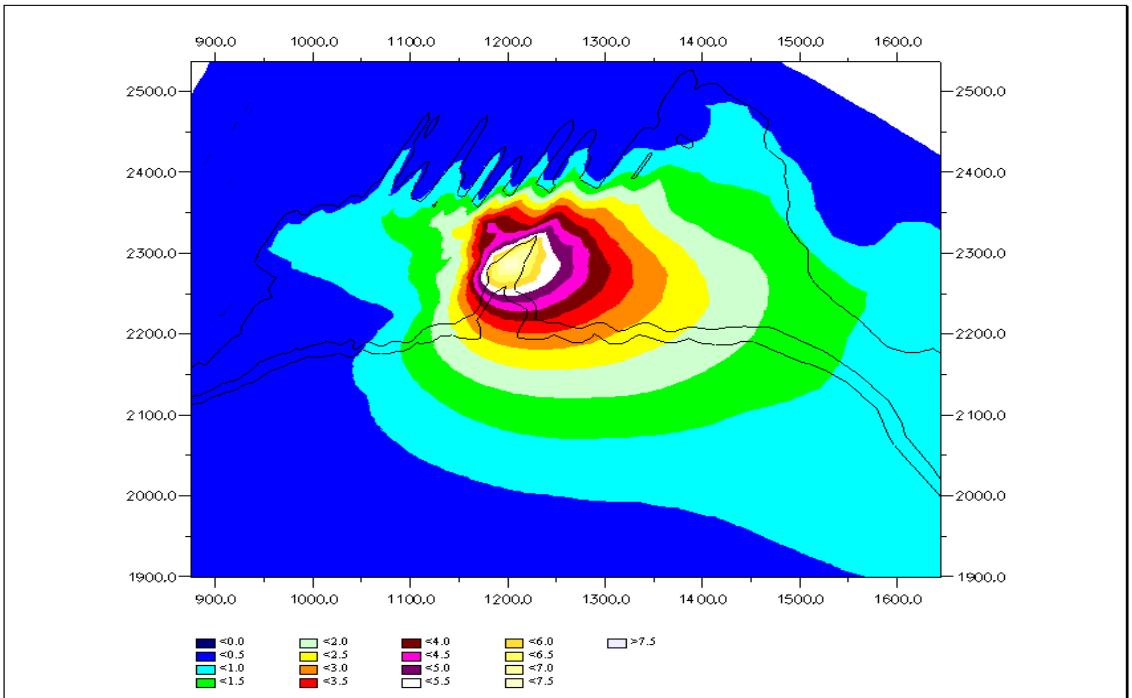

Colours represent the root mean square wave height [m] The solid lines represent the 0, 500 and 1000 metres depth isolines	Date: 06/11/1996	Time: 22:00:00
	Figure C-121	
3D Ganges Delta		

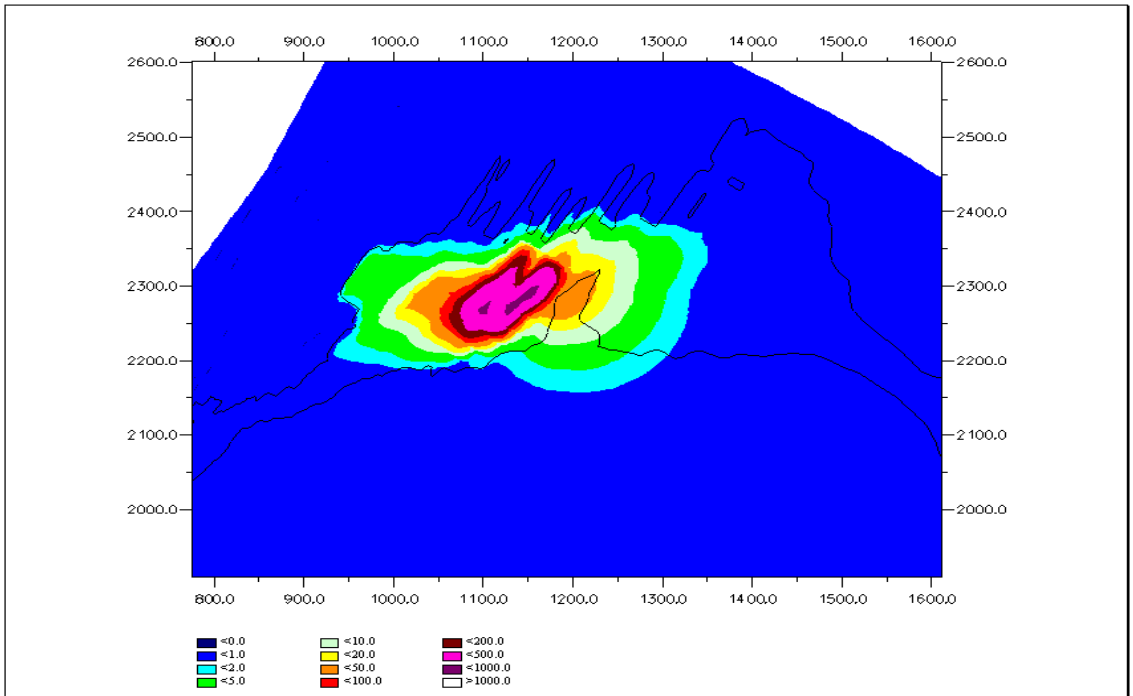

Colours represent the dissipation of energy Solid lines represent a water depth of 0 and 500 metres	Date: 06/11/1996	Time: 22:00:00
	Figure C-122	
3D Ganges Delta		

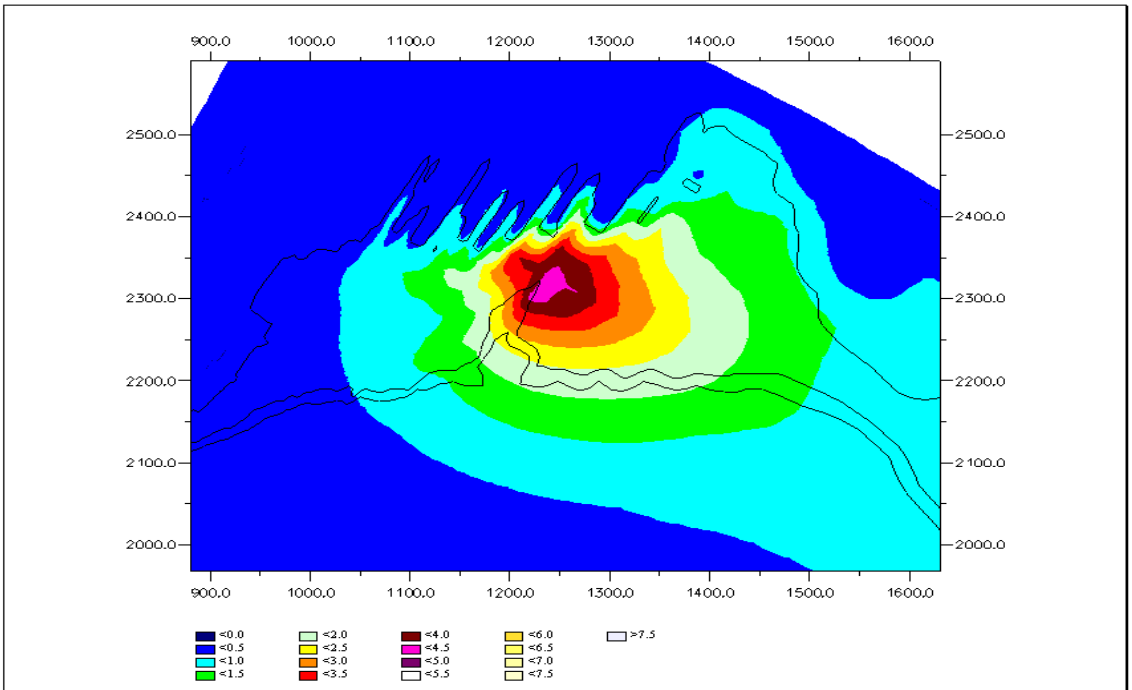

Colours represent the root mean square wave height [m] The solid lines represent the 0, 500 and 1000 metres depth isolines	Date: 07/11/1996	Time: 02:00:00
	Figure C-123	
3D Ganges Delta		

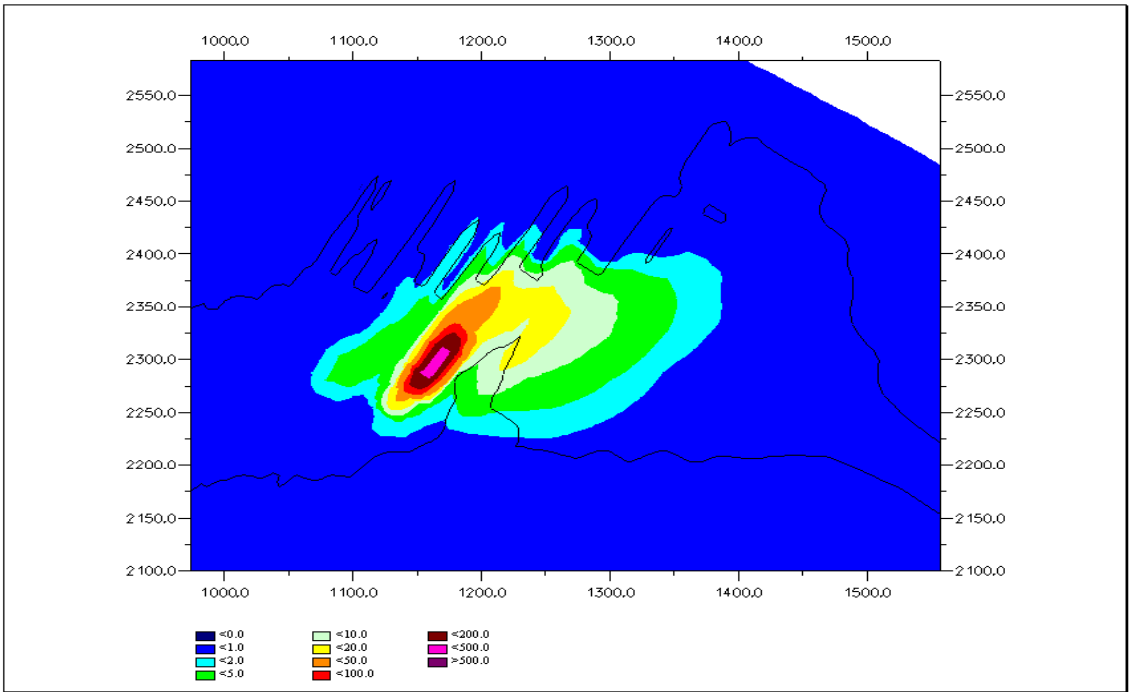

Colours represent the dissipation of energy Solid lines represent a water depth of 0 and 500 metres	Date: 07/11/1996	Time: 02:00:00
	Figure C-124	
3D Ganges Delta		

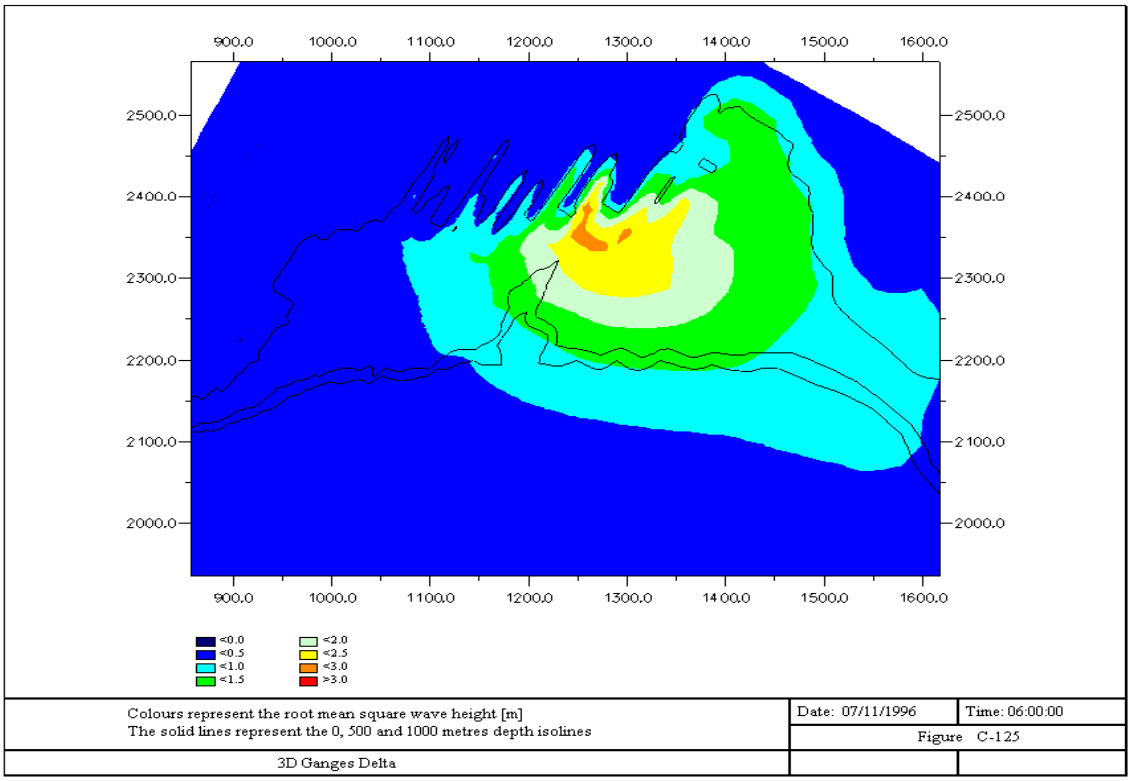

Colours represent the root mean square wave height [m] The solid lines represent the 0, 500 and 1000 metres depth isolines	Date: 07/11/1996	Time: 06:00:00
	Figure C-125	
3D Ganges Delta		

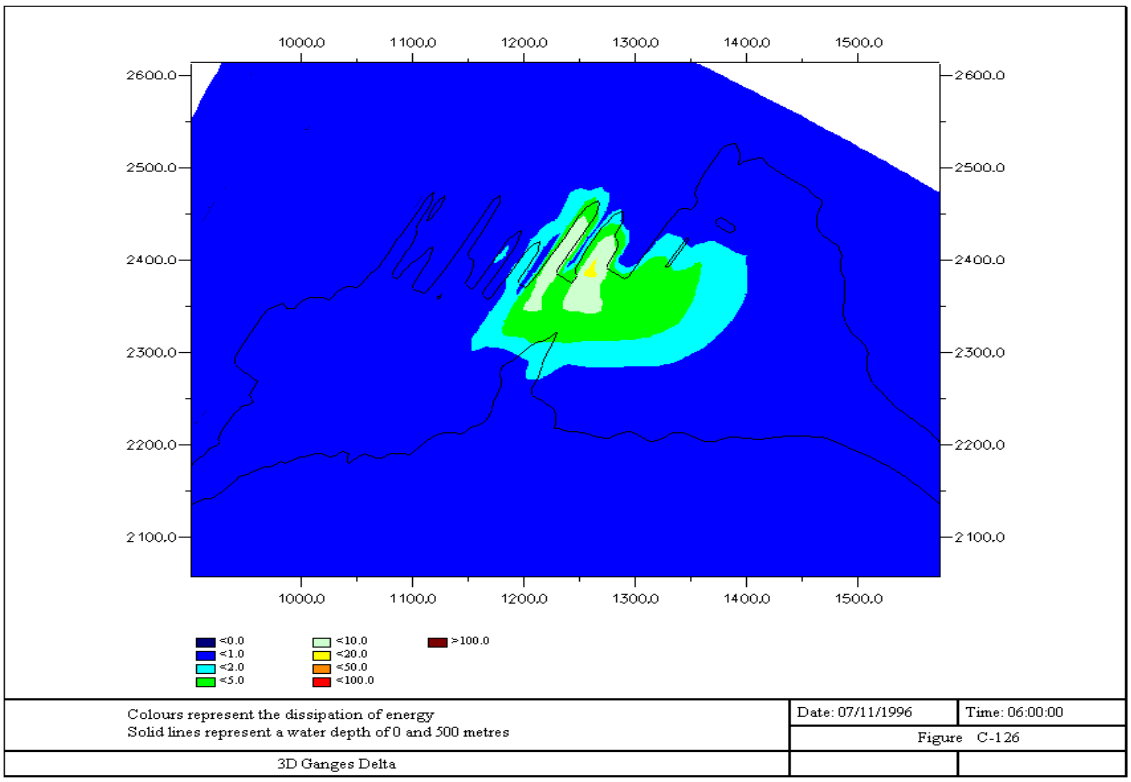

Colours represent the dissipation of energy Solid lines represent a water depth of 0 and 500 metres	Date: 07/11/1996	Time: 06:00:00
	Figure C-126	
3D Ganges Delta		

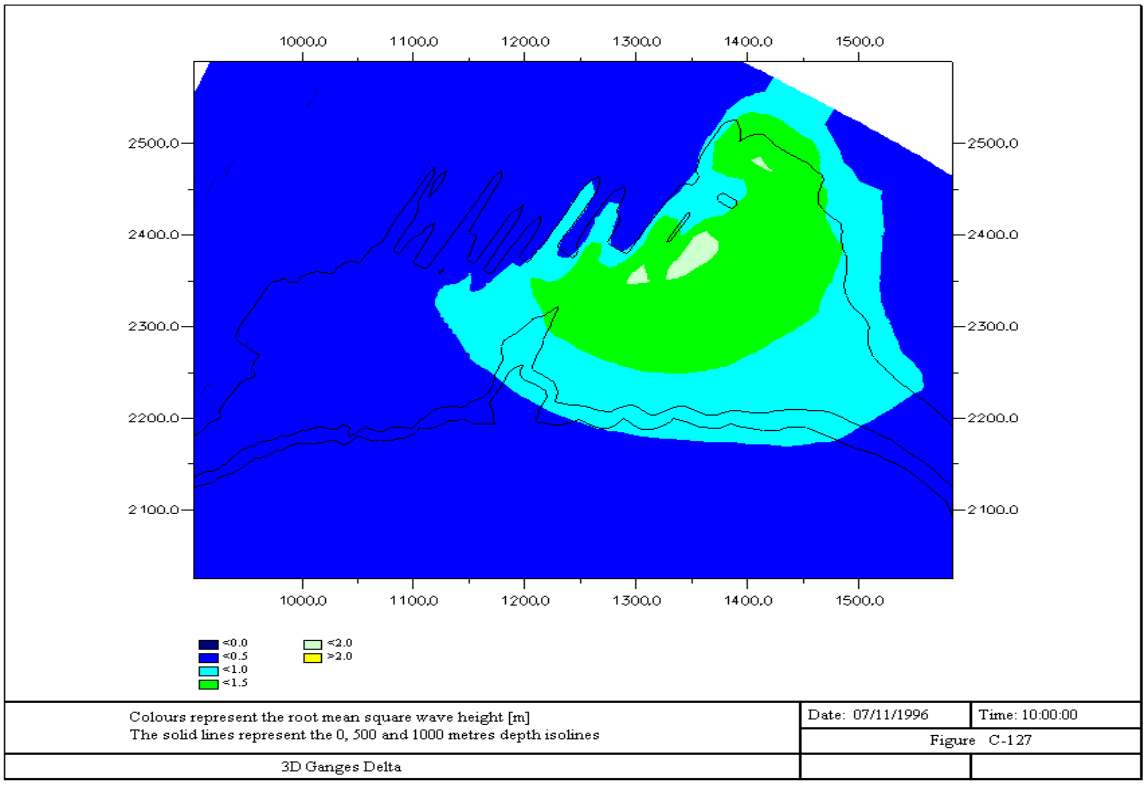

Colours represent the root mean square wave height [m] The solid lines represent the 0, 500 and 1000 metres depth isolines	Date: 07/11/1996	Time: 10:00:00
	Figure C-127	
3D Ganges Delta		

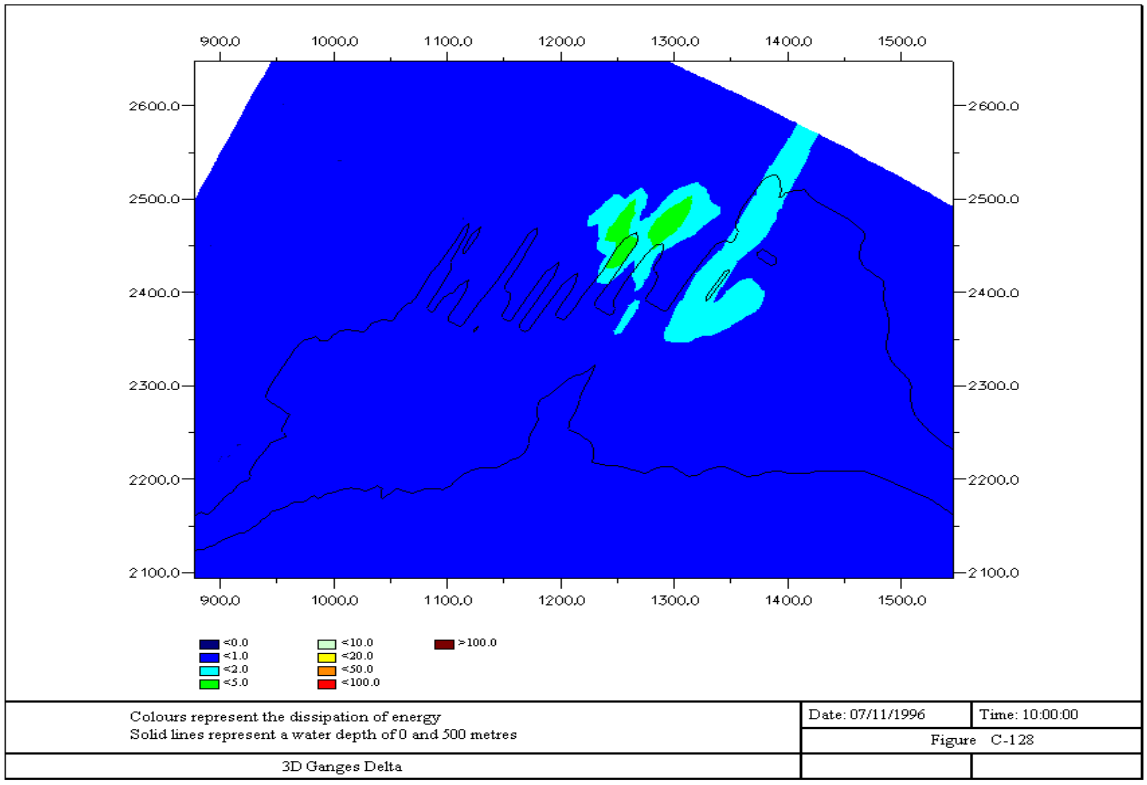

Colours represent the dissipation of energy Solid lines represent a water depth of 0 and 500 metres	Date: 07/11/1996	Time: 10:00:00
	Figure C-128	
3D Ganges Delta		

C.12 Set-up computation with wind profile B

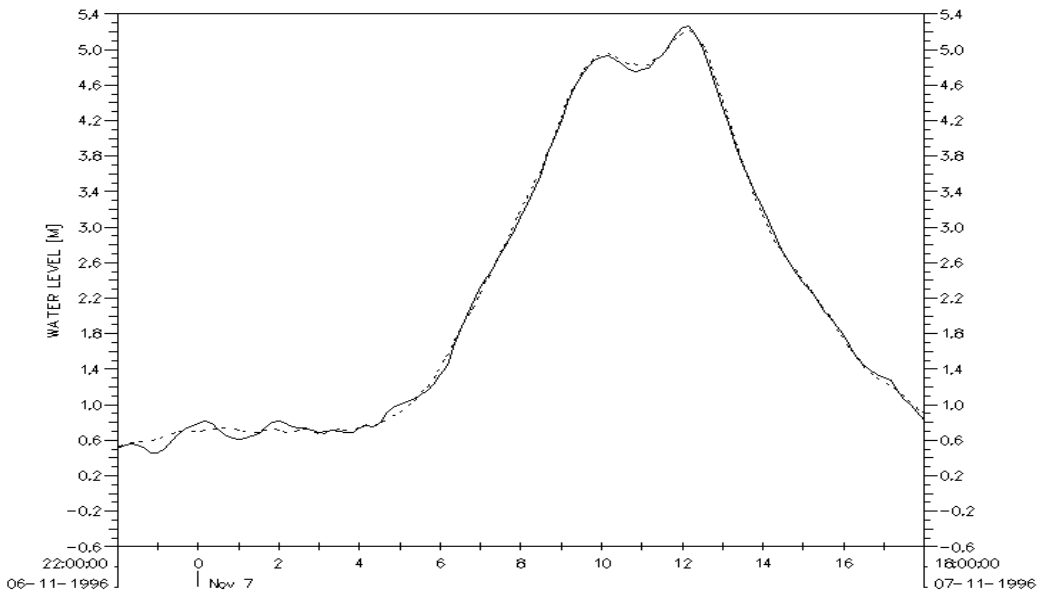

Dashed line represents the water level without including the effects of waves Solid line represents the water level including the effects of waves	Station 6	
	Figure C-129	
Water level at the coast as registered in specified station during cyclone event	2D Andhra Pradesh	Wind Profile B

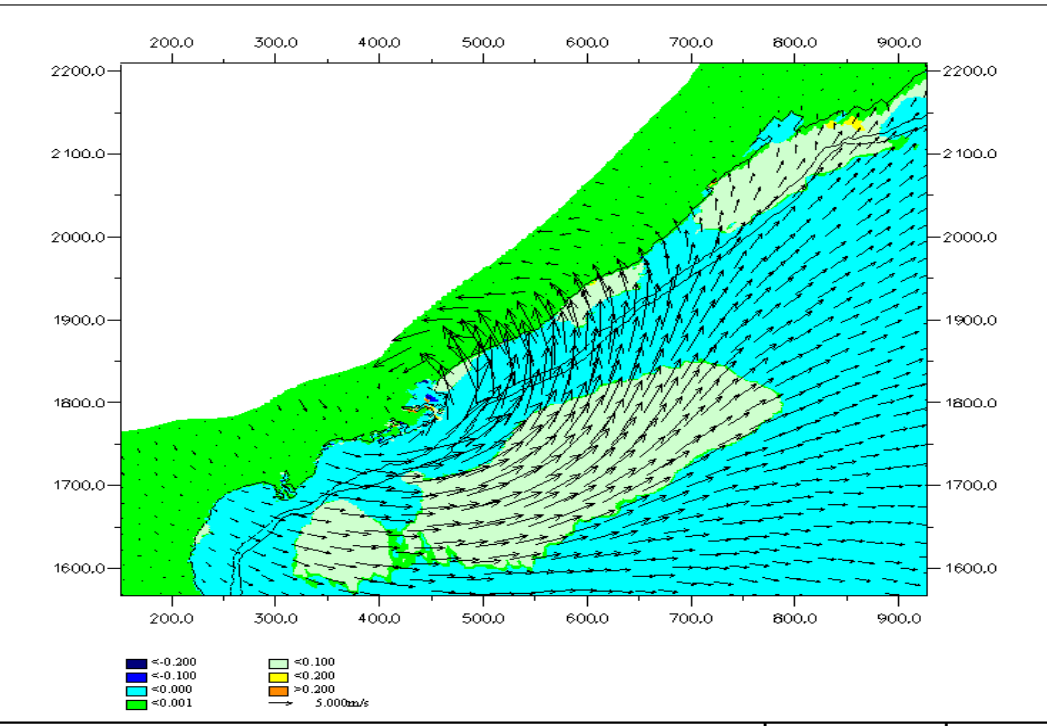

Black solid lines represent 0, 500 and 1000 metres depth isolines Vectors represent the wave direction Colours represent water level difference between computation with and without waves	Date: 07/11/1996	Time: 12:00:00
	Figure C-130	
2D Andhra Pradesh	Wind Profile B	